A UNIFIED APPROACH FOR STEEL AND COMPOSITE BEAMS WITH WEB OPENINGS

KO CHI HANG

M. PHIL.

THE HONG KONG
POLYTECHNIC UNIVERSITY

2002

ABSTRACT

A unified design method incorporating tee-section approach and perforated section approach is developed. The method provides a harmonized design method for steel beams and composite beams with web openings of various sizes and shapes. Hot rolled or fabricated compact steel sections with symmetric cross-section geometry are covered. No local buckling problem is considered.

In the tee-section approach, simple design formulas for the determination of plastic moment resistances of both composite tee-sections and steel tee-sections at the low moment side and the high moment side of the web openings under co-existing axial force and shear force are derived analytically based on plastic stress blocks. The beneficial effect of axial force on the moment resistances is identified. Complete shear-axial-moment interaction curves are produced for the tee-sections.

In order to assess the load capacities of beams with web openings, the design formulas from the tee-sections approach are extended for the analyses of the entire perforated sections by considering the equilibrium of forces around the web openings. Moment-shear interaction curves are generated for steel beams with web openings and the results are compared with those obtained from a separate finite element study. Similar moment-shear interaction curves for composite beams with web openings are also produced and discussed.

Harmonized design of beams with web openings of different shapes is achieved through the use of equivalent octagonal openings. Transformation expression for steel beams with circular web openings has been proposed. Moment-shear interaction curves for these beams have also been generated and compared with finite element results.

Over a hundred test data have been collected from various sources and a comprehensive database is established. Forty test data of composite beams with rectangular web openings, fourteen test data of steel beams with rectangular web openings, and nine test data of steel beams with circular web openings are selected from the database for the calibration of the proposed unified design method with the use of a specifically developed computer program.

The proposed unified design method is considered to be straightforward and easy to understand. It may facilitate practicing engineers to take advantages of composite construction to build commercial buildings with improved performance and full integration with building services. Furthermore, based on the step-by-step design procedures provided, engineers will be able to perform quick and practical scheming design on steel and composite beams with large web openings.

ACKNOWLEDGEMENTS

The author feels indebted and would like to express his sincere thanks to Dr. K. F. Chung for his knowledgeable and skillful guidance, his continual encouragement and his patience throughout his research study.

Special appreciation has to be directed to Dr. T. C. H. Liu of the Manchester University in the United Kingdom. Results predicted by the proposed design method for steel beams with web openings have been frequently compared with those obtained from the finite element studies performed by Dr. Liu. His findings have provided invaluable reference and have made possible a more accurate and reliable design method to be delivered. Details of the finite element studies are discussed in specific sections of Chapters 3 and 4.

The financial assistance provided by the Hong Kong Research Grant Council (Project No. PolyU5085/97E) and the tuition scholarship for my Mphil study awarded by the Faculty Research Committee of the Hong Kong Polytechnic University are gratefully acknowledged.

Thanks are also extended to Miss Natalie Wong for her drafting of the test data presented in Appendix A. Encouragement and humor from Mr. Dominic Yu should also be mentioned.

CONTENTS

CHAPTER 6 DESIGN PROCEDURES AND EXAMPLES

LIST OF FIGURES

LIST OF TABLES

LIST OF SYMBOLS

A_f	Area of steel flange
A_v	Shear area of un-perforated section
A_{vf}	Shear area of steel flange
A_{vo}	Shear area of perforated section
A_{vw}	Shear area of steel web
M_{Rd}	Plastic moment resistance of an un-perforated section
M_{Sd}	Global bending moment at the centerline of a web opening
$M_{o,Rd}$	Plastic moment resistance of a perforated section
$M_{T,Rd}$	Plastic moment resistance of a tee-section
$M_{v,Rd}$	Vierendeel resistance of a perforated section
$M_{bh,Sd}$	Local bending moment acting at HMS of the bottom tee-section
$M_{bl,Sd}$	Local bending moment acting at LMS of the bottom tee-section
$M_{th,Sd}$	Local bending moment acting at HMS of the top tee-section
$M_{tl,Sd}$	Local bending moment acting at LMS of the top tee-section
$M_{vc,Rd}$	Moment resistance derived from the composite action of the top steel tee-section and the concrete slab
$M_{T,N,Rd}$	Plastic moment resistance of a tee-section under axial force
$M_{T,V,Rd}$	Plastic moment resistance of a tee-section under shear force
$M_{T,VN,Rd}$	Plastic moment resistance of a tee-section under shear force and axial force
$M_{Tl,V,Rd}$	Plastic moment resistance of a top tee-section at LMS under shear force
$M_{Th,V,Rd}$	Plastic moment resistance of a top tee-section at HMS under shear force
$M_{Tbl,V,Rd}$	Plastic moment resistance of a bottom tee-section at LMS under shear force
$M_{Tbh,V,Rd}$	Plastic moment resistance of a bottom tee-section at HMS under shear force
$M_{Tl,VN,Rd}$	Plastic moment resistance of a top tee-section at LMS under shear force and axial force
$M_{Th,VN,Rd}$	Plastic moment resistance of a top tee-section at HMS under shear force and axial force

$M_{Tbl,VN,Rd}$	Plastic moment resistance of a bottom tee-section at LMS under shear force and axial force
$M_{Tbh,VN,Rd}$	Plastic moment resistance of a bottom tee-section at HMS under shear force and axial force
N_{Rd}	Axial force transferred across the concrete-steel interface
$N_{ao,Rd}$	Axial resistance of a perforated steel I-section
$N_{c,Rd}$	Axial resistance of concrete slab
$N_{f,Rd}$	Axial resistance of steel flange
$N_{f,Sd}$	Axial force applied to steel flange
$N_{o,Rd}$	Axial resistance of the removed web due to presence of an opening
$N_{H,Rd}$	Compressive force in the concrete slab at HMS
$N_{L,Rd}$	Compressive force in the concrete slab at LMS
$N_{sh,Rd}$	Resistance of shear connectors from support to a point under consideration
$N_{T,Rd}$	Axial resistance of a tee-section
$N_{T,Sd}$	Axial force applied to a tee-section
$N_{w,Rd}$	Axial resistance of web of an steel I-section
$N_{w,Sd}$	Applied axial force carried by steel web
$N_{a,V,Rd}$	Axial resistance of a steel tee-section under shear force
$N_{f,V,Rd}$	Axial resistance of steel flange under shear force
$N_{w,V,Rd}$	Axial resistance of steel web under shear force
V_{Sd}	Global shear force at the centerline of a web opening
$V_{a,Rd}$	Shear resistance of a steel perforated I-section
$V_{c,Rd}$	Shear resistance of concrete slab
$V_{c,Sd}$	Shear resisted by concrete slab
$V_{f,Rd}$	Shear resistance of steel flange
$V_{f,Sd}$	Shear force resisted by steel flange
$V_{o,Rd}$	Shear resistance of a perforated section
$V_{t,Sd}$	Shear force resistance by a top tee-section
$V_{t,Rd}$	Shear resistance of a top tee-section
$V_{T,Rd}$	Shear resistance of a tee cross-section
$V_{T,Sd}$	Shear force applied to a tee cross-section
$V_{w,Rd}$	Shear resistance of steel web
$V_{w,Sd}$	Shear force resisted by steel web

$V_{ab,Sd}$	Shear resisted by bottom steel tee-section
$V_{ab,Rd}$	Shear resistance of the bottom steel tee-section
$V_{at,Rd}$	Shear resistance by top steel tee-section
$V_{at,Sd}$	Shear resisted by top steel tee-section
W_{pl}	Plastic modulus of un-perforated section
$W_{o,pl}$	Plastic modulus of perforated section
a_o	Length of a rectangular web opening
b_e	Effective breadth of concrete slab
b_f	Width of steel flange
d_1	Depth of web of a steel tee-section
d_e	Effective depth of concrete slab
d_L	Distance from centroid of compressive in the concrete slab to the top of steel section at LMS
d_H	Distance from centroid of compressive in the concrete slab to the top of steel section at HMS
d_o	Diameter of a circular web opening
f_{cd}	Design strength of concrete
f_{ck}	Compressive cylinder strength of concrete
f_{vf}	Average reduced bending strength of steel flange under shear force
f_{vw}	Reduced bending strength of steel web under shear force
f_{vfl}	Reduced bending strength of flange shear area under shear force
f_y	Yield strength of a steel
f_{yd}	Design strength of steel
h	Depth of steel beam
h_c	Height of concrete over decking
h_o	Height of a rectangular web opening
h_p	Height of profiled steel decking
h_t	Total height of concrete slab
h_w	Depth of the steel web in un-perforated section
m	Bending moment ratio
n	Axial force ratio
n_H	Number of shear connector from support to HMS of a perforated section
n_L	Number of shear connector from support to LMS of a perforated section
n_o	Number of shear connector over a web opening

r_o	Radius of a circular web opening
t_e	Reduced web thickness of steel under shear force
t_f	Thickness of steel flange
t_w	Thickness of steel web
v	Shear force ratio
v_c	Concrete shear strength
x_o	Distance of centerline of web opening from support
y_I	Distance between PNA and bottom of flange for I section under bending
y_L	Distance between PNA and top of concrete slab at LMS of composite tee-section
y_H	Distance between PNA and top of concrete slab at HMS of composite tee-section
y_{pc}	Depth of PC from top of flange in a steel tee-section
y_{po}	Depth of PNA from top of flange in a steel tee-section
y_{pob}	Depth of PNA from top of flange in a bottom steel tee-section
y_{pcb}	Depth of PC from top of flange of a bottom steel tee-section
y_{pcth}	Depth of PC from top of flange of a top composite tee-section at HMS
y_{pctl}	Depth of PC from top of flange of a top composite tee-section at LMS
z	Lever arm between axial forces acting on the top and the bottom steel tee-sections
z_H	Lever arm between the applied axial forces on top and bottom composite tee-sections at HMS
z_L	Lever arm between the applied axial forces on top and bottom composite tee-sections at LMS
α	Depth of stress block in concrete due to bending
α_c	Depth of stress block in concrete due to applied axial force
α_f	Depth of stress block in steel flange due to applied axial force
α_w	Depth of stress block in steel web due to applied axial force
β_o	Constant for converting the diameter of a circular web opening into the length of an equivalent octagonal web opening
β_c	Distance from center of axial stress block in concrete to PC
β_f	Distance from center of axial stress block in steel flange to PC

β_h	Constant for calculating the height based on the length of an equivalent octagonal web opening
β_w	Distance from center of axial stress block in steel web to PC
γ_a	material factor for steel
γ_c	material factor for concrete
γ_v	material factor for shear connector
τ_f	Shear stress in steel flange
τ_w	Shear stress in steel web

CHAPTER 1

INTRODUCTION

1.1 Background

Steel beams with multiple web openings found applications for ships, aircrafts and vehicles in early days because of their increased section moduli and stiffnesses over the un-perforated steel beams. Due to their easy and economic fabrication, these beams have been used in exposed roof structures for architectural reasons, as shown in Figure 1.1. They are also used with concrete slabs in modern composite commercial buildings, as shown in Figure 1.2. The regular spacing of the web openings along the beam length allows flexible layout for the passage of building services such as air ducts and water pipes. The result is a combination of reduced storey height and more efficient use of steel materials, and easy installation of building services, leading to significant saving of overall construction cost. When irregular layout of building services is required, discrete or single web openings can be provided at specific locations along the beam span.

The strength and stiffness of a beam with web openings are often reduced when compared to its un-perforated counterpart, and the reduction is a function of the opening configuration such as:

- Shapes and sizes of the web openings,
- Locations of the web openings along the beam span,
- Spacing between adjacent web openings,
- Reinforcement or stiffener plates provided around the web openings, and
- Position of the web openings with respect to the mid-depth of the steel beam.

Due to the presence of openings in the web of the steel sections, both the moment and the shear resistances of the steel or composite beams are reduced. As the size of the web openings increases, the flexural and the shear failures may be found at points of high bending moment and high shear force along a beam as shown in Figure 1.3a and 1.3b. Furthermore, depending on the length of the web openings and the moment to shear (M/V) ratio at the perforated sections, the shear force acting across the web openings produces "Vierendeel" moments which may cause local flexural failure in the top and the bottom tee-sections above and below the web openings, as shown in Figure 1.3c. This mode of failure is usually referred as the Vierendeel mechanism, which deserves much attention in studying the structural behavior of beams with web openings. All the three failure modes may occur in composite beams with web openings as well. However, the Vierendeel mechanism is more complicated due to the presence of the concrete slab and the different degrees of shear connection at the low moment side (LMS) and the high moment side (HMS) of the web opening. As shown in Figure 1.3d, concrete cracking may occur at the top of the concrete slab at the LMS while there is concrete crushing at the top of the concrete slab at the HMS. Thus, the stress distributions of the composite tee-sections at the LMS and the HMS above the web opening are different.

1.2 Current Design Rules

The provision of web openings in structural members is a subject of extensive research for the last few decades and there are many experimental tests, analysis techniques, and design methods available in the literature. For beams with multiple web openings, that is, castellated beams, many design rules are usually simple, empirical, and 'product-specific'. Their applications are very restrictive and are not valid for large web openings with different opening configurations.

For beams with discrete or single web openings without web buckling problems, most of the works are only intended for small openings with an opening depth of less than 60% of the section depth of the steel beam. There are also no consistent design methods for beams with different opening shapes. All strength design methods based on plastic stress block analysis may be classified into two categories as follows:

1) Design methods utilizing moment-shear interaction curves on perforated sections
2) Design methods based on interaction of shear force, axial force, and bending moment acting on tee-sections

The stress distribution around a perforated section at failure varies according to the M/V ratios at the centerline of the perforated section. Design methods utilizing the moment-shear interaction curve approach involves, based on a particular stress distribution, the evaluation of the global moment resistance of the perforated section, M_{oRd}, under a specific applied shear force, V_{oRd}. Complete interaction curves can be generated by calculating the global moment resistances at different M/V ratios and thus, many different stress blocks must be considered in order to achieve a complete solution. A typical moment-shear interaction curve is shown in Figure 1.4. To simplify the calculation efforts, many design methods require only the calculation of the resistances of two or three stress blocks for the perforated sections, typically the pure moment and the pure shear resistances. Interaction curves are then generated by joining these points with simple empirical curves.

These simplified design methods have the advantages of being easier to apply because closed-form formulas are usually given, and manual calculations are usually performed to give conservative results. Moreover, the same interaction curve can be

used for the same beam section even when the web opening is placed at a different location, provided that the size of the opening does not change. However, since different design methods may adopt different stress blocks, the formulas derived are unique and thus are not compatible with other methods. Some of the formulas may also be considered to be "over-developed", as the structural principles are usually implicitly stated and often quite complicated for comprehension.

In the tee-section approach, the moment resistances of the tee-sections above and below the web openings are evaluated explicitly under co-existing axial force and shear force due to global actions. The three failure modes mentioned in Section 1.1 are then checked to ensure that the beam is structurally adequate. Since this method considers directly the applied force and moment against the corresponding resistances of the beam, it does not involve any pre-determined stress distribution. Furthermore, the generation of interaction curves is not always necessary. A complete interaction curve for a steel tee-section subjects to different combinations of axial force and bending moment under constant shear force is shown in Figure 1.5, where the moment and the axial force ratios are defined as the applied moment divided by the moment resistance, and the applied axial force divided by the axial resistance of the tee-section, respectively. As all the formulas are based on simple structural principles, the design method may be considered to be simplistic and easily understood while the calculation effort may be considerable. The calculations of the moment resistances of the tee-sections are rather inaccurate in some cases as only empirical design rules are used for the shear force-axial force-moment (V-N-M)$_T$ interaction on the tee-sections. Moreover, calculations have to be repeated if either the location or the size of the web opening is changed.

1.3 Objectives

The objectives of this research project are:

a) To predict analytically the plastic moment resistances of both steel and composite tee-sections in the presence of co-existing axial force and shear force.

b) To develop analytical moment-shear interaction curves for perforated sections of both steel and composite beams for general design.

c) To develop a unified design method for steel and composite beams with large web openings of various sizes and shapes based on plastic design method and formulated in accordance with analytical structural design principles.

d) To propose transformation expression for converting a circular web opening into equivalent octagonal opening.

e) To implement a specialist computer program for the calibration of the proposed unified design method with test data. Step-by-step design procedures in accordance with Eurocodes are also provided to assist engineers to perform practical scheming design.

1.4 Scope of Work

This thesis reports the findings of a two-year research project in which a unified design method for both steel beams and composite beams with large un-reinforced concentric web openings is developed through basic structural design principles. The design development involves the harmonization of both the tee-section approach and the perforated section approach for both steel beams and composite beams with single rectangular or circular web openings of various sizes. However, instabilities such as web buckling, web post buckling, and local flange buckling are not considered. Neither is flexural deflection considered.

The scopes of the research project are:

*a) **Literature review***

Comprehensive study on published research works is carried out to collect and extract information on the structural behavior of steel and composite beams with single and multiple web openings. Based on published experimental investigations, a database for steel and composite beams with web openings is established, which is then used subsequently in the calibration of the proposed unified design method.

*b) **Design method for steel beams with single web openings***

Following the direction of the tee-section approach and based on structural design principles with rectangular stress blocks, a set of analytical design formulas is developed for the evaluation of the moment resistances of tee-sections in the presence of co-existing axial force and shear force. Moreover, complete interaction curves of tee-sections under a full range of tensile and compressive forces and shear force, or the local $(V\text{-}N\text{-}M)_T$ interaction curves, may be traced out analytically. Based on the tee-section analysis and by considering web openings subject to different M/V ratios, a set of moment-shear interaction curves for perforated section, or the global $(M\text{-}V)_o$ interaction curves are generated following the perforated section approach. It is, thus, possible to evaluate both the applied moment, M_{Sd}, and the applied shear force, V_{Sd}, at failure of the perforated section along the beam span. These $(M\text{-}V)_o$ interaction curves are compared with those derived from a separate finite element study. The proposed design method for steel beams with single web openings is also calibrated with test data, and a step-by-step design procedure is presented together with a fully worked example.

*c) **Transformation expression for beams with circular web openings***

The proposed analytical design method is suitable for beams with rectangular

web openings assuming the formation of four plastic hinges at the corner of the web openings. Its applicability to beams with circular web openings requires a transformation expression in which the circular web opening is transformed into an equivalent octagonal web opening, resulting in tee-sections of constant depth so that the tee-section analysis can be performed. Different transformation expressions assuming different octagonal web openings are investigated to establish analytical global $(M\text{-}V)_o$ interaction curves for direct comparison with results derived from finite element study and other design methods. After calibration against the finite element results, a transformation expression for converting circular web opening into an equivalent octagonal web opening is proposed. Transformation expressions for other opening shapes are not considered in this project.

d) Design method for composite beams with single web openings

A similar set of analytical design formulas for composite tee-sections is also developed, taking into account the effect of the degree of shear connections. In order to illustrate the effect of shear connections on the moment resistance of the composite tee-sections, local $(V\text{-}N\text{-}M)_T$ interaction curves are generated for comparison. These design formulas are then used to generate global $(M\text{-}V)_o$ interaction curves for the perforated sections based on the equilibrium condition around the web openings. Since no results from finite element study are available, the proposed design method for composite beams with single web opening is directly calibrated with test data, and a step-by-step design procedure is presented together with a fully worked example.

1.5 Layout of Thesis

The layout of thesis is divided into the following chapters:

a) Chapter 2

Available literature on the topic of steel and composite beams with web openings is reviewed in details. Major aspects on structural performance of steel and composite beams with web openings such as failure behaviors, yielding pattern of steel, crushing of concrete, and slippage of shear connectors are summarized. Key design assumptions and principles in current design methods directly relevant to the research project are discussed. The design procedures of two widely used design guides are selected and discussed in order to illustrate the primary difference between the perforated section approach and the tee-section approach. Abstracts of three publications which are published by the candidate as an author or as a co-author related to the research project are also included.

b) Chapter 3

Practical analytical design formulas based on structural design principles with rectangular stress blocks are derived for determining local moment resistance of steel tee-section under co-existing axial and shear forces and local $(V\text{-}N\text{-}M)_T$ interaction curves may be generated for the tee-sections. The proposed design formulas for tee-section are then extended and a complete analytical design method for perforated section is proposed to generate global $(M\text{-}V)_o$ interaction curves for practical design. The design results are then compared with those obtained from a separate finite element study. Test results of steel beams with rectangular web openings are used to calibrate the proposed design method.

c) Chapter 4

Three transformation expressions using equivalent octagonal web openings are incorporated in the proposed design method in order to extend the method for the design of steel beams with circular web openings. The results are then compared

with those obtained from a finite element study and the best transformation expression is chosen for use with the proposed design method. Finally, test data of steel beams with circular web openings are used to calibrate the proposed design method.

d) Chapter 5

A similar set of analytical design formulas is also developed for composite beams with web openings. Composite tee-sections with both full and partial shear connections and different slab details such as solid slabs and slabs with profiled steel decking placed either transversely or parallel to the steel beam are included. The tee-section analysis of the bottom steel tee-section and the composite tee-section analysis of the top composite tee-section are then combined to derive a complete analytical design method for composite perforated section. The method is then calibrated with test data from the established database of composite beams with web openings.

e) *Chapter 6*

A step-by-step design procedure is presented for each of the steel and the composite beams with web openings. The design procedures are fully illustrated with two worked examples. A description of the capability of the specialist computer program specifically developed in this project for calibration of the proposed design method is also provided.

f) Chapter 7

This chapter presents the conclusion to the research project.

g) Appendix A

This appendix presents a comprehensive listing of test data for both steel beams and composite beams with web openings collected from the literature.

1.6 Related Publications Published by the Candidate

In conjunction with the development of this research project, three papers are published by the candidate as an author or as a co-author and they are listed as follows:

1. Chung, K. F., Liu, T. C. H., and **Ko, A. C. H.** "Investigation on Vierendeel mechanism in steel beams with circular web openings". *Journal of Constructional Steel Research*, Vol. 57, pp. 467-490 (2001)

2. **Ko, C. H.** and Chung, K. F. "A comparative study on existing design rules for steel beams with circular web openings". In Yang, Y. B., Leu, L. L., and Hsieh, S. H., eds., *Proceedings of the First International Conference on Structural Stability and Dynamics*, Taipei, Taiwan, December 2000, pp. 733-738 (2000)

3. Liu, T. C. H., Chung, K. F., and **Ko, A. C. H.** "Finite element modeling on Vierendeel mechanism in steel beams with large circular web openings". *Proceedings of the International Conference on Structural Engineering, Mechanics and Computation*, Cape Town, South Africa, April 2001, pp. 1567-1574 (2001)

Figure 1.1 Typical usages of steel beams with web openings

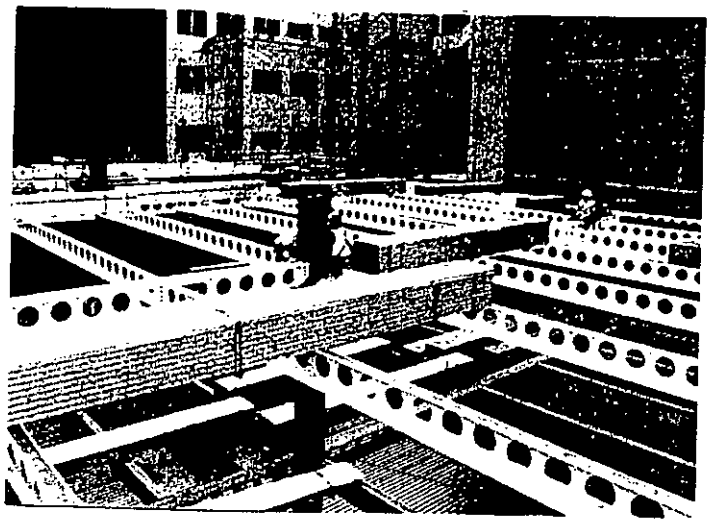

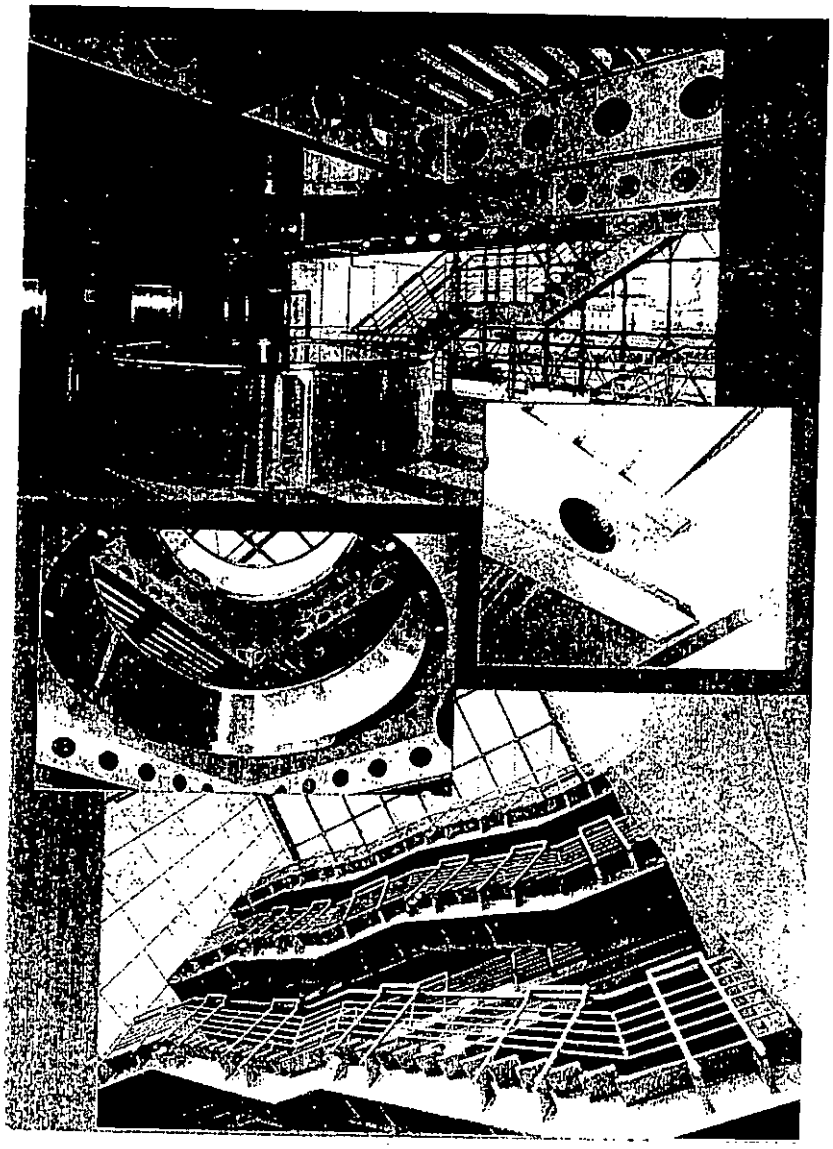

Figure 1.2 Typical usages of composite beams with web openings

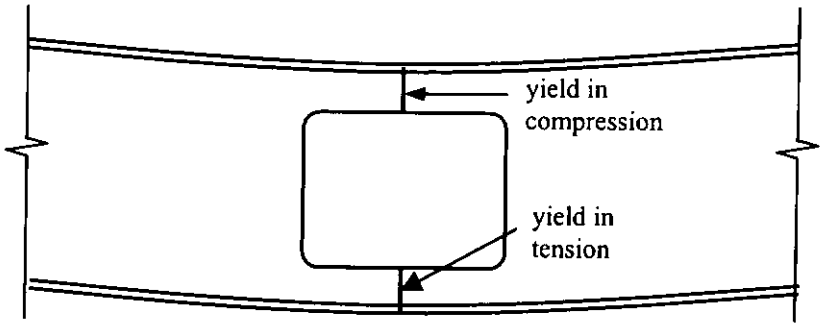

a) Flexural failure

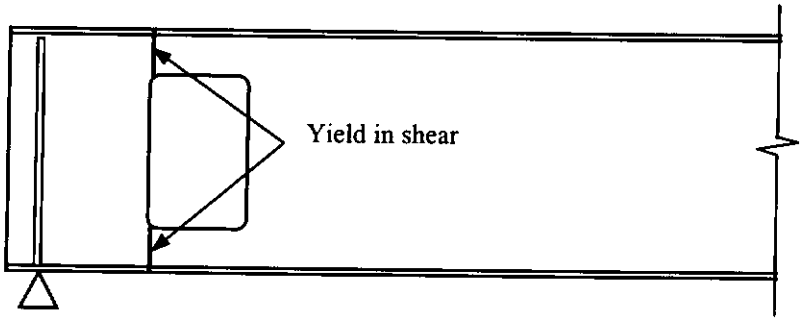

b) Shear failure

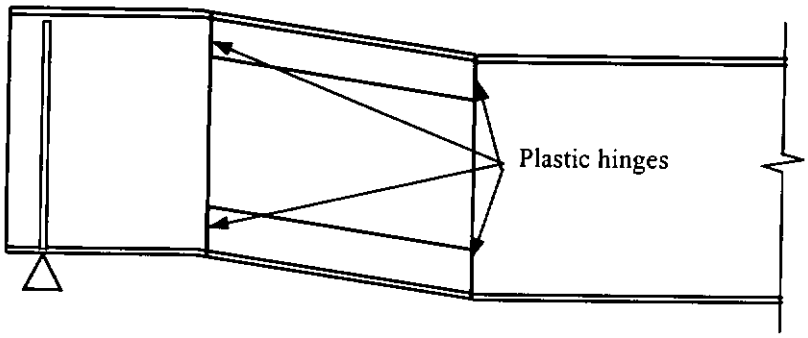

c) Vierendeel mechanism in steel beam

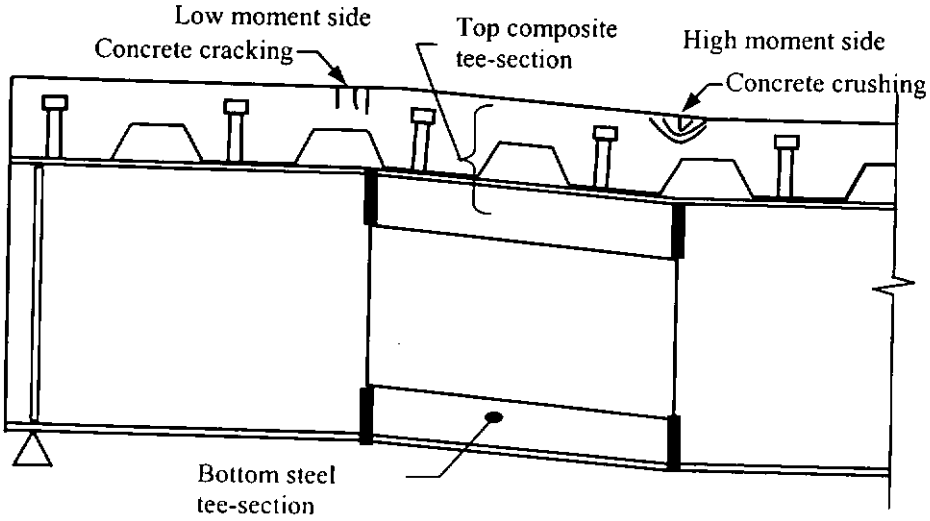

d) Vierendeel mechanism in composite beam with web opening

Figure 1.3 Failure modes of beams with web opening

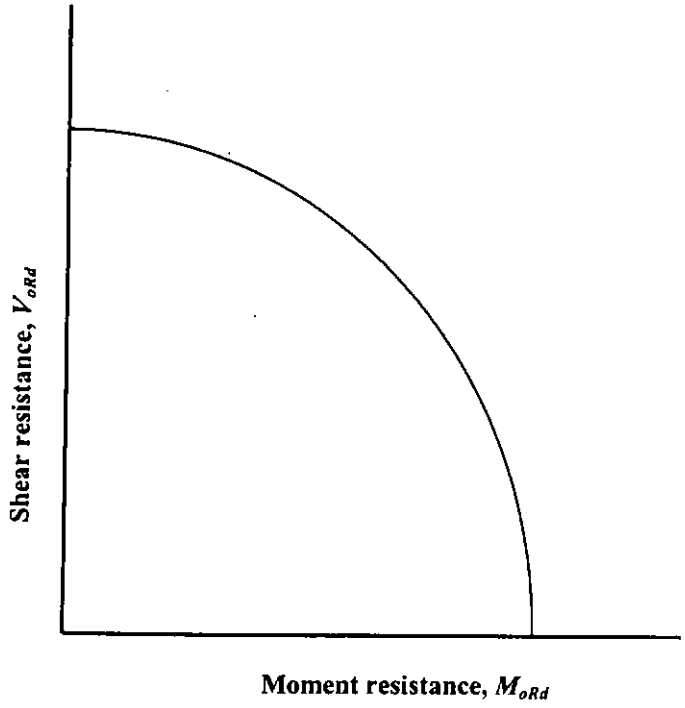

Figure 1.4 Typical moment-shear interaction curve for perforated section

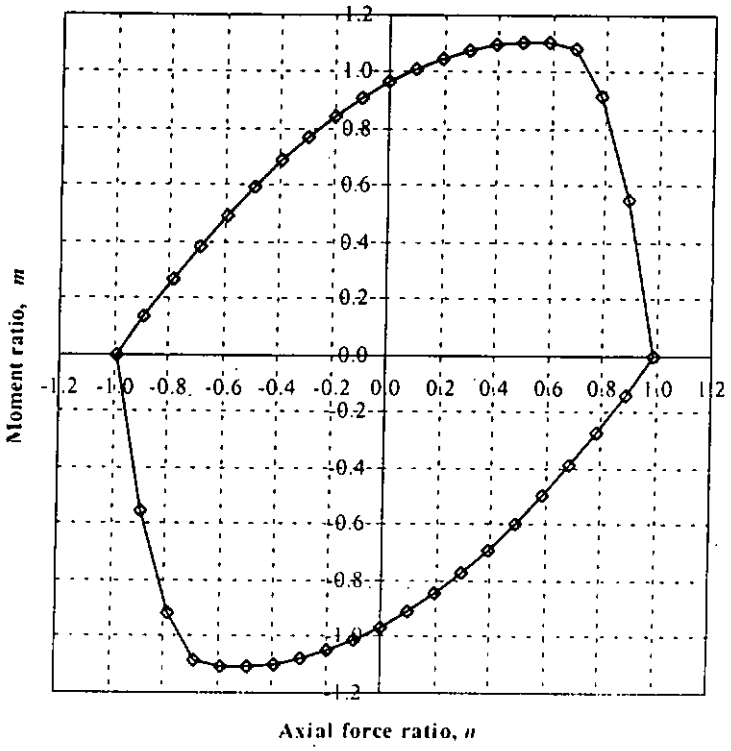

Figure 1.5 Axial-moment interaction curve for a steel tee-section under constant shear force

CHAPTER 2

LITERATURE REVIEW

2.1 General

A large number of experimental investigations and numerical analyses have been carried out to study the behavior of steel and composite beams with web openings over the past few decades. Alongside with these studies was the establishment of theoretical detailed strength design models and simplified design methods to predict the load capacities of beams with web openings. Amongst the methods proposed, almost all of them are for single rectangular web openings since multiple web openings are usually associated with castellated beams, which are often "product-specific" and are analyzed empirically. Single circular web openings are usually treated with the same methods through the use of equivalent rectangular openings.

In the analysis and design of steel beams with web openings, the plastic stress block method is usually employed because of its simplicity in analysis and rationality in design. However, it should be noted that its application is guaranteed only for compact sections that can undergo considerable inelastic rotation without local buckling. Elastic analysis is also used, particularly for non-compact sections, which is outside the scope of the current project.

With the advance of composite construction techniques, steel beams are readily connected to concrete slabs via shear connectors to develop composite action. The two materials act as a monolithic unit when subject to loading in order to provide greater strength and stiffness over that of a non-composite steel section. Much larger web openings can be provided in the steel sections without reinforcements around

the web openings. The concrete contributes to both the moment and shear resistances of the composite section, thus reduces both the fabrication and the construction cost. The failure behavior of such composite beams with web openings is similar to that of steel beams with web openings, although force distribution is much more complicated, and more design efforts are needed in general.

This chapter summarizes important experimental observations and structural behavior of both steel and composite beams with web openings relevant to the current research project. The design procedures from two widely used design guides are briefly discussed in order to illustrate the difference between the perforated section approach and the tee-section approach in the design of beams with web openings.

There is a large amount of experimental investigations on the structural behavior of both steel and composite beams with web openings. The test programs, details and scopes of the steel beams and the composite beams with web openings, and also the test loads are re-presented in a consistent format for ease of comparison in Appendix A.

2.2 Steel Beams with Web Openings

A large number of test data have been collected for steel beams with web openings. The test beams are generally short in span with a maximum span length of about 5 meters. These beams are usually loaded under concentrated loads to simulate the situation of a primary beam (or girder) in a floor system. A summary of test data for steel beams with web openings is presented in Appendix A. In most of the tests, rectangular web openings are present because of their prevalence in practice. Furthermore, the test results may be directly compared with analytical design methods derived from plastic stress blocks. Various key observations from the tests

are discussed below.

2.2.1 Failure mechanisms

Elastic stress analysis of steel beams with web openings was quite popular in the early days. However, when the size of a web opening is larger than 50% of the beam depth or when a more accurate design is needed, plastic stress analysis should be used. Steel beams with single web openings subject to pure bending are found to be failed in a way similar to that of un-perforated beams, that is, complete yielding of the top and the bottom tee-sections (Redwood & McCutcheon, 1968) as shown in Figure 2.1. However, in the presence of a shear force, the mode of failure will be different. The beams will exhibit "Vierendeel" behavior, which is related to the transfer of shear force across the web openings by the top and the bottom tee-sections. Under the Vierendeel action, each end of the tee-sections above and below the web openings is subjected to co-existing shear force, axial force, and bending moment. At failure, these local forces and moments will cause the tee-sections to yield, forming plastic hinges as shown in Figure 2.2.

The plastic analysis of the Vierendeel mechanism usually assumes the formation of plastic hinges at both ends of the tee-sections above and below the rectangular web openings. In the rare case when the perforated section is subject to a very high shear force and that the opening depth is large but the opening length is short, the perforated section may exhibit a pure shear failure as shown in Figure 2.3.

It should be noted that in order to utilize the plastic design method, local buckling of various elements, especially the web, of the steel member around the web opening must be prevented. Web instability problems have been investigated by Redwood et al. (1978) for un-reinforced web opening, Shrivastava and Redwood (1977) for web opening reinforced on both sides of the web, and Lupien and

Redwood (1978) for web opening reinforced on one side of the web.

2.2.2 Moment-shear interaction curves

A number of plastic design methods for beams with un-reinforced rectangular web openings are very similar in checking against both the moment and the shear resistances of the perforated section. However, they differ in the assumed stress distributions corresponding to the relative values of shear force, axial force, and bending moment in the tee-sections above and below the web openings. Except Lawson's design method (1987), a number of the methods require the strength of the perforated section to be plotted in the form of a complete moment-shear $(M\text{-}V)_o$ interaction curve. These methods are usually simplified in practical design in which it is only required to calculate two or three points on the graph. Then the points will be either connected by straight lines, or curves to obtain an approximate interaction curve, as shown in Figure 2.4. The applied moment and shear forces at the centerline of the web openings will then be pinpointed on the graph. If the design point falls below the strength curve, then the design is structurally adequate. Although it seems to be quite simple to calculate only two or three points on the graph, the expressions are often quite involved when calculating the Vierendeel shear resistance of the perforated section.

A number of design methods (Bower, 1968; Redwood, 1968; Aglan and Qaqish, 1982) have been derived for beams with un-reinforced web openings. All of these methods consider the interaction of the assumed local uniform shear stress and the bending stress in the steel web according to von Mises' yielding criterion. The predictions by all these methods have made use of the complete $(M\text{-}V)_o$ interaction curves.

It should be noted that as moment to shear (M/V) ratio changes from zero to

infinity at the perforated section, the plastic neutral axis (PNA) usually remains in the flanges of the tee-sections at the LMS. However, the PNA may shift from the flanges to the webs at the HMS. Figure 2.5 illustrates the stress distributions at the plastic hinges when M/V ratio is equal to zero or infinity. As a result, several combinations of stress blocks of the tee cross-sections at the LMS and the HMS have to be considered if a complete $(M\text{-}V)_o$ interaction curve is to be generated. Redwood (1968) has compared several stress blocks and amongst all the stress blocks the one giving the highest load capacity is adopted. Thus, this method does not necessarily produce a lower bound solution since equilibrium is not achieved in every aspect.

While most methods assume the pure shear yielding load to be the maximum value of the shear resistance, the effect of strain hardening ignored in those methods can cause the beams to sustain shear loads considerably above their pure shear resistances in the case of high M/V ratio. Shrivastava and Redwood (1979) has extended Redwood's method to consider explicitly the shear force carried by the flanges, and they also point out the possibility of horizontal shear yielding at the web-flange interface, which introduces a restriction on the shear resistance in some cases. In general, the consideration of horizontal shear yielding may lead to under-estimation of load capacity in those cases where horizontal shear yielding does not arise, i.e. when the shear force is low.

In all these design methods using the von Mises' yielding criterion, a minor error is usually introduced. As there is no shear force at the edge of the web opening, the shear stress is theoretically zero at the edge. Thus, the assumed shear stress distribution violates this boundary condition. However, since the shear stress may increase rapidly from zero at the opening edge to a high value over a short distance from the edge of the opening, this violation is probably not serious, as suggested by

Bower (1968).

2.2.3 Explicit consideration of shear-axial-moment interaction in tee-sections

Lawson has proposed a unique design method for beams with web openings in which the moment and the shear resistances of a perforated section at the mid-length of the opening are first assessed. Then the applied Vierendeel moment across the opening is compared with the total local moment resistances of the tee-sections above and below the opening, as modified according to the co-existing axial and shear forces due to global action. Thus, it is not required to generate the complete $(M\text{-}V)_o$ interaction curve and this method can be referred to as a point-by-point method.

Under normal circumstances, there is seldom a chance for a single tee-shaped member to be subjected to co-existing axial force, shear force, and bending moment. However, such situation always occurs in a beam with web opening whenever shear force is presented, as shown in Figure 2.6. Cantilever beams are often used to investigate the interactions among shear force, axial force, and bending moment. For beams with symmetrical cross-sections, the effect of axial force on the plastic moment resistance is well understood in the absence of shear force. Studies on the effect of shear force on the plastic moment resistance were made for rectangular beams (Drucker, 1956; Hodge, 1957) and for I-beams (Heyman and Dutton, 1954; Hodge, 1957; Neal, 1961a). Extension to incorporate the effect of axial force was undertaken by Neal (1961b) for rectangular beams, and by Horne (1958) and Neal (1961c) for I-beams. A lower bound solution has been suggested by Sherbourne and Oostom (1972a) for a long cantilever beam with a tee cross-section, under the effect of co-existing shear force and low axial force. As pointed out by Drucker (1956), a general true interaction curve for co-existing shear force, axial force, and bending

moment is never attainable whenever a shear force is present, as the solution for any particular situation is unique, depending on the loading and the support conditions. As a result, the outcomes of all of the aforementioned studies may be considered as lower bound or upper bound solutions with empirical formulation.

Since this research project has adopted the point-by-point method of Lawson's, it is thus important to evaluate the plastic moment resistances of the tee-sections under co-existing axial and shear forces in order to assess the Vierendeel resistance of a perforated section. In his method, Lawson has proposed the use of reduced web thickness to allow for the effect of shear force on the axial and the moment resistances rather than the reduced bending strength in accordance with von Mises' yielding criterion, which is normally used. Moreover, his method also ignores the beneficial effect of axial force on the plastic moment resistance through the use of a linear equation for the axial-moment interaction, leading to significant conservatism. Chapter 3 is devoted to the derivation of simple design formulas for the calculation of moment resistance of tee-section under the effect of co-existing axial force and shear force.

2.2.4 Equivalent rectangular web openings

If the Vierendeel mechanism of steel beams with rectangular web openings is considered in terms of localized plastic hinges, the positions of them may be considered to be located almost exactly at the corners of the web openings. However, the Vierendeel mechanism of steel beams with circular web openings under shear force is not as clear as those observed in steel beams with rectangular web openings. Instead of localized hinges, it appears that extensive shear yielding of the web takes place between these positions. In general the yielding is not symmetrical about the centerline of the web opening, but is slightly displaced towards the loaded position

(Redwood & McCutcheon, 1968), as shown in Figure 2.7.

The curve beam analysis proposed by Olander (1953) and Sahmel (1963) considers the section capacities of the tee-sections around the circular web openings explicitly under both global and local actions, and the location of the first plastic hinge in the tee-sections is established through iterations. This method was adopted by Ward (1990) to assess the load capacities of composite beams with multiple circular web openings. After minor modification, the method was incorporated into the Amendment A2 of Eurocode 3: Part 1.1: Annex N in 1998 for steel beams with multiple circular web openings. However, the curve beam analysis is very tedious and it considers only the formation of plastic hinges on one side of the web openings only, which can lead to either conservative or un-conservative results (Chung, Liu, and Ko; 2001).

In general, most of the current design methods adopt the use of equivalent rectangular transformation as suggested by Redwood (1969) to analyze and design beams with circular web openings as shown in Figure 2.8. However, the transformation expression is only suitable for a specific design method (Ko and Chung, 2000) and thus, new transformation expression is needed whenever a new design method is proposed. This is fully discussed in Chapter 4.

Through finite element analysis, Chung, Liu, and Ko (2001) have investigated the Vierendeel mechanism in steel beams with circular web opening. The load carrying capacities of typical universal steel beams with circular web opening are presented and discussed. An empirical moment-shear interaction curve at the perforated sections is also suggested for practical design of steel beams with circular web opening.

2.3 Composite Beams with Web Openings

Before 1970s, design methods for non-composite steel beams with web openings have been indirectly applied to the widely used composite beams, which were becoming more popular at that time. However, these design methods often result in uneconomic and over-conservative design of the steel sections since they do not take into account of any strength contribution of the concrete slab. The concrete contributes to both the moment and the shear resistances of the beams, and improves their structural behavior significantly. The need to understand the structural behavior of composite perforated sections and the urge to devise more suitable strength models have initiated a series of experimental investigations on composite beams with web openings. A summary of the tests data for composite beams with web openings is presented in Appendix A. Along with the tests, many strength design models have also been developed to predict the structural performance of the test beams. The failure behavior of composite beams with web openings is similar to that of steel beams with web openings, although force distribution around the web opening is more complicated. Besides, concrete cracking and shear connection are also very important factors in determining the stress distribution in the concrete slabs, the force distribution around the web openings, and also the load capacities of the beams. The force distribution around the web opening in a composite beam under intermediate M/V ratio is illustrated in Figure 2.9.

2.3.1 Failure mechanisms

The failure of composite beams with web openings was found to be quite ductile for both solid slabs and slabs utilizing profiled steel deckings (Clawson and Darwin, 1980; Donahey and Darwin, 1986; Lawson, 1992). For composite beams under high M/V ratios, the mode of deformation and failure is primarily flexural in

nature. At the ultimate load, the concrete at the top of the slabs failed by crushing, preceded by the full yielding of steel section as shown in Figure 2.10. In this case, secondary moments and shear forces have only minor effect on the overall behavior of the composite beams.

As the shear force increases, the Vierendeel effect becomes more dominant. Under medium M/V ratios, the bottom steel tee-section is subjected to a combination of local axial force, shear force, and bending moment. At failure, two plastic hinges will form at both ends of the bottom steel tee-section. However, only the cross-section of the top tee at the HMS of the web opening will fail because this is the critical section where the secondary bending moment adds to the primary bending moment. As a result, the Vierendeel failure is initiated by the formation of a "three-hinge mechanism", named by Clawson and Darwin (1980), as shown in Figure 2.11.

Under high shear force or low M/V ratios, the Vierendeel moment is severe and may cause one of the following two failure modes. The first one is a "four-hinge mechanism" shown in Figure 2.12 in which plastic hinges are formed at both ends of the top and the bottom tee-sections, resulting in a traditional Vierendeel mechanism as those observed in steel beams with web openings. Another failure mode, which is called the "shear failure", maybe resulted when the shear resistance of the top composite tee-section (concrete and steel) is exceeded at the point of contraflexure before the Vierendeel mechanism occurs. In this latter case, the bottom tee-section again fails with the formation of two plastic hinges at its ends as shown in Figure 2.13. It should be noted that the "shear failure" was not considered by Wong and Redwood (1982), and Poumbouras and Redwood (1983) since they observed that this failure mode always leads to a higher load capacity than those associated with the "four-hinge" Vierendeel mechanism. Clawson and Darwin (1980) suggested that

the load capacities of the beams obtained for the two failure modes are within 10%.

All of the beam behaviors discussed so far are related to short span beams. For long span beams, similar behaviors may occur; however, the Vierendeel effect reduces in significance as the beam becomes longer. In the tests carried out by Lawson in 1992, neither concrete splitting or crushing, nor bridging (separation between the concrete slabs and the steel beams) was observed. However, on breaking out the concrete after the tests, it was clear that the shear connectors adjacent to the web openings had deformed considerably. Moreover, it was very difficult to differentiate the pure flexure failure at high M/V ratios from the Vierendeel mechanism at low M/V ratios by judging merely from the deflected shapes of the beams around the web openings.

2.3.2 Moment-shear interaction curves

Clawson and Darwin (1980), Donahey and Darwin (1986), and Lawson (1992) have observed that steel yielding always occurred at relatively low loads and thus, they concluded that the first yield does not give an accurate measure of the load capacities of the composite beams with web openings. As a result, most of the analytical design methods adopt plastic design, which employs the ultimate capacities of the beams with rectangular stress blocks. In the experimental investigations, most of the test beams were loaded to failure with prohibition on lateral torsion buckling, local bucking, or any other effects that might initiate premature failure in the beams. It is common to ignore the effect of strain hardening, which in fact, may increases the strength of a section significantly, especially for web openings located at points of high M/V ratios (Clawson and Darwin, 1980).

The interaction between moment and shear is usually considered to be weak for composite beams with web openings. The composite section can carry a

considerable moment without a significant reduction in its shear resistance, or vice versa.

Based on test observations, many researchers (Todd and Cooper, 1980; Clawson and Darwin, 1980; Poumbouras and Redwood, 1983; Donahey and Darwin, 1986) have derived detailed strength design models which require the generation of moment-shear (M-V) interaction curves by varying the value of applied shear force to a perforated section and calculating the corresponding moment resistances of the top and bottom tee-sections, similar to those used for the design of steel beams with web openings. Again, since this type of detailed models involves very complicated procedures and iterations, it is meant primarily for research purposes and thus, not suitable for practical uses. Considerable efforts have been made to simplify the detailed models into practical design methods through rational assumptions and approximations.

Some of the simplified strength methods (Clawson and Darwin, 1980; Darwin and Lucas, 1990; Oehlers and Bradford, 1995) involve calculations of only two points on the moment-shear interaction curves, namely, the maximum moment resistance at zero global shear and the maximum shear resistance at zero global moment. Other methods (Wong and Redwood, 1982; Poumbouras and Redwood, 1983; Redwood and Cho, 1993) require the calculation of one additional point, which corresponds to the maximum moment resistance that can be carried by the beam under maximum shear force. However, since only the end points of the curve are calculated in these methods, the actual resistance of the composite perforated section under any intermediate value of the M/V ratio can only be approximated by the actual curve used. Typical $(M\text{-}V)_o$ interaction curves suggested by various design methods are shown in Figure 2.14. It should also be noted that since no point is

calculated for any intermediate value of the M/V ratio, the three-hinge Vierendeel mechanism is usually ignored, and thus all of the methods are based on a four-hinge Vierendeel mechanism.

Lawson's method (1987) also covers composite beams with web openings by considering the Vierendeel resistance contributed by the concrete slab, in addition to the moment resistances of the steel tee-sections under co-existing axial force and shear force. As a result, this method doesn't consider explicitly the moment resistances of the composite tee-sections.

2.3.3 Shear connection

Shear connectors play an important role in both solid slabs and slabs with profiled steel decking. The degree of shear connection is a very important structural parameter in composite structure in many experimental investigations (Poumbouras and Redwood, 1983; Donahey and Darwin, 1986; Cho and Redwood, 1992, Lawson, 1992). It can affect slippage, modes of concrete cracking, and the load capacities of the beams.

Transverse cracks often form at the top of a composite slab at the LMS of the web openings due to the Vierendeel effect and also the slippage at the concrete-steel interface. Experiments indicate a lack of strain compatibility between the top and the bottom tee-sections, and also between the top steel tee-section and the composite slab. Since a web opening is frequently placed away from the region of maximum moment, where lower degrees of shear connection are provided, and where the M/V ratios are low, large slippage may usually be expected at these locations. The slippage will place the lower portion of the concrete slab in compression and the upper portion of the concrete slab in tension at the LMS of the perforated section, which results in transverse cracking as shown in Figure 2.15. Such compressive

stress has been observed by Clawson and Darwin (1980) in composite beams with solid slabs and slabs with profiled steel decking (Donahey and Darwin, 1986). As the M/V ratio decreases, transverse cracks tend to appear at lower applied loads. As the applied load increases, the cracks increase in width and in depth, and eventually may propagate to the bottom of the concrete slab.

Some analytical design methods (Clawson and Darwin, 1980; Wong and Redwood, 1982) assume the concrete slab is fully cracked at the LMS so that no compressive force exists at all. However, Clawson and Darwin have considered the contribution of bending resistance of steel reinforcement. While the concrete slab appears to be cracked at the LMS under the Vierendeel effect, it will crush at the HMS at failure and thus it is usually assumed that the full concrete slab at the HMS can contribute to the moment resistance of the composite tee-section. Wong and Redwood (1982) have assumed that the compressive resistance of the concrete slab at the HMS is equal to the shear resistance of the shear connectors provided over the length of the web opening; this was generally considered to be conservative. The compression is assumed to be located at the top of the concrete slab where compressive strains are often very large as shown in Figure 2.15.

Poumbouras and Redwood (1983) have developed a detailed analysis procedure for beams with web openings that incorporates the compressive strengths of the concrete slab at both the LMS and the HMS of the web openings. The compressive force of the concrete slab at the LMS is assumed to be located at the top of the concrete slab at zero global shear; however, it is allowed to shift to the bottom of the concrete slab as the shear force at the web opening increases. The compressive force of the concrete slab at the HMS is selected in such a way that moment equilibrium is satisfied at the web opening. In their simplified version of the method,

Poumbouras and Redwood (1983) proposed that the compressive force in the concrete slab at the HMS is limited to the smaller of the resistances of the shear connectors at this point or the full compressive resistance of the concrete slab. All other design methods (Redwood, 1986; Donahey and Darwin, 1986; Lawson, 1987, and Cho and Redwood, 1993) thereafter have included the compressive force in the concrete slab at both the LMS and the HMS of the perforated section. Their difference being the assumptions made regarding different stress blocks and the positions of the resultant axial forces.

For beams subjected to high M/V ratios, the omission of a shear connector between the ends of the web opening may not lead to any problem since the concrete slab over the web opening is subjected to high compressive stresses. However, the omission of shear connectors between the ends of the web openings may prevent the concrete slab in participating fully in the Vierendeel action at the web opening under low M/V ratios. This will cause a significant reduction in the ultimate capacity of the beams in the region of the web opening (Wong and Redwood, 1982; Poumbouras and Redwood, 1983). As a result, any shear connector in the proximity of the web opening should be included for strength calculation in order to produce load capacities close to test results.

Solid slabs and composite slabs with longitudinal profiled steel decking can accommodate more shear connectors than composite slabs with transverse profiled steel decking. In addition, the strength of shear connectors decreases progressively from solid concrete slabs to concrete slabs with longitudinal profiled steel decking, then to composite slabs with transverse ribs. As a result, for solid concrete slabs, the resistance of shear connectors is generally large enough to force crushing or diagonal tension failure in the slabs, while for composite slabs with profiled steel decking,

strength is usually limited to the resistance of the shear connectors. This strongly suggests that for composite slabs with profiled steel decking, any increase in the resistance of the shear connectors will also increase the load capacities of the perforated sections. As a general rule, both the moment and the shear resistances of a composite beam with web openings will be increased as the number of shear connectors is increased over the web opening, and also between the openings and the closest point of zero moment.

2.3.4 Shear force distribution

The mechanism with which the concrete slab carries shear force in a composite beam with web openings has long been an unknown. In the absence of a clear understanding of this mechanism, all theories or strength design methods have taken steps either to assign vertical shear forces to the concrete slab and the steel tee-section arbitrarily, or to limit the shear resistance of the composite tee-section.

In the detailed model reported by Clawson and Darwin (1980) for unreinforced web openings, a biaxial state of shear and compressive stresses is assumed in the concrete slab; the tensile strength of the concrete slab is ignored. Shear stresses based on a punching shear phenomenon in the concrete slab are assumed to be effective over a width of the concrete slab equal to three times the slab thickness. The shear force is assumed to be carried by both the steel web and the steel flange in the composite tee-section; however, only the steel web of the bottom tee-section is assumed to resist any shear force. Furthermore, the combined direct and shear stress in the steel section is accounted for through the reduction of the bending strength using the von Mises' yielding criterion. This method is generally considered to be conservative, except at low M/V ratios.

Although Wong and Redwood (1982) recognize that the inclusion of the

compression in the lower part of the concrete slab at the LMS together with the compression near the top of the concrete slab at the HMS of the web opening has allowed the concrete slab to carry certain shear force, the shear resistance at the HMS of the perforated section is limited to that of the resistance of the steel web as there is only a limited number of shear connectors placed within the opening length. The steel flanges are assumed not to resist any secondary bending moment. The method is conservative when compared against test data, and Wong suggested that the conservatism comes mainly from the fact that i) the compressive stress in the concrete slab at the LMS of the web opening resulted from the slippage between the concrete slab and the steel decking is ignored, and ii) the resistance of the shear connectors obtained from the push-out tests was lower than the actual values for shear connectors embedded in concrete slabs. In fact, the ignorance of the shear resistance of the concrete slab may also contribute to the conservatism.

In order to calculate the shear resistance of a concrete slab, Lawson (1987) has suggested that the permissible shear stress in BS 8110 may be used, taking into account the steel areas of the profiled steel decking, and also the mesh reinforcement in resisting shear in the zone of the web opening. However, this should not exceed $0.25\sqrt{f_{cu}}$ as suggested by Donahey and Darwin (1986). The shear resistance of the concrete slab is then obtained by considering an effective width against local punching shear of 1.5 times the slab depth on either side of the beam. Then the remaining shear force may be distributed to the top and the bottom steel tee-sections. In order to simplify the calculation, Lawson has suggested that the shear force resisted by the steel web in the bottom tee-section may be conservatively ignored.

In 1990, Cho has proposed a theory utilizing the truss analogy in an attempt to clarify the fundamental behavior of the concrete slab and the shear connectors in

resisting vertical shear. In this theory, the shear connectors above the opening region are considered as vertical tension-carrying members, while inclined struts in the concrete are considered to act between the bearing zones near the heads of the shear connectors and at their bases at the steel flange as shown in Figure 2.16. The action between the concrete slab and the shear connectors is thus identified and the shear resistance is found to be related directly to the location of the shear connectors. Refer to the reference for details. This method predicts explicitly the shear resistance of the concrete slab for different shear connector configurations and the result may be used in the usual way to determine the load capacities of composite beams with web openings. Comparison of the results of this theory with available test data from the literature has proven that the model is generally satisfactory despite some conservatism is inherent, particularly for beams with solid slabs. Although the truss analogy does not give any more accurate results than other available models based on pre-determined shear distribution, it does provide a more satisfactory conceptual model for the determination of the shear resistance contributed by the concrete slab.

With the help of the truss analogy, it is confirmed that for those shear connectors placed either within the opening length or sufficiently close to the ends of the web opening, they should be incorporated in the assessment of the shear resistance of the perforated section in composite beams. It is also showed that the shear resistance of the concrete slab is largely dependent on the tensile capacity of the shear connectors near the HMS of the web opening.

2.4 Summary of Experimental Test Data

Seventy tests data of steel beams with web openings and forty-four tests data of composite beams with web openings have been collected. A database is established for easy interpretation of the data. All test beams were loaded with point

loads to failure and the failure locations were constrained to the regions of the web openings. Load-deflection curves were re-presented based on the information provided by various researchers wherever available.

2.4.1 Test data for steel beams with web openings

All of the seventy test beams collected from nine test series were carried out before 1980 and the details of each individual test series are presented in Table 2.1. The span/depth ratios of the test beams range from 4.6 to 13.2. The measured yield strengths of the components of the steel beams vary greatly from 222 N/mm^2 to 461 N/mm^2. Only one test was performed on each beam and the moment to shear (M/V) ratios fall in the range of zero to 10.54 m. Out of the seventy test beams, fifty-three of them have rectangular web openings and the rest have either circular or extended rectangular web openings. Twenty-nine of the rectangular web openings are reinforced with either one sided or two sided reinforcement plates on the webs above and below the openings. Overall, only six of the web openings are placed eccentrically to the mid-depth of the beams. The opening height ranges from 13% to 67% of the depth of the steel beams, and the aspect ratios for rectangular web openings range from 1.0 to 3.0. A detailed re-presentation of the tests is presented in Appendix A.

2.4.2 Test data for composite beams with web openings

Six test series are reported by various researchers in both North America and the UK, and the details of each individual test series are tabulated in Table 2.2. In some of the test series two individual tests were carried on the same beam and there are forty-four tests in total. Thirty-three tests utilize profiled steel decking placed transversely to the steel beams while three tests utilize profile steel decking placed parallel to the steel beams. Solid slabs are used in the remaining eight tests. The

span/depth ratios of the beams range from 7.3 to 15.9 while the strength of the steel beams and the cylinder strength of the concrete slabs range from 238 to 386 N/mm^2 and 17.1 to 48.2 N/mm^2, respectively. Rectangular web openings were tested in all test series and only two of the openings were reinforced with reinforcement plates, which were placed on one side of the web openings. The smallest size of the web opening has a depth equal to 37% of the depth of the steel beam while the largest one is equal to 71% depth of the steel beam. The aspect ratios of the openings range from 1.0 to 3.0 and the moment to shear ratio ranges from 0 to 13.66 m. A detailed representation of the tests is presented in Appendix A.

2.5 Selected Current Design Methods

As discussed previously, all strength design methods based on plastic stress analysis may be classified into two categories as follows:

1) Design methods utilizing moment-shear interaction curves on perforated sections
2) Design methods based on interaction of shear force, axial force, and bending moment acting on tee-sections

One design method chosen from each of the category is elaborated in this section so as to illustrate the primary difference between the two approaches.

2.5.1 Design methods utilizing moment-shear interaction curves on perforated sections

This approach involves the calculation of the maximum moment resistance under zero shear force and the maximum shear resistance under zero bending moment at the perforated section. Then the capacity of the perforated section is checked using an interaction expression. Among all design methods following this approach, the one developed by Darwin and Lucas (1990) remains the easiest to apply and is the most comprehensive and accurate. It should be noted that the

method has been adopted in the Steel Design Guide series (Darwin, 1990) of the American Institute of Steel Construction (ASIC). It is also the principal design technique in the Structural Engineering Institute/American Society of Civil Engineers (SEI/ASCE) Standard 23-97 (1997).

This method gives explicit, closed-form formulas to calculate the maximum moment resistance and the maximum shear resistance.

a) Maximum moment resistance under zero shear force

The design expressions for maximum moment resistance of the perforated section, $M_{o,Rd}$ are based on well-established strength procedures. They involve the subtraction of the moment resistance contributed by the removed web element from the original plastic moment resistance of the composite section. Depending on the opening configurations, the expressions may take several different forms. The design expression for the maximum moment resistance, $M_{o,Rd}$, of a steel beams with rectangular web opening is given by:

$$M_{o,Rd} = M_{Rd}\left[\frac{1-\Delta A_s\left(\frac{h_o}{4}\right)}{W_{pl}}\right]$$

in which $\Delta A_s = h_o t_w$ and $M_{Rd} = f_y W_{pl}$, where W_{pl} is the plastic modulus of the un-perforated section.

b) Maximum shear resistance under zero bending moment

The maximum shear resistance of the composite perforated section, $V_{o,Rd}$, is the sum of the shear resistance of the top composite tee-section, $V_{t,Rd}$, and the shear resistance of the bottom steel tee-section, $V_{ab,Rd}$.

$$V_{o,Rd} = V_{t,Rd} + V_{ab,Rd}$$

Both $V_{t,Rd}$ and $V_{ab,Rd}$ can be expressed as ratios of the plastic shear resistance of a steel tee-section, $V_{t,Rd}$, and they are given by:

Bottom steel tee-section: $V_{ab,Rd} = (\frac{\sqrt{6}+\mu}{\eta+\sqrt{3}})V_{T,Rd} \le V_{T,Rd}$

Top composite tee-section: $V_{t,Rd} = (\frac{\sqrt{6}+\mu}{\eta+\sqrt{3}})V_{T,Rd} \le V_{T,Rd}$ or

$$V_{t,Rd} = \frac{\mu}{\eta}V_{T,Rd} \le V_{T,Rd} + 0.11A_{vc}\sqrt{f'_c} \quad \text{if } \frac{\mu}{\eta} \ge 1$$

where $V_{T,Rd} = \frac{f_y t_w d_1}{\sqrt{3}}$, $\eta = \frac{a_o}{t_f + d_1}$ is the aspect ratio of the tee-section, $A_{vc} = 3d_e b_e$ is the effective concrete shear area, and μ is given by:

$$\mu = \frac{N_{H,Rd}d_H - N_{L,Rd}d_L}{V_{T,Rd}(t_f + d_1)}$$

where $N_{H,Rd}$ and $N_{L,Rd}$ are the compressive forces in the concrete slab at the HMS and the LMS of the perforated section, respectively, and d_H and d_L are their respective distances to the top of the steel section.

c) Moment-shear interaction curve

After $M_{o,Rd}$ and $V_{o,Rd}$ are determined, the following cubic interaction curve is used to check the structural adequacy of the perforated section:

$$(\frac{M_{Sd}}{M_{o,Rd}})^3 + (\frac{V_{Sd}}{V_{o,Rd}})^3 \le 1$$

where M_{Sd} and V_{Sd} are the applied moment and shear at the centerline of the perforated section, respectively.

2.5.2 Design methods based on interaction of shear force, axial force, and bending moment acting on tee-sections

This approach involves the direct calculation of the moment and the shear resistances of a perforated section. Moreover, it is required to evaluate the plastic moment resistances of individual top and bottom tee-sections at both the HMS and the LMS of the web opening under co-existing axial force and shear force. The

prime example of this approach appears in the joint publication by the Construction Industry Research and Information Association (CIRIA) and the Steel Construction Institute (SCI) (Lawson, 1987). This design method involves the checking of the flexural, the shear, and the Vierendeel failures of the perforated section as follows:

a) Flexural failure of the perforated section

The applied moment at the LMS of the web opening is used to determine the axial forces in the bottom steel tee-section, the top steel tee-section, and the concrete slab. The axial resistances of the steel tee-sections and the concrete slab are also evaluated accordingly. Then the flexural failure of the perforated section is checked by comparing the axial resistances of the bottom steel tee-section and the concrete slab with the applied axial forces. It should be noted that iterations are required to establish equilibrium in order to determine the applied axial forces.

b) Shear failure of the perforated section

The maximum shear resistance of the perforated section, $V_{o,Rd}$, is the sum of the shear resistances of the top steel tee-section, the bottom steel tee-section, and the concrete slab given as follows:

$$V_{o,Rd} = V_{at,Rd} + V_{ab,Rd} + V_{c,Rd}$$

The shear resistances of both the top and the bottom steel tee-sections, $V_{at,Rd}$ and $V_{ab,Rd}$, are based on the following formula:

$$V_{at,Rd} \text{ or } V_{ab,Rd} = 0.9t_w(d_1 + t_f)(0.6f_y)$$

while the shear resistance of the concrete slab, $V_{c,Rd}$, is given by:

$$V_{c,Rd} = 3h_t h_c v_c \leq 0.25\sqrt{f_{cu}}$$

where v_c and f_{cu} are the shear strength and the compressive cube strength of the concrete, respectively. The shear failure is then checked using the following equation:

$$V_{o,Rd} \geq V_{Sd}$$

c) Vierendeel failure of the perforated section

The Vierendeel resistance of a composite perforated section, $M_{v,Rd}$, consists of the plastic moment resistances, $M_{T,VN,Rd}$, of the individual top and bottom steel tee-sections at both the HMS and the LMS of the web opening under co-existing axial force and shear force, and also the moment resistance, $M_{vc,Rd}$, derived from the composite action of the top steel tee-section and the concrete slab. Thus,

$$M_{v,Rd} = 4M_{T,VN,Rd} + M_{vc,Rd}$$

The moment resistance of a steel tee-section under shear force alone, $M_{T,V,Rd}$, is determined on the basis of the first moment of area of the section using a reduced web thickness, t_e, which is given by:

$$t_e = t_w \sqrt{1 - (\frac{V_{T,Sd}}{V_{T,Rd}})^2}$$

where $V_{T,Sd}$ is the applied shear force on a tee-section and $V_{T,Rd}$ is the shear resistance of the section. The effect of axial force on the moment resistance is then considered through the linear equation:

$$M_{T,VN,Rd} = M_{T,V,Rd}(1 - \frac{N_{T,Sd}}{N_{T,Rd}})$$

where $N_{T,Sd}$ is the applied axial force on a tee-section and $N_{T,Rd}$ is the axial resistance of the section. Referring to Figure 2.17, the Vierendeel moment resistance of the concrete slab is given by:

$$M_{vc,Rd} = (h_t + x_{cr})N_{2,Sd} + h_c N_{1,Sd}[1 - \frac{N_{1,Sd} + N_{2,Sd}}{N_{c,Rd}}]$$

where $N_{1,Sd}$ and $N_{2,Sd}$ are the forces transferred by the shear connectors from the support to the LMS of the web opening and over the web opening, respectively. $N_{c,Rd}$.

is the axial resistance of the concrete slab. The Vierendeel resistance of the perforated section is finally compared to the applied Vierendeel moment across the web opening:

$$M_{v,Rd} \geq V_{Sd} a_o$$

Complete design procedures of the two methods can be found in the literature.

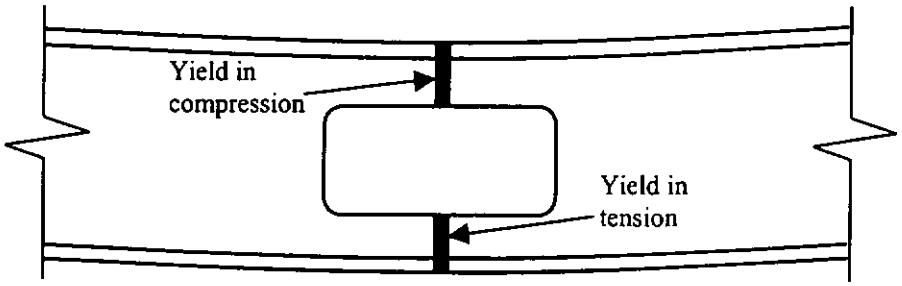

Figure 2.1 Flexure failure of perforated section

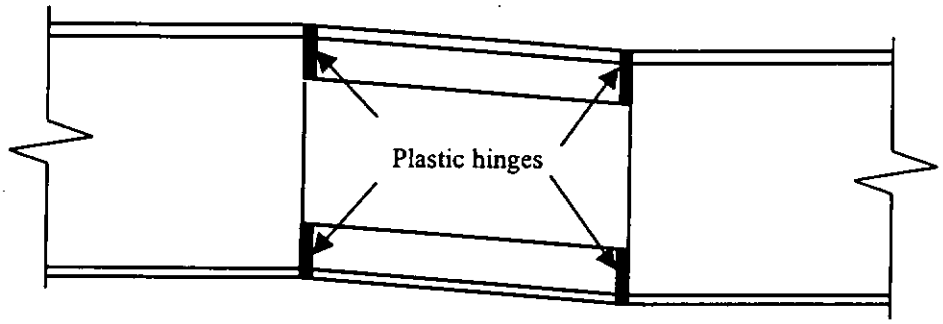

Figure 2.2 Vierendeel mechanism

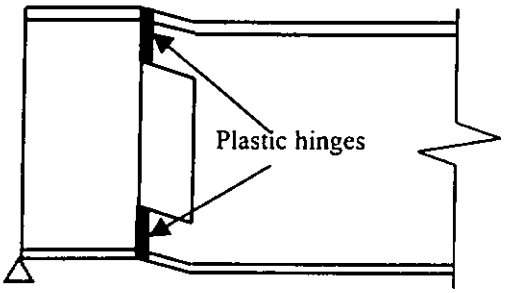

Figure 2.3 Shear failure of perforated section

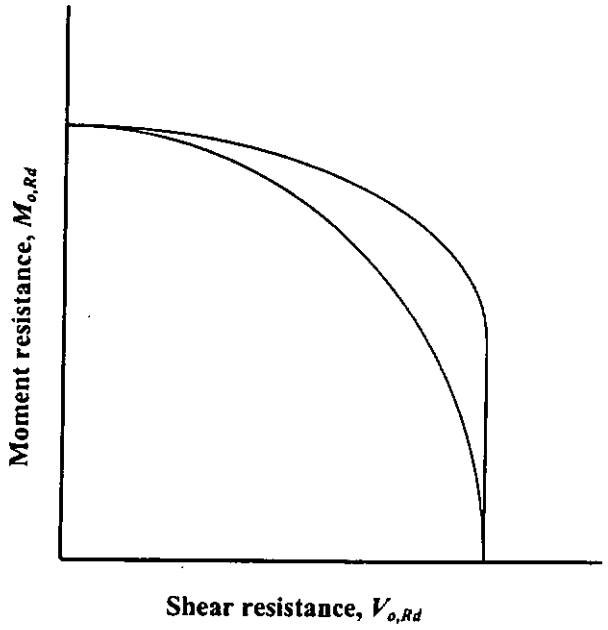

Figure 2.4 Moment-shear interaction curves suggested by various design methods for steel beams with web openings

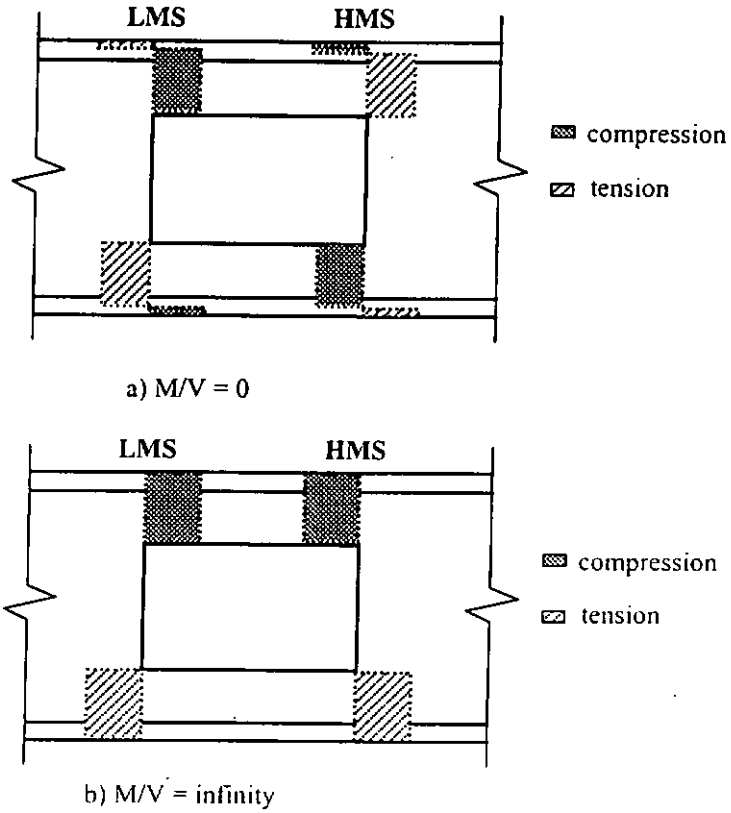

Figure 2.5 Stress distributions at plastic hinges when M/V ratio is equal to zero or infinity

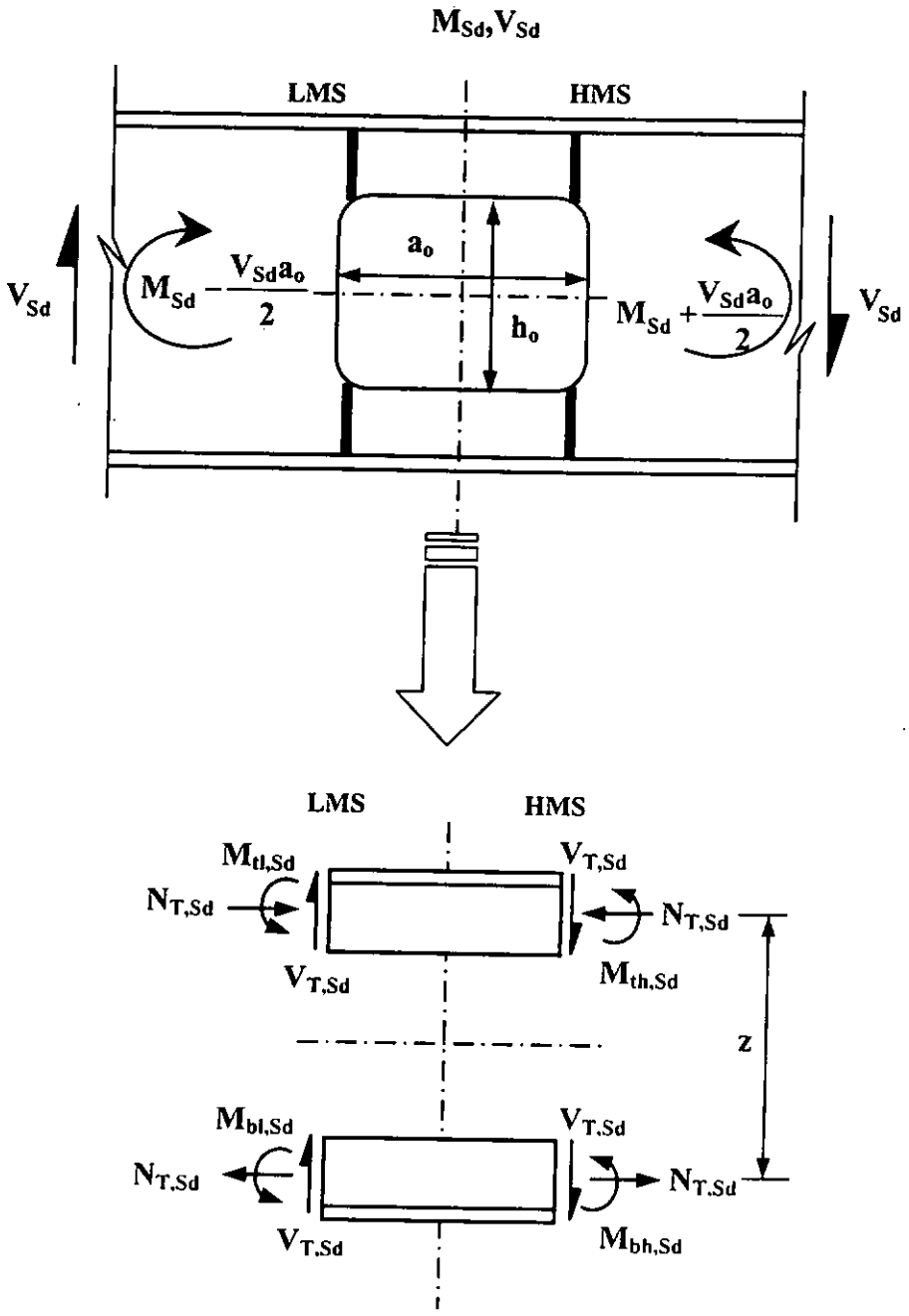

Figure 2.6 Global and local actions at perforated section of a steel beam

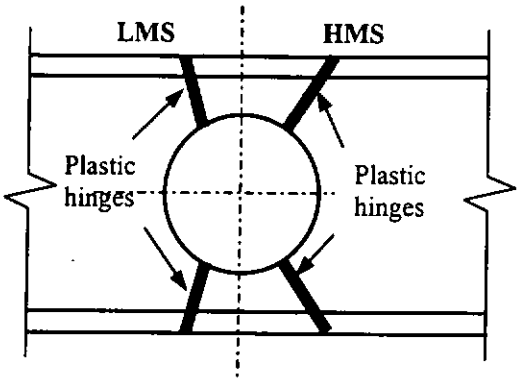

Figure 2.7 Vierendeel mechanism around circular web opening

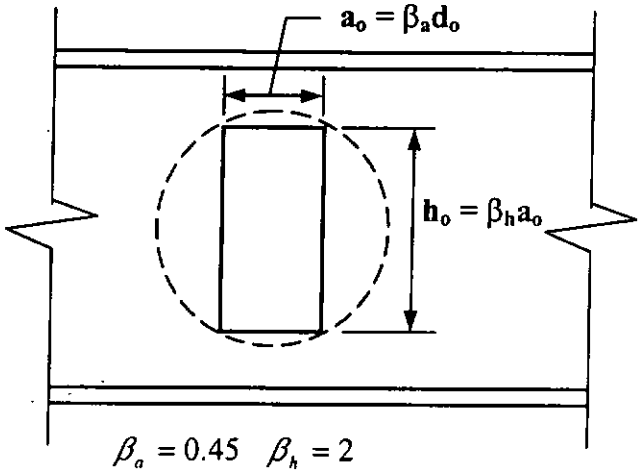

Figure 2.8 Equivalent rectangular web opening

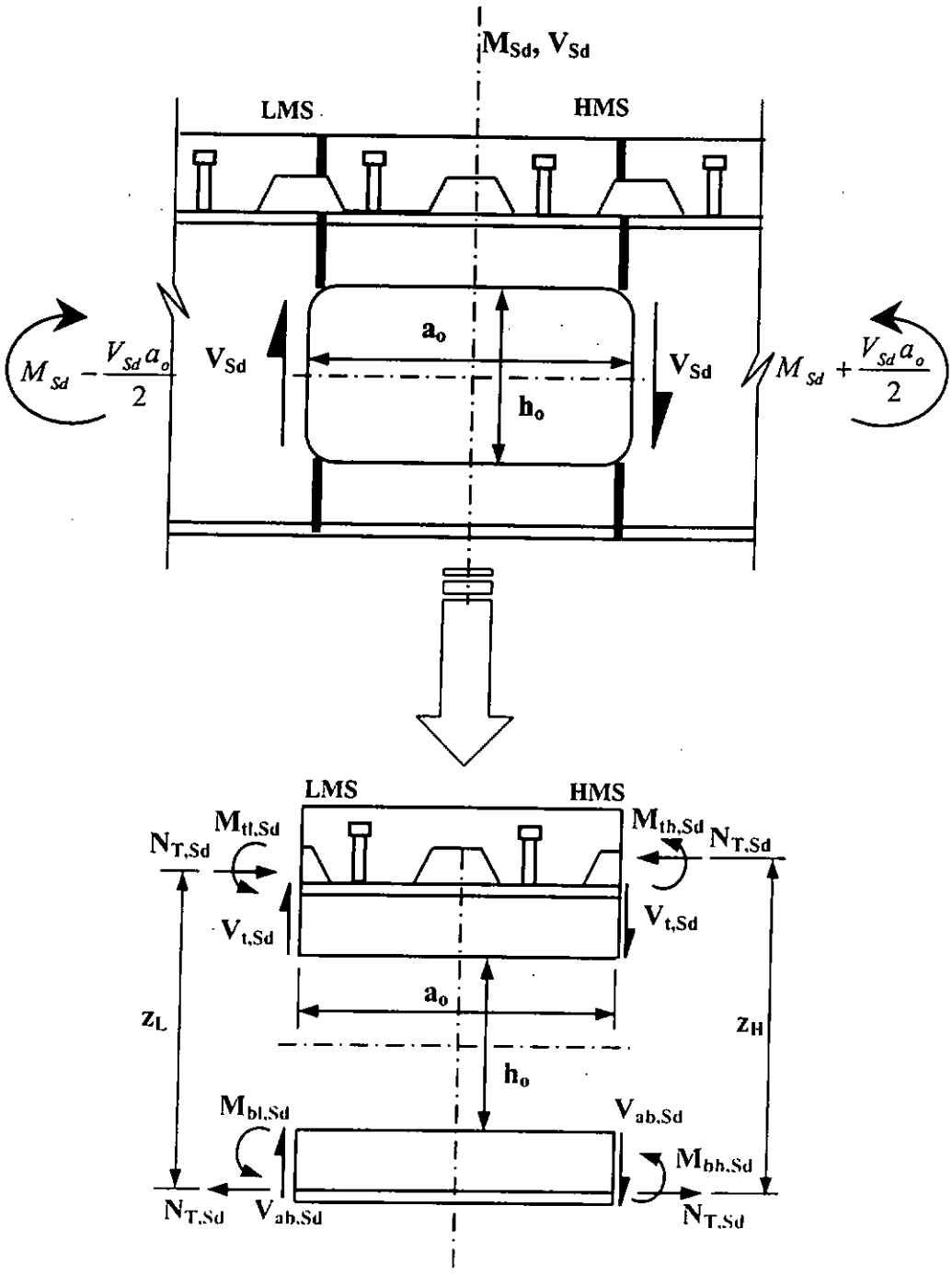

Figure 2.9 Global and local actions at perforated section of a composite beam

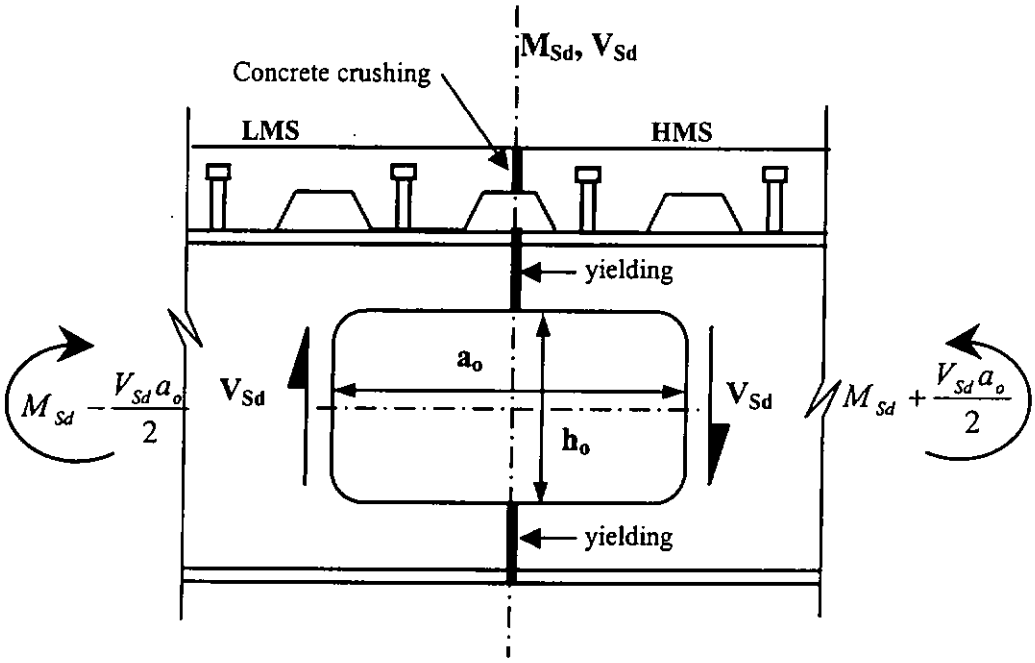

Figure 2.10 Flexural failure in composite beam with web opening

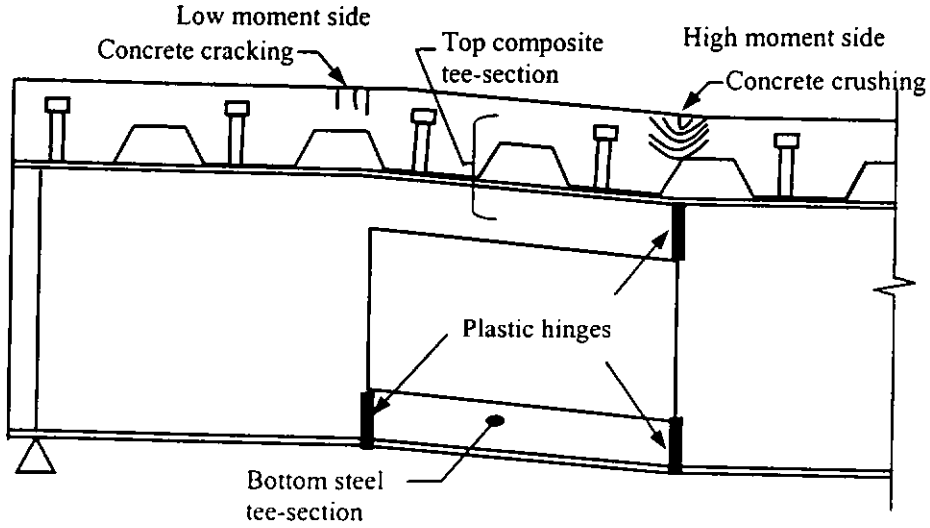

Figure 2.11 "Three-hinge" Vierendeel mechanism in composite beam with web opening

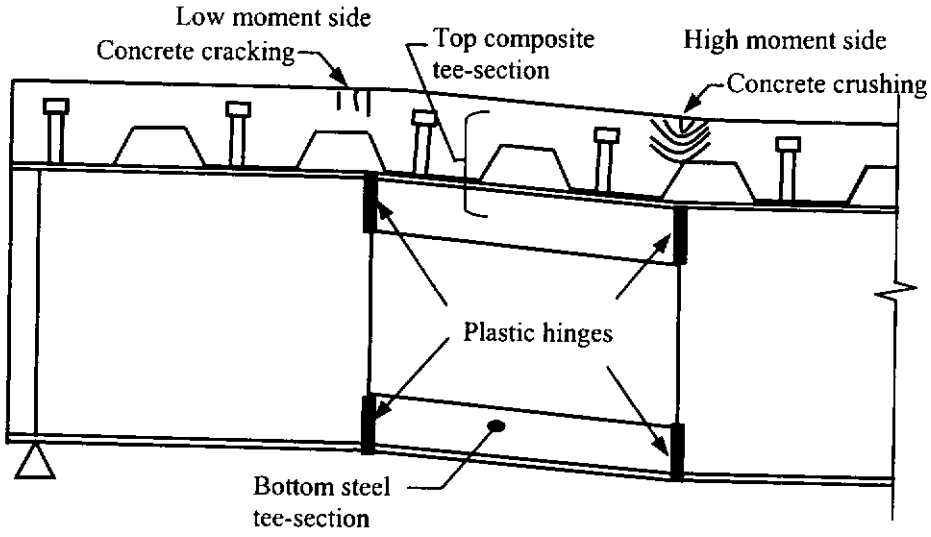

Figure 2.12 "Four-hinge" Vierendeel mechanism in composite beam with web opening

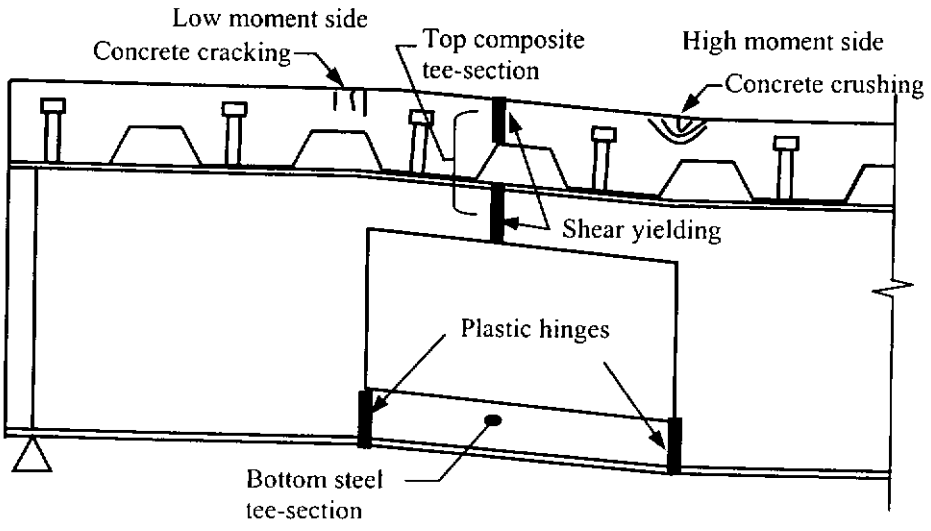

Figure 2.13 Vierendeel "shear-failure" mechanism in composite beam with web opening

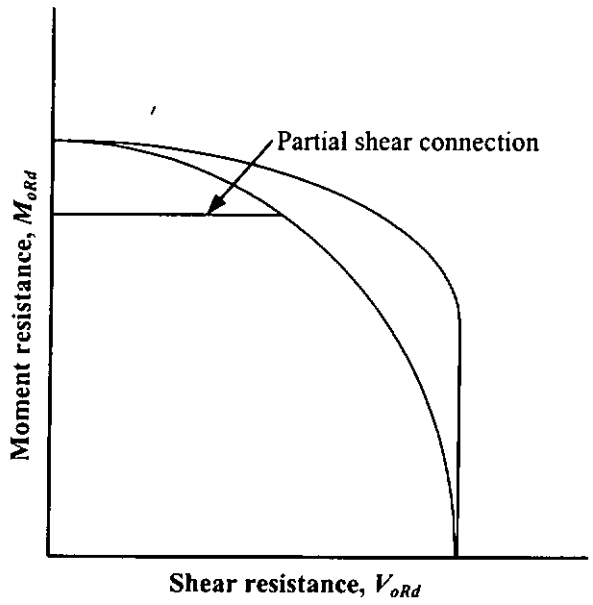

Figure 2.14 Moment-shear interaction curves suggested by various design methods for composite beam with web openings

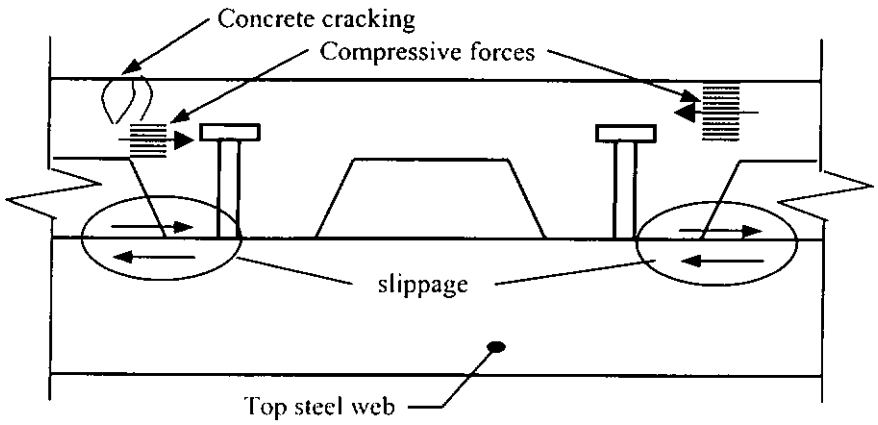

Figure 2.15 Compressive forces in concrete slab

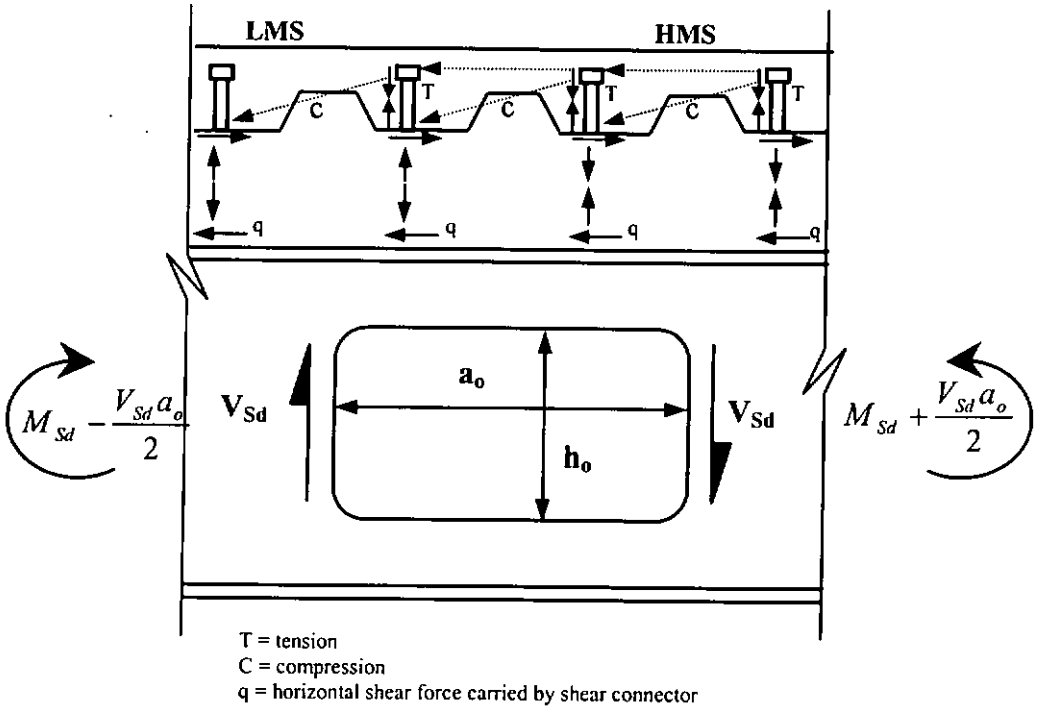

Figure 2.16 Truss idealization for the slab at the composite perforated section

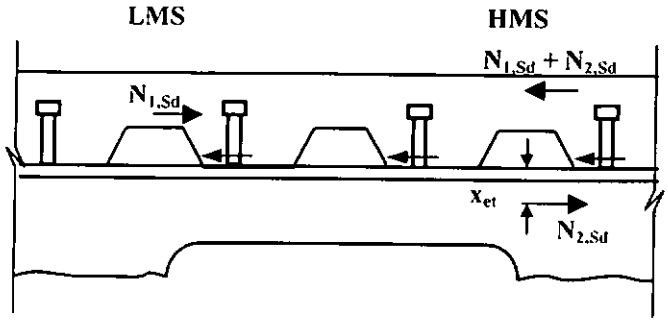

Figure 2.17 Equilibrium of forces in top composite perforated section

Table 2.1 Summary of test data for steel beams with web openings

References	Year of publication	Number of beams (tests)	Number of reinforced openings	Number of unreinforced openings	Number of eccentric openings	Ratio of opening dimension (h_o/h)	Ratio of opening dimension (a_o/h_o)	Span/depth ratio	M/V ratio at opening center (m)	Measured yield strength (N/mm^2)
Bower	1968	4(4)	0	4R	0	0.45-0.46	1.01-1.26	7.53-7.59	0-1.02	232.4-303.4
Clawson and Darwin	1980	1(1)	0	1R	0	0.6	1.99	10	0.91	309.5-358.5
Congdon and Redwood	1970	13(13)	2R-one sided 10R-two sided	1R	0	0.49-0.63	1.49-1.99	6.3-9.1	0.43-1.14	274.4-395.1
Cooper and Snell	1972	3(3)	1R-one sided 2R-two sided	0	0	0.49	1.50	9.9-13.2	1.02-1.52	222.0-258.6
Cooper, Snell, and Knostman	1977	5(5)	3R-one sided 1R-two sided	1R	3R-upward 2R-downward	0.37-0.49	1.5-2.0	6.6-6.9	0.76	244.9-317.6
Redwood and McCutcheon	1968	19(19)	0	4C(S), 5C(M) 2R(S), 5R(M) 3ER(S)	0	0.27-0.56	1.0-1.5	7.3-12.3	0.46-1.22, ∞	277.2-399.9
Lupien and Redwood	1978	6(6)	6R-one sided	0	0	0.43-0.65	2.48-2.50	6.0-8.4	0.6-1.24,∞	262.9-461.9
Redwood, Baranda, and Daly	1978	11(15)	0	10R, 5C	1R-downward	0.13-0.62	1.0-3.0	4.6-10.5	0.54-10.54	297.2-409.5
Shrivastava and Redwood	1977	4(4)	4R-two sided	0	0	0.29-0.67	1.58-3.00	5.5-6.9	0.6-0.8	255.1-402.0
Total	-	**66(70)**	**12R-one sided 17R-two sided**	**19R(S), 5R(M) 9C(S), 5C(M) 3ER(S)**	**3R-upward 3R-downward**	**0.13-0.67**	**1.00-3.00**	**4.6-13.2**	**0-10.54**	**222.0-461.9**

Notes:
- h_o = height of web opening
- h = height of steel beam
- a_o = length of web opening
- R = rectangular web opening
- C = circular web opening
- ER = extended rectangular web opening
- S = Single
- M = Multiple

Table 2.2 Summary of test data for composite beams with rectangular web openings

References	Year of publication	No. of beams (tests)	Reinforced rectangular opening	Eccentric opening	Ratio of opening dimension (h_o/h)	Ratio of opening dimension (a_o/h_o)	Profiled steel decking (no. of tests)	Span/ depth ratio	M/V ratio at opening center (m)	Measured yield strength (N/mm^2)	Measured cylinder strength of concrete (N/mm^2)
Cho and Redwood	1992	6(9)	0	0	0.68-0.69	1.70-1.72	7T, 2S	7.9-8.6	0-1.0	301-347	22.2-24.9
Clawson and Darwin	1980	6(6)	0	0	0.57-0.60	2.0	6S	8.2-15.9	0.9-9.9	238-335	27.7-48.2
Donahey & Darwin	1986	9(15)	0	1-downward	0.58-0.71	1.0-2.92	12T, 3L	7.3-10.3	0-13.66	264-357	27.1-36.4
Lawson, Chung, and Price	1992	3(5)	2-one sided	1-downward	0.37-0.65	1.0-3.0	5T	15.3	0.3-4.1	309-349	25.6-33.9
Redwood and Poumbouras	1983	2(3)	0	0	0.59-0.60	2.0	3T	7.6	0.95	301-325	17.1-18.8
Redwood and Redwood	1982	5(6)	0	1-upward	0.59	2.0	6T	7.8-12.0	0.95-6.0	276-386	19.5-29.6
Total	-	**31(44)**	**2-one sided**	**1-upward 2-downward**	**0.37-0.71**	**1.0-3.0**	**33T, 3L, 8S**	**7.3-15.9**	**0-13.66**	**238-386**	**17.1-48.2**

Notes:
- h_o = height of web opening
- h = height of steel beam
- a_o = length of web opening
- T = decking placed transversely to steel beam
- L = decking placed parallel to steel beam
- S = solid slab

CHAPTER 3

V-N-M INTERACTION FOR STEEL TEE-SECTION AND PERFORATED SECTION ANALYSIS

3.1 General

As depicted in Figure 3.1, global actions acting at the perforated section of a beam may be resolved into local axial force (tension and compression), shear force, and bending moment, all of which acting simultaneously on the cross-sections at both ends of the top and the bottom tee-sections. Thus, it is important to evaluate the plastic moment resistances of tee-sections under the effect of co-existing axial and shear forces in order to assess the Vierendeel resistance of a perforated section. Section 3.2 presents the basic resistances of a tee-section against axial force, shear force, and bending moment separately. Simple design formulas based on plastic stress blocks are derived in Section 3.3 to allow for the effect of axial force on the moment resistance of a tee-section. Also, the beneficial effect of axial force on the plastic moment resistance will also be discussed. Interaction curves generated by the proposed design formulas are compared with those obtained by other empirical formulas. Effect of shear on both the axial and the moment resistances of a tee-section is considered in Section 3.4. In order to propose a design method for the analysis of beams with web openings, the design formulas for tee-sections are extended for analysis of perforated section in Section 3.5. Finally, results predicted by the proposed design method are compared with those obtained from finite element analyses and experimental investigations.

3.2 Basic Resistances of a Tee-section

While application of heavy concentrated load directly over a perforated section of a beam should be avoided whenever possible, uniformly distributed load is often

encountered in beams with web openings such that variation of applied shear force occurs along the length of the web opening and so does the applied bending moment. For simplicity, values of applied shear force and bending moment at the centerline of the web opening are often used for analysis and design, leading to a constant value of applied shear at both ends of the tee-sections above and below the web opening. The applied shear force is assumed to be distributed equally between the top and the bottom tee-sections in the case of a concentric web opening. The axial force, arising from global bending action, is assumed to act at the elastic or plastic centroid of the tee-sections. Local bending moment is caused by the transfer of shear force between the two ends of the tee-sections above and below the web opening. This is shown in Figure 3.1, where "HMS" and "LMS" denote the high moment side and the low moment side of the perforated section, respectively.

3.2.1 Axial resistance

A tee-section is shown in Figure 3.2a. The greatest possible axial force, or the squash load, that the cross-section can resist occurs when it is fully yielded in tension or compression, so that

$$N_{T,Rd} = N_{f,Rd} + N_{w,Rd}$$

where $N_{f,Rd} = t_f b_f f_{yf}$ and $N_{w,Rd} = t_w d_1 f_{yw}$

In case of pure axial force, it must be distributed over the tee-section in such a way that no moment is created, as shown in Figure 3.2b. In other words, the axial force resultant is considered as being applied at a specific point on the tee-section creating no moment. This point is referred to as the plastic axial centroid (PC), and its distance from the top of the flange is designated as y_{pc}, which is given as follows:

$$y_{pc} = \frac{N_{f,Rd}(\frac{t_f}{2}) + N_{w,Rd}(\frac{d_1}{2} + t_f)}{N_{T,Rd}}$$

The plastic axial centroid will coincide with the elastic centroid of the tee-section if the yield strengths of both the flange and the web are the same.

3.2.2 Shear resistance

According to Eurocode 3, the ultimate shear resistance, $V_{T,Rd}$, of the tee-section is limited to that contributed by the full depth of the web and a portion of the flange, and is given by:

$$V_{T,Rd} = V_{f,Rd} + V_{w,Rd} \qquad \text{Equation 3.1}$$

where $V_{f,Rd} = A_{vf}(\frac{f_{yf}}{\sqrt{3}})$ and $V_{w,Rd} = A_{vw}(\frac{f_{yw}}{\sqrt{3}})$ are the shear resistances of the flange and the web, respectively. The flange shear area, A_{vf}, and the web shear area, A_{vw}, defined in Eurocode 3 are $t_w t_f$ and $d_1 t_w$, respectively, if fillets are ignored. However, in a parallel study by Chung, Liu, and Ko (to be published), a finite element analysis of the perforated section has consistently shown that the flange shear area is actually larger than assumed conventionally. In the perforated section analysis, the upper and lower tee-sections are separated and the shear stress distribution becomes independent from each other. The centroid of shallow tee-sections, where maximum shear flow is found, may lie near to or even inside the flanges. The shear resistance of the flange in a tee-section at failure is found to be larger than that of a symmetrical I-section. The equivalent shear area contributed by the flange as obtained from the calibration against the finite element results is

$$A_{vf} = (0.75t_f + t_w)t_f$$

This flange shear area is used instead of that given by Eurocode 3 throughout this text.

3.2.3 Plastic moment resistance

The strength distribution of a tee-section under pure bending is depicted in

Figure 3.2c, where "C" denotes compressive strength and "T" denotes tensile strength. Under the principle of equilibrium, the compressive force is equal to the tensile force and the dividing line is referred as the plastic neutral axis (PNA). The distance of the PNA from the top of the flange is denoted as y_{po}, which is given as follows:

$$y_{po} = \frac{N_{w,Rd} + N_{f,Rd}}{2N_{f,Rd}}(t_f)$$

The plastic moment resistance of the tee-section, $M_{T,Rd}$, may be evaluated by taking moment of the forces about the PNA as follows:

$$M_{T,Rd} = N_{f,Rd}[\frac{y_{po}^{\ 2} + (t_f - y_{po})^2}{2t_f}] + N_{w,Rd}[\frac{d_1}{2} + t_f - y_{po}] \qquad \text{Equation 3.2}$$

Obviously, the plastic moment resistance can also be taken about any axis and still gives the same answer. Thus, if moment is to be taken about the axis passing through the PC, the expression of the plastic moment resistance is given by:

$$M_{T,Rd} = N_{f,Rd}[(\frac{y_{po}}{t_f})(y_{pc} - \frac{y_{po}}{2}) + \frac{(t_f - y_{po})}{t_f}(\frac{t_f + y_{po}}{2} - y_{pc})] + N_{w,Rd}[\frac{d_1}{2} + t_f - y_{pc}]$$

if the PNA is located within the flange. For hot rolled I beams with web openings of practical sizes, the PNA of the tee-sections always falls within the flanges, and thus only this case is considered.

3.3 Axial-Moment Interaction for Tee-section

It is well known that the presence of axial force to a symmetrical I-section will have a penalty on its plastic moment resistance. However, for an asymmetrical tee-section, the effect of axial force on its plastic moment resistance is not so clear as it is related to the distribution of the axial force, the sense of axial force (tension or compression) and bending moment (sagging or hogging), and also the relative

position of the axis to the centroid about which the moment is calculated. In the following sections, formulas for the interaction of axial force and bending moment are derived for a tee-section. Both axial force and bending moment are considered to be positive if they produce compressive stress in the flange of a tee-section. The sign convention is shown in Figure 3.3 for both the top and the bottom tee-sections above and below a web opening and is used primarily for the plotting of the interaction curves discussed in the next section.

3.3.1 Complete axial-moment interaction curve

A complete interaction curve for a tee-section subjects to different combinations of bending moment and axial force is plotted in Figure 3.5. The curve is explicitly calculated for a tee-section of the dimensions shown in Figure 3.4. Each quadrant of the interaction curve contains an axial-moment interaction curve for each individual tee cross-section at different locations of a perforated section and is identified in Figure 3.5. For example, the interaction curve in Quadrant I is identified as the top tee-section at the HMS of the perforated section. The axial force ratio, n, and the bending moment ratio, m, are defined as follows:

$$n = \frac{N_{T,Sd}}{N_{T,Rd}} \quad \text{and} \quad m = \frac{M_{T,Sd}}{M_{T,Rd}}$$

where $N_{T,Sd}$ and $M_{T,Sd}$ are the axial force and the bending moment applied to a tee-section, respectively. $N_{T,Rd}$ and $M_{T,Rd}$ are the axial and the moment resistances of the tee-section, respectively. The stress blocks for $n = 1$ and $m = 1$ are drawn next to the perforated section for the four tee cross-sections in Figure 3.5. In general, there is also a co-existing shear force acting at the centerline of the web opening, V_{Sd}, and the shear force ratio, v, is defined as follows:

$$v = \frac{V_{T,Sd}}{V_{T,Rd}}$$

is also zero where $V_{T,Sd}$ and $V_{T,Rd}$ are the applied shear force and the shear resistance of the tee-section, respectively. In subsequent discussions, references are frequently made to the interaction curve shown in Figure 3.5, where V_{Sd} and hence v are equal to zero.

3.3.2 Top Tee-section at LMS: Quadrant IV

The top tee-section at the LMS of the perforated section is subjected to a compressive axial force and a negative bending moment causing tensile stress in the flange. The situation is depicted by the axial-moment interaction curve in Quadrant IV in Figure 3.5. Consider a tee-section shown in Figure 3.6a, the moment resistance of the tee-section under zero axial force is equal to its nominal value $M_{T,Rd}$, which corresponds to a point with the coordinates (0,-1) in the interaction curve. The corresponding stress block is shown in Figure 3.6b. If a compressive axial force, $N_{T,Sd}$, is applied to the tee-section, a stress block of depth α_f, is thus introduced as:

$$\alpha_f = \frac{N_{T,Sd}}{2b_f f_{yf}}$$

as shown in Figure 3.6c. The PNA will shift towards the top of the flange to maintain equilibrium, and the result is a shifted PNA as shown in Figure 3.6d.

The application of the axial force, which is deviated from the plastic axial centroid, causes a reduction in the plastic moment resistance and the modified moment resistance, $M_{T,N,Rd}$, is given by:

$$M_{T,N,Rd} = M_{T,Rd} - N_{f,Sd}\beta_f$$

where β_f is the distance from the center of the axial stress block to the plastic axial centroid. The modified moment resistance, $M_{T,N,Rd}$, can also be found by using Equation 3.2 based on the shifted PNA. It can be seen that a positive axial force acting in addition to a negative bending moment always causes a reduction in the

moment resistance of the tee-section since the PNA shifts towards the top of the flange. The reduction of the moment resistance due to the presence of axial force is also shown by the interaction curve in Quadrant IV in Figure 3.5, where it can be seen that the moment resistance reaches zero when the axial force ratio is unity. The reduction in the plastic moment resistance is gradual and slow.

3.3.3 Top Tee-section at HMS: Quadrant I

The top tee-section at the HMS of the perforated section is subjected to a positive axial force and a positive bending moment, and the axial-moment interaction is represented by the Quadrant I of the interaction curve in Figure 3.5. A brief look at the interaction curve reveals that the effect of a positive axial force on a tee-section subjected to a positive bending moment is somehow complicated as the plastic moment resistance may be either increased or decreased, depending on the magnitude of the axial force.

Consider a tee-section under a positive pure bending moment, the stress block is shown in Figure 3.7b. This corresponds to a point with the coordinates of (0,1) on the interaction curve. Suppose a positive axial force of magnitude $N_{T,Sd}$ is applied to the tee-section and assuming that $N_{T,Sd}$ is less than or equal to the residual compressive strength of the flange, $2(t_f-y_{po})b_f f_{yf}$, then the shifted PNA of the section will remain within the flange as shown in Figure 3.7d. The axial stress block can be assumed to act at a distance of β_f (see Figure 3.7c) from the plastic axial centroid as discussed previously, but this time it induces a beneficial effect to the plastic moment resistance as it is acting in the same sense of the moment resistance. Thus, the modified moment resistance, $M_{T,N,Rd}$, is larger than the nominal value of $M_{T,Rd}$ and is given by:

$$M_{T,N,Rd} = M_{T,Rd} + N_{T,Sd}\beta_f$$

where $N_{f,Sd} = 2\alpha_f t_f f_{yf}$ and $\beta_f = y_{pc} - (y_{po} + \frac{\alpha_f}{2})$. However, if the axial force continues to increase and exceeds the residual compressive strength of the flange, the axial stress block will extend to the web, which shifts the PNA down to the web as illustrated in Figures 3.8c and 3.8d. The axial force resisted by the web is then given by:

$$N_{w,Sd} = N_{T,Sd} - N_{f,Sd}$$

where $N_{f,Sd} = 2(t_f - y_{po})b_f f_{yf}$. The depth of the axial stress block in the web is given by:

$$\alpha_w = \frac{N_{w,Sd}}{2t_w f_{yw}}$$

The modified plastic moment resistance is given by:

$$M_{T,N,Rd} = M_{T,Rd} + N_{f,Sd}\beta_f + N_{w,Sd}\beta_w$$

where β_w is the distance between the center of the axial stress block in the web and the plastic axial centroid. The plastic moment resistance will increase with an increase in the axial force until a peak value is reached on the interaction curve in Quadrant I in Figure 3.5. The peak value represents a specific stress block at which the applied axial force is large enough to shift the PNA below the plastic axial centroid, and hence further increase in the axial force will have a non-beneficial effect on the moment resistance. The non-beneficial effect may be significant and cause large reduction in the moment resistance as shown by the steep slope of the interaction curve when the axial force ratio is large. The moment resistance will drop to zero eventually when the axial force is large enough to yield the entire section in compression.

3.3.4 Bottom Tee-section at LMS: Quadrant II

The bottom tee-section at the LMS of the perforated section is subjected to a negative (tensile) axial force and a positive bending moment. The axial-moment interaction is a duplication of that shown in Figures 3.6b to 3.6d, only with the stress blocks and the forces being reversed in direction. The interaction curve for this tee-section is shown in Quadrant II of the complete axial-moment interaction curve in Figure 3.4. The moment resistance of the section always decreases gradually from its full value to zero when axial force is applied. The procedures for the calculation of the modified moment resistance are identical to those given in Section 3.3.2, hence they are not repeated here.

3.3.5 Bottom Tee-section at HMS: Quadrant III

Quadrant III of the complete axial-moment interaction curve in Figure 3.5 shows the axial-moment interaction curve for the bottom tee-section at the HMS of the perforated section. The section is subjected to both a negative (tensile) axial force and a negative bending moment causing tensile stress in the flange. With the increase of axial force, the moment resistance of the section is first increased gradually until a peak value is reached. Then it decreases sharply to zero when the axial force ratio reaches unity. This resembles the case of the top tee-section at the HMS of the perforated section, as shown in Figures 3.7 and 3.8 with the stress blocks and the forces being applied in the opposite direction. As a result, the procedures for the calculation of the modified moment resistance are identical to those given in Section 3.3.3, and hence they are not repeated here.

It is interesting to note that for steel beams with concentric rectangular web openings, the axial-moment interaction curves for the bottom tee-sections can be obtained by rotating those of the top tee-section about the origin by 180°. Thus, the

modified moment resistances for the bottom tee-section at the LMS and the HMS under the effect of axial force are the same as those for the top tee-section at the LMS and the HMS of the perforated section, respectively, and they need not be calculated again. Similar axial-moment interaction curves are also commonly used in designing reinforced concrete and composite columns. However, the sections are often symmetrical in practice and thus, the interaction curves are very similar to the interaction curve shown in Quadrant I of Figure 3.5, as concrete cannot resist significant tensile force. In the presence of small axial force, the moment resistance of a short column may be larger than its moment resistance under zero axial force because the compressive force prevents concrete cracking, and thus makes the cross-section of the short column more effective in resisting moments (Kong and Evans, 1987; MacGinley and Choo, 1990).

3.3.6 Comparisons of proposed interaction curves with other empirical formulas

Current design methods often use empirical interaction formulas with different power indices to allow for axial-moment interaction. Linear and quadratic interaction curves are drawn together with the proposed interaction curves in Figure 3.9 for the tee-section shown in Figure 3.4. As indicated by the interaction curves obtained by the proposed design formulas, there is always reduction in the plastic moment resistance of the tee-sections at the LMS of the perforated section whenever an axial force is presented. However, the movement of the PNA from the flange to the web in the tee-section at the HMS of the perforated section renders an increase in the plastic moment resistances; the increase can be as high as 20%.

As shown in the figure, the linear interaction curves are always below the curves derived from the proposed design formulas, indicating that the linear interaction curves are always conservative. However, the conservatism may

considered to be acceptable.

Although the quadratic interaction curves have less conservatism than the linear ones, they still ignore any beneficial effect of the axial force on the plastic moment resistance of tee-sections and thus, they fall far below the curves derived from the proposed design formulas in both Quadrants I and III. Meanwhile, the quadratic interaction curves are un-conservative as shown in both Quadrants II and IV.

So far, no shear force is present yet, and the effect of shear force is considered in the next section.

3.4 Shear-Axial-Moment Interaction for Tee-section

The interaction of shear force, axial force, and bending moment is very complicated, and a general analytical solution for sections of arbitrary shapes has not been obtained so far. Instead, it is more practical to obtain general and simple design formulas for typical sections based on rational assumptions. To this end, the effect of shear force on a tee-section is allowed for through reduced bending strengths of both the web and the flange based on von Mises' yielding criterion. For a given tee-section, the shear resistance is given by Equation 3.1. The applied shear force is assumed to be distributed between the flange and the web according to their respective shear resistances:

$$V_{w,Sd} = V_{T,Sd}\left(\frac{V_{w,Rd}}{V_{T,Rd}}\right) \quad \text{and} \quad V_{f,Sd} = V_{T,Sd}\left(\frac{V_{f,Rd}}{V_{T,Rd}}\right)$$

where $V_{f,Sd}$ and $V_{w,Sd}$ are the shear forces resisted by the shear areas of the web and the flange, respectively. $V_{T,Sd}$ is the applied shear force on the tee-section. Other terms have been defined previously. The effect of shear stress is then taken into account by reducing the bending strengths of the flange and the web through von

Mises' yielding criterion as follows:

$$f_{vw} = \sqrt{f_y^{\,2} - 3\tau_w^{\,2}} \qquad \text{and} \qquad f_{vf1} = \sqrt{f_y^{\,2} - 3\tau_f^{\,2}}$$

where $\tau_w = \frac{V_{w,Sd}}{A_{vw}}$ and $\tau_f = \frac{V_{f,Sd}}{A_{vf}}$. f_{vw} and f_{vf1} are the reduced bending strengths of the shear areas of the web and the flange, respectively. Since the bending strength of a significant area of the flange is not reduced, an average reduced bending strength, f_{vf}, is calculated for the whole flange as follows:

$$f_{vf} = \frac{f_y(A_f - A_{vf}) + f_{vf1}A_{vf}}{A_f}$$

where A_f is the total area of the flange and A_{vf} is the shear area of the flange. After the reduced bending strengths of both the web and the flange are found, the basic axial and the moment resistances of a tee-section are then calculated. Finally, the effect of axial force on the plastic moment resistance can be considered using the proposed design formulas given in Section 3.3. The axial-moment interaction curves for the tee-section shown in Figure 3.5 are plotted in Figure 3.10 for various shear force ratios.

The shear force ratio, the axial force ratio and the moment ratio have been defined previously. It is shown in Figure 3.10 that when the shear force is small, the reduction in the plastic moment resistance is insignificant. However, when the shear force ratio is large, say 0.8, the plastic moment resistance under zero axial force reaches only about 70% of its nominal value. In general, the reduction in the axial resistance is less severe for all values of shear force ratio as the shear area of the flange is only a fraction of the total area of the flange. All interaction curves are found to be of similar shapes.

3.5 Perforated Section Analysis

The proposed design formulas presented in Sections 3.3 and 3.4 are primarily for analysis of interaction of co-existing axial force, shear force, and bending moment occurring on individual tee-sections. By considering the four critical cross-sections at the top and the bottom tee sections in a perforated section under specific combination of global shear force and moment, the proposed design formulas are integrated to predict the resistances of the perforated section against shear and flexural failures, and also Vierendeel mechanism. Comparisons are also made with results obtained from finite element analyses and experimental investigations.

3.5.1 Extension of proposed design formulas for perforated sections

The global and the local actions in a perforated section are illustrated in Figure 3.1. Based on equilibrium of the HMS of the perforated section, the global moment at the centerline of the web opening may be expressed as:

$$M_{Sd} = zN_{T,Sd} + M_{th,Sd} + M_{bh,Sd} - \frac{V_{Sd}a_o}{2}$$

where z is the lever arm between the axial forces acting on the top and the bottom tee-sections. Similarly, considering the equilibrium of the LMS of the perforated section, the global moment may also be expressed as:

$$M_{Sd} = zN_{T,Sd} - M_{tl,Sd} - M_{bl,Sd} + \frac{V_{Sd}a_o}{2}$$

For concentric web opening, the local bending moments $M_{bh,Sd}$ and $M_{bl,Sd}$ are the same as $M_{th,Sd}$ and $M_{tl,Sd}$, respectively. By summing the above two equations and eliminating $M_{bh,Sd}$ and $M_{bl,Sd}$ in terms of $M_{th,Sd}$ and $M_{tl,Sd}$, the moment becomes:

$$M_{Sd} = zN_{T,Sd} + M_{th,Sd} - M_{tl,Sd}$$

For any given global bending moment, the axial force acting on the top and the bottom tee-sections may be found after manipulation on the above equation as

follows:

$$N_{T,Sd} = \frac{M_{Sd} - (M_{th,Sd} - M_{tl,Sd})}{z} \quad \text{Equation 3.3}$$

The axial force is used to obtain the modified moment resistances of the top tee-sections through the proposed design formulas presented in Sections 3.3 and 3.4. Vierendeel failure is then checked by considering the equilibrium of the top tee-section as follows:

$$M_{th,Sd} + M_{tl,Sd} = V_{T,Sd} a_o \quad \text{Equation 3.4}$$

where $V_{T,Sd} = \frac{V_{Sd}}{2}$. Since the axial force calculated using Equation 3.3 also depends on the magnitudes of the moment resistances of the top tee-sections, an iteration process is required until both Equations 3.3 and 3.4 are satisfied. A detailed design procedure for steel beams with web openings is presented in Chapter 6.

3.5.2 Finite element analysis results

A finite element model was set up by Liu, Chung, and Ko (2001) to investigate the global moment-shear $(M\text{-}V)_o$ interaction at the perforated sections of four universal steel beams. The beam sizes used are:

- Series I: UB457x152x52 and UB457x152x82,
- Series II: UB610x229x101 and UB610x229x140

All beams are of grade S275 and have yield strengths of 275 N/mm^2. The two series are chosen to cover a range of steel beams used in practice. Two different section sizes in each series are used for the illustration of the effect of flange thickness on the shear resistance of the perforated section. Rectangular web openings with an aspect ratio of two, and square web openings are investigated. The openings have a height equal to either 50% or 75% depth of the beam. Refer to the reference paper for details of the modeling. The $(M\text{-}V)_o$ interaction curves based on finite

element results have been plotted in Figures 3.11a to 3.11d for each beam section using resistances of the perforated sections with respective opening shapes and sizes. In the figures, the shear force ratio, v, and the moment ratio, m, are defined as:

$$v = \frac{V_{Sd}}{V_{o,Rd}}, \qquad m = \frac{M_{Sd}}{M_{o,Rd}}$$

where V_{Sd} and M_{Sd} are the global applied shear force and the applied bending moment at the centerline of the web opening, respectively. $V_{o,Rd}$ and $M_{o,Rd}$ are the shear and the moment resistances of the perforated section, respectively.

A comparison of Figures 3.11a to 3.11d reveals that all steel beams have interaction curves of similar shapes. This suggests that the use of the new flange shear area has taken into account the effect of the flange thickness on the shear resistances of the perforated sections.

3.5.3 Comparisons of the proposed design method with finite element analysis

The $(M\text{-}V)_o$ interaction curves for the beam sections of Series I from finite element analyses are re-plotted in both Figures 3.12 and 3.13 together with the results predicted by the proposed design method for perforated sections. The results from the current SCI design method for beams with web openings (Lawson, 1987) are also included for comparison. In addition, two different variations for the calculation of shear area, A_{vf}, of the flange are used with the proposed design method to illustrate the relative contribution of shear resistance of the flange. These variations are:

a) Variation I: $A_{vf} = t_w t_f$ from Eurocode 3 and

b) Variation II: $A_{vf} = (0.75t_f + t_w)t_f$ from Chung, Liu, and Ko (to be published) as given in Section 3.2.2.

In general, the current SCI design method always gives the most conservative

results, except for very low moment ratios. Moreover, since the SCI method assumes there is no reduction in the moment resistance when the shear force ratio is less than 0.5 according to BS5950, there is a sudden drop in the moment resistance when the shear force ratio is equal to 0.5. This is shown as a "horizontal slope" on the SCI curve in both Figures 3.12a and 3.13a. However, no sudden drop in those SCI curves in other figures is found since the shear force ratios of the perforated sections do not exceed 0.5.

The different variations of the proposed design method for perforated sections produce results that lie between the SCI curve and the FEM curve. Variation I always predicts shear resistances less than those by Variation II as a smaller shear area in the flange is assumed. The difference is apparent when the shear force ratio is large as shown in Figures 3.12a and 3.13a. However, the difference becomes negligible when the shear force ratio is small as shown in the case of small square openings and rectangular openings as depicted in Figures 3.12b,c,d and 3.13b,c,d. All design methods are generally conservative when compared with the FEM results as the interactions curves are below the FEM curves.

3.5.4 Comparisons with the proposed design method with experimental results

The established database contains twenty-two test data of steel beams with concentric rectangular web openings. However, among the twenty-two test data, only fourteen of them with compact steel sections can be used directly to verify the validity of the proposed design method. The remaining eight test beams failed in modes associated with instability and are thus not included for calibration.

The depths of the selected test beams range from 206mm to 454mm and the span/depth ratios range from 4.6 to 12.5. All of them are loaded with concentrated loads at specific locations along the spans to give particular M/V ratios at the

perforated sections. The sizes of the openings range from 45% to 63% depth of the test beams. During the calibration exercise, measured dimensions and properties of the test beams are used and all material partial safety factors of the proposed design method are set to unity.

In order to illustrate the improvement of the proposed design method over the current SCI design method, both of them are used in the calibration of the test data and the results are compared. Table 3.1 presents the results from calibrations of the selected test data with the two design methods, together with other information for the test beams. Items in the columns of the table are self-explanatory, except that a few of them deserve more attention and they are described below.

There are six sub-columns under the main column of the results predicted by each design method. The first four sub-columns (*m, v, mv, and FM*) indicate whether a test beam fail in flexural, shear, or Vierendeel mode, as predicted by the design method. For example, both design methods indicate that the Test Beam RM11H has a moment utilization ratio (*m*) of 1.0, thus both of the methods predict that the beam fails in a flexural mode (F) as indicated in the "*FM*" sub-column.

A model factor for load capacity is calculated for each test beam for both design methods. The model factor is considered as a measure on the adequacy of a design method against a specific type of failure mode, and it is defined as:

$$\text{Model factor}, \psi = \frac{\text{Capacity measured from tests}}{\text{Predicted capacity}}$$

An improvement is achieved whenever the proposed design method predicts a model factor that is closer to unity than that predicted by the SCI design method. From Table 3.1, it can be seen that the model factors predicted by the proposed design method range from 1.01 to 1.49 with an average of 1.18 for model factors that are above unity, while those predicted by the SCI design method range from 1.03 to

1.59 with an average of 1.29 for model factors that are above unity. It is thus observed that the proposed design method can produce more consistent results and an average improvement of about 8% can be achieved when compared with the SCI design method. The proposed design method is shown to be effective with high structural adequacy and economy.

3.6 Conclusions

Based on the study of the tee-sections and the perforated section of steel beams with rectangular web openings, the following conclusions can be made.

1) Design formulas for the axial resistance, the shear resistance, and the nominal plastic moment resistance of a tee-section are derived in accordance with basic structural design principles and plastic stress blocks. A modified formula is used to evaluate the flange shear area in order to incorporate the effect of the flange thickness. The axial forces arising from global bending action are assumed to act at the plastic axial centroid of the tee-section.

2) Simple design formulas for tee-sections based on plastic stress block are also derived analytically to allow for interaction of axial force and bending moment. It is found that the plastic moment resistance of a tee-section can either be increased or decreased, depending on the signs and the magnitudes of both the moment and the axial force acting on the tee-section. The moment resistances of the tee-sections at the LMS are always reduced while those of the tee-sections at the HMS are increased under low axial force, but both of them are decreased under high axial force. In general, the current empirical interaction formulas with different power indices are conservative as they do not account for the possibility of any increase in the moment resistance of the tee-section in the presence of low axial force

3) The shear effect on the plastic moment resistance of a tee-section is allowed for through the reduction of the bending strengths of both the web and the flange based on von Mises' yielding criterion. A complete axial-moment interaction curve for a tee-section under different values of shear force is also developed. It is found that low shear force often has a smaller effect on the plastic moment resistance of a tee-section than the axial force. However, a high shear force can cause significant reduction in the plastic moment resistance even when the co-existing axial force is low. A high axial force can cause significant reduction in the plastic moment resistance for all values of applied shear force.

4) In order to assess the load capacities of steel beams with web openings, the design formulas for tee-section analysis are extended for analysis of perforated section by considering the equilibrium of forces around the perforated section. The proposed design method is used to generate moment-shear interaction curves for a number of steel beams with rectangular web openings, which are compared with those obtained from finite element analyses. The results indicate that the proposed design method is accurate and conservative.

5) Fourteen test data of steel beams with rectangular web openings are selected from the established database for the calibration of the proposed design method. Model factors predicted by both the proposed design method and the current SCI design method are compared. It is confirmed that the proposed design method is more accurate than the current SCI design method for design of steel beams with rectangular web openings and an average improvement of about 8% on the model factors is achieved.

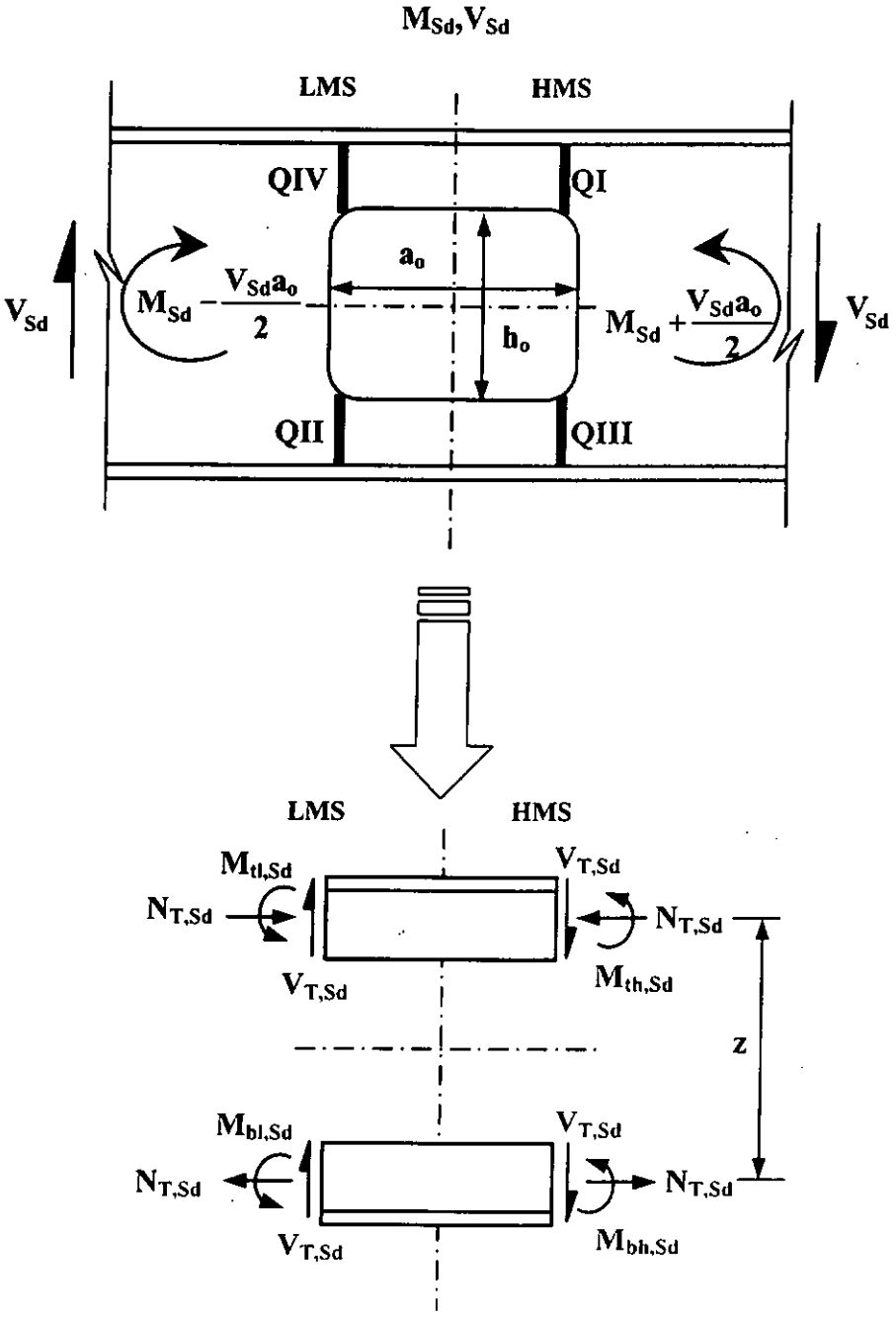

Figure 3.1 Global and local actions at perforated section of a steel beam

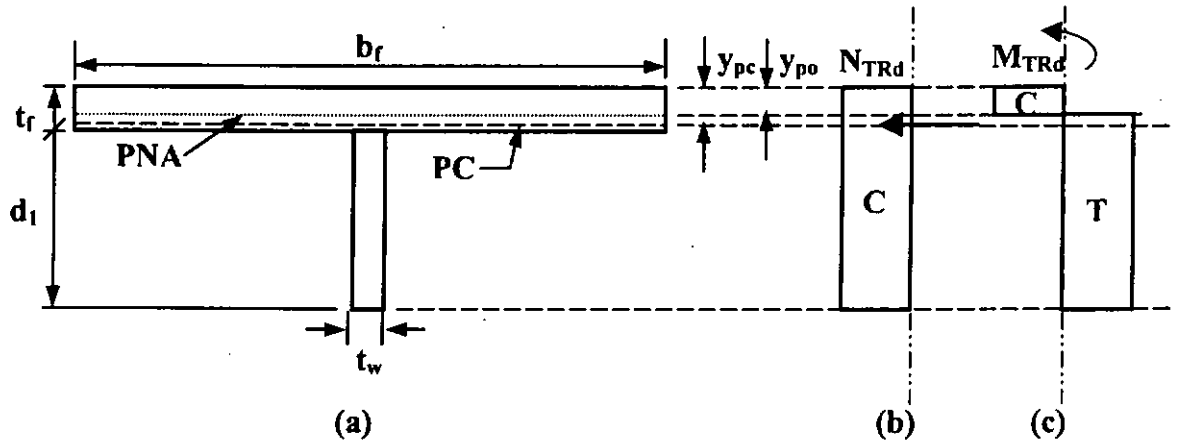

Figure 3.2 Stress blocks of a tee-section under pure axial force and bending moment

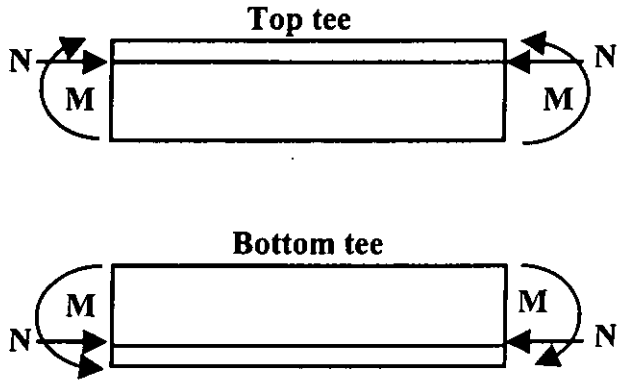

Figure 3.3 Sign convention for positive axial force and bending moment in Tee-section analysis

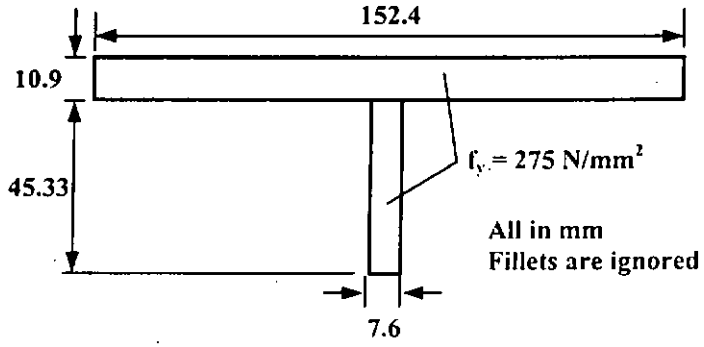

Figure 3.4 Dimensions of the reference tee-section, 56x152x15T S275

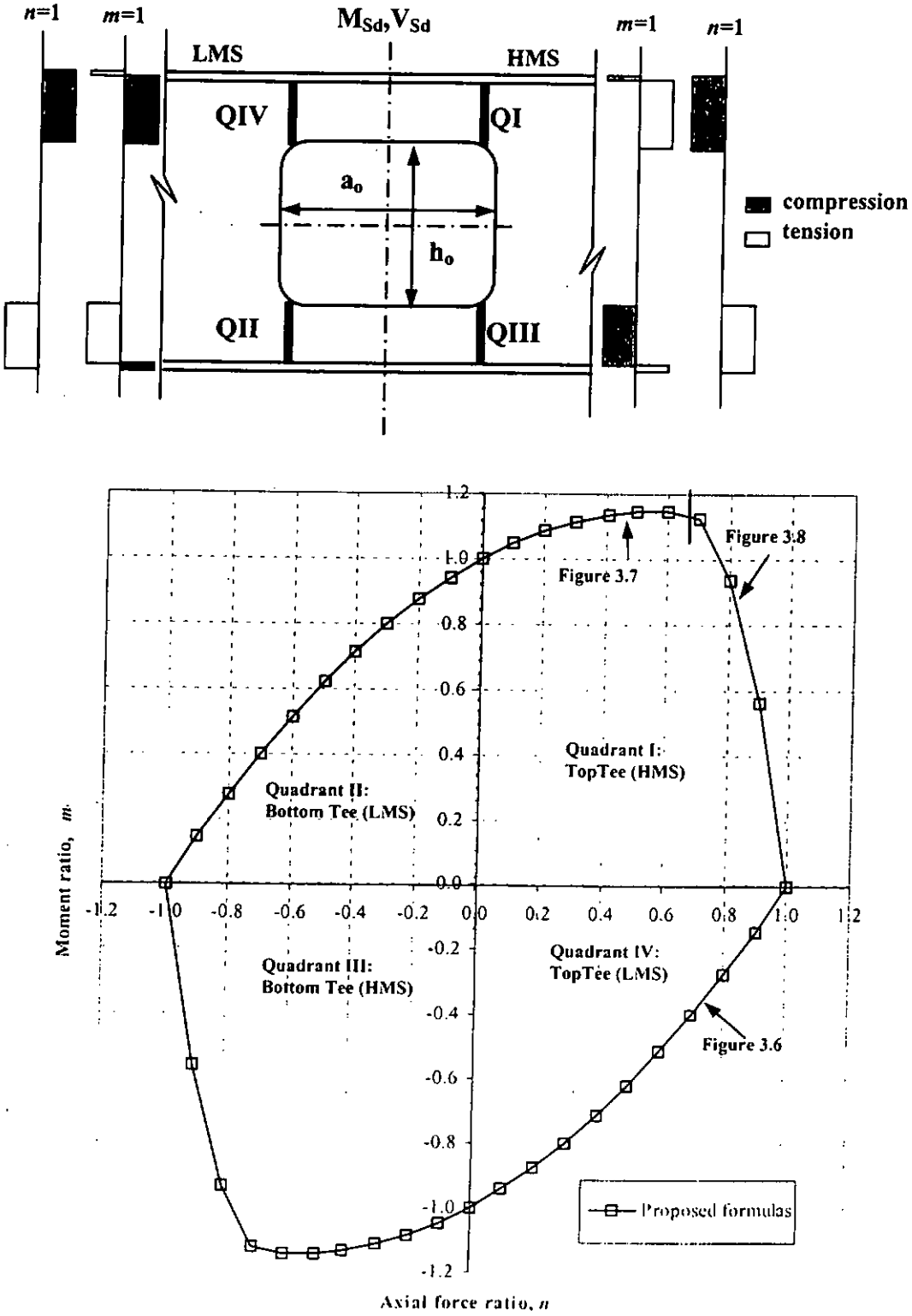

Figure 3.5 Interaction of axial force and bending moment on 56x152x15T S275 for $\nu = 0$

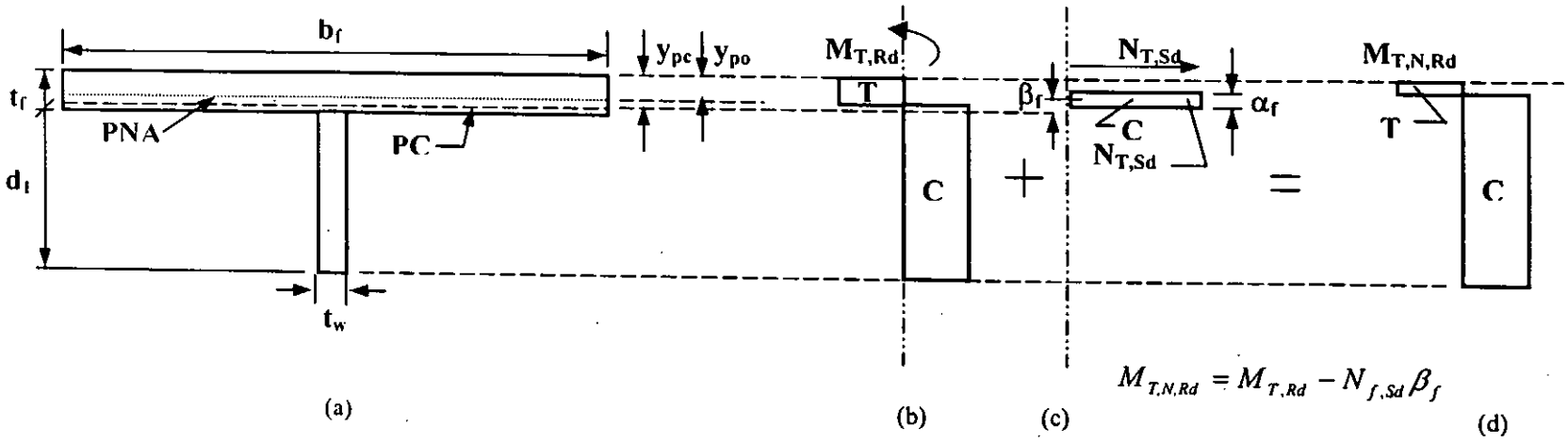

Figure 3.6 Axial-moment interaction of top tee-section at LMS: Quadrant IV

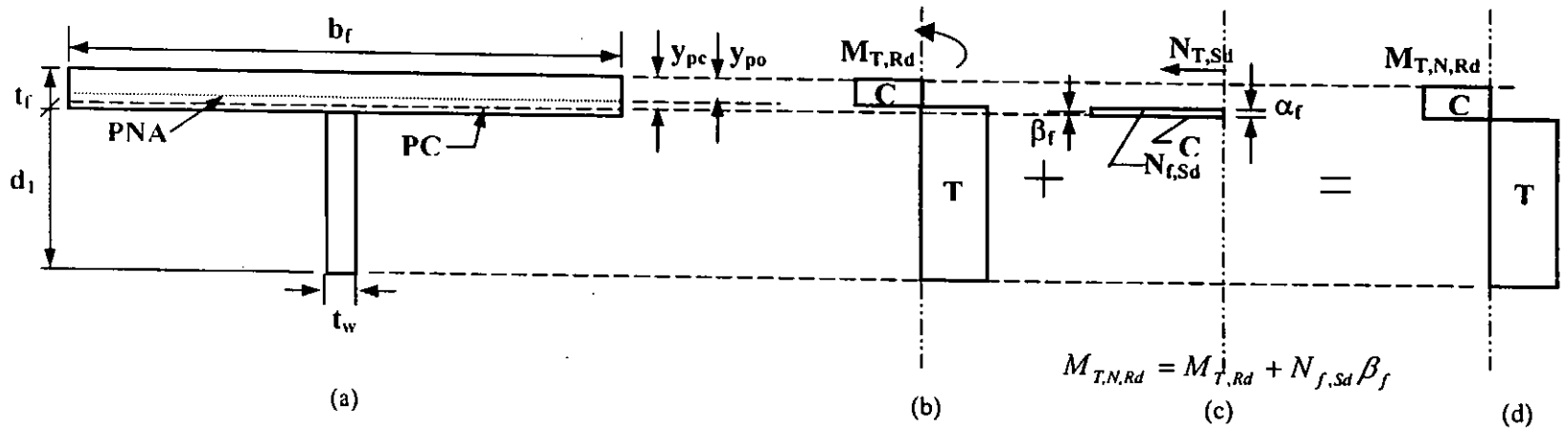

Figure 3.7 Axial-moment interaction of top tee-section at HMS: Quadrant I (PNA in flange)

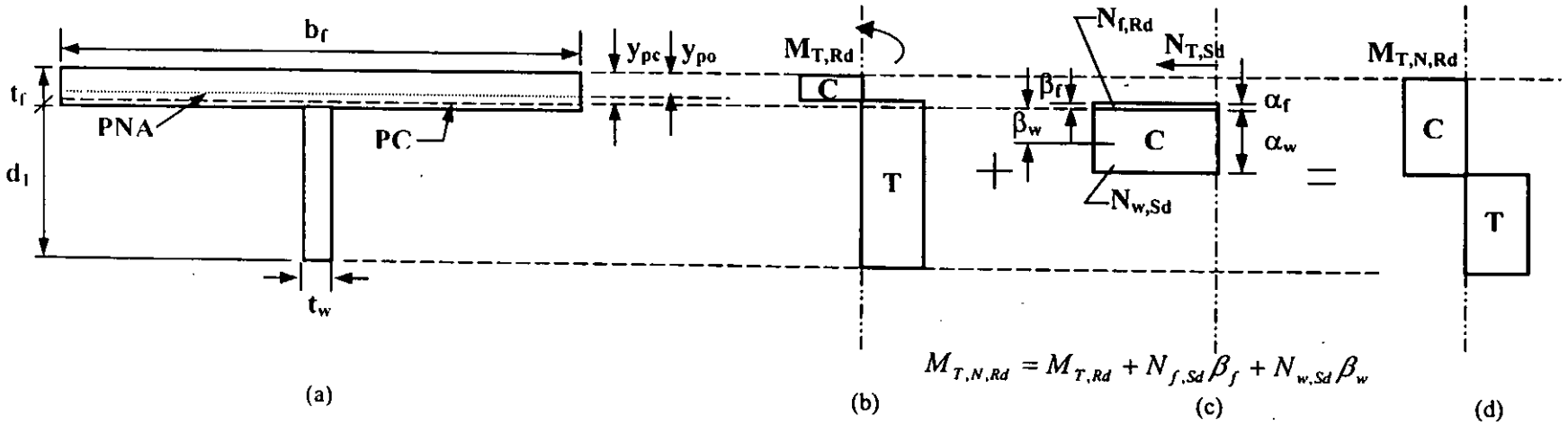

Figure 3.8 Axial-moment interaction of top tee-section at HMS: Quadrant I (PNA in web)

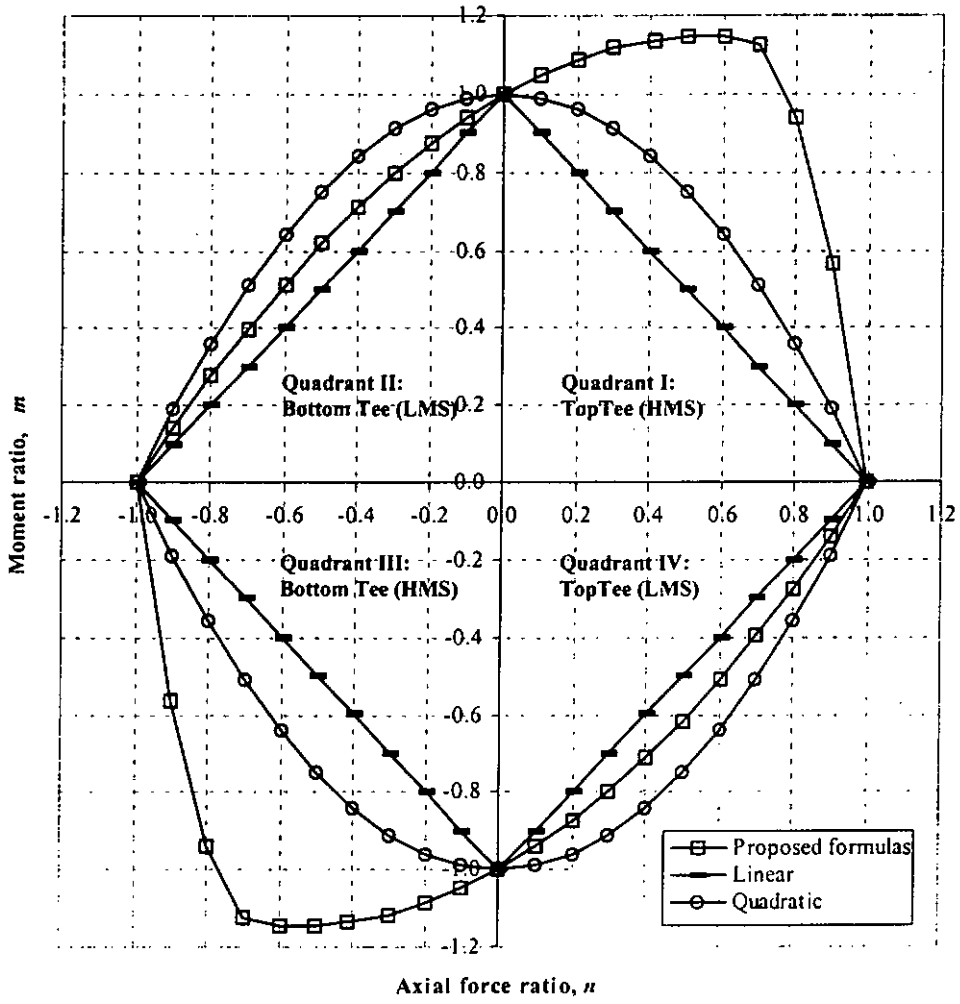

Figure 3.9 Interaction of axial force and bending moment on 56x152x15T S275 for $\nu = 0$

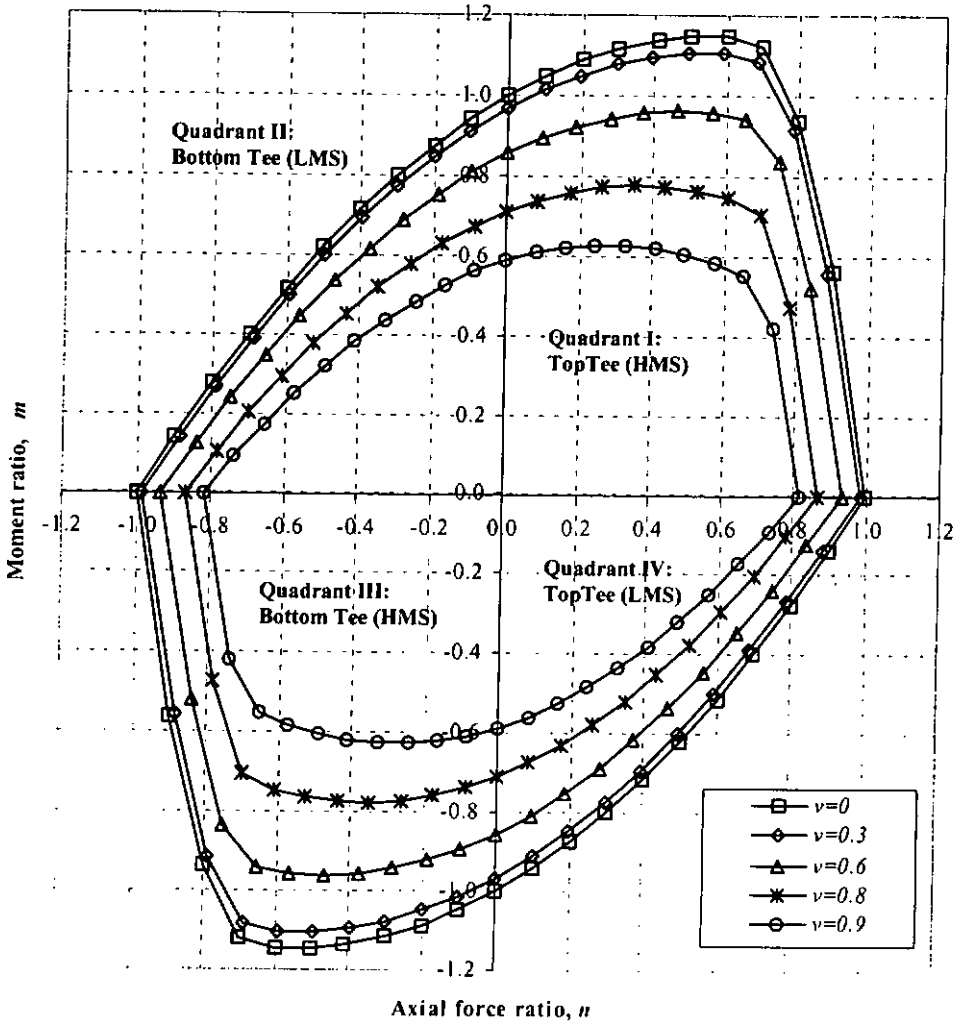

Figure 3.10 Interaction of shear force, axial force, and bending moment on 56x152x15T S275 predicted by proposed design formulas

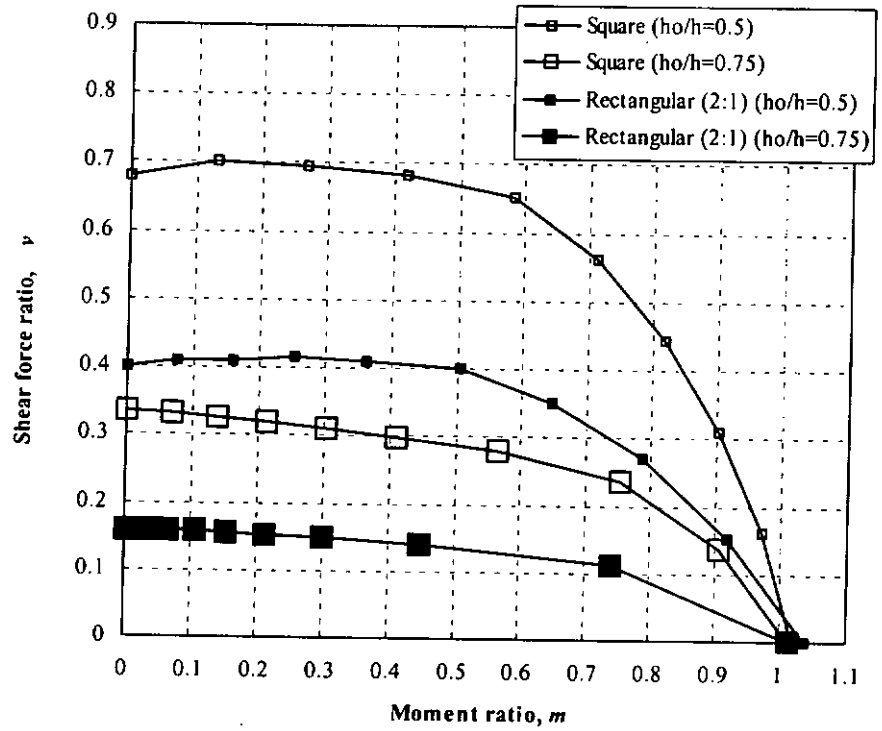

Figure 3.11a Moment-shear interaction curves for UB457x152x52 S275 with square or rectangular web openings

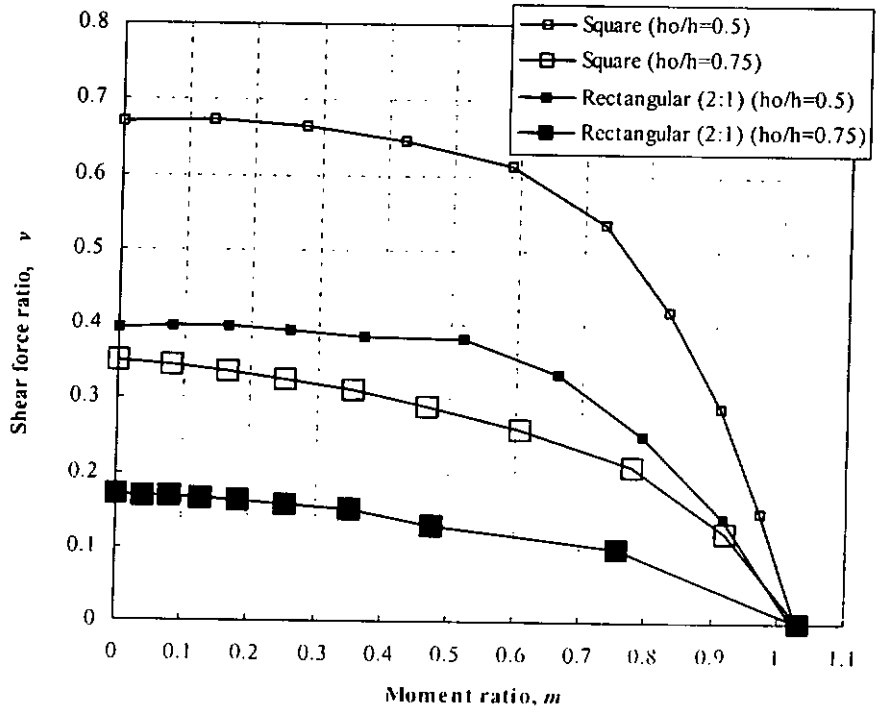

Figure 3.11b Moment-shear interaction curves for UB457x152x82 S275 with square or rectangular web openings

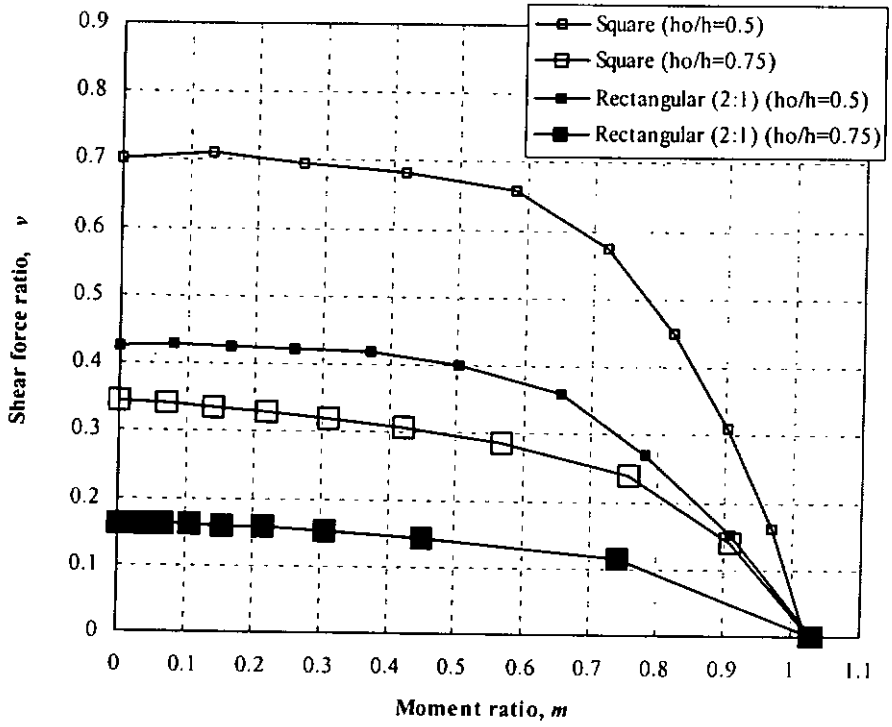

Figure 3.11c Moment-shear interaction curves for UB610x229x101 S275 with square or rectangular web openings

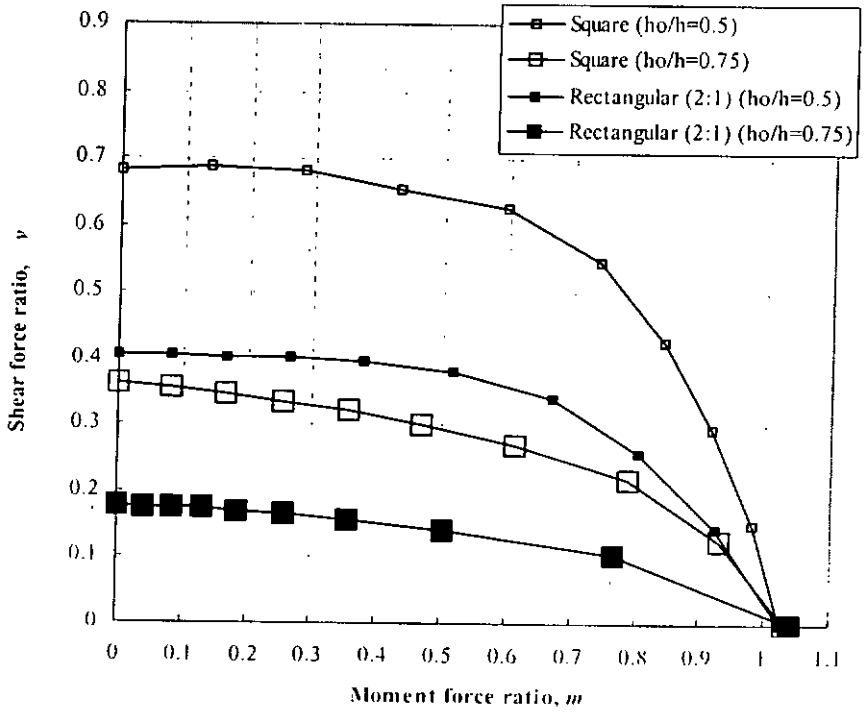

Figure 3.11d Moment-shear interaction curves for UB610x229x140 S275 with square or rectangular web openings

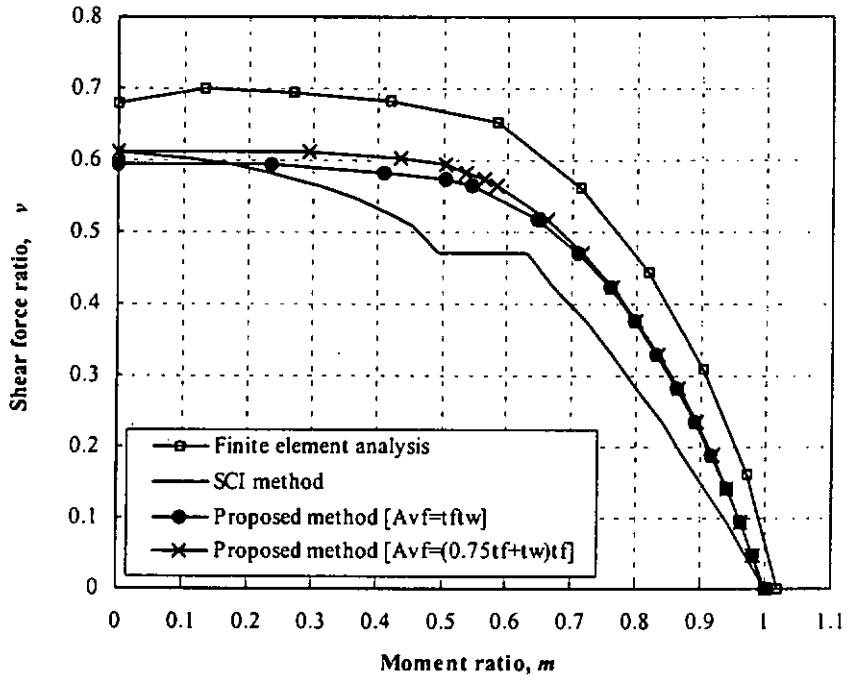

Figure 3.12a Comparisons of moment-shear interaction curves for UB457x152x52 S275 with square web openings (h_o/h=0.5)

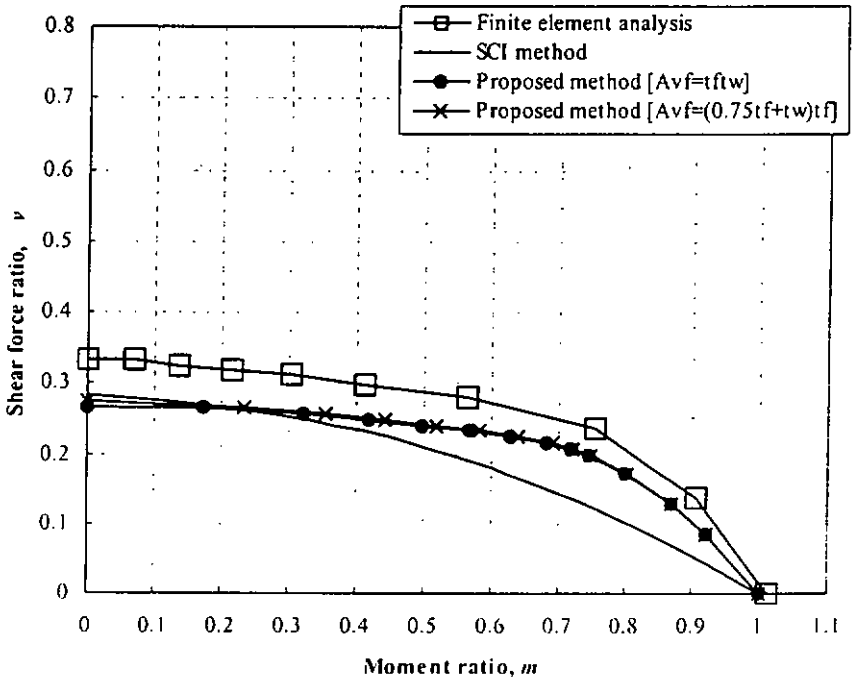

Figure 3.12b Comparisons of moment-shear interaction curves for UB457x152x52 S275 with square web openings (h_o/h=0.75)

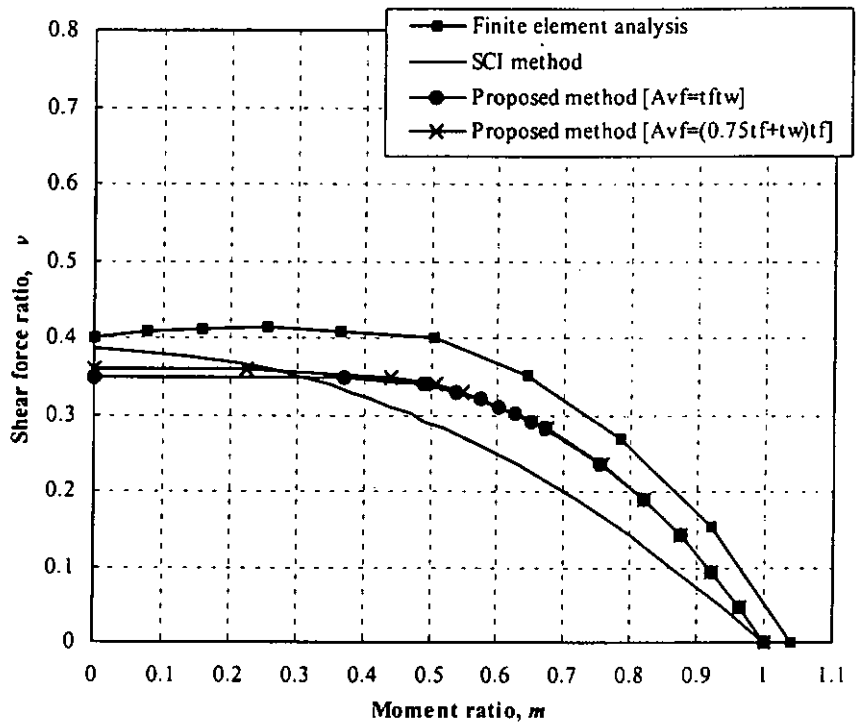

Figure 3.12c Comparisons of moment-shear interaction curves for UB457x152x52 S275 with rectangular web openings (h_o/h=0.5)

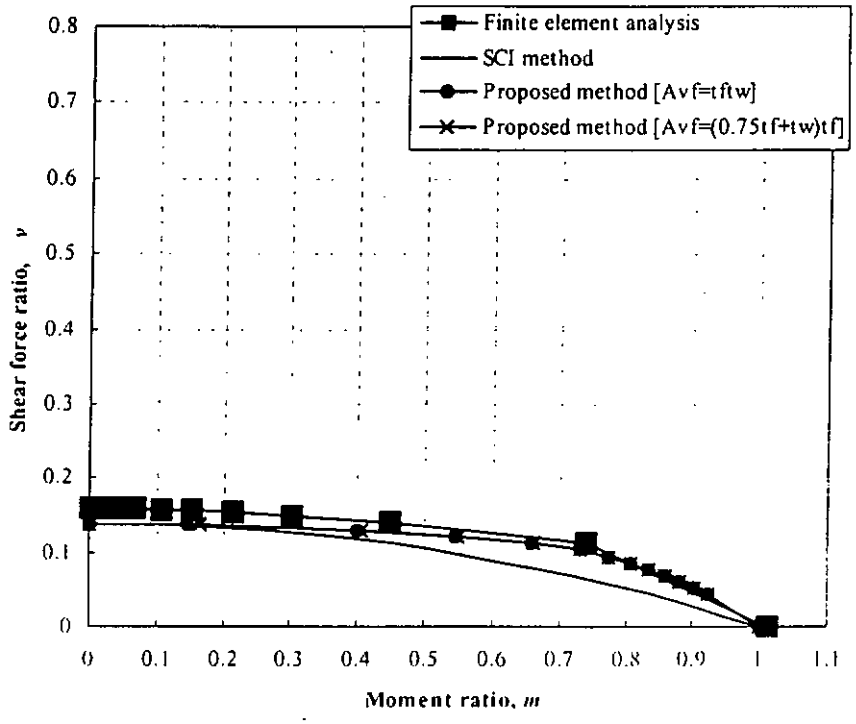

Figure 3.12d Comparisons of moment-shear interaction curves for UB457x152x52 S275 with rectangular web openings (h_o/h=0.75)

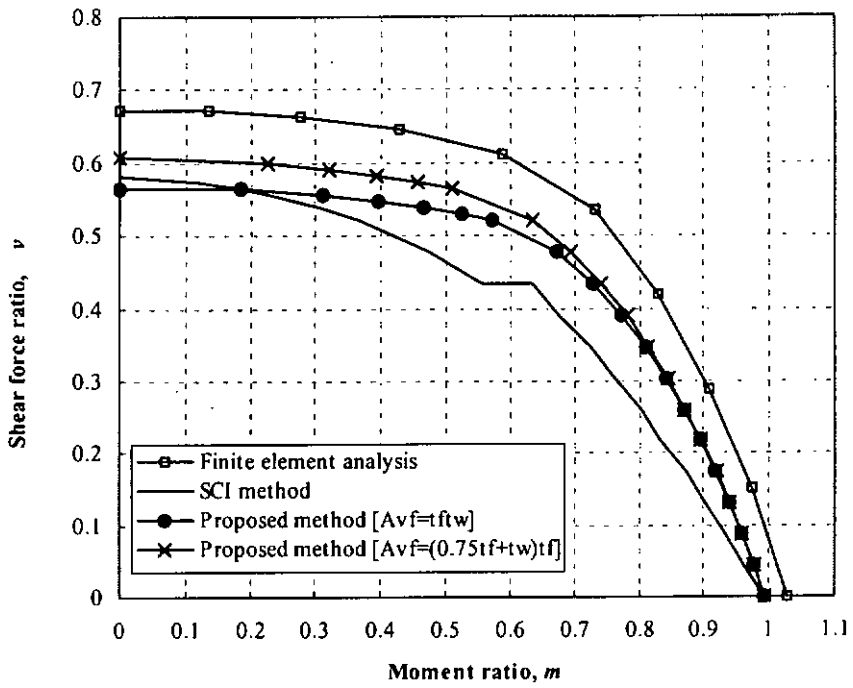

Figure 3.13a Comparisons of moment-shear interaction curves for UB457x152x82 S275 with square web openings (h_o/h=0.5)

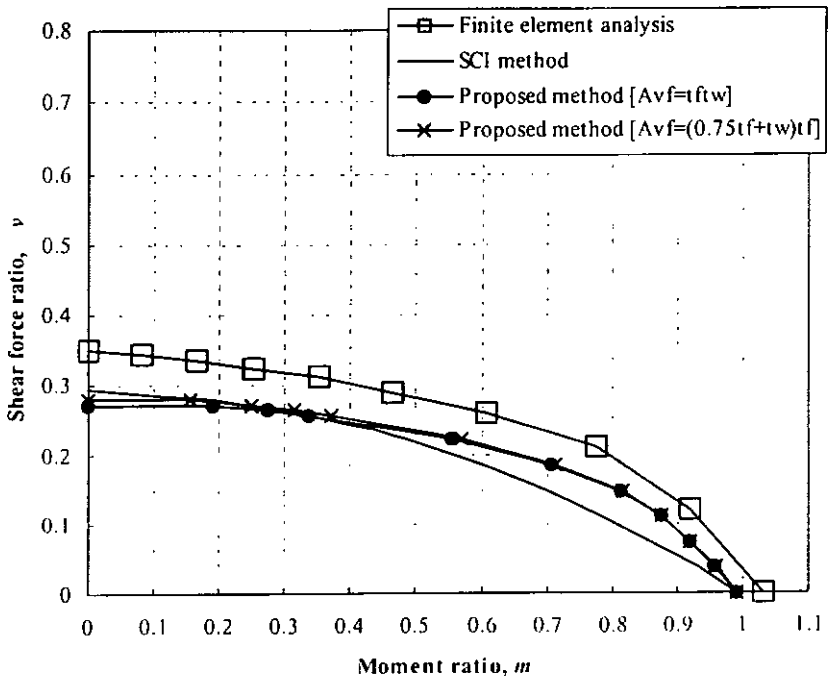

Figure 3.13b Comparisons of moment-shear interaction curves for UB457x152x82 S275 with square web openings (h_o/h=0.75)

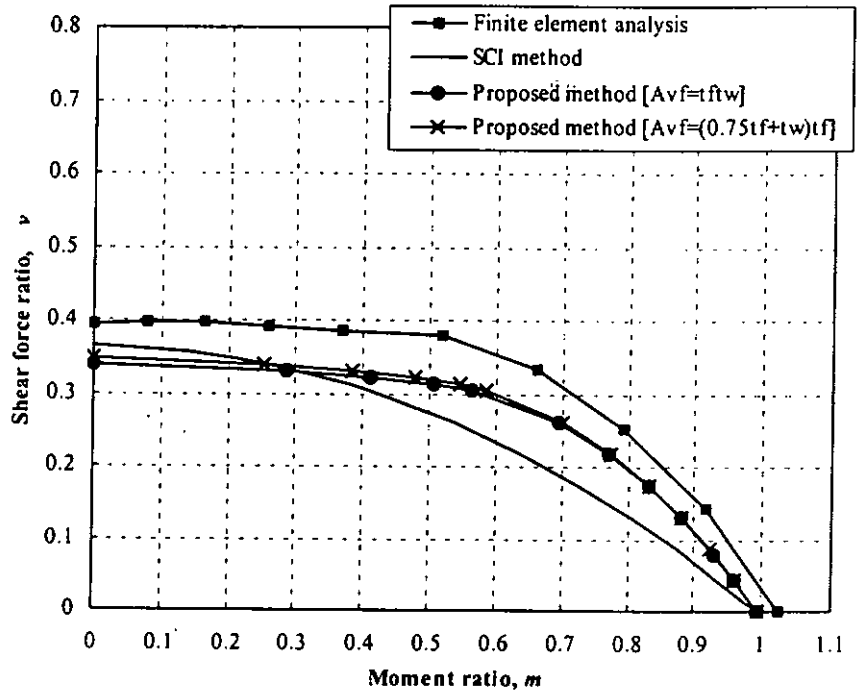

Figure 3.13c Comparisons of moment-shear interaction curves for UB457x152x82 S275 with rectangular web openings (h_o/h=0.5)

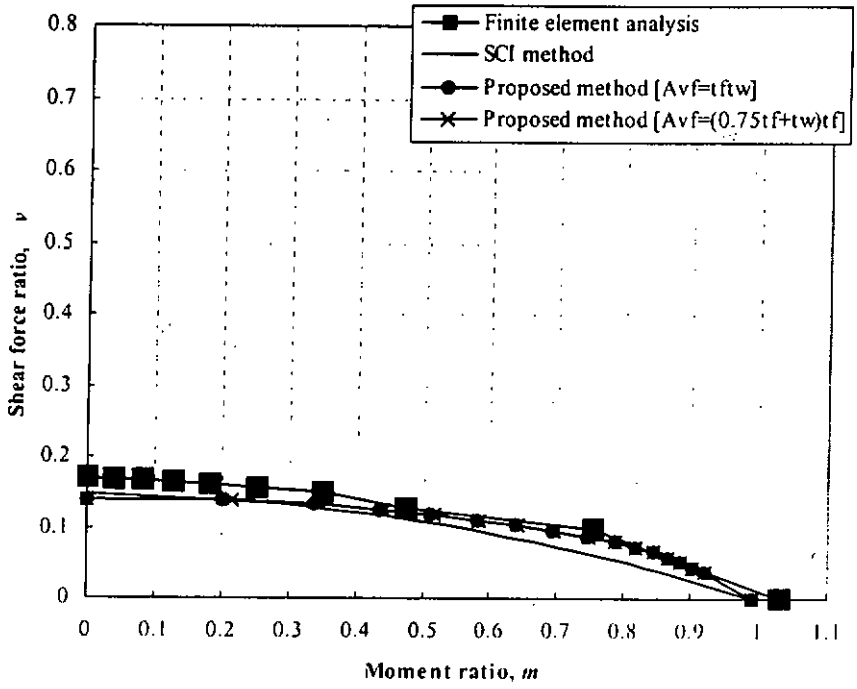

Figure 3.13d Comparisons of moment-shear interaction curves for UB457x152x82 S275 with rectangular web openings (h_o/h=0.75)

Table 3.1 Comparison of the results from proposed design method and SCI design method on steel beams with rectangular web openings

Test number	Experiment designation	Span to depth ratio	Opening aspect ratio	Opening height to beam depth	Location of opening along beam span	Failure M/V ratio at opening centerline	Load capacity in test	Failure mode observed in test	Results from proposed design method						Results from SCI design method					
		L/h	a_o/h_o	h_o/h	x_o/L	M_{Sd}/V_{Sd} (m)	P_{test} (kN)	FM	*m*	*v*	*mv*	*FM*	P_1	Ψ_1	*m*	*v*	*mv*	*FM*	P_2	Ψ_2
1	RM11H	10.58	1.50	0.55	0.43	-	122.2	F	1.00	0.00	0.00	F	117.6	1.04	1.00	0.00	0.00	F	118.9	1.03
2	RM2F	7.44	1.50	0.56	0.30	0.46	136.0	Vi	0.29	0.40	1.00	Vi	91.3	1.49	0.28	0.46	1.00	Vi	85.6	1.59
3	RM21G	8.98	1.50	0.56	0.33	0.61	93.9	Vi	0.40	0.39	1.00	Vi	87.2	1.08	0.37	0.43	1.00	Vi	79.7	1.18
4	RM21H	9.00	1.50	0.56	0.33	0.61	122.2	Vi	0.38	0.39	1.00	Vi	87.9	1.39	0.36	0.44	1.00	Vi	80.7	1.52
5	RM4F	12.31	1.50	0.55	0.48	1.22	125.2	Vi	0.69	0.33	1.00	Vi	116.4	1.08	0.59	0.35	1.00	Vi	99.1	1.26
6	RM4G	12.31	1.50	0.55	0.48	1.22	120.1	Vi	0.69	0.33	1.00	Vi	118.5	1.01	0.59	0.35	1.00	Vi	100.7	1.19
7	RM4H	12.45	1.50	0.56	0.48	1.22	106.6	Vi	0.68	0.34	1.00	Vi	99.3	1.07	0.57	0.35	1.00	Vi	83.9	1.27
8	CR6A	6.33	1.49	0.49	0.24	0.56	400.3	Vi	0.32	0.47	1.00	Vi	329.9	1.21	0.30	0.53	1.00	Vi	302.7	1.32
9	B11	7.53	1.21	0.47	0.17	0.51	419.0	Vi	0.37	0.59	1.00	Vi	381.3	1.10	0.35	0.62	1.00	Vi	341.5	1.23
10	B21	7.59	1.26	0.45	0.33	1.02	378.1	Vi	0.63	0.52	1.00	Vi	303.2	1.25	0.56	0.53	1.00	Vi	262.4	1.44
11	B31	7.56	1.23	0.46	0.50	0.00	442.2	Vi	0.00	0.61	1.00	Vi	338.7	1.31	0.00	0.67	1.00	Vi	320.1	1.38
12	CD4B	10.07	2.00	0.60	0.20	0.91	123.7	Vi	0.20	0.25	1.00	Vi	89.8	1.38	0.20	0.29	1.00	Vi	87.1	1.42
13	RBD-HB5	5.78	2.00	0.53	0.22	0.66	265.1	Vi	0.19	0.33	1.00	Vi	262.2	1.01	0.19	0.37	1.00	Vi	251.3	1.06
14	RBD-HB2	4.63	1.00	0.63	0.27	0.66	254.4	Vi	0.21	0.43	1.00	Vi	218.1	1.17	0.20	0.48	1.00	Vi	206.4	1.23
													Maximum =	**1.49**					**Maximum =**	**1.59**
													Minimum =	**1.01**					**Minimum =**	**1.03**
													Average (above unity) =	**1.18**					**Average (above unity) =**	**1.29**
													Average (below unity) =	**-**					**Average (below unity) =**	**-**
													No. of Ψ_1 above unity =	**14**					**No. of Ψ_2 above unity =**	**14**
													No. of Ψ_1 below unity =	**0**					**No. of Ψ_2 below unity =**	**0**

Notations:

m	Moment utilization ratio
v	Shear utilization ratio
mv	Vierendeel moment utilization ratio
P_1	Load capacity predicted by proposed method
P_2	Load capacity predicted by SCI method
FM	Failure mode: F = Flexural, V = Shear, and Vi = Vierendeel
Ψ_1	Model factor for load capacity predicted by proposed method = P_{test}/P_1
Ψ_2	Model factor for load capacity predicted by SCI method = P_{test}/P_2

CHAPTER 4

DESIGN OF STEEL BEAMS WITH CIRCULAR WEB OPENINGS

4.1 General

The proposed design method presented in Chapter 3 is developed for steel beams with rectangular web openings and thus, it is not applicable for beams with circular web openings. It is considered that the use of a transformation expression is effective to design beams with circular web openings using design methods developed specifically for beams with rectangular web openings. Conventionally, the circular web opening is converted into a rectangular web opening with predetermined transformation parameters for both opening length and height. This procedure and an alternate transformation expression to convert the circular opening into an equivalent octagonal web opening are incorporated in the current SCI design method to investigate the structural behavior of steel beams with circular web openings. The results are compared with those from a finite element study and the findings are presented in a publication (Ko and Chung; 2000). It is shown that the accuracy of the current SCI design method is improved when the equivalent octagonal web opening is used in designing steel beams with circular web openings. This implies that specific transformation expressions should be used for different design methods. For this reason, it is necessary to re-formulate the transformation expression for the proposed design method when designing steel beams with circular web openings. In this chapter, different transformation expressions for equivalent octagonal web openings are investigated. After comparison among themselves, the best transformation expression is selected for use with the proposed design method to generate moment-shear $(M\text{-}V)_o$ interaction curves to compare with those obtained

from finite element analysis and other design methods. The proposed design method has also been calibrated with test data to establish its validity.

4.2 Finite Element Modeling

In order to simulate the structural behavior of steel beams with circular web openings, a finite element model was established with both material and geometrical non-linearity incorporated. The finite element model is calibrated against the test data of two steel I beams with single circular web openings, reported by Redwood and McCutcheon (1968). It is shown that both the moment resistances of the perforated sections and the deformation characteristics of the beams are modeled satisfactorily. A parametric study is then performed to assess the structural performance of simply supported steel beams with circular web openings of different sizes at different locations along the beams. The finite element model shown in Figure 4.1 is used to generate the moment-shear $(M\text{-}V)_o$ interaction curves of the perforated sections for these beams. By varying the position of the opening along the beam span, a non-dimensional interaction curve, namely, Curve FEM, relating the shear force ratio, v, and the moment ratio, m, was obtained. The shear force ratio and the moment ratio are defined previously in Chapter 3. Figures 4.2a to 4.2d present the $(M\text{-}V)_o$ interaction curves for four beams of different sections, and the beam sizes used are:

- Series I: UB457x152x52 and UB457x152x82,
- Series II: UB610x229x101 and UB610x229x140

All beams are of grade S275 steel and they have yield strengths of 275 N/mm^2. The two series are chosen to cover a range of steel beams used in practice. The two different beam sizes used in each series are for the illustration of the effect of flange thickness on the shear resistance of the perforated section. For each steel beam, two

FEM curves for a web opening of diameter d_o equals to both *0.5h* and *0.75h* are plotted together in the same graph for direct comparison. It is shown that in all cases both curves are highly non-linear, and they are very close to each other in shape, despite the significant difference in the opening sizes. The Vierendeel action is less severe in beams with circular web opening when compared with beams with rectangular web openings.

The basic moment and shear resistances of the perforated section are given by:

A) Moment resistance:

$$M_{o,Rd} = f_y W_{o,pl} \geq M_{Sd} \qquad \text{Equation 6.1}$$

$$W_{o,pl} = W_{pl} - \frac{d_o^{\,2} t_w}{4}$$

where

W_{pl} is the plastic modulus of the un-perforated section,

t_w is the web thickness,

d_o is the diameter of the opening, and

f_y is the design yield strength of the steel beam

B) Shear resistance:

$$V_{o,Rd} = f_v A_{vo} \geq V_{Sd} \qquad \text{Equation 6.2}$$

$$A_{vo} = A_v - d_o t_w$$

where

f_v is the shear strength of the steel, which is taken as $\frac{f_y}{\sqrt{3}\gamma_a}$,

A_v is the shear area of the un-perforated section, and

4.3 Equivalent Web Openings

4.3.1 Different transformation expressions

In order to achieve a simple and yet accurate prediction of the load capacity of steel beams with circular web openings, four sets of transformation expressions are

investigated and the best is selected for use with the proposed design method developed in Chapter 3. The first three sets of transformation expressions require the transformation of the circular web opening into equivalent octagonal web opening, as shown in Figure 4.3. Figure 4.3b illustrates Transformation Expression-1 (TE-1) in which the transformed octagonal web opening circumscribes the circular web opening. The transformed octagonal web opening has a length of a_o and a depth of h_o, which are given as follows:

1) TE-1: $a_o = \beta_a d_o$ where $\beta_a = \tan\frac{\pi}{8}$ and

$$h_o = \beta_h a_o \text{ where } \beta_h = 1+\sqrt{2}$$

This expression is simple because it only involves one simple transformation parameter for the equivalent opening length.

In Figure 4.3c, the transformed equivalent octagonal web opening has the same area as the circular web opening. This is referred as Transformation Expression-2 (TE-2). The transformed octagonal web opening has a length of a_o and a depth of h_o, which are given as follows:

2) TE-2 $a_o = \beta_a d_o$ where $\beta_a = \sqrt{\frac{\pi}{8}\tan(\frac{\pi}{8})}$ and

$$h_o = \beta_h a_o \text{ where } \beta_h = 1+\sqrt{2}$$

Finally, the Transformation Expression-3 (TE-3) is illustrated in Figure 4.3d where the transformed octagonal web opening is inscribed by the circular web opening. The transformed octagonal web opening has a length of a_o and a depth of d_o, which are given as follows:

3) TE-3 $a_o = \beta_a d_o$ where $\beta_a = \sin\frac{\pi}{8}$ and

$$h_o = \beta_h a_o \text{ where } \beta_h = 1+\sqrt{2}$$

The transformation parameters β_a and β_h for the above three sets of transformation expressions are obtained readily from the relations between the geometries of the circle and the octagons. The traditional equivalent rectangular web opening is also included for investigation and it is designated as Transformation Expression-4 (TE-4). As shown in Figure 4.3e, this procedure requires transforming the circular web opening into a rectangular web opening and the equivalent length, a_o, and equivalent height, h_o, are given by:

4) TE-4 $a_o = \beta_a d_o$ where $\beta_a = 0.45$ and

$$h_o = \beta_h a_o \text{ where } \beta_h = 2$$

All of the transformation expressions are used with the proposed design method for a parametric study on steel beams with circular web openings reported in the next section.

4.3.2 Comparison of proposed design method with FEM results

Different transformation expressions are used in the proposed design method to generate moment-shear $(M\text{-}V)_o$ interaction curves for four steel beams with circular web openings so that the results can be compared directly with those of the finite element study. Since the FEM results for beams in Series I and II are similar to each other, only the results of Series I are presented here and they are shown in Figures 4.4a to 4.4b for UB457x152x52 and Figures 4.5a to 4.5b for UB457x152x82.

It is convenient to compare the results according to the opening sizes used. For beams with small web openings, the proposed design method can predict results that are either conservative or un-conservative with respect to the FEM results when different transformation expressions are used. As illustrated in Figures 4.4a and 4.5a,

the use of both TE-1 and TE-2 generally gives conservative results while the use of TE-3 and TE-4 produces the opposite. Since the Vierendeel effect is not significant in steel beams with small web openings, the results predicted by the various transformation expressions are within $\pm$ 10% when compared to the FEM results.

However, for larger web openings, the variation of the results is more widespread, which can be seen in Figures 4.4b and 4.5b. In this case, all curves are below the FEM curves, indicating that all the transformation expressions are conservative for steel beams with large circular web openings. Among all the transformation expressions, it is shown that TE-1 predicts results that are significantly lower than those FEM results because of the longer equivalent opening length. For large web opening, it seems that TE-3 is the most desirable.

4.3.3 Final proposed transformation expression

In the previous comparison with FEM results, it is shown that TE-1 is more suitable for small circular web openings while TE-3 is the best for large circular web opening. As a result, it is not possible to use just one particular transformation expression for all opening sizes. It is thus proposed to use interpolated transformation parameters between TE-1 and TE-3 for opening sizes ranging from 50% to 75% depth of the steel beam. The final proposed transformation expression uses the equivalent circumscribed octagon as a basis and the equivalent opening length and height diminish in values when the circular opening becomes larger as follows:

$$a_o = \beta_a d_o,\ h_o = \beta_h a_o$$

where $\beta_a = \tan\frac{\pi}{8} + 4(\frac{d_o}{h} - 0.5)(\sin\frac{\pi}{8} - \tan\frac{\pi}{8})$ and $\beta_h = 1 + \sqrt{2}$.

4.4 Comparisons of Various Design Methods with Finite Element Results

4.4.1 General

The proposed transformation expression is used in conjunction with the proposed design method to generate moment-shear interaction curves for comparison with those obtained from FEM and other existing design methods for design and analysis of steel beams with circular web openings as follows:

1. Design formulas for steel beams with single circular web opening from the Annex N of Eurocode 3
2. The proposed design method using equivalent octagonal web opening based on the proposed transformation expression
3. The current SCI design method using traditional equivalent rectangular web opening using the new flange shear area

Again, since the FEM results for beams in Series I and II are similar to each other, only the results of Series I are presented here and they are shown in Figures 4.6a to 4.6b for UB457x152x52 and Figures 4.7a to 4.7b for UB457x152x82.

4.4.2 Results for beams with small web openings

From Figures 4.6a and 4.7a, it is shown that all design methods generally predict conservative results when compared to those obtained from FEM for small web openings. Results from the proposed design method and the SCI method are similar to each other. However, the SCI curves always have a "horizontal slope" at some particular shear force ratios due to the way in which the SCI method allows for the effect of shear force. In general, the SCI curves match closer to the FEM curves at high moment and shear force ratios while the proposed design method is more accurate at medium moment and shear force ratios. The Annex N design method is generally the least accurate of all.

4.4.3 Results for beams with large web openings

The shear resistances predicted by various design methods are reduced differently when the web opening increases in size. Among the design methods, the results from Annex N of Eurocode 3 are the most conservative. For large web openings, the proposed design method seems to outrank the SCI method for all moment and shear force ratios as it matches closer to the FEM results. This is probably due to the fact that the proposed design method has adopted the proposed transformation expression of equivalent octagonal web openings.

4.5 Calibration of Proposed Design Method with Test Data

A total number of nine tests with compact steel section are selected from the established database to compare the accuracy of the proposed design method in conjunction with the proposed transformation expression. All of the selected test beams have small circular web openings when compared with the beam depth. Various M/V ratios are covered.

Utilization ratios for moment, shear, and Vierendeel moment resistances, failure modes, load capacities, and model factors for each of the test beams predicted by the proposed design method are presented in Table 4.1. The results obtained from the current SCI design method using conventional equivalent rectangular web opening are also included for direct comparison.

An improvement is achieved whenever the proposed design method predicts a model factor that is closer to unity than that predicted by the SCI design method. From Table 4.1, it can be seen that the model factors predicted by the proposed design method range from 0.93 to 1.24, while those predicted by the SCI design method range from 0.93 to 1.39. The number of model factors that are less than unity has increased from two to five as predicted by the proposed design method.

indicating that the method is slightly un-conservative. However, the averages of the model factors that are above unity are 1.09 and 1.12 as predicted by the proposed method and the SCI method, respectively. Similarly, the averages of the model factors that are below unity are 0.95 and 0.93 as predicted by the proposed method and the SCI method, respectively. Thus, both the averages above and below unity have shown that the proposed design method is slightly more accurate than the SCI method.

4.6 Conclusions

Based on the study of steel beams with circular web openings, the following conclusions are made:

1) Specific transformation expression is required for different design methods in designing beams with circular web openings. Transformation expressions using equivalent octagonal web openings of various criteria are incorporated in the proposed design method to generate moment-shear interaction curves for a number of steel beams with circular web openings, and the results are compared with those obtained from a finite element study. It is found that the transformation expression using equivalent circumscribed octagon is the most suitable for small circular web openings, while the transformation expression using equivalent inscribed octagon is the most suitable for medium to large circular web openings. As a result, a transformation expression utilizing interpolated transformation parameters between these two expressions is proposed for circular web openings of all sizes.

2) The proposed design method using the proposed transformation expression and two other design methods are used to generate moment-shear interaction curves for a number of steel beams with circular web openings, and the results

are compared with those obtained from a finite element study. It is found that the proposed design method is at least as accurate as the current SCI design method for small circular web openings. It is the most accurate among all design methods for large circular web openings.

3) Nine test data of steel beams with circular web openings are selected from the established database for the calibration of the proposed design method. Model factors predicted by both the proposed design method and the current SCI design method are compared. In general, the proposed design method predicts higher load capacities than the SCI design method and shows a slight improvement of about 2% on average on the model factors. The diameters of all the circular web openings are considered to be small.

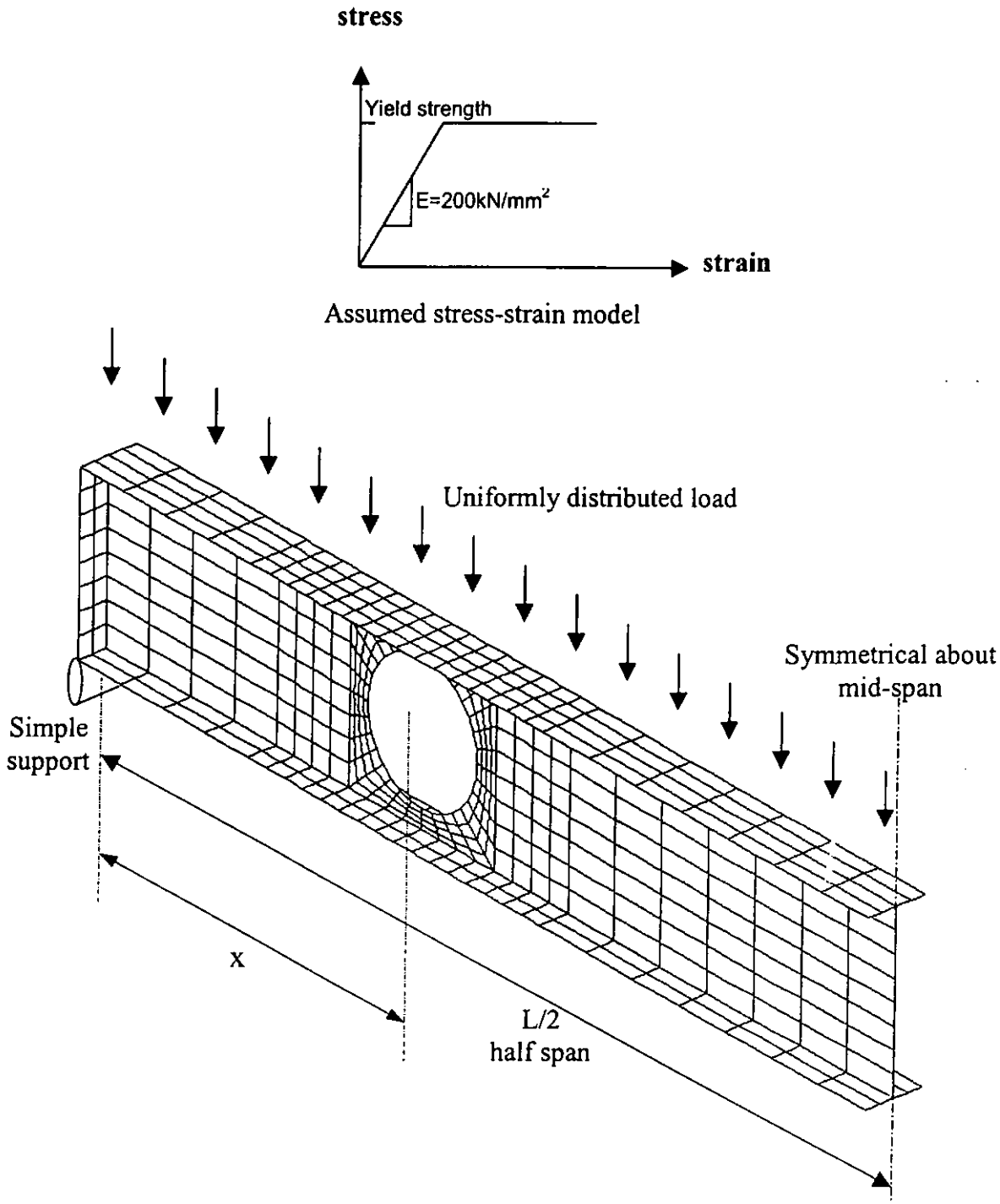

Figure 4.1 Finite element model for a steel beam with circular web opening

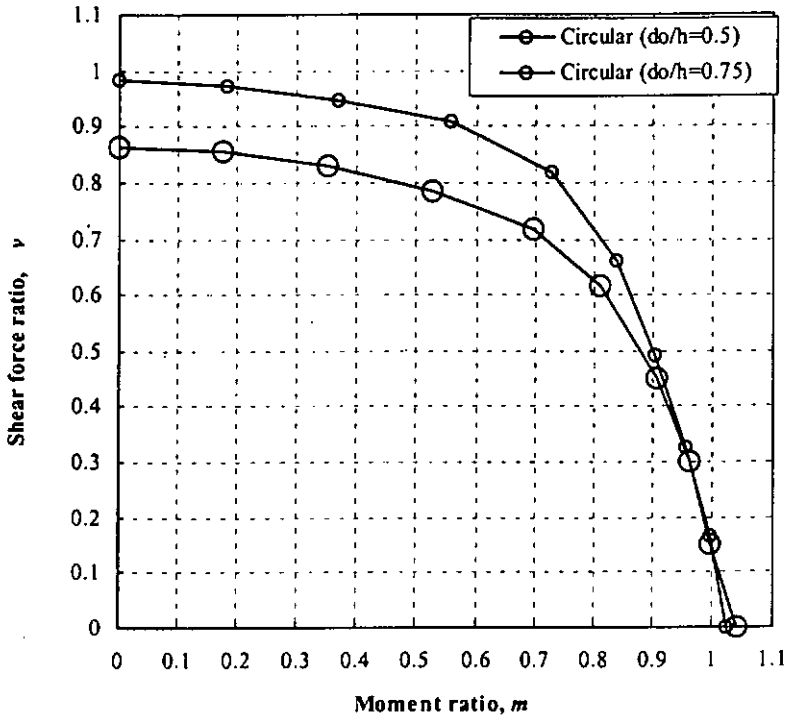

Figure 4.2a Moment-shear interaction curves for UB457x152x52 S275 with circular web openings from finite element analysis

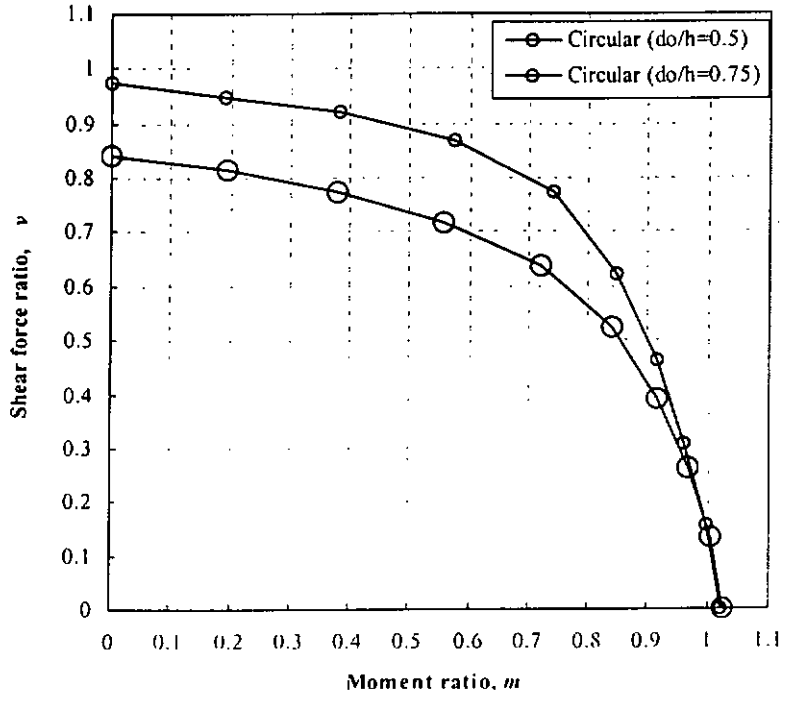

Figure 4.2b Moment-shear interaction curves for UB457x152x82 S275 with circular web openings from finite element analysis

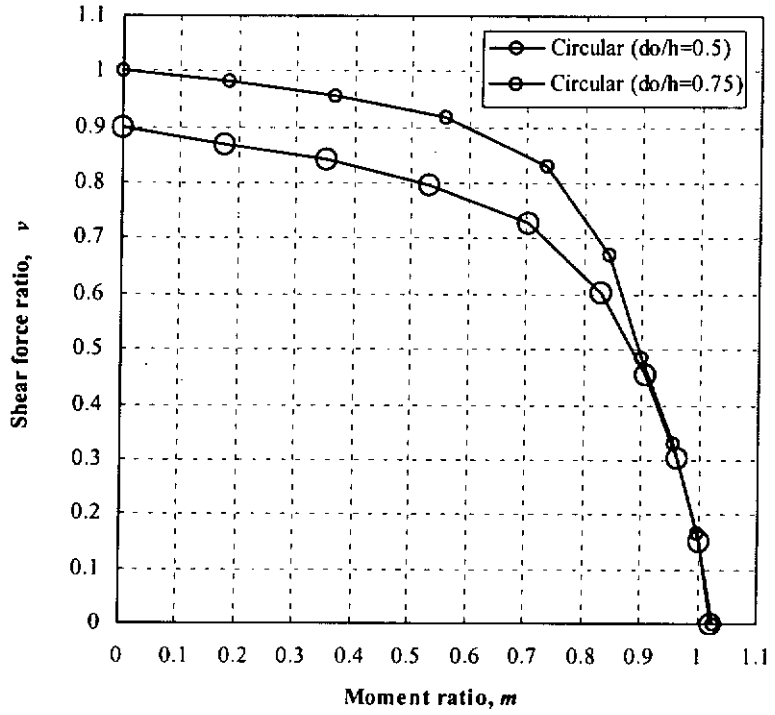

Figure 4.2c Moment-shear interaction curves for UB610x229x101 S275 with circular web openings from finite element analysis

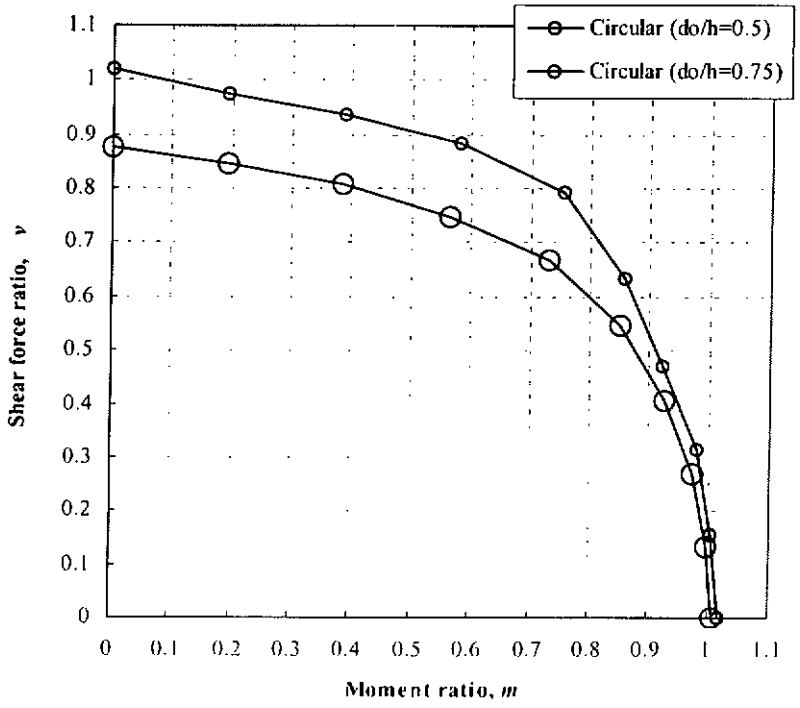

Figure 4.2d Moment-shear interaction curves for UB610x229x140 S275 with circular web openings from finite element analysis

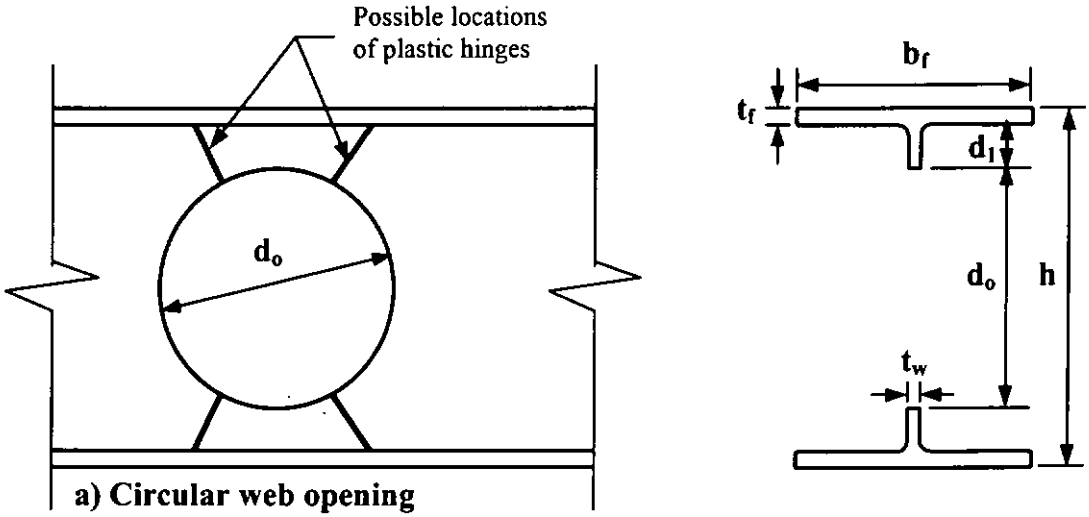

a) Circular web opening

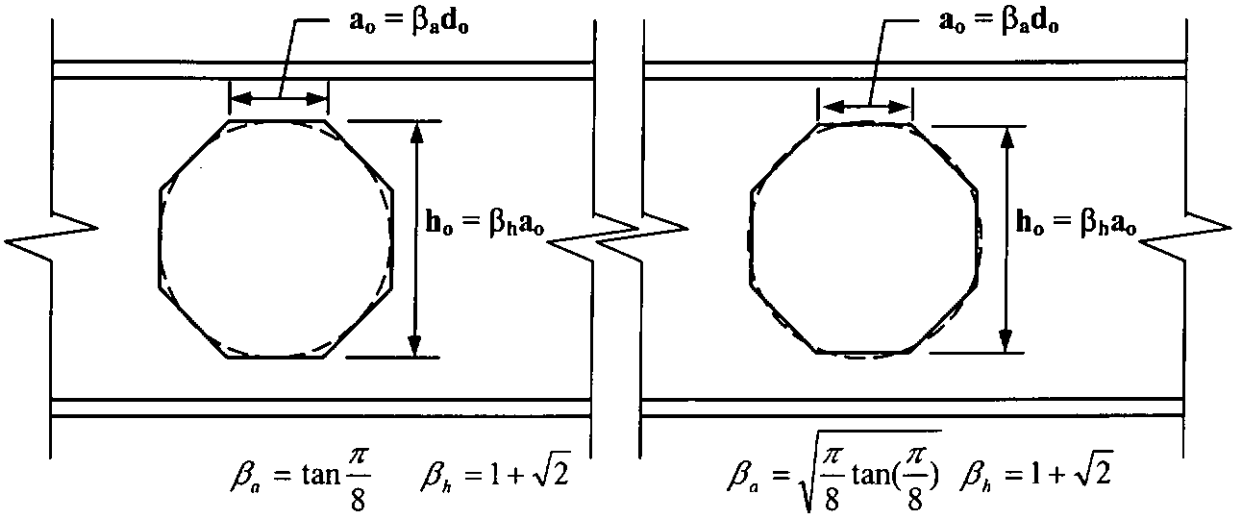

$\beta_a = \tan\frac{\pi}{8}$ $\beta_h = 1+\sqrt{2}$

b) TE-1

$\beta_a = \sqrt{\frac{\pi}{8}\tan(\frac{\pi}{8})}$ $\beta_h = 1+\sqrt{2}$

c) TE-2

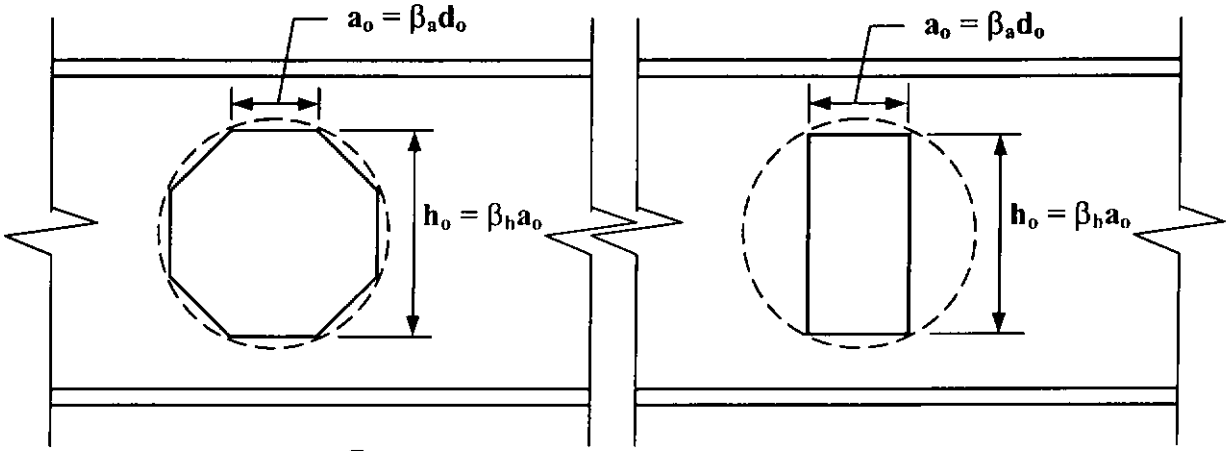

$\beta_a = \sin\frac{\pi}{8}$ $\beta_h = 1+\sqrt{2}$

d) TE-3

$\beta_a = 0.45$ $\beta_h = 2$

e) TE-4

Figure 4.3 Transformed shapes for circular web openings

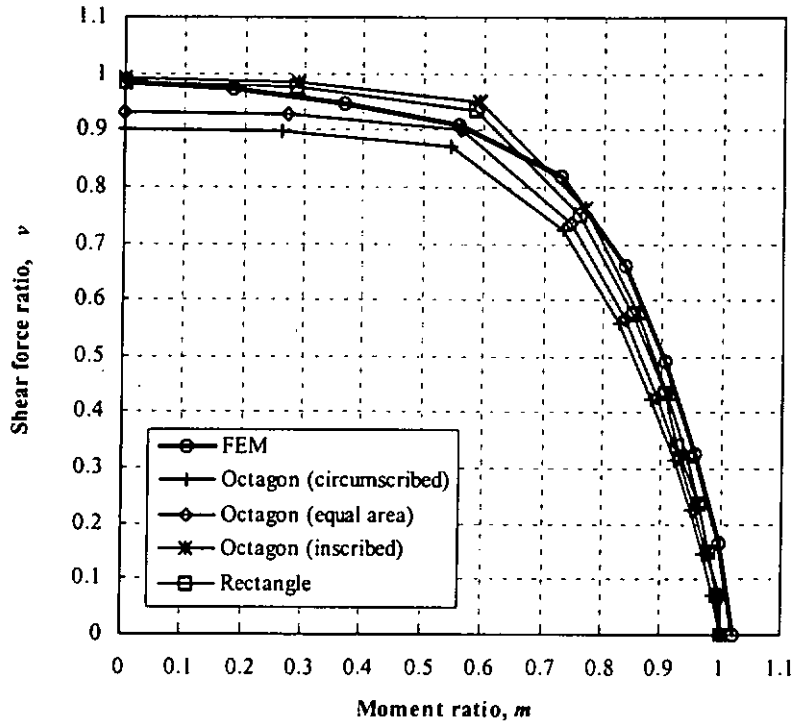

Figure 4.4a Comparisons of moment-shear interaction curves for UB457x152x52 S275 with circular web openings (d_o/h=0.5)

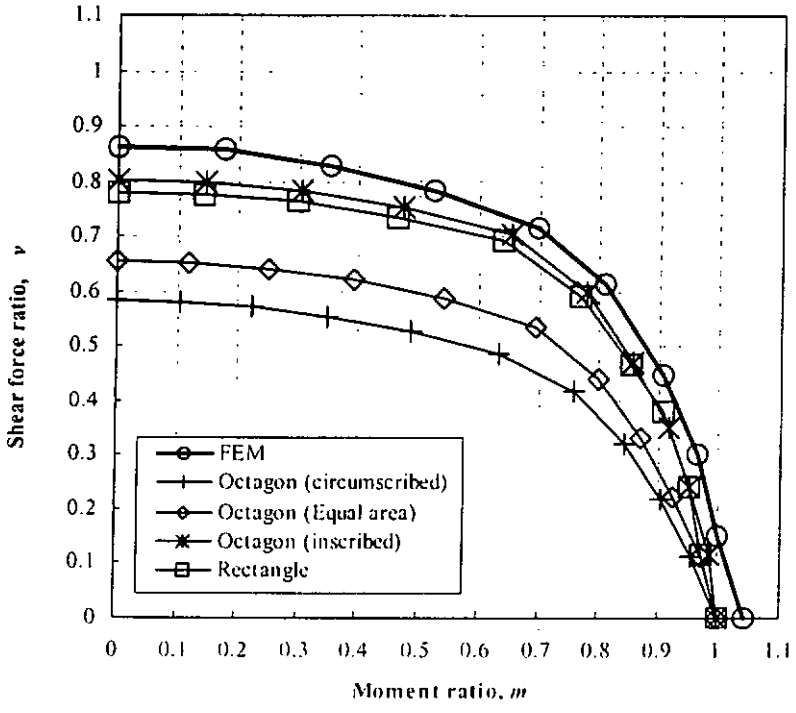

Figure 4.4b Comparisons of moment-shear interaction curves for UB457x152x52 S275 with circular web openings (d_o/h=0.75)

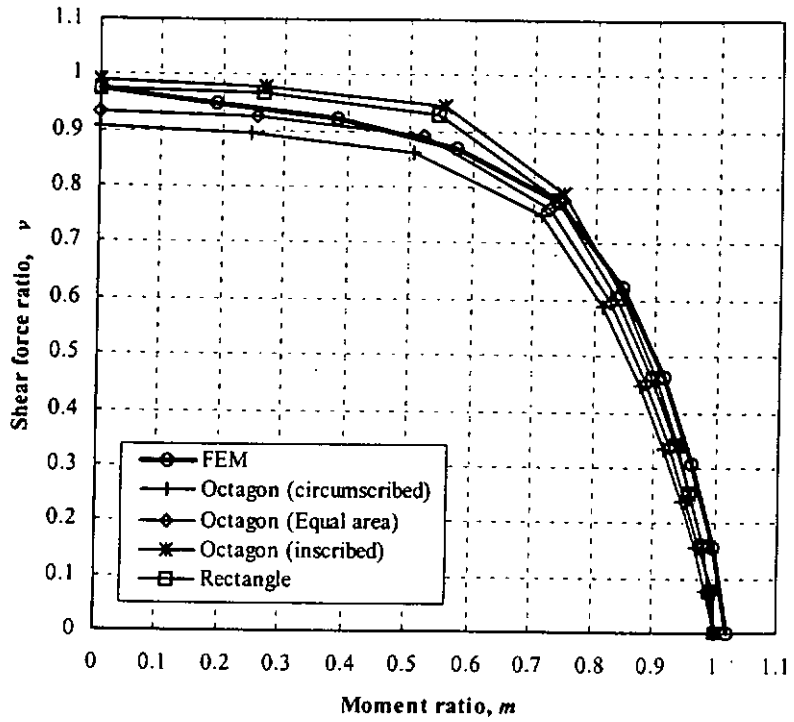

Figure 4.5a Comparisons of moment-shear interaction curves for UB457x152x82 S275 with circular web openings (d_o/h=0.5)

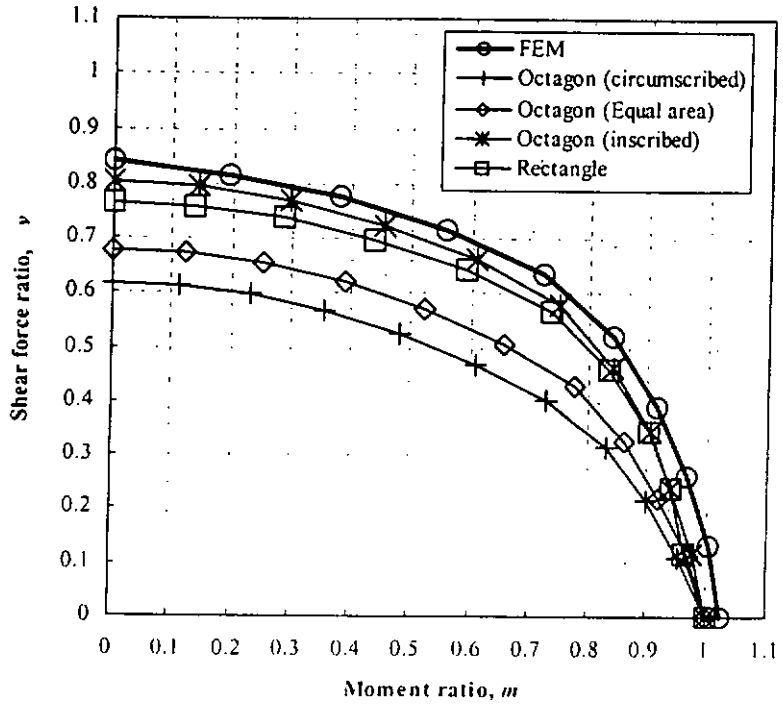

Figure 4.5b Comparisons of moment-shear interaction curves for UB457x152x82 S275 with circular web openings (d_o/h=0.75)

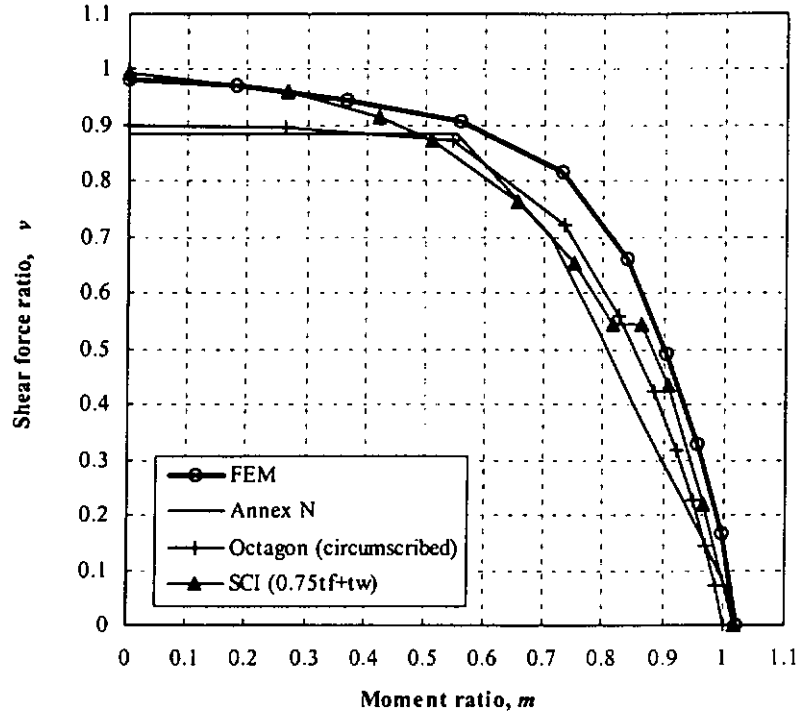

Figure 4.6a Comparisons of moment-shear interaction curves for UB457x152x52 S275 with circular web openings (d_o/h=0.5)

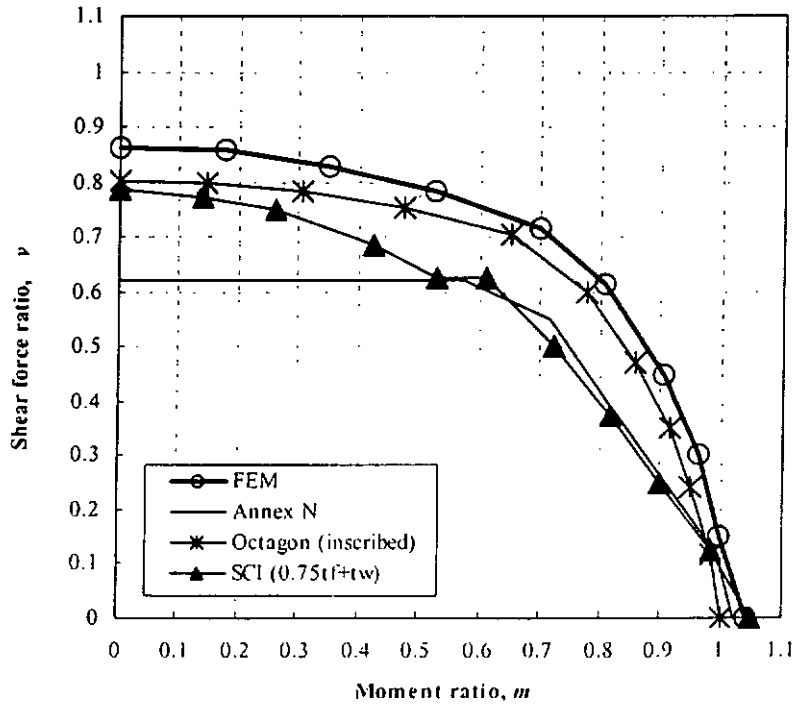

Figure 4.6b Comparisons of moment-shear interaction curves for UB457x152x52 S275 with circular web openings (d_o/h=0.75)

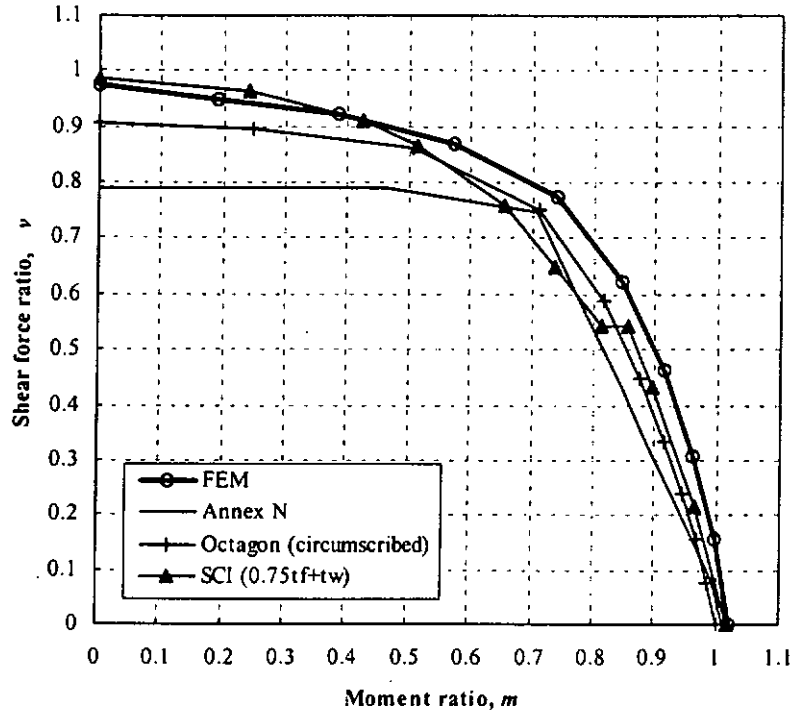

Figure 4.7a Comparisons of moment-shear interaction curves for UB457x152x82 S275 with circular web openings (d_o/h=0.5)

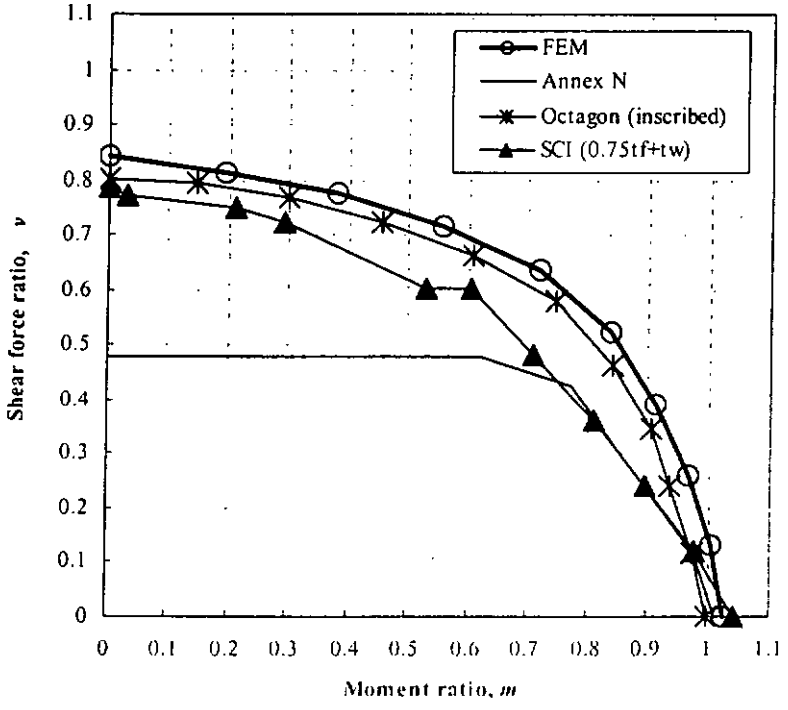

Figure 4.7b Comparisons of moment-shear interaction curves for UB457x152x82 S275 with circular web openings (d_o/h=0.75)

Table 4.1 Comparison of the results from proposed design method and SCI design method on steel beams with circular web openings

Test number	Experiment designation	Span to depth ratio	Opening aspect ratio	Opening height to beam depth	Location of opening along beam span	Failure M/V ratio at opening centerline	Load capacity in test	Failure mode observed in test	Results from Proposed design method						Results from SCI design method					
		L/h	a_o/h_o	h_o/h	x_o/L	M_{Sd}/V_{Sd} (m)	P_{test} (kN)	FM	m	v	mv	P_1	FM	Ψ_1	m	v	mv	P_2	FM	Ψ_2
1	RM1A	9.85	1.00	0.54	0.50	-	111.2	F	1.00	0.00	0.00	113.2	F	**0.98**	1.00	0.00	0.00	115.9	F	**0.96**
2	RM1D	9.98	1.00	0.55	0.46	-	98.8	F	1.00	0.00	0.00	104.4	F	**0.95**	1.00	0.00	0.00	106.6	F	**0.93**
3	RM2A	7.38	1.00	0.54	0.30	0.46	262.8	Vi	0.63	0.85	1.00	247.8	Vi	**1.06**	0.60	0.84	1.00	221.3	Vi	**1.19**
4	RM2C	7.46	1.00	0.55	0.30	0.46	230.3	Vi	0.62	0.86	1.00	185.4	Vi	**1.24**	0.59	0.84	1.00	165.8	Vi	**1.39**
5	RM2D	7.38	1.00	0.54	0.30	0.46	246.1	Vi	0.66	0.84	1.00	234.0	Vi	**1.05**	0.62	0.82	1.00	208.4	Vi	**1.18**
6	RM3A	12.31	1.00	0.54	0.30	0.76	145.6	Vi	0.83	0.65	1.01	149.8	Vi	**0.97**	0.78	0.65	1.00	137.9	Vi	**1.06**
7	RM4C	12.31	1.00	0.54	0.48	1.22	146.6	Vi	0.91	0.40	1.01	145.4	Vi	**1.01**	0.88	0.43	1.00	142.5	Vi	**1.03**
8	RM4D	12.31	1.00	0.54	0.48	1.22	154.6	Vi	0.90	0.45	1.01	158.8	Vi	**0.97**	0.86	0.47	1.01	151.8	Vi	**1.02**
9	RBD-C1	4.71	1.00	0.29	0.27	0.54	751.8	Vi	0.66	0.94	1.00	811.1	Vi	**0.93**	0.73	0.95	1.01	742.0	Vi	**1.01**
													Maximum =	**1.24**					**Maximum =**	**1.39**
													Minimum =	**0.93**					**Minimum =**	**0.93**
													Average (above unity) =	**1.09**					**Average (above unity) =**	**1.12**
													Average (below unity) =	**0.96**					**Average (below unity) =**	**0.94**
													No. of Ψ_1 above unity =	**4**					**No. of Ψ_2 above unity =**	**7**
													No. of Ψ_1 below unity =	**5**					**No. of Ψ_2 below unity =**	**2**

Notations:

m	Moment utilization ratio
v	Shear utilization ratio
mv	Vierendeel moment utilization ratio
P_1	Load capacity predicted by proposed method
P_2	Load capacity predicted by SCI method
FM	Failure mode: F = Flexural, V = Shear, and Vi = Vierendeel
Ψ_1	Model factor for load capacity predicted by proposed method = P_{test}/P_1
Ψ_2	Model factor for load capacity predicted by SCI method = P_{test}/P_2

CHAPTER 5

V-N-M INTERACTION FOR COMPOSITE TEE-SECTION AND PREFORATED SECTION ANAYSIS

5.1 General

Composite beams with web openings are widely used in floor construction, and concrete slabs increase both the shear and the moment resistances of the beams tremendously. For composite beams with rectangular web openings, the Vierendeel failure is often critical with the formation of plastic "hinges" near the corners of the web openings as shown in Figure 5.1. The hinges take place at two steel tee cross-sections below the web opening and two composite tee cross-sections above the web opening. The moment resistances of the steel tee-sections under the effect of co-existing shear force and axial force can be evaluated using the method presented in Chapter 3. The analysis of the composite tee-sections is more complicated since shear connection between the concrete slab and the steel tee-section have to be considered. Moreover, the composite tee-sections at the LMS and the HMS have to be considered separately because of different stress blocks presented under both global and local bending actions. The nominal resistances of the composite tee-sections are discussed first in Section 5.2. Then the interaction of axial force and bending moment is considered in Sections 5.3 and 5.4 for composite tee cross-sections at the HMS and the LMS of the perforated section, respectively. The proposed design formulas are then extended to incorporate the design of perforated section after calibration with test data in Section 5.6.

5.2 Nominal Resistances of Composite Tee-sections

In this section, formulas for the shear resistances, the moment resistances and the plastic axial centroids of the composite tee-sections are present. The effect of

shear force on composite tee-section is also discussed and presented in details.

5.2.1 Shear resistances of composite tee-section

Experiments indicate that the concrete slab contributes significantly to the shear resistance of a composite beam with web openings. Eurocode 2 provides design rules to calculate the shear resistance of reinforced concrete beams and slabs and they are convenient for use in composite beams with web openings after suitable modifications.

The shear resistance of a composite tee-section is contributed both by the steel tee-sections and the concrete slab. For rational design, the concrete slab is assumed to take up a portion of the applied shear force up to its shear resistance according to Eurocode 2, and any remaining shear force is then distributed to the top and the bottom steel tee-sections. The steel tee-section is assumed to resist the applied shear force through a portion of its flange and the full depth of its web, i.e. the shear areas of the flange and the web. The design rules have been discussed in Section 3.2.2 and they are not repeated here.

5.2.2 Moment resistance of composite tee-section at HMS

Under pure bending, the nominal plastic neutral axis (PNA) of the composite tee-section at the HMS of the perforated section may locate within the concrete slab, the steel flange, or the steel web, depending on the relative axial resistances of the steel tee-section, the concrete slab, and also the degree of shear connection. The stress blocks of all three cases are illustrated in Figure 5.2. In the figure, "C" denotes compressive strength while "T" denotes tensile strength. It is important to note that compressive force in the concrete is assumed to act at the top of the concrete slab as observed from experiments while the tensile strength of the concrete is neglected. The axial resistances of the three components of the composite tee-section are given

as follows:

1. Concrete slab: $N_{c,Rd} = 0.85 b_e d_e f_{ck}$, where f_{ck} is the compressive cylinder strength of the concrete, b_e is the effective width of the concrete slab, and d_e is the effective concrete depth.
2. Steel tee-section: $N_{a,V,Rd} = N_{w,V,Rd} + N_{f,V,Rd}$, where $N_{w,V,Rd} = d_1 t_w f_{vw}$ and $N_{f,V,Rd} = t_f b_f f_{vf}$.
3. Shear connectors: $N_{sh,Rd} = n_H P_{Rd}$, where n_H is the number of shear connectors from the nearest support to the HMS of the perforated section and P_{Rd} is the design strength of a shear connector according to Eurocode 4.

If the resistance of the shear connectors is larger than the resistances of both the concrete slab and the steel tee-section, that is, $N_{sh,Rd}$ is larger than either $N_{c,Rd}$ or $N_{a,V,Rd}$, then the composite tee-section has full shear connection. In general, the depth of the compressive strength block in the concrete is given by:

$$\alpha = \frac{N_{Rd} d_e}{N_{c,Rd}} \qquad \text{Equation 5.1}$$

where $N_{Rd} = Minimum\,(N_{a,V,Rd}, N_{c,Rd}, N_{sh,Rd})$

The nominal PNA locates within the concrete slab as shown in Figure 5.2b if $N_{c,Rd}$ is larger than $N_{a,V,Rd}$, and the position of the PNA, y_{po}, is always smaller than h_t. For convenience of subsequent calculations, the nominal PNA is assumed to be located at the top of the steel flange. Suppose that $N_{a,V,Rd}$ is larger than $N_{c,Rd}$ and the PNA locates within the steel flange, which is illustrated in Figure 5.2c. The depth of the portion of the flange under tension is given as follows:

$$y_{II} = \frac{N_{f,V,Rd} + N_{Rd} - N_{w,V,Rd}}{2 b_f f_{vf}}$$

and the position of the PNA is given by:

$$y_{po} = h_t + t_f - y_H$$

In the rare case where the nominal PNA locates within the web, the depth of the portion of the web under compression is given by:

$$y_H = \frac{N_{w,V,Rd} - N_{Rd} - N_{f,V,Rd}}{2t_w f_{vw}}$$

and the position of the PNA is given as follows:

$$y_{po} = h_t + t_f + y_H$$

The plastic moment resistance, $M_{Tih,V,Rd}$, of the composite tee-section may be found by summing up the moments of all the resistances of both the concrete slab and the steel tee-section about the bottom of the steel flange. Explicit formulas are given in Chapter 6. However, if there is only partial shear connection, that is, $N_{Rd} = N_{sh,Rd}$, then the full compressive strength of the concrete is not attainable and the possible stress blocks are shown in Figure 5.2c and 5.2d. The depth of the compressive stress block in the concrete slab may be found by using Equation 5.1. In general, this equation is valid for composite tee-sections with both full and partial shear connections.

5.2.3 Moment resistance of composite tee-section at LMS

Whenever a composite beam with a perforated steel section is subjected to both moment and shear, tensile cracks always form at the top of the concrete slab at the LMS of the perforated section at failure, and at the same time the lower part of the concrete slab is under compression. When global bending moment is increased, the axial force acting on the composite tee-section also increases, causing the cracks to close up, and hence larger compressive resistance may be developed in the concrete slab. Thus, it is reasonable to consider that under pure shear, the moment resistance of the composite tee-section at the LMS assumes the stress block as

illustrated in Figure 5.3, depending on the relative axial resistances of the concrete slab, the steel tee-section, and also the degree of shear connection.

The axial resistances of the concrete slab and the steel tee-section are defined in Section 5.2.2 while the resistance of the shear connectors is given by:

$$N_{sh,Rd} = n_L P_{Rd}$$

where n_L is the number of shear connectors from the LMS of the perforated section to the nearest support.

The types of stress block for the composite tee-section at the LMS are similar to those for the cross-section at the HMS except that the resistance of shear connectors is smaller, i.e. the PNA may locate within the concrete slab, the flange, or the web in the case of full shear connection while it may only locate within the flange or the web in the case of partial shear connection. The stress blocks shown in Figure 5.3 are valid for composite tee-section with both full and partial shear connections.

The nominal moment resistance, $M_{Tld,V,Rd}$, of the cross-section can be found by summing up the moments of each of the resistances of the concrete slab and the tee-section about the bottom of the flange. All relevant strength quantities are defined in Section 5.2.2, and explicit formulas are given in Chapter 6.

5.2.4 Plastic axial centroids of the composite tee-sections

The plastic axial centroid (PC) of a composite tee-section is a point at which the resultant axial force is assumed to pass through such that both the concrete slab and the steel tee-section are fully yielded without creating any moment under axial force. With reference to Figure 5.4, the PCs of the composite tee-sections at both the LMS and the HMS are different because of the different stress blocks assumed. The concrete compressive force is assumed to act at the top and the bottom parts of the

concrete slab at the HMS and the LMS, respectively. The position of the plastic axial centroid, y_{pctl}, from the top of the concrete slab at the LMS is given by:

$$y_{pctl} = \frac{N_{Rd}(d_e - \frac{\alpha}{2}) + N_{f,V,Rd}(\frac{t_f}{2} + h_t) + N_{w,V,Rd}(h_t + t_f + \frac{d_1}{2})}{N_{Rd} + N_{f,V,Rd} + N_{w,V,Rd}}$$

where

N_{Rd} is the minimum of $N_{sh,Rd}$ and $N_{c,Rd}$

$N_{sh,Rd}$ is the resistance of shear connectors at the point under consideration

$N_{c,Rd}$ is the compressive strength of the concrete slab

$N_{a,V,Rd}$ is the axial resistance of the steel tee-section

The position of the plastic axial centroid, y_{pcth}, from the top of the concrete slab at the HMS is given by:

$$y_{pcth} = \frac{N_{Rd}(\frac{\alpha}{2}) + N_{f,V,Rd}(\frac{t_f}{2} + h_t) + N_{w,V,Rd}(h_t + t_f + \frac{d_1}{2})}{N_{Rd} + N_{f,V,Rd} + N_{w,V,Rd}}$$

The PC is a point of significant importance since any effect of axial force on the moment resistance of the composite tee-section is derived with reference to this point.

5.2.5 Effect of shear force on composite tee-sections

Shear force is assumed to affect both the axial and the moment resistances of composite tee-section and the effect of shear is taken into account by reducing the bending strengths of both the flange and the web of the steel tee-sections through von Mises' yielding criterion. It is assumed that only the steel tee-sections are affected and the design rules are presented in Section 3.4. Similarly, both the axial and the moment resistances of the composite tee-sections are calculated using the reduced bending strengths of the flange and the web in the presence of high shear force. For convenience, all the formulas used in the previous sections and also the

following sections are presented with the effect of shear force being considered.

5.3 Modified Moment Resistances of Composite Tee-section at HMS under Axial Force

When the axial force arising from global bending action is applied to the composite tee-section at the HMS, its plastic moment resistance is modified. The modification depends on the position of the nominal PNA, the magnitude of the axial force, and also the degree of shear connection in the composite tee-section.

5.3.1 Full shear connection and nominal PNA in concrete.

Figure 5.5 shows a composite tee-section together with its stress block when the nominal plastic neutral axial (PNA) locates within the concrete slab. A number of cases for different stress blocks are considered as follows.

Case 1) Shifted PNA in concrete

Assume an axial force, $N_{T,Sd}$, is applied to the section and that the residual strength of the concrete, smaller of $N_{c,Rd}$ and $N_{sh,Rd}$ minus $N_{a,V,Rd}$, is large enough to resist the applied force, then the stress block of the axial force in the concrete is given by:

$$\alpha_c = \frac{N_{T,Sd}}{0.85 b_e f_{ck}}$$

This axial force is acting along the direction of the positive bending moment resistance with a lever arm, β_c, measured from the plastic axial centroid (PC). So it has a beneficial effect and the moment resistance of the composite tee-section is increased. The modified moment resistance, $M_{Tth,VN,Rd}$, is given by:

$$M_{Tth,VN,Rd} = M_{Tth,V,Rd} + N_{c,Sd}\beta_c$$

where $\beta_c = y_{pcth} - (\alpha + \frac{\alpha_c}{2})$ and $N_{c,Sd} = N_{T,Sd}$.

Case 2) Shifted PNA in steel web

If the magnitude of the axial force is larger than the residual strength of the concrete, then the shifted PNA may locate within either the flange or the web. Suppose the axial force is large enough to cause the PNA to locate within the web as shown in Figure 5.5d. The stress block has shown that the residual compressive strength of the concrete and the yield strength of the flange are reached such that a portion of the web is in compression while the remaining portion is in tension. As the stress blocks in the flange and the web due to the axial force are below the PC, the effect due to these two forces are non-beneficial. The magnitudes of the forces are given by:

$$N_{c,Sd} = MIN(N_{c,Rd}, N_{sh,Rd}) - N_{a,V,Rd}, \quad N_{f,Sd} = 2\alpha_f b_f f_{vf}, \quad N_{w,Sd} = 2\alpha_w t_w f_{vw}$$

where $\alpha_f = t_f$ and $\alpha_w = \dfrac{N_{T,Sd} - N_{c,Sd} - N_{f,Sd}}{2t_w f_{vw}}$. The modified moment resistance of the composite tee-section is thus given by:

$$M_{Tth,VN,Rd} = M_{Tth,V,Rd} + N_{c,Sd}\beta_c + N_{f,Sd}\beta_f + N_{w,Sd}\beta_w \qquad \text{Equation 5.2}$$

where $\beta_f = y_{pcth} - (y_{po} + \dfrac{\alpha_f}{2})$ and $\beta_w = y_{pcth} - (y_{po} + \alpha_f + \dfrac{\alpha_w}{2})$.

Case 3) Shifted PNA in steel flange

However, if the applied axial force is only large enough to shift the PNA to the flange, then all quantities related to the web will vanish. The depth of the stress block in the flange is given by:

$$\alpha_f = \frac{N_{T,Sd} - N_{c,Sd}}{2b_f f_{vf}}$$

where $N_{c,Sd} = MIN(N_{c,Rd}, N_{sh,Rd}) - N_{a,V,Rd}$. The modified moment resistance, $M_{Tth,VN,Rd}$, is given by:

$$M_{Tth,VN,Rd} = M_{Tth,V,Rd} + N_{c,Sd}\beta_c + N_{f,Sd}\beta_f$$

where $\beta_c = y_{pcth} - (\alpha + \frac{\alpha_c}{2})$ and $\beta_f = y_{pcth} - (y_{po} + \frac{\alpha_f}{2})$.

5.3.2 Full shear connection and nominal PNA in flange or web

In the rare case in which the axial resistance of the concrete slab is less than both the resistances of the shear connectors and the steel tee-section, the nominal PNA locates within either the flange or the web as shown in Figures 5.6 and 5.7, respectively.

Case 1) Nominal PNA in steel flange and shifted PNA in steel web

When the axial force is applied to the section, the PNA shifts towards the bottom of the web of the steel tee-section. Since the concrete slab is not able to take any applied axial force, the axial force is distributed to the steel flange first and is then resisted by the steel web after the flange is fully yielded in compression if the nominal PNA is in the steel flange. This is shown in Figure 5.6c and 5.6d. Since the beneficial effect from the concrete stress block does not exist, there is always a reduction in the moment resistance due to the applied force resisted by both the flange and the web. The modified moment resistance, $M_{Tth,VN,Rd}$, may be calculated using Equation 5.2, with the second term on the right hand side of the equation set to zero. Thus,

$$M_{Tth,VN,Rd} = M_{Tth,V,Rd} + N_{f,Sd}\beta_f + N_{w,Sd}\beta_w$$

The depth of the stress block in the flange in this case is given by:

$$\alpha_f = y_{II}$$

where y_{II} is defined previously in Section 5.2.2.

Case 2) Nominal PNA in steel flange and shifted PNA in steel flange

If the nominal PNA is located within the steel flange and if the applied axial

force is not large enough to shift the PNA to be located in the web, then the PNA may remain in the flange. In this case, the modified moment resistance, $M_{Tth,VN,Rd}$, may be calculated using Equation 5.2, with the second and the fourth terms on the right hand side of the equation being set to zero. Thus,

$$M_{Tth,VN,Rd} = M_{Tth,V,Rd} + N_{f,Sd}\beta_f$$

where $\beta_f = y_{pcth} - (y_{po} + \frac{\alpha_f}{2})$ and $N_{f,Sd} = 2\alpha_f b_f f_{vf}$. The depth of the stress block in the flange in this case is given by:

$$\alpha_f = \frac{N_{T,Sd}}{2b_f f_{vf}}$$

Case 3) Nominal PNA in steel web and shifted PNA in steel web

The same reasoning can be applied to the calculation of the modified moment resistance if the nominal PNA is located within the web. In this case, $M_{Tth,VN,Rd}$ can be found using Equation 5.2 with the second and third terms being set to zero. Thus,

$$M_{Tth,VN,Rd} = M_{Tth,V,Rd} + N_{w,Sd}\beta_w$$

The force resisted by the web is equal to the applied axial force and the depth of the stress block in the web, α_w, is given by:

$$\alpha_w = \frac{N_{T,Sd}}{2t_w f_{vw}}$$

This case is illustrated in Figure 5.7.

5.3.3 Partial shear connection and nominal PNA in steel flange or web

For a composite tee-section under pure bending with partial shear connection, the concrete strength is always not fully utilized. As a result, there is always compression in the top steel tee-section in order to maintain equilibrium, and thus the nominal PNA may locate within the flange or the web. The effect of axial force on the moment resistance may be assessed using the method outlined in the previous

section for full shear connection. Figures 5.6 and 5.7 again illustrate these two cases, respectively.

5.4 Modified Moment Resistances of Composite Tee-section at LMS under Axial Force

The effect of axial force on the moment resistance of the composite tee-section at the LMS follows the same philosophy as presented in Section 5.3 for composite tee-section at the HMS. The axial force arising from the global bending action is assumed to act at the plastic axial centroid (PC) of the composite tee-section. The stress block for pure bending is modified by shifting the PNA to a new position allowing for the presence of the applied axial force. The modified moment resistance may then be found by adding or subtracting the moments contributed by the axial forces resisted by the concrete, the flange, and the steel web as appropriate.

5.4.1 Full shear connection and nominal PNA in concrete

Consider a case where there is full shear connection and $N_{c,Rd}$ is larger than $N_{a,V,Rd}$, the composite tee-section at the LMS under pure bending may assume a stress block as shown in Figure 5.8b.

Case 1) Shifted PNA in steel web

If a large axial force is applied to the composite tee-section, it will be distributed to the concrete first, then to the flange, and finally to the web. The force resisted by each element is shown in Figure 5.8c and the final stress block is shown in Figure 5.8d where the nominal PNA is shifted to be located within the web. The concrete slab can resist an axial force which is equal to its residual strength, the smaller of $N_{c,Rd}$ and $N_{sh,Rd}$ minus $N_{a,V,Rd}$, and the depth of the stress block is given by:

$$\alpha_c = \frac{Minimum\,(N_{c,Rd}, N_{sh,Rd}) - N_{a,V,Rd}}{0.85 b_c f_{ck}}$$

This concrete force is acting opposite to the positive moment resistance with a lever arm, β_c, measured from the PC. So it has a non-beneficial effect and the moment resistance of the composite tee-section is reduced. The remaining applied axial force is then distributed to the flange and also the web if the strength of the former is fully utilized. The depths of the stress blocks in these two elements are given as follows:

$$\alpha_f = t_f \qquad \text{and } \alpha_w = \frac{N_{T,Sd} - N_{c,Sd} - N_{f,Sd}}{2t_w f_{vw}}$$

where $N_{f,Sd} = 2\alpha_f b_f f_{vf}$ and $N_{c,Sd} = 0.85\alpha_c b_e f_{ck}$. The force in the web, $N_{w,Sd}$, is given by:

$$N_{w,Sd} = 2\alpha_w t_w f_{vw}$$

Since the forces in the flange and the web are located below the PC and act in the direction of positive moment resistance, they are considered to have beneficial effect on the moment resistance of the composite tee-section. The modified moment resistance due to the additional moments created by all these three forces can be calculated as follows:

$$M_{Tll,VN,Rd} = M_{Tll,V,Rd} - N_{c,Sd}\beta_c - N_{f,Sd}\beta_f - N_{w,Sd}\beta_w \qquad \text{Equation 5.3}$$

where: $\beta_c = y_{pctl} - (d_e - \alpha - \frac{\alpha_c}{2})$, $\beta_f = y_{pctl} - (h_t + \frac{\alpha_f}{2})$, and

$\beta_w = y_{pctl} - (h_t + a_f + \frac{\alpha_w}{2})$.

Case 2) Shifted PNA in steel flange

If the applied axial force is large enough to shift the PNA to be located in the steel flange only, then the fourth term on the right hand side of Equation 5.3 will vanish. Thus, the modified moment resistance of the composite tee-section is given

by:

$$M_{Tfl,VN,Rd} = M_{Tfl,V,Rd} - N_{c,Sd}\beta_c - N_{f,Sd}\beta_f$$

and other quantities defined in Case 1 remain valid.

Case 3) Shifted PNA in concrete

The same reasoning can be applied to the calculation of the modified moment resistance of the composite tee-section if the shifted PNA is located within the concrete. In this case, $M_{Tfh,VN,Rd}$ may be found using Equation 5.3 with the third and the fourth terms set to zero. Thus,

$$M_{Tfl,VN,Rd} = M_{Tfl,V,Rd} - N_{c,Sd}\beta_c$$

and other quantities defined in Case 1 remain valid.

5.4.2 Full shear connection and nominal PNA in flange or web

Similar to the case of composite tee-section at the HMS, the nominal PNA locates within the flange or the web when the strength of the concrete is less than that of the top steel tee-section. In this case, only the part of the steel tee-section originally under tension is able to resist any applied axial compressive force.

Case 1) Nominal PNA in steel web and shifted PNA in steel web

When the nominal PNA locates within the web as shown in Figure 5.9, both the flange and part of the web may take axial forces. The axial resistance of the flange is fully utilized and the applied axial force resisted by the web, $N_{w,Sd}$, is given by:

$$N_{w,Sd} = N_{T,Sd} - N_{f,Sd}$$

where $N_{f,Sd} = 2\alpha_f b_f f_{yf}$ and $\alpha_f = t_f$. The depth of the stress block in the web is given by:

$$\alpha_w = \frac{N_{w,Sd}}{2t_w f_{yw}}$$

The modified moment resistance of the composite tee-section is given by:

$$M_{Ttl,VN,Rd} = M_{Ttl,V,Rd} - N_{f,Sd}\beta_f - N_{w,Sd}\beta_w$$

where $\beta_f = y_{pctl} - (h_t + \frac{\alpha_f}{2})$, and $\beta_w = y_{pctl} - (h_t + a_f + \frac{\alpha_w}{2})$.

Case 2) Nominal PNA in steel web and shifted PNA in steel flange

When the axial force is not large enough to shift the PNA to be located within the web, only part of the flange is resisting the axial force and the depth of the stress block is given by:

$$\alpha_f = \frac{N_{T,Sd}}{2b_f f_{vf}}$$

The modified moment resistance of the composite tee-section is given by:

$$M_{Ttl,VN,Rd} = M_{Ttl,V,Rd} - N_{f,Sd}\beta_f$$

where $\beta_f = y_{pctl} - (h_t + \frac{\alpha_f}{2})$.

Case 3) Nominal PNA in steel flange and shifted PNA in steel flange

When the nominal PNA is located within the steel flange as shown in Figure 5.10, then the shifted PNA always stay within the flange. Thus, all quantities defined in Case 2 are valid and the modified moment resistance of the composite tee-section is again given by:

$$M_{Ttl,VN,Rd} = M_{Ttl,V,Rd} - N_{f,Sd}\beta_f$$

5.4.3 Partial shear connection and nominal PNA in flange or web

For those composite tee-sections with partial shear connection, the nominal PNA falls either in the flange or the web. The procedures for assessing the effect of the axial force on the moment resistance are exactly the same as discussed in Section 5.4.2; both the quantities and the formulas in that section can be used to calculate the

modified moment resistances. The stress blocks are shown in Figures 5.9 and 5.10 while explicit formulas are given in Chapter 6.

5.5 Axial-Moment Interaction Curves for Composite Tee-sections

In order to examine the structural behavior of composite beams with web openings, axial-moment interaction curves are plotted for the composite tee-sections at both the LMS and the HMS of the perforated section shown in Figure 5.11. The depth of the web opening is equal to 65% depth of the steel beam of UB457x152x82 S355. For direct comparison, the degree of shear connection is assumed to be the same at both the LMS and the HMS. The following two cases are considered:

1) Full shear connection with nominal PNA in concrete with n_o =1 and n_L = 20

2) Partial shear connection with nominal PNA in flange with n_o = 1 and n_L = 6

Shear force ratios of 0, 0.5, and 0.9 are considered. Figure 5.12a shows the interaction curves for the composite tee-sections with full shear connection with nominal PNA in the concrete slab. Under different shear force ratios, all interaction curves have similar shapes. Basically, the presence of shear force causes a reduction in the moment resistances of composite tee-sections at both the LMS and the HMS. The reduction is not significant when the shear force ratio, v, is small, but is apparent when v is large. The moment resistance of composite tee-section at the HMS is always higher than that of the composite tee-section at the LMS. Since there is full shear connection and the nominal PNA is located in the concrete slab, the concrete slab is able to resist any additional axial force. As can be seen from the graph, addition of axial force to the concrete slab has caused the moment resistance to increase until the compressive strength of the concrete is fully utilized. Any further increase of axial force will cause a reduction in the moment resistance.

Figure 5.12b shows the interaction curves for the composite tee-sections with

partial shear connection with nominal PNA in the steel flange. In this case, the concrete slab cannot resist any additional axial force and thus, there is always reduction in the moment resistance whenever the axial force is applied to the composite tee-sections. Everything else is similar to the case shown in Figure 5.12a.

5.6 Perforated Section Analysis

The perforated section analysis for a composite beam with a web opening is similar to that of a steel beam with a web opening. It includes the checking of the flexural, the shear, and also the Vierendeel failures of the perforated section. Flexural and shear failures can be checked using conventional methods by considering the moment and shear resistances of the perforated section. To check for the Vierendeel failure, the moment resistances of the top composite tee cross-section and the bottom steel tee cross-section at both the LMS and the HMS of the perforated section under global shear force and moment should be checked.

5.6.1 Philosophy

Consider the force distribution in the perforated section of a composite beam as shown in Figure 5.1. Each tee-section near the corners of the web opening is subjected to local shear and axial force, and bending moment simultaneously. These local forces and moments can be related to the global shear force and moment at the centerline of the web opening by considering the equilibrium at the LMS and the HMS of the perforated section, respectively. It should be noted that the lines of action of the axial forces at both the LMS and the HMS of the composite tee-section do not coincide due to the different degrees of shear connection, and also the stress blocks modified by local moments.

Considering the equilibrium at the HMS of the perforated section, the global moment at the centerline of the opening, M_{SH}, can be written as:

$$M_{Sd} = N_{T,Sd} z_H + M_{th,Sd} + M_{bh,Sd} - \frac{V_{Sd} a_o}{2} \quad \text{Equation 5.4}$$

where z_H is the moment arm between the axial forces acting on the top composite and the bottom steel tee-sections at the HMS of the perforated section. Similarly, the global moment can also be obtained by considering the equilibrium at the LMS of the perforated section as follows:

$$M_{Sd} = N_{T,Sd} z_L - M_{tl,Sd} - M_{bl,Sd} + \frac{V_{Sd} a_o}{2} \quad \text{Equation 5.5}$$

where z_L is the moment arm between the axial forces acting on the top composite and the bottom steel tee-sections at the LMS.

By summing the above two equations to eliminate the shear force, the global moment can be expressed in terms of only the local axial forces and bending moments given as follows:

$$M_{Sd} = N_{T,Sd} \left(\frac{z_H + z_L}{2}\right) + \frac{M_{th,Sd} + M_{bh,Sd} - M_{tl,Sd} - M_{bl,Sd}}{2}$$

For any given global moment at the centerline of the perforated section, the above equation can be rearranged to give the axial force acting on the top composite and the bottom steel tee-sections as follows:

$$N_{T,Sd} = \frac{2M_{Sd} - (M_{th,Sd} + M_{bh,Sd} - M_{tl,Sd} - M_{bl,Sd})}{z_H + z_L} \quad \text{Equation 5.6}$$

The moment resistances of the composite and steel tee-sections can be evaluated through the use of formulae based on the methods outlined in Sections 5.3 and 5.4. However, since the axial force also depends on the magnitudes of the moment resistances, iterations are required. The moment resistances found for the tee-sections must also satisfy the equilibrium of the top composite and the bottom steel tee-sections. Since the axial forces at both ends of the bottom tee-sections

coincide, the equilibrium equation can be written as:

$$M_{bl,Sd} + M_{bh,Sd} = V_{ab,Sd} a_o \qquad \text{Equation 5.7}$$

where $V_{ab,Sd}$ is the shear force applied to the bottom tee-section and a_o is the horizontal dimension of the web opening. The equilibrium of the composite tee-section requires that:

$$N_{T,Sd}(z_H - z_L) + M_{tl,Sd} + M_{th,Sd} = (V_{at,Sd} + V_{c,Sd}) a_o \qquad \text{Equation 5.8}$$

where $V_{at,Sd}$ and $V_{c,Sd}$ are the shear forces resisted by the top steel tee-section and concrete slab, respectively. A complete design procedure for composite beams with web openings is given in Chapter 6.

5.6.2 Moment-shear interaction curves for perforated sections

The proposed design method is used to generate moment-shear $(M\text{-}V)_o$ interaction curves for perforated sections in composite beams with web openings. Details of the composite beam are shown in Figure 5.13. Universal steel beam sections of UB457x152x52 S355 and UB457x152x82 S355 are considered. Rectangular web openings with an aspect ratio of two, and square web openings are investigated. The openings have a height equal to either 50% or 75% of the depth of the steel beam. The results are presented in Figures 5.14a and 5.14b. Both figures can be considered together as the interaction curves are basically of the same shape. The interaction curves are obtained by determining the load capacities of the beams when web openings are placed at different locations along the beam spans. The shear connector configurations around the perforated section when the web openings are placed at various locations along the beam length are presented in Table 5.1.

When the web openings are located at the support, where the moment is zero, the shear resistances are less than the pure shear resistances of the perforated sections due to the Vierendeel action. Although this situation is not physically

possible in practice, it indicates a scenario where there is no local axial force acting on the tee-sections above and below the web openings.

As the applied moment increases, the shear resistances of the beams with small square and rectangular web openings with h_o/h equals 50% depth of the steel section increase slightly at the beginning and then drop steadily. However, the shear resistances of the beams with large square and rectangular web openings with h_o/h equals 75% depth of the steel section decrease at the beginning and may increase slightly thereafter.

At high moment, the $(M\text{-}V)_o$ interaction curves of the composite beams with web openings of the same height finally converge. At the points of convergence, the failure mode for these beams becomes that of flexure. This is because the moment resistances of the composite perforated sections are lower than the Vierendeel resistances. As indicated by the interaction curves, the beams with the deepest and the longest web openings are the weakest of all.

5.6.3 Calibration of the proposed design method with experimental results

A total number of forty test data of composite beams with concentric rectangular web openings are selected from the established database to calibrate the proposed design method. Moreover, back analysis of the current SCI design method is also presented for comparison. The calibrations are divided into three groups based on the type of the concrete slabs as follows:

Calibration I: Composite beams with solid slabs, i.e. no decking

Calibration II: Composite beams with decking placed parallel to the steel beams

Calibration III: Composite beams with decking placed transversely to the steel beams

Only composite beams with un-reinforced rectangular web openings are

considered. Tables 5.2a through 5.2c contain information pertaining to the above three groups of test data and also the calibration results for the two design methods. Items in the columns of the tables are self-explanatory. The model factors for load capacity, as defined in Section 3.5.4, are used here again to compare the relative accuracy of the two design methods.

a) Calibration I

In Table 5.2a, results for eight composite beams with rectangular web openings utilizing solid concrete slabs are presented. The ratios of the opening heights to depths of the steel sections range from 59% to 69% and thus the sizes of the openings can be considered to be medium to large. The model factors predicted by the proposed design method range from 0.73 to 1.19 with an average of 1.09 for model factors that are above unity, while those predicted by the SCI design method range from 0.7 to 1.64 with an average of 1.31 for model factors that are above unity. This indicates an improvement of about 16% with the use of the proposed design method. Meanwhile, the averages of the model factors that are below unity are 0.76 and 0.78 as predicted by the proposed method and the SCI method, respectively.

b) Calibration II

Only three beams have composite slabs with decking placed parallel to the steel beams. The model factors predicted by the proposed design method range from 1.34 to 1.42 with an average of 1.39, while those predicted by the SCI design method range from 1.03 to 1.3 with an average of 1.13. The difference between the averages is about 23%. The proposed design method seems to be more conservative for this type of deck orientation. However, it is not conclusive as the number of test data is scarce.

c) Calibration III

The majority of the composite beams have concrete slabs with decking placed transversely to the steel beams and this accounts for twenty-nine beams of the selected test data. The ratios of the opening depths to the steel sections vary from 38% to 71% and the opening aspect ratios range from 1.0 to 2.92. Table 5.2c summarizes the results predicted by both the SCI method and the proposed design method. While the numbers of model factors that are above and below unity are 23 and 6, respectively, as predicted by the proposed method, the numbers are 21 and 8, respectively, as predicted by the SCI method. The proposed design method predicts a range of model factors from 0.71 to 1.37 with an average of 1.15 for model factors that are above unity. Meanwhile, the model factors predicted by the SCI method range from 0.71 to 2.00 with an average of 1.21 for model factors which are above unity. The improvement with the proposed design method is about 5%. There is no difference between the averages for the model factors that are below unity as predicted by the two methods, which is 0.86.

5.7 Conclusions

Based on the study of the composite tee-sections and the perforated section of composite beams with rectangular web openings, the following conclusions can be made.

1) Design formulas for the axial resistance, the shear resistance, and the nominal plastic moment resistance of composite tee-sections are derived based on basic structural design principles and plastic stress blocks. Due to global moment at the perforated section and different degrees of shear connection at different locations along a composite beam, the stress blocks at both the LMS and the HMS of the web opening are different and thus the nominal plastic moment resistances are considered separately. The axial forces arising from global

bending action are assumed to act at the plastic axial centroids of the composite tee-sections.

2) Simple design formulas for composite tee-sections based on plastic stress blocks are derived analytically to allow for interaction of axial force and bending moment. It is found that the plastic moment resistances of the composite tee-sections at both the LMS and the HMS of the web openings are always modified in the presence of axial force. In the case of full shear connection, the plastic moment resistances of the composite tee-sections are always increased under low axial force. However, there is always reduction in the plastic moment resistances of the composite tee-sections in the presence of axial force when there is partial shear connection. The moment resistance of the composite tee-section at the HMS is always higher than that of the composite tee-section at the LMS.

3) The shear effect on the plastic moment resistance of a composite tee-section is allowed for through the reduction of the bending strengths of both the web and the flange based on von Mises' yielding criterion. The concrete slab is allowed to carry shear force. Axial-moment interaction curves for the composite tee-sections at both the LMS and the HMS of the web opening under different values of shear force are also developed. It is found that the effect of shear force on the plastic moment resistance of a composite tee-section is not as significant as the axial force does.

4) In order to assess the load capacities of composite beams with web openings, the design formulas for composite tee-section analysis are extended for the analysis of perforated section by considering the equilibrium of forces around the perforated section. Moment-shear interaction curves for composite beams

with rectangular web openings are also presented and discussed.

5) Forty test data are selected from the established database for the calibration of the proposed design method. Model factors predicted by both the proposed design method and the current SCI design method are compared. It is demonstrated that the proposed design method is able to provide improvement over the SCI design method, especially for composite beams with rectangular web openings utilizing solid slabs and slabs with profiled steel decking placed transversely to the steel beams.

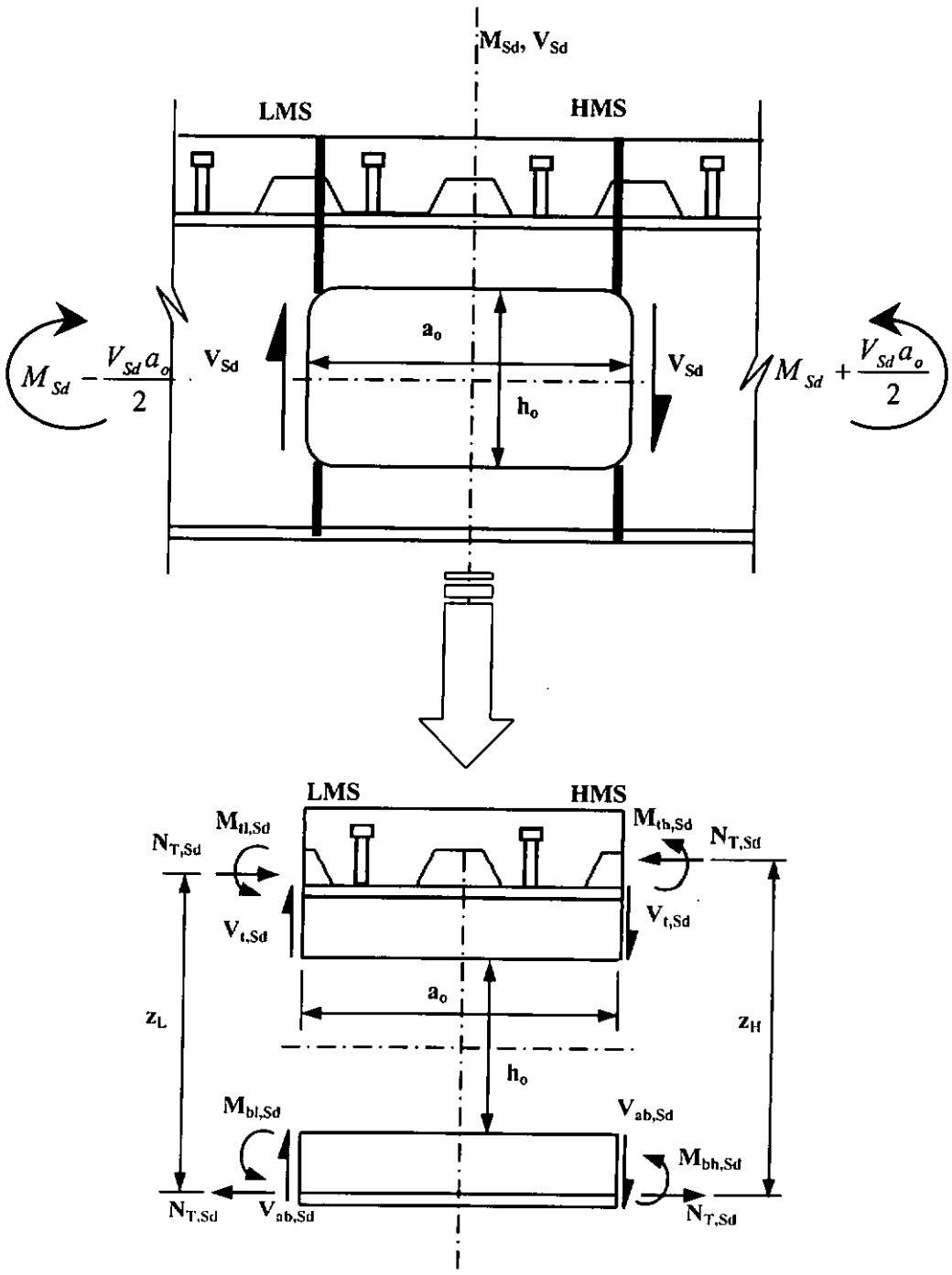

Figure 5.1 Global and local actions at perforated section of a composite beam

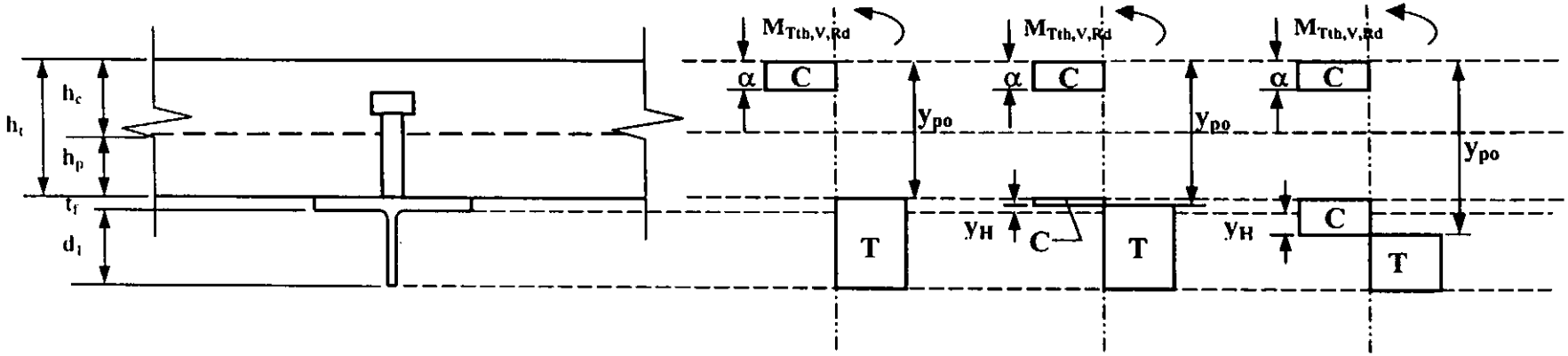

(a) (b) PNA in concrete (c) PNA in flange (d) PNA in web

Figure 5.2 Bending stress blocks of composite tee-section at HMS under zero axial force

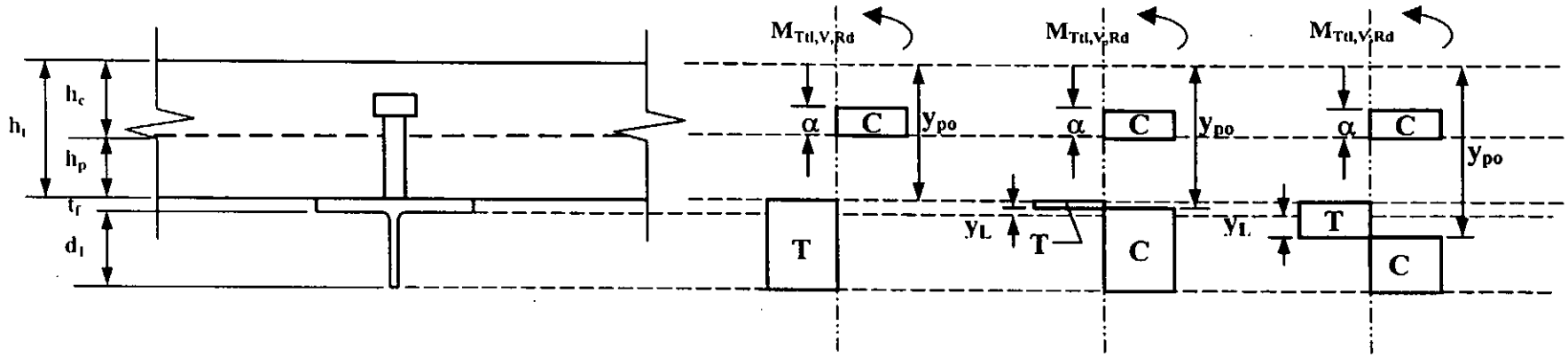

(a) (b) PNA in concrete (c) PNA in flange (d) PNA in web

Figure 5.3 Bending stress blocks of composite tee-section at LMS under zero axial force

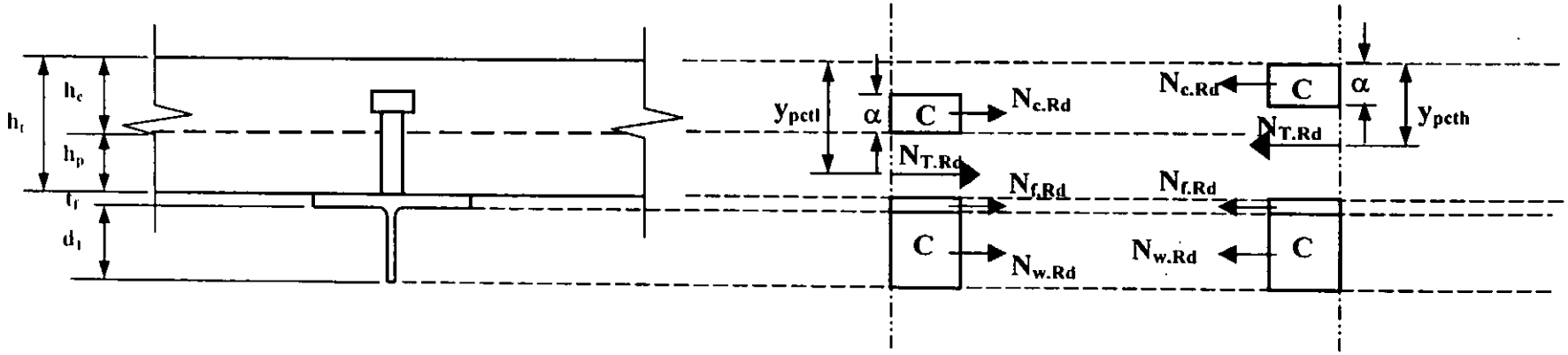

Figure 5.4 Plastic axial centroids of composite tee-sections

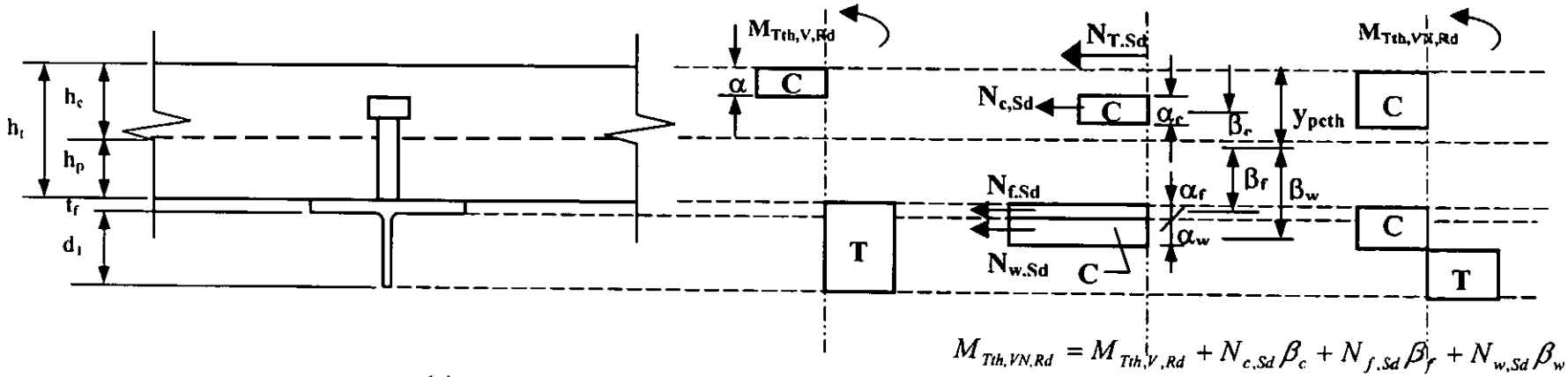

Figure 5.5 Bending stress blocks of composite tee-section at HMS under axial force (nominal PNA in concrete)

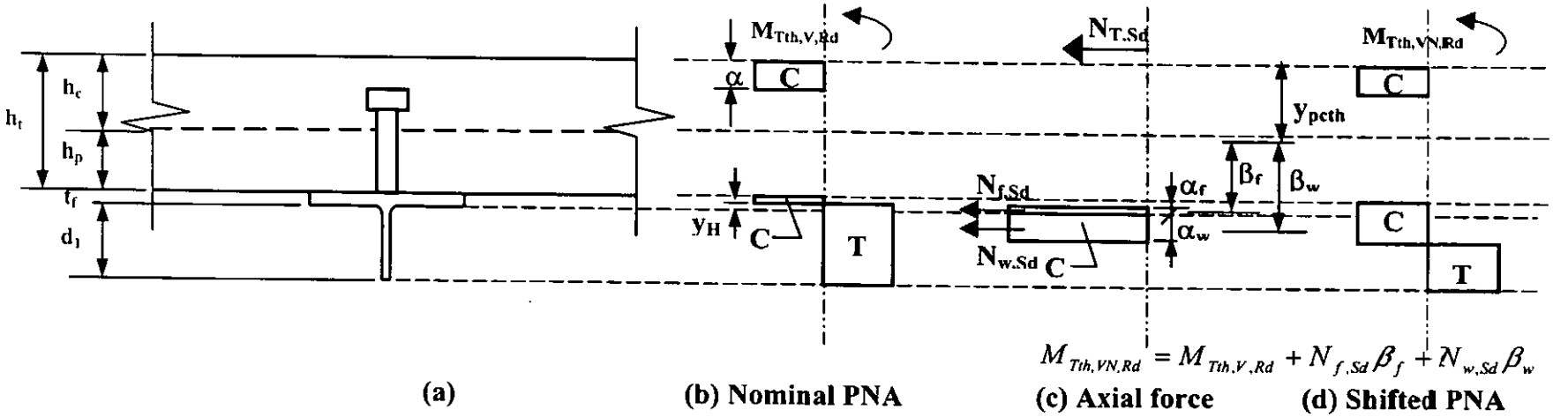

Figure 5.6 Bending stress blocks of composite tee-section at HMS under axial force (nominal PNA in flange)

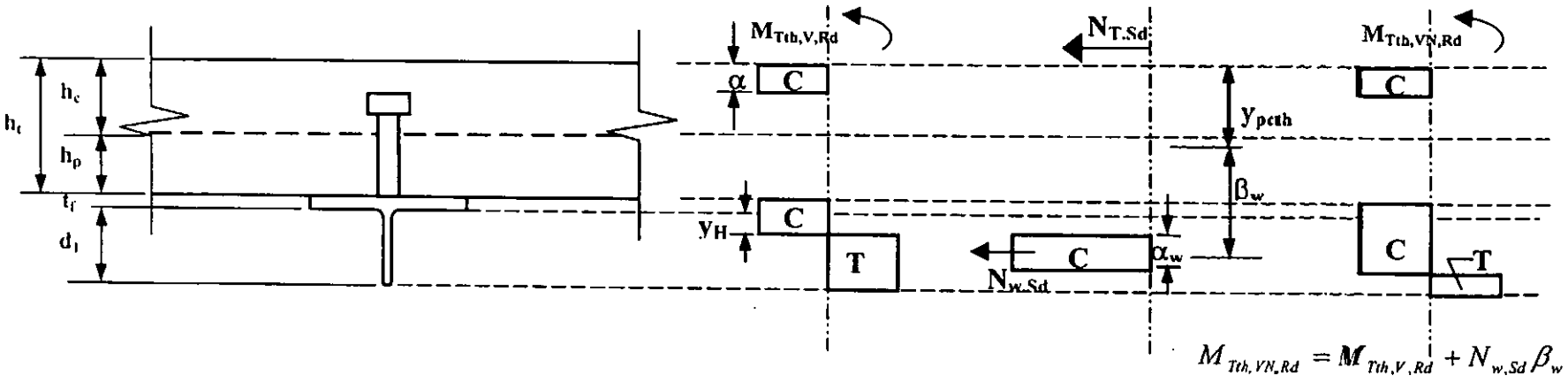

Figure 5.7 Bending stress blocks of composite tee-section at HMS under axial force (nominal PNA in web)

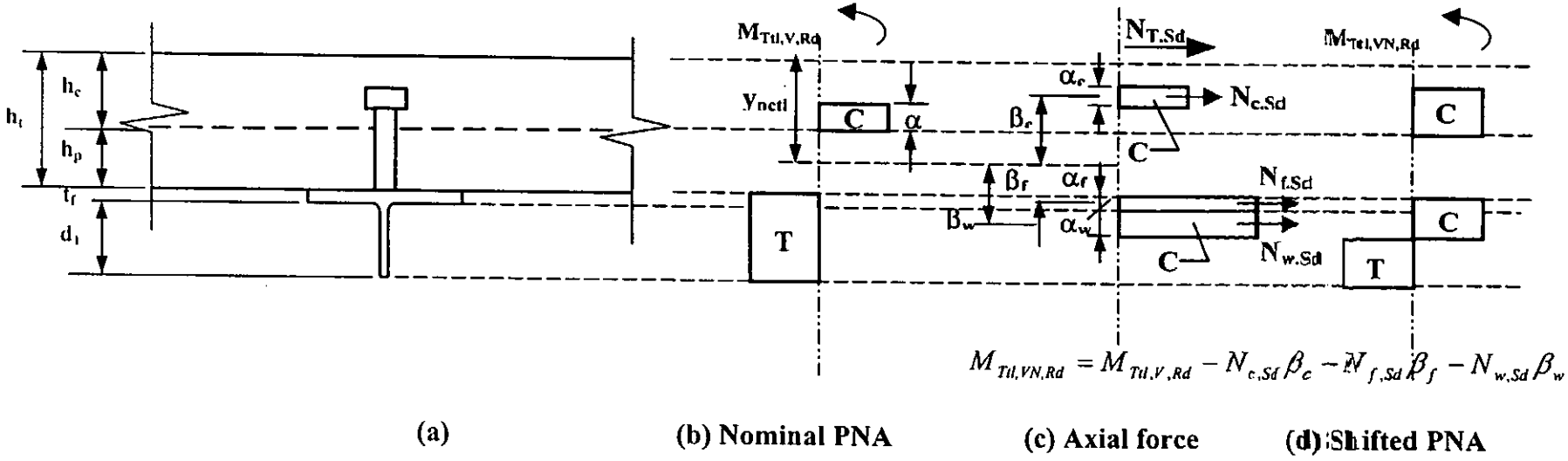

Figure 5.8 Bending stress blocks of composite tee-section at LMS under axial force (nominal PNA in concrete)

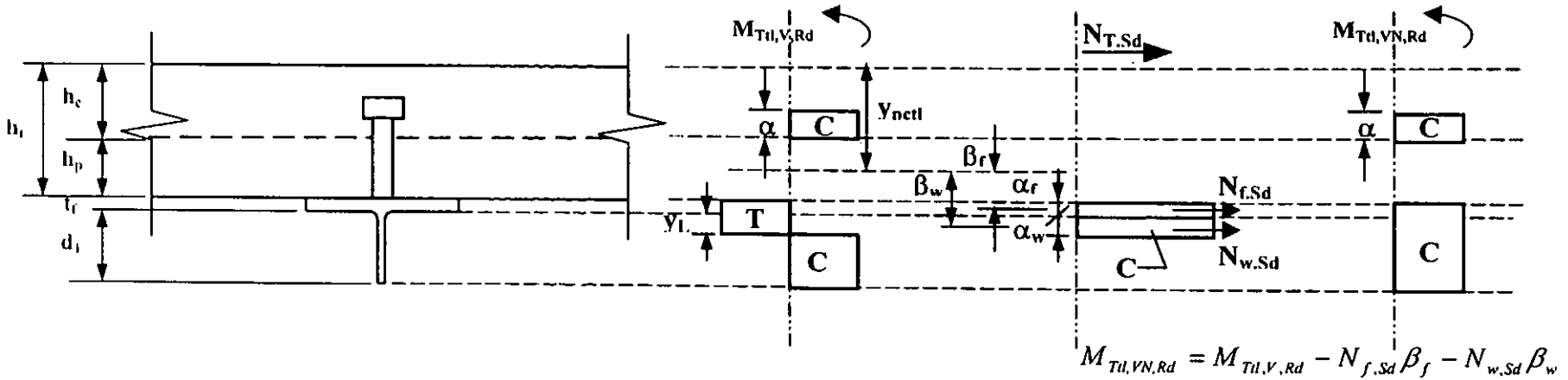

Figure 5.9 Bending stress blocks of composite tee-section at LMS under axial force (nominal PNA in web)

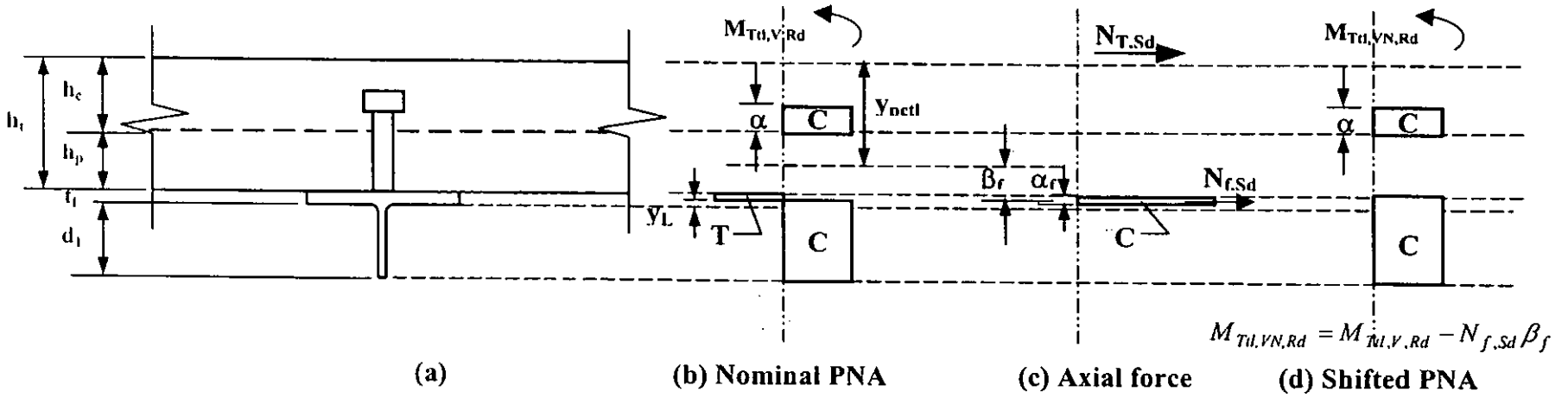

Figure 5.10 Bending stress blocks of composite tee-section at LMS under axial force (nominal PNA in flange)

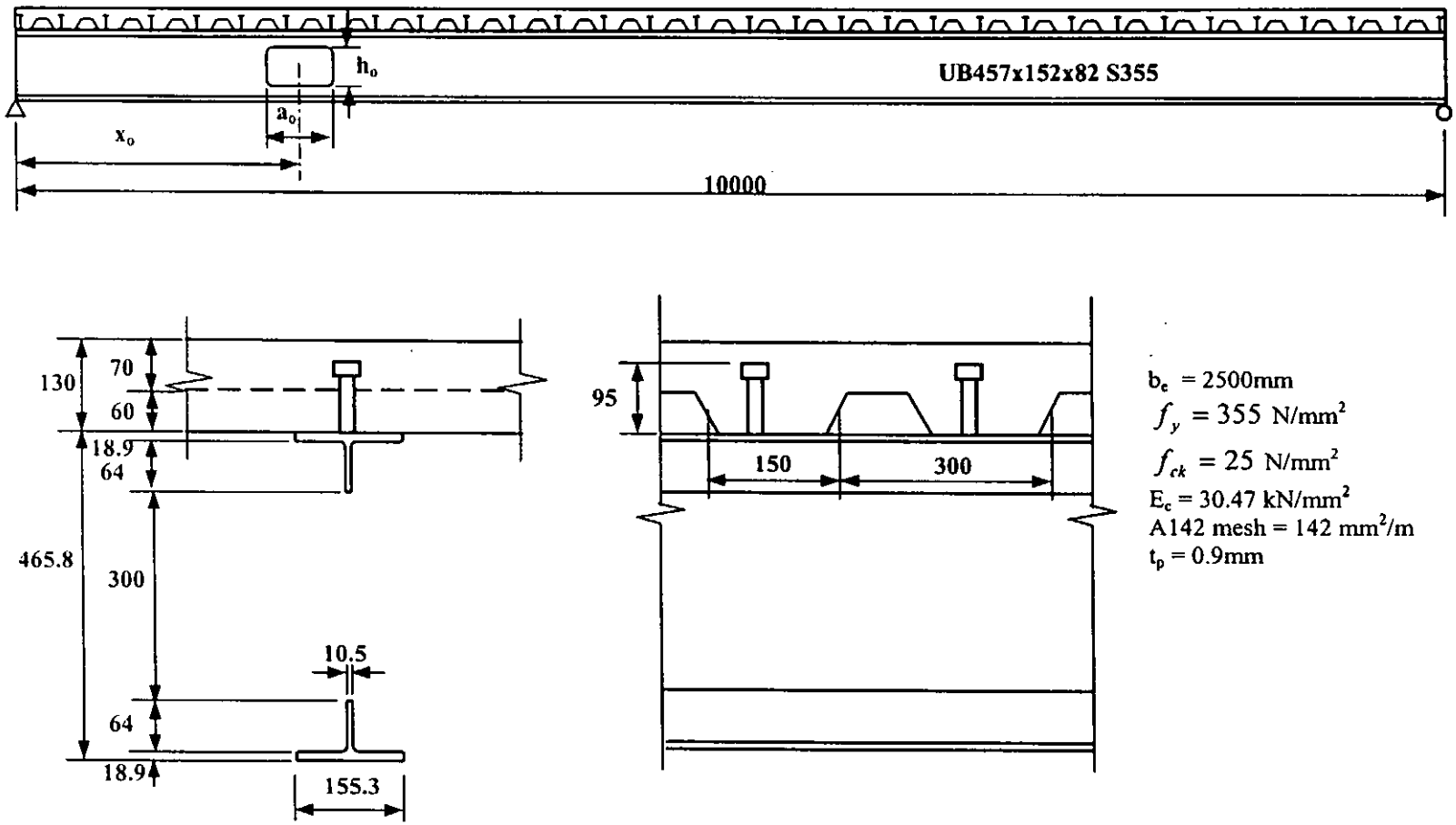

Figure 5.11 Configuration of the reference composite beam for tee-section analysis

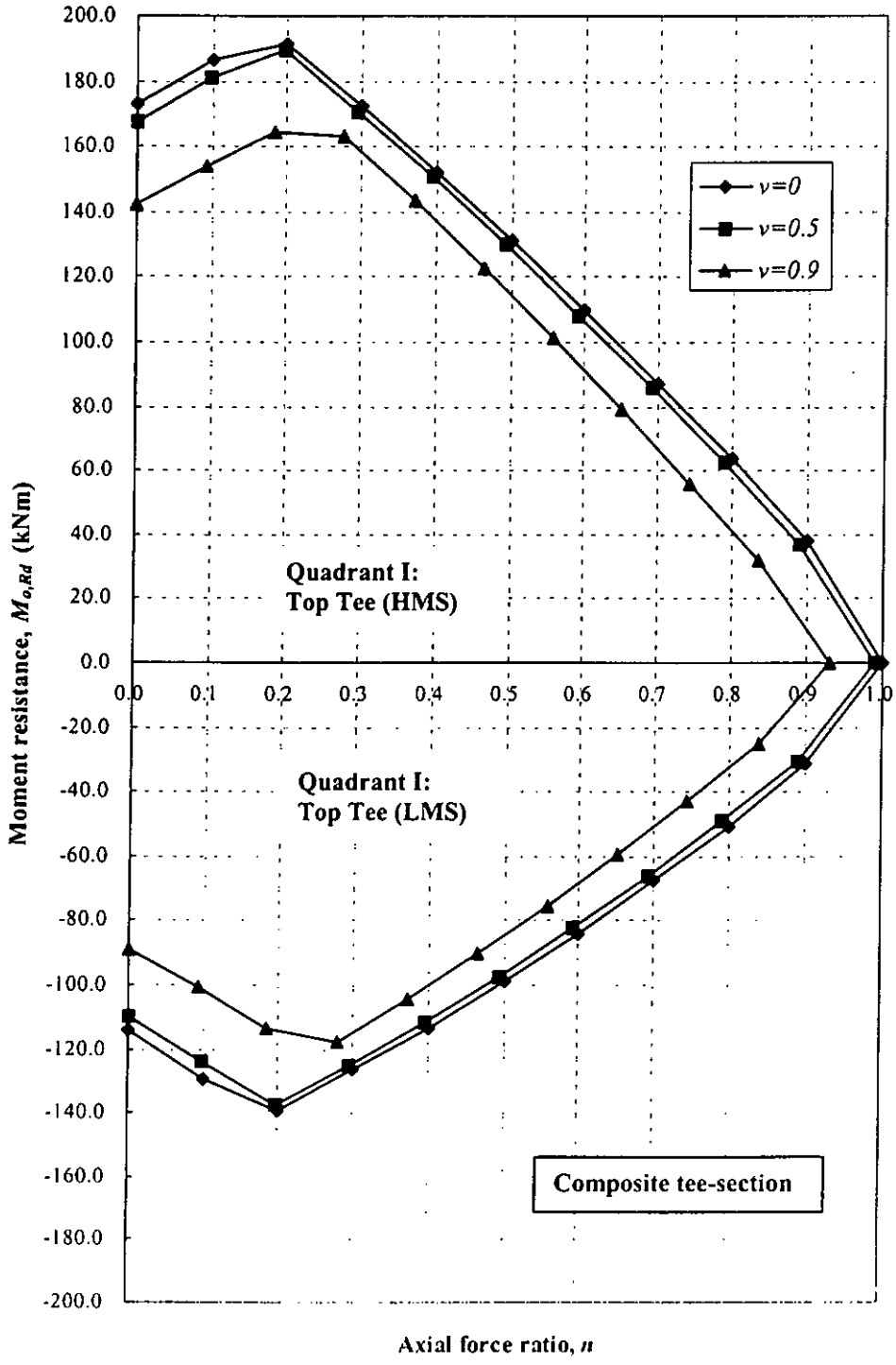

Figure 5.12a Axial-moment interaction curves for composite tee-sections (full shear connection with nominal PNA in concrete)

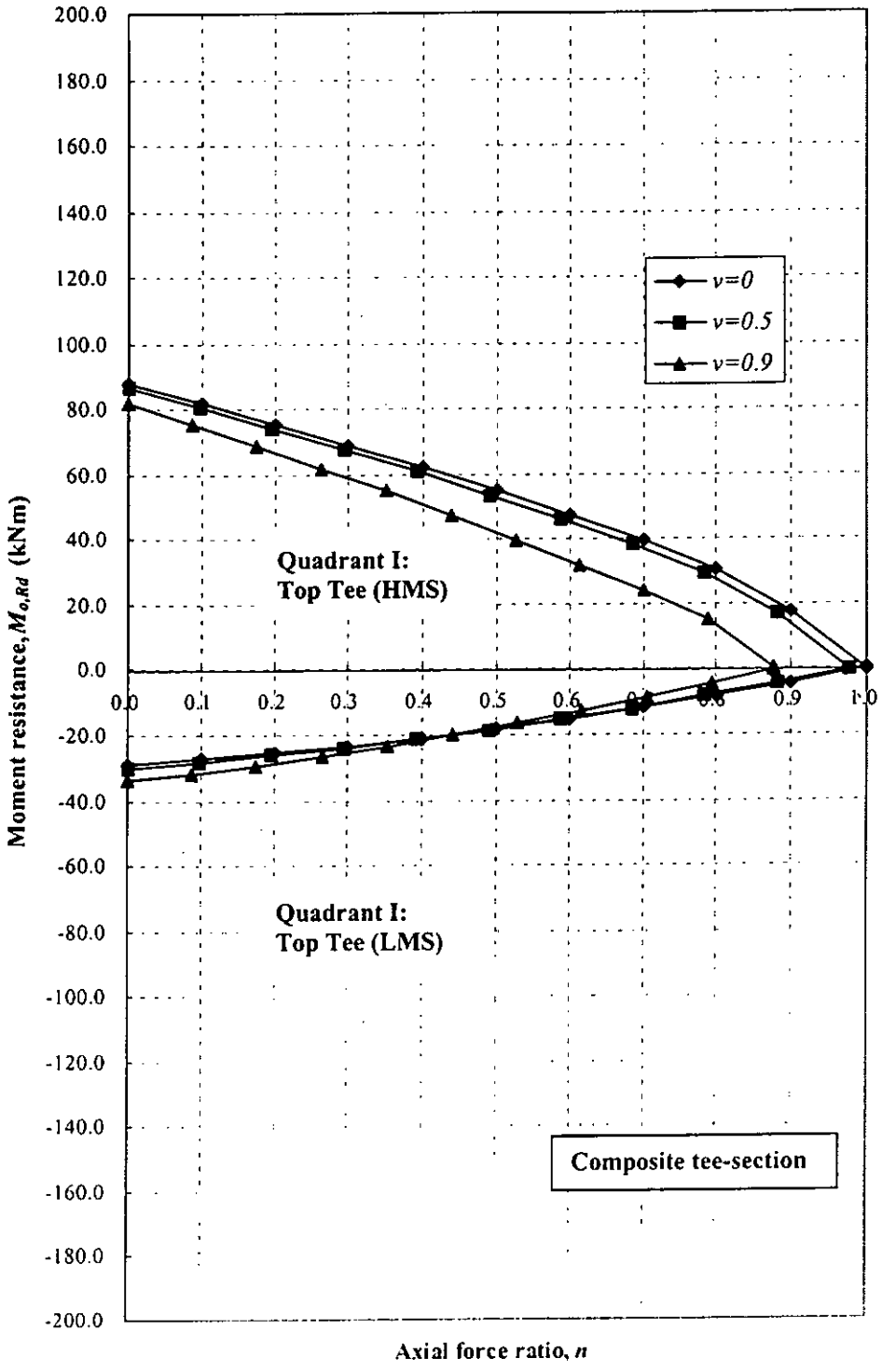

Figure 5.12b Axial-moment interaction curves for composite tee-sections (partial shear connection with nominal PNA in flange)

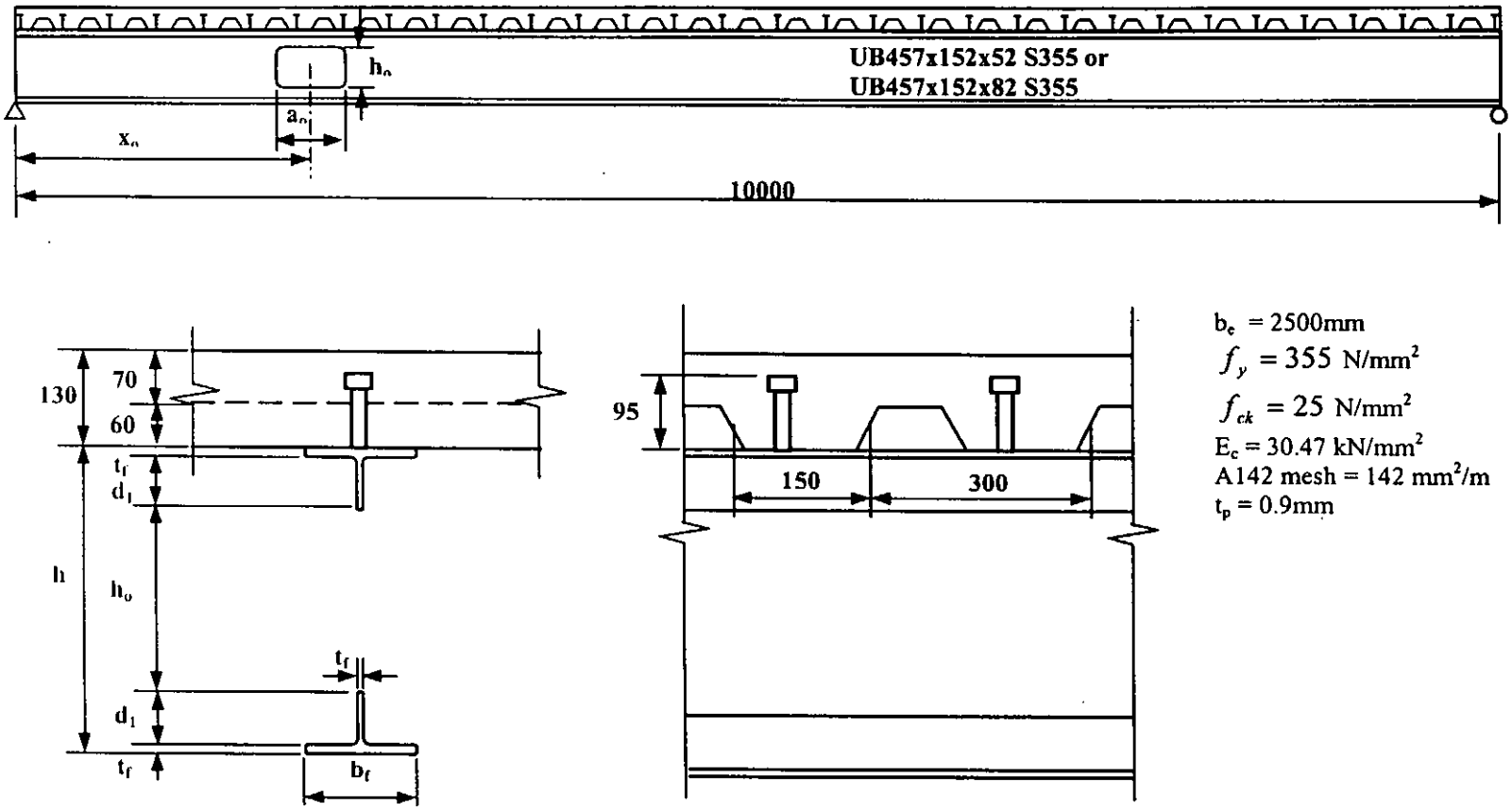

Figure 5.13 Configuration of the reference composite beam for perforated section analysis

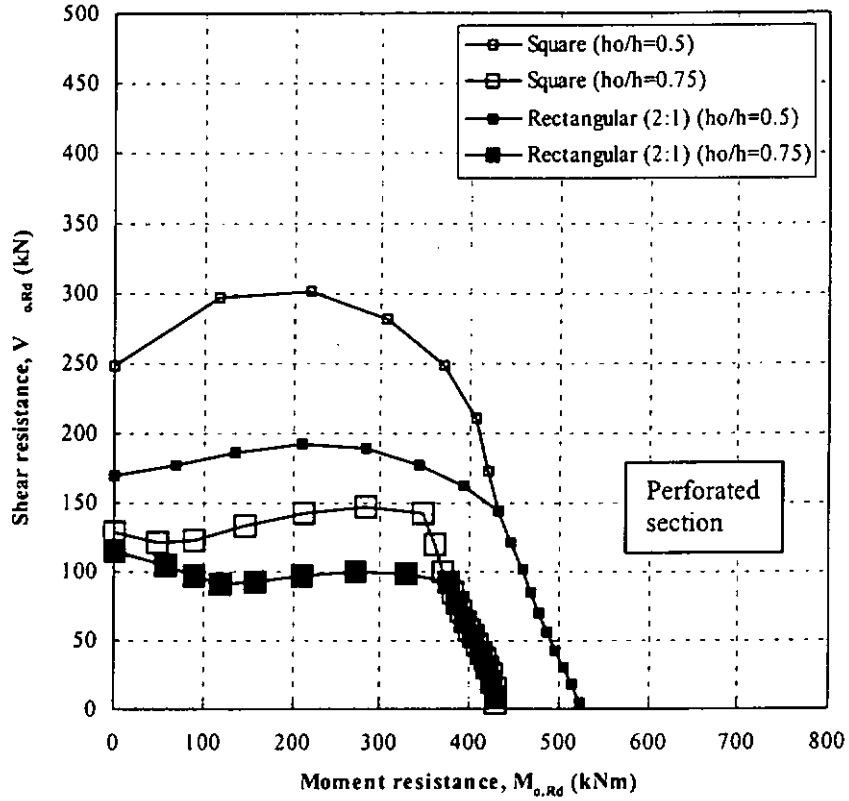

Figure 5.14a Moment-shear interaction curves for composite beam using UB457x152x52 S355 with square or rectangular web openings

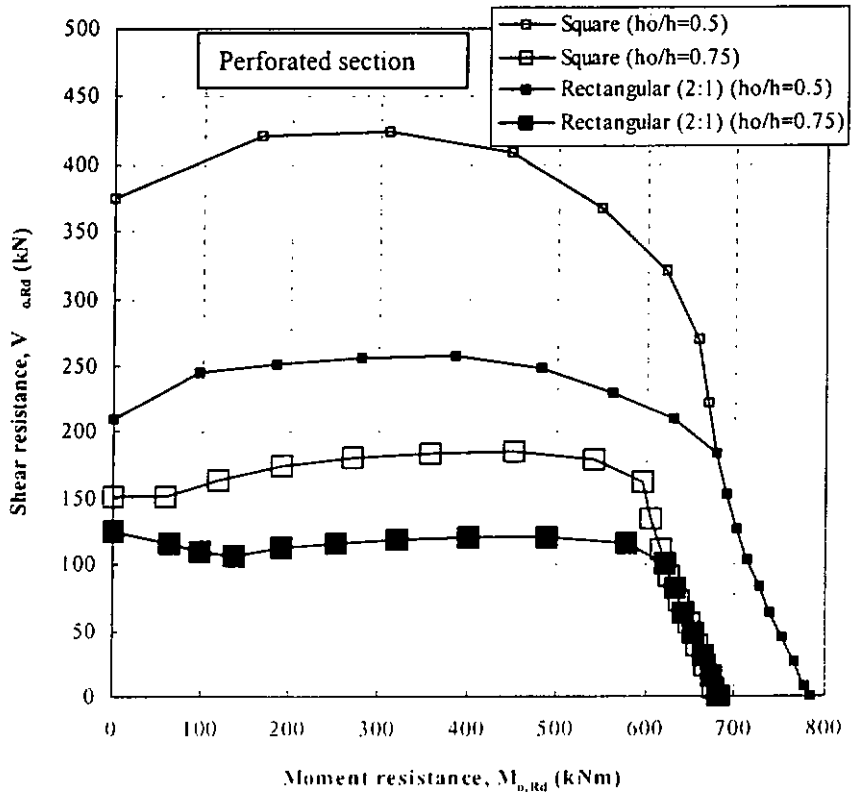

Figure 5.14b Moment-shear interaction curves for composite beam using UB457x152x82 S355 with square or rectangular web openings

Table 5.1 Shear connector configurations

UB457x152x52 and UB457x152x82 S355					
Square (h_o/h=0.5, h_o/h=0.75), Rectangular (h_o/h=0.5)			Rectangular (h_o/h=0.75)		
x_o (mm)	n_L	n_o	x_o (mm)	n_L	n_o
0	0	0	0	0	0
375	1	1	525	1	2
675	2	1	825	2	2
975	3	1	1125	3	2
1275	4	1	1425	4	2
1575	5	1	1725	5	2
1875	6	1	2025	6	2
2175	7	1	2325	7	2
2475	8	1	2625	8	2
2775	9	1	2925	9	2
3075	10	1	3225	10	2
3375	11	1	3525	11	2
3675	12	1	3825	12	2
3975	13	1	4125	13	2
4275	14	1	4425	14	2
4575	15	1	4725	15	2
4875	16	1	-	-	-

Notation:

x_o = Location of opening centerline from support

n_o = Number of shear connectors over web opening

n_L = Number of shear connectors from support to LMS of the opening

Table 5.2a Comparison of the results from proposed design method and SCI design method on composite beams with concentric rectangular web openings (no decking) - Calibration 1

Test number	Experiment designation	Span to depth ratio	Opening aspect ratio	Opening height to beam depth	Location of opening along beam span	Failure M/V ratio at opening centerline	Load capacity in test	Failure mode observed in test	Results from Proposed design method						Results from SCI design method					
		L/h	a_o/h_o	h_o/h	x_o/L	M_{Sd}/V_{Sd} (m)	P_{test} (kN)	FM	m	v	mv	P_1	FM	Ψ_1	m	v	mv	P_2	FM	Ψ_2
1	CR66	11.16	1.73	0.69	0.24	0.95	167.2	Vi	0.40	0.51	0.99	230.1	Vi	**0.73**	0.45	0.63	1.00	238.1	Vi	**0.70**
2	CR69	11.16	1.72	0.69	0.26	1.05	191.2	Vi	0.47	0.54	1.00	238.6	Vi	**0.80**	0.53	0.66	1.00	248.9	Vi	**0.77**
3	CD1	20.56	2.00	0.57	0.29	2.20	143.5	F	1.00	0.60	0.62	133.3	F	**1.08**	1.00	0.48	0.37	87.5	F	**1.64**
4	CD2	15.95	2.00	0.60	0.38	2.83	214.0	Vi	0.87	0.46	0.95	203.9	Vi	**1.05**	0.99	0.48	0.82	183.8	F	**1.16**
5	CD3	15.94	2.00	0.60	0.38	9.92	236.9	F	1.00	0.15	0.28	198.5	F	**1.19**	1.00	0.14	0.21	151.4	F	**1.56**
6	CD4	10.08	2.00	0.61	0.20	0.92	206.8	Vi	0.42	0.56	1.00	206.4	Vi	**1.00**	0.46	0.61	1.00	193.8	Vi	**1.07**
7	CD5	13.82	2.00	0.59	0.29	1.86	209.1	Vi	0.66	0.47	0.92	178.3	Vi	**1.17**	0.86	0.61	1.00	189.0	Vi	**1.11**
8	CD6	13.18	2.00	0.59	0.20	0.92	173.0	Vi	0.58	0.68	0.88	165.8	Vi	**1.04**	0.91	0.93	1.00	196.6	Vi	**0.88**
													Maximum =	**1.19**						**1.64**
													Minimum =	**0.73**						**0.70**
													Average (above unity) =	**1.09**						**1.31**
													Average (below unity) =	**0.76**						**0.78**
													No. of Ψ_1 above unity =	**6**						**5**
													No. of Ψ_1 below unity =	**2**						**3**

Notations:

- m Moment utilization ratio
- v Shear utilization ratio
- mv Vierendeel moment utilization ratio
- P_1 Load capacity predicted by proposed method
- P_2 Load capacity predicted by SCI method
- FM Failure mode: F = Flexural, V = Shear, and Vi = Vierendeel
- Ψ_1 Model factor for load capacity predicted by proposed method = P_{test}/P_1
- Ψ_2 Model factor for load capacity predicted by SCI method = P_{test}/P_2

Table 5.2b Comparison of the results from proposed design method and SCI design method on composite beams with concentric rectangular web openings (decking placed parallel to the steel beams) - Calibration 2

Test number	Experiment designation	Span to depth ratio	Opening aspect ratio	Opening height to beam depth	Location of opening along beam span	Failure M/V ratio at opening centerline	Load capacity in test	Failure mode observed in test	Results from Proposed design method						Results from SCI design method					
		L/h	a_o/h_o	h_o/h	x_o/L	M_{Sd}/V_{Sd} (m)	P_{test} (kN)	FM	*m*	*v*	*mv*	P_1	*FM*	Ψ_1	*m*	*v*	*mv*	P_2	*FM*	Ψ_2
1	DD6B	10.47	2.00	0.60	0.19	1.08	329.6	Vi	0.31	0.36	1.02	245.2	Vi	1.34	0.42	0.53	1.00	307.9	Vi	1.07
2	DD7A	12.80	2.00	0.60	0.16	1.08	167.0	Vi	0.34	0.40	1.65	119.9	Vi	1.39	0.49	0.61	1.00	162.9	Vi	1.03
3	DD7B	12.80	2.00	0.60	0.30	2.02	203.3	Vi	0.58	0.38	1.55	142.7	Vi	1.42	0.73	0.48	1.00	156.9	Vi	1.30
													Maximum =	**1.42**					**Maximum =**	**1.30**
													Minimum =	**1.34**					**Minimum =**	**1.03**
													Average (above unity) =	**1.39**					**Average (above unity) =**	**1.13**
													Average (below unity) =	**-**					**Average (below unity) =**	**-**
													No. of Ψ_1 above unity =	**3**					**No. of Ψ_2 above unity =**	**3**
													No. of Ψ_1 below unity =	**0**					**No. of Ψ_2 below unity =**	**0**

Notations:

m Moment utilization ratio

v Shear utilization ratio

mv Vierendeel moment utilization ratio

P_1 Load capacity predicted by proposed method

P_2 Load capacity predicted by SCI method

FM Failure mode: F = Flexural, V = Shear, and Vi = Vierendeel

Ψ_1 Model factor for load capacity predicted by proposed method = P_{test}/P_1

Ψ_2 Model factor for load capacity predicted by SCI method = P_{test}/P_2

Table 5.2c Comparison of the results from proposed design method and SCI design method on composite beams with concentric rectangular web openings (decking placed transversely to the steel beams) - Calibration 3

Test number	Experiment designation	Span to depth ratio	Opening aspect ratio	Opening height to beam depth	Location of opening along beam span	Failure M/V ratio at opening centerline	Load capacity in test	Failure mode observed in test	Results from Proposed design method						Results from SCI design method					
		L/h	a_o/h_o	h_o/h	x_o/L	M_{Sd}/V_{Sd} (m)	P_{test} (kN)	FM	m	v	mv	P_1	FM	Ψ_1	m	v	mv	P_2	FM	Ψ_2
1	L2N	18.80	1.00	0.66	0.27	3.95	77.5	F	1.00	0.41	0.88	77.0	F	1.01	0.99	0.44	0.83	70.7	F	1.10
2	L3N	18.80	1.80	0.47	0.08	1.02	92.0	Vi	0.47	0.50	1.01	90.0	Vi	1.02	0.47	0.53	1.00	83.8	Vi	1.10
3	L3S	18.80	3.00	0.38	0.09	1.10	92.0	Vi	0.50	0.45	1.01	94.3	Vi	0.98	0.51	0.48	1.00	88.7	Vi	1.04
4	CR11	11.20	1.72	0.69	0.44	0.00	71.6	Vi	0.00	0.30	1.02	52.5	Vi	1.36	0.00	0.24	1.05	35.8	Vi	2.00
5	CR22	11.17	1.72	0.69	0.44	0.00	54.7	Vi	0.00	0.44	0.99	76.8	Vi	0.71	0.00	0.52	1.00	74.6	Vi	0.73
6	CR33	11.13	1.71	0.69	0.44	0.00	53.1	Vi	0.00	0.40	0.99	72.6	Vi	0.73	0.00	0.50	1.00	75.1	Vi	0.71
7	CR44	11.18	1.71	0.69	0.24	0.95	183.6	Vi	0.35	0.46	1.00	203.4	Vi	0.90	0.41	0.62	1.00	227.3	Vi	0.81
8	CR47	11.18	1.71	0.69	0.26	1.05	210.3	Vi	0.36	0.44	1.00	196.2	Vi	1.07	0.41	0.58	1.00	211.8	Vi	0.99
9	CR55	11.16	1.72	0.69	0.24	0.95	183.9	Vi	0.24	0.30	1.03	134.1	Vi	1.37	0.23	0.34	1.00	124.7	Vi	1.47
10	CR58	11.16	1.71	0.69	0.26	1.05	237.7	Vi	0.36	0.43	1.00	191.3	Vi	1.24	0.41	0.57	1.00	206.1	Vi	1.15
11	DD1	10.47	2.00	0.60	0.19	1.08	207.3	Vi	0.34	0.35	1.00	199.2	Vi	1.04	0.38	0.43	1.00	210.4	Vi	0.99
12	DD2	10.47	2.00	0.60	0.36	2.01	217.5	Vi	0.47	0.31	1.15	174.4	Vi	1.25	0.60	0.42	1.00	205.3	Vi	1.06
13	DD3	11.63	2.00	0.60	0.43	13.65	322.7	F	1.00	0.09	0.38	273.0	F	1.18	1.00	0.10	0.28	257.5	F	1.25
14	DD4A	11.05	2.00	0.60	0.34	2.03	282.0	Vi	0.48	0.27	1.02	240.3	Vi	1.17	0.49	0.31	1.00	232.7	Vi	1.21
15	DD4B	11.05	2.00	0.60	0.34	2.03	338.5	Vi	0.49	0.31	1.29	270.1	Vi	1.25	0.45	0.31	1.00	233.6	Vi	1.45
16	DD5A	11.05	2.00	0.60	0.34	2.05	299.4	Vi	0.58	0.32	1.00	278.1	Vi	1.08	0.63	0.38	1.00	285.6	Vi	1.05
17	DD6A	10.18	2.00	0.60	0.46	0.00	304.0	Vi	0.00	0.35	0.99	263.6	Vi	1.15	0.00	0.40	1.00	259.3	Vi	1.17
18	DD8A	14.22	1.99	0.59	0.25	1.01	141.9	Vi	0.82	0.56	0.99	127.1	Vi	1.12	0.95	0.67	1.00	137.4	Vi	1.03
19	DD8B	14.22	2.92	0.63	0.20	0.76	102.8	Vi	0.47	0.39	0.99	103.3	Vi	1.00	0.57	0.49	1.00	111.9	Vi	0.92
20	DD9A	9.89	1.68	0.71	0.21	1.08	290.5	Vi	0.42	0.52	0.94	306.2	Vi	0.95	0.49	0.61	1.00	318.9	Vi	0.91
21	DD9B	9.89	1.00	0.71	0.18	0.95	403.0	Vi	0.51	0.70	1.00	361.5	Vi	1.11	0.53	0.72	1.00	320.8	Vi	1.26
22	RW00	15.77	2.00	0.59	0.25	1.00	162.0	Vi	0.81	0.50	0.99	180.1	Vi	0.90	0.94	0.59	1.00	191.2	Vi	0.85
23	RW11	10.93	2.00	0.60	0.24	0.95	225.0	Vi	0.35	0.39	1.00	193.5	Vi	1.16	0.40	0.49	1.00	209.0	Vi	1.08
24	RW22	16.82	2.00	0.60	0.42	2.50	340.0	Vi	0.77	0.38	0.99	280.8	Vi	1.21	0.86	0.48	1.00	298.5	Vi	1.14
25	RW33	16.84	2.00	0.60	0.50	6.00	146.0	F	1.00	0.22	0.44	124.1	F	1.18	1.00	0.22	0.29	103.5	F	1.41
26	RW44	16.83	2.00	0.60	0.50	6.00	117.0	F	1.00	0.18	0.68	102.0	F	1.15	1.00	0.20	0.62	96.4	F	1.21
27	RP56	10.61	2.00	0.60	0.25	0.95	189.0	Vi	0.28	0.30	1.00	162.5	Vi	1.16	0.31	0.37	1.00	169.9	Vi	1.11
28	RP57	10.61	2.00	0.60	0.25	0.95	272.0	Vi	0.43	0.46	1.00	248.1	Vi	1.10	0.49	0.59	1.00	267.9	Vi	1.02
29	RP68	10.67	2.00	0.60	0.25	0.95	258.0	Vi	0.41	0.47	1.00	229.6	Vi	1.12	0.46	0.61	1.00	249.5	Vi	1.03
													Maximum =	1.37					Maximum =	2.00
													Minimum =	0.71					Minimum =	0.71
													Average (above unity) =	1.15					Average (above unity) =	1.21
													Average (below unity) =	0.86					Average (below unity) =	0.86
													No. of Ψ_1 above unity =	23					No. of Ψ_2 above unity =	21
													No. of Ψ_1 below unity =	6					No. of Ψ_2 below unity =	8

Notations:

- m Moment utilization ratio
- v Shear utilization ratio
- mv Vierendeel moment utilization ratio
- P_1 Load capacity predicted by proposed method
- P_2 Load capacity predicted by SCI method
- FM Failure mode: F = Flexural, V = Shear, and Vi = Vierendeel
- Ψ_1 Model factor for load capacity predicted by proposed method = P_{test}/P_1
- Ψ_2 Model factor for load capacity predicted by SCI method = P_{test}/P_2

CHAPTER 6

DESIGN PROCEDURES AND EXAMPLES

6.1 General

Analytical design formulas are developed in Chapter 3 to determine the plastic moment resistance of tee-sections under co-existing axial and shear forces, which are also extended for the analysis of steel perforated section. Similar design formulas have also been developed for composite tee-sections and composite perforated section in Chapter 5. In this chapter, the complete proposed design procedures for steel beams and composite beams with web openings are presented. Section 6.2 deals with the design of steel beams with web openings, accompanied by a fully worked design example in Section 6.3. The proposed design procedures for composite beams with web openings are presented in Section 6.4, supplemented by a fully worked design example in Section 6.5. The details of a specialist computer program developed for the analysis of both steel beams and composite beams with web openings are presented in Section 6.6.

6.2 Design Procedures for Steel Beams with Web Openings

This section provides a formal presentation of the design procedures for steel beams with web openings. The design procedures are based on the design formulas proposed in Chapter 3 for both tee-sections and perforated sections and the equivalent transformation expression in Chapter 4 for beams with circular web openings. It is assumed that the flange and the web are either plastic or compact sections such that plastic analysis can be used without instability problems.

Step 1: Evaluate the applied forces at the perforated section

Determine the ultimate design shear force V_{sd} and moment M_{sd} at the centerline of the web opening, which is located at a distance of x_o from the

nearest support or point of zero moment.

Step 2: Evaluate the resistances of the perforated section

It is assumed that the yield strength of steel, f_y, is reduced using the material factor, γ_a, for steel, which is equal to 1.05 according to Eurocode 3. Hence, the design yield strength, f_{yd}, is given by:

$$f_{yd} = \frac{f_y}{1.05}$$

a) Plastic moment resistance:

$$M_{o,Rd} = f_{yd}(W_{pl} - \frac{t_w h_o^2}{4})$$

where:

W_{pl} is the plastic modulus of un-perforated cross-section
h_o is the opening height
t_w is the web thickness

b) Shear resistances:

$$V_{f,Rd} = \frac{A_{vf} f_{yd}}{\sqrt{3}}, \quad V_{w,Rd} = \frac{A_{vw} f_{yd}}{\sqrt{3}} \quad V_{o,Rd} = 2(V_{f,Rd} + V_{w,Rd})$$

where:

$V_{f,Rd}$ is the shear resistance of the flange of a tee-section with a shear area A_{vf} equals to $(0.75t_f+t_w)t_f$
$V_{w,Rd}$ is the shear resistance of the web of a tee-section with a shear area A_{vw} equals to $d_1 t_w$
$V_{o,Rd}$ is the shear resistance of the perforated section

Step 3: Check against shear and flexure failures

$$V_{o,Rd} \geq V_{Sd} \quad \text{and} \quad M_{o,Rd} \geq M_{Sd}$$

If either of the inequalities is not satisfied, then another steel section should be selected.

Step 4: Transformation of circular web opening into equivalent octagonal web opening

For beams with circular web openings, transform the circular web openings into equivalent octagonal web openings with the following formulas for the opening height, h_o, and the opening length, a_o:

$$a_o = \beta_a d_o \quad \text{and} \quad h_o = \beta_h a_o$$

where $\beta_a = \tan\frac{\pi}{8} + 4(\frac{d_o}{h} - 0.5)(\sin\frac{\pi}{8} - \tan\frac{\pi}{8})$ and $\beta_h = 1 + \sqrt{2}$. Calculate the depth of the web, which is given by:

$$d_1 = \frac{h - h_o}{2} - t_f$$

and then repeat Step 2b to calculate the shear resistances of the flange and the web.

Step 5: Evaluate the shear force resisted by the flange and the web of both the top and the bottom tee-sections

For concentric web openings, the applied shear force is assumed to be resisted equally by the top and the bottom tee-sections; that is, $V_{T,Sd} = \frac{V_{Sd}}{2}$. Then $V_{T,Sd}$ is distributed to the flange and the web as follows:

$$V_{f,Sd} = \frac{V_{f,Rd}}{V_{T,Rd}}(V_{T,Sd}) \quad \text{and} \quad V_{w,Sd} = \frac{V_{w,Rd}}{V_{T,Rd}}(V_{T,Sd})$$

where $V_{T,Rd}$ is the shear resistance of a tee-section

Step 6: Evaluate the reduced bending strengths of the flange and the web

The design bending strengths of the shear areas of both the web and the flange are reduced according to the shear forces they carry. The reduction is made through the von Mises' yielding criterion as follows:

$$f_{vw} = \sqrt{f_{yd}^{\ 2} - 3\tau_w^{\ 2}} \quad \text{and} \quad f_{vf1} = \sqrt{f_{yd}^{\ 2} - 3\tau_f^{\ 2}}$$

where $\tau_w = \frac{V_{w,Sd}}{A_{vw}}$ and $\tau_f = \frac{V_{f,Sd}}{A_{vf}}$. The average reduced bending strength of the flange, f_{vf}, can then be calculated as follows:

$$f_{vf} = \frac{f_{vf1} A_{vf} + f_y (A_f - A_{vf})}{A_f}$$

where A_f is the area of the flange.

Step 7: Determine the position of the plastic axial centroid and the plastic moment resistance of a tee-section

a) Plastic axial centroid (PC)
It is a point at which the axial force arising from the global bending action is assumed to pass through. Its distance from the top of a tee-section, y_{pc}, is given as follows:

$$y_{pc} = \frac{N_{f,Rd}(\frac{t_f}{2}) + N_{w,Rd}(\frac{d_1}{2} + t_f)}{N_{f,Rd} + N_{w,Rd}}$$

where $N_{f,Rd} = b_f t_f f_{vf}$ and $N_{w,Rd} = d_1 t_w f_{vw}$

b) Plastic moment resistance, $M_{T,V,Rd}$
The distance of the plastic neutral axis (PNA) from the top of the flange is given as:

$$y_{po} = t_f[\frac{N_{f,Rd} + N_{w,Rd}}{2N_{f,Rd}}]$$

The plastic moment resistance of a tee-section is thus found by summing moments of the forces about the PNA and is given as follows:

$$M_{T,V,Rd} = N_{f,Rd}[\frac{y_{po}^{\ 2} + (t_f - y_{po})^2}{2t_f}] + N_{w,Rd}[\frac{d_1}{2} + t_f - y_{po}]$$

Step 8: Evaluate the applied axial force on the tee-sections

The axial force, $N_{T,Sd}$, arising from the global bending action is assumed to act at the plastic axial centroid of the tee section and is given by:

$$N_{T,Sd} = \frac{M_{Sd} - M_{Tth,VN,Rd} - M_{Ttl,VN,Rd}}{z}$$

where z is the lever arm between the compressive normal force acting on the top tee and the tensile normal force acting on the bottom tee and is equal to $h-2y_{pc}$. $M_{Tth,VN,Rd}$ and $M_{Ttl,VN,Rd}$ are the modified moment resistances of the top tee sections at the HMS and the LMS of the perforated section, respectively. The following equation may be used as a first trial to find $N_{T,Sd}$ whenever iterations are needed:

$$N_{T,Sd} = \frac{M_{Sd}}{z}$$

Step 9 Evaluate the modified moment resistances of the tee-sections

a) Top tee-section at LMS
The modified moment resistance, $M_{Ttl,VN,Rd}$ is given by:

$$M_{Ttl,VN,Rd} = M_{T,V,Rd} - N_{f,Sd}\beta_f$$

where $\beta_f = y_{pc} - (y_{po} - \frac{\alpha_f}{2})$, $N_{f,Sd} = 2\alpha_f b_f f_{vf}$, and $\alpha_f = \frac{N_{f,Sd}}{2b_1 f_{vf}}$.

b) Top tee-section at HMS

The modified moment resistance, $M_{Tth,VN,Rd}$ is given by:

$$M_{Tth,VN,Rd} = M_{T,V,Rd} + N_{f,Sd}\beta_f + N_{w,Sd}\beta_w$$

where $\beta_f = y_{pc} - (y_{po} + \frac{\alpha_f}{2})$, $\beta_w = y_{pc} - (y_{po} + \alpha_f + \frac{\alpha_w}{2})$,

$N_{w,Sd} = 2\alpha_w t_w f_{vw}$.

If $N_{T,Sd}$ is larger than the residual strength of the flange, $2(t_f - y_{po})b_f f_{vf}$, then $\alpha_f = t_f - y_{po}$.

Step 10: Check Vierendeel failure mode

Since the sum of the modified moment resistances in the top tee-section is the same as those of the bottom tee-section, only the top tee-section need to be checked as follows:

$$M_{Tll,VN,Rd} + M_{Tth,VN,Rd} \geq \frac{V_{Sd}}{2} a_o$$

A more accurate solution can be achieved by repeating Steps 8 through 10, until a stable $N_{T,Sd}$ is found. The proposed design method is illustrated with a fully worked design example in Section 6.3.

6.3 Design Example 1 – A Steel Beam with Two Rectangular Web Openings

Consider the steel beam with two rectangular web openings as shown below:

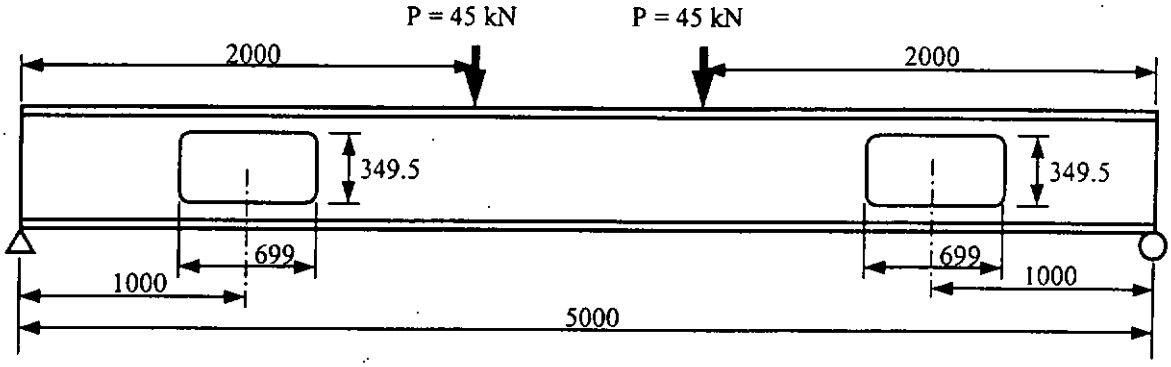

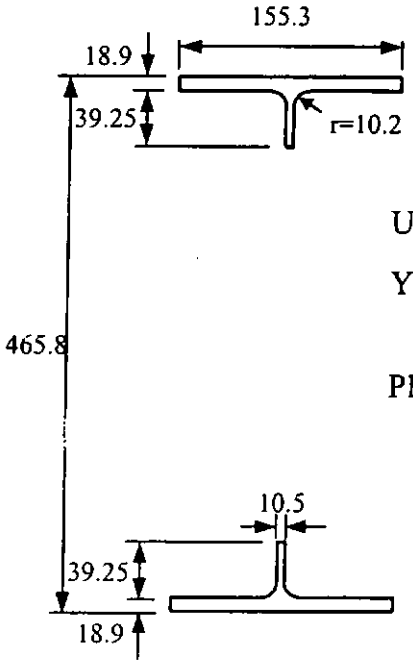

UB457x152x82 S355

Yield strength, $f_{yd} = \frac{355}{1.05} = 338.1$ N/mm^2

Plastic modulus, $W_{pl} = 1811$ cm^3

Check the structural adequacy of the beam in accordance with the proposed design method.

Step 1: Evaluate the applied forces at the perforated section

Ultimate design shear force, $V_{Sd} = P = 45kN$

Ultimate design moment, $M_{Sd} = V_{Sd}x_o = 45(1) = 45kNm$

Steps 2&3: Evaluate the resistances of the perforated section and check against shear and flexural failures

a) Pure bending moment resistance:

$$M_{o,Rd} = f_{yd}(W_{pl.} - \frac{t_w h_o^{\ 2}}{4})$$

$$= \frac{338.1(1811x1000 - \frac{10.5\times 349.5^2}{4})}{1000000}$$

$$= 503.88kNm > M_{Sd} = 45 \text{ kNm} \quad \textbf{(OK)}$$

b) Shear Resistances:

$$A_{vf} = (0.75t_f + t_w)t_f = (0.75\text{x}18.9+10.5)\text{ x}18.9 = 466.36 \text{ mm}^2$$

$$A_{vw} = d_1 t_w = 39.25\text{x}10.5 = 412.125 \text{ mm}^2$$

$$V_{f,Rd} = \frac{A_{vf} f_{yd}}{\sqrt{3}} = \frac{466.36\times 338.1}{\sqrt{3}\times 1000} = 91.03 \text{ kN}$$

$$V_{w,Rd} = \frac{A_{vw} f_{yd}}{\sqrt{3}} = \frac{412.125\times 338.1}{\sqrt{3}\times 1000} = 80.45 \text{ kN}$$

$$V_{o,Rd} = 2(V_{f,Rd} + V_{w,Rd}) = 2(91.03+80.45) = 342.97 \text{ kN} > V_{Sd} = 45 \text{ kN} \quad \textbf{(OK)}$$

Step 4: Transformation of circular web opening into equivalent octagonal web opening

- Not applicable to rectangular web opening

Step 5: Evaluate the shear force resisted by the flange and the web of both top and bottom tee-sections

$$V_{T.Sd} = \frac{V_{Sd}}{2} = \frac{45}{2} = 22.5 \text{ kN}$$

$$V_{f.Sd} = \frac{V_{f.Rd}}{V_{T.Rd}}(V_{T.Sd}) = \frac{91.03}{171.48}(22.5) = 11.94 \text{ kN}$$

$$V_{w.Sd} = \frac{V_{w.Rd}}{V_{T.Rd}}(V_{T.Sd}) = \frac{80.45}{171.48}(22.5) = 10.56 \text{ kN}$$

Step 6: Evaluate the reduced bending strengths of the flange and the web

$$\tau_w = \frac{V_{w,Sd}}{A_{vw}} = \frac{10.56\times1000}{412.125} = 25.62 \text{ N/mm}^2$$

$$\tau_f = \frac{V_{f,Sd}}{A_{vf}} = \frac{11.94\times1000}{466.36} = 25.62 \text{ N/mm}^2$$

$$f_{vw} = \sqrt{f_{yd}{}^2 - 3\tau_w{}^2} = \sqrt{338.1^2 - 3\times25.62^2} = 335.2 \text{ N/mm}^2$$

$$f_{vf1} = \sqrt{f_{yd}{}^2 - 3\tau_f{}^2} = \sqrt{338.1^2 - 3\times25.62^2} = 335.2 \text{ N/mm}^2$$

$$f_{vf} = \frac{f_{vf1}A_{vf} + f_y(A_f - A_{vf})}{A_f}$$

$$= \frac{335.2\times466.36 + 338.1(155.3\times18.9 - 466.36)}{155.3\times18.9} = 337.6 \text{ N/mm}^2$$

Step 7: Determine the position of the plastic axial centroid and the plastic moment resistance of a tee-section

a) Plastic axial centroid:

$$N_{f,Rd} = b_f t_f f_{vf} = \frac{155.3\times18.9\times337.6}{1000} = 990.9 \text{ kN}$$

$$N_{w,Rd} = d_1 t_w f_{vw} = \frac{39.25\times10.5\times335.2}{1000} = 138.14 \text{ kN}$$

$$y_{pc} = \frac{N_{f,Rd}(\frac{t_f}{2}) + N_{w,Rd}(\frac{d_1}{2} + t_f)}{N_{f,Rd} + N_{w,Rd}} = \frac{990.9(\frac{18.9}{2}) + 138.14(\frac{39.25}{2} + 18.9)}{990.9 + 138.14}$$

$$= 13.01 \text{ mm}$$

b) Plastic moment resistance:

$$y_{po} = t_f[\frac{N_{f,Rd} + N_{w,Rd}}{2N_{f,Rd}}] = 18.9[\frac{990.9 + 138.14}{2\times990.9}] = 10.77 \text{ mm}$$

$$M_{T,V,Rd} = N_{f,Rd}[\frac{y_{po}{}^2 + (t_f - y_{po})^2}{2t_f}] + N_{w,Rd}[\frac{d_1}{2} + t_f - y_{po}]$$

$$= \frac{990.9}{1000}[\frac{10.77^2 + (18.9 - 10.77)^2}{2\times18.9}] + \frac{138.14}{1000}[\frac{39.25}{2} + 18.9 - 10.77]$$

$$= 4.77 + 3.84$$

$$= 8.61 \text{ kNm}$$

Step 8: Evaluate the applied axial force acting on the tee-sections

First trial:

$$N_{T,Sd} = \frac{M_{Sd}}{z} = \frac{45\times1000}{465.8 - 2\times13.01} = 102.32 \text{ kN}$$

Step 9: Evaluate the modified moment resistance of tee-sections

a) Top tee-section at LMS

$$\alpha_f = \frac{N_{T,Sd}}{2b_f f_{vf}} = \frac{102.32 \times 1000}{2 \times 155.3 \times 337.6} = 0.976 \text{ mm}$$

$$\beta_f = y_{pc} - (y_{po} - \frac{\alpha_f}{2}) = 13.01 - (10.77 - \frac{0.976}{2}) = 2.728 \text{ mm}$$

$$N_{f,Sd} = 2\alpha_f b_f f_{vf} = N_{T,Sd} = 102.32 \text{ kN}$$

$$M_{Tfl,VN,Rd} = M_{T,V,Rd} - N_{f,Sd}\beta_f = 8.61 - \frac{102.32 \times 2.728}{1000} = 8.33 \text{ kNm}$$

b) Top tee-section at HMS

$$2(t_f - y_{po})b_f f_{vf} = \frac{2(18.9 - 10.77) \times 155.3 \times 337.6}{1000} = 852.5 \text{ kN} > N_{T,Sd}$$

So

$$\alpha_f = \frac{N_{T,Sd}}{2b_f f_{vf}} = 0.976 \text{ mm},$$

$$\beta_f = y_{pc} - (y_{po} + \frac{\alpha_f}{2}) = 13.01 - (10.77 + \frac{0.976}{2}) = 1.752 \text{ mm}$$

$$N_{f,Sd} = 2\alpha_f b_f f_{vf} = N_{T,Sd} = 102.32 \text{ kN}$$

$$M_{Tfh,VN,Rd} = M_{T,V,Rd} + N_{f,Sd}\beta_f + N_{w,Sd}\beta_w = 8.61 + \frac{102.32 \times 1.752}{1000} = 8.79 \text{ kNm}$$

Step 10: Check Vierendeel failure mode

$$M_{Tfl,VN,Rd} + M_{Tfh,VN,Rd} = 8.33 + 8.79 = 17.12 kNm$$

$$\frac{V_{Sd}}{2} a_o = \frac{45x699}{2x1000} = 15.73 kNm$$

So $M_{Tfl,VN,Rd} + M_{Tfh,VN,Rd} > \frac{V_{Sd}}{2} a_o$ **(OK)**

Comments:

(1) The design can be refined by repeating Steps 8 through 10. After several iterations, it is found that:

$N_{T,Sd}$ = 101.28 kN
$M_{Tfl,VN,Rd}$ = 8.33 kNm
$M_{Tfh,VN,Rd}$ = 8.79 kNm

$$M_{Tfl,VN,Rd} + M_{Tfh,VN,Rd} = 8.33 + 8.79 = 17.12 kNm > \frac{V_{Sd}}{2} a_o \quad \textbf{(OK)}$$

Thus, there is basically no improvement by performing the iterations to find a stable $N_{T,Sd}$.

(2) For illustration purpose, a detailed analysis has been performed to determine the load capacity of the beam. The beam is found to fail at point loads of 48.9 kN, which is about 8% higher than the current loading. The force distributions around the web opening at failure are shown in Figure 6.1. At failure, the perforated section is subjected to a low shear force ratio of about 0.14. An axial-moment interaction curve for the tee-sections under such shear force ratio is plotted in Figure 6.2. The plastic moment resistances of the four tee-sections are also marked on the curve for comparison. From the curve it is shown the plastic moment resistances of the tee-sections at the HMS of the perforated section has been increased over their nominal values.

(3) A global moment-shear interaction curve for the perforated section in the example at failure is shown in Figure 6.3. The design shear and moment under the current design load are below the $(M\text{-}V)_O$ interaction curve so that the beam does not fail.

6.4 Design Procedures for Composite Beams with Web Openings

This section provides a formal description of the design procedures for composite beams with web openings. The design procedures are based on the design formulas proposed in Chapter 5 for composite perforated section. It is assumed that both section classifications of both the flange and the web are either "plastic" or "compact" and plastic analysis can be used; no stability is considered. The design formulation of the composite beam design is in accordance with Eurocode 4.

Step 1: Evaluate the applied forces at the perforated section

Determine the ultimate design shear force V_{Sd} and moment M_{Sd} at the centerline of the opening, which is located at a distance of x_o from the nearest support.

Step 2: Evaluate the moment resistances of perforated section

The design strengths of the steel, f_{yd}, and the concrete, f_{cd}, are evaluated as follows:

$$f_{yd} = \frac{f_y}{\gamma_a} \quad \text{and} \quad f_{cd} = \frac{f_{ck}}{\gamma_c}$$

where:

γ_a is the material factor for steel and is equal to 1.05 according to Eurocode 3

γ_c is the material factor for concrete and is equal to 1.5 according to Eurocode 2

The axial resistances of the concrete and the steel tee-section are calculated as follows:

$$N_{c,Rd} = 0.85 f_{cd} b_e d_c, \quad N_{sh,Rd} = n_L P_{Rd}, \quad N_{o,Rd} = h_o t_w f_{yd}$$
$$N_{f,Rd} = t_f b_f f_{yd}, \quad N_{w,Rd} = h_w t_w f_{yd},$$
$$N_{a,Rd} = 2(N_{f,Rd}) + N_{w,Rd} - N_{o,Rd}$$

N_{Rd} = minimum of ($N_{c,Rd}$, $N_{sh,Rd}$, $N_{a,Rd}$)

$$\alpha = \frac{N_{Rd}}{N_{cRd}} d_c$$

The moment resistance of the perforated section can be calculated by considering the following cases:

Case I: Full shear connection, ($N_{sh,Rd} > N_{c,Rd} > Na_{,Rd}$ or $N_{c,Rd} > N_{sh,Rd} > N_{a,Rd}$)

PNA in concrete

$$M_{o,Rd} = N_{Rd}(t_f + h_t - \frac{\alpha}{2}) - N_{f,Rd}(\frac{t_f}{2}) + N_{w,Rd}(\frac{h_w}{2}) + N_{f,Rd}(h_w + \frac{t_f}{2}) - N_{o,Rd}(\frac{h_w}{2})$$

Case II: Full-shear connection, ($N_{sh,Rd} > N_{a,Rd} > N_{c,Rd}$ or $N_{a,Rd} > N_{sh,Rd} > N_{c,Rd}$)

a) PNA in steel flange, $N_{Rd} + N_{f,Rd} \geq N_{a,Rd} - N_{f,Rd}$

$$y_1 = t_f(\frac{N_{Rd} + N_{o,Rd} - N_{w,Rd}}{2N_{f,Rd}}), \qquad N_{f1,Rd} = (t_f - y_1)b_f f_{yd},$$
$$N_{f2,Rd} = y_1 b_f f_{yd}$$

$$M_{o,Rd} = N_{Rd}(t_f + h_t - \frac{\alpha}{2}) + N_{f1,Rd}(\frac{t_f + y_1}{2}) - N_{f2,Rd}(\frac{y_1}{2})$$
$$+ N_{w,Rd}(\frac{h_w}{2}) + N_{f,Rd}(h_w + \frac{t_f}{2}) - N_{o,Rd}(\frac{h_w}{2})$$

b) PNA in steel web, $N_{Rd} + N_{f,Rd} < N_{a,Rd} - N_{f,Rd}$

$$y_1 = h_w(\frac{N_{w,Rd} - N_{Rd} - N_{o,Rd}}{2N_{w,Rd}}), \qquad N_{w1,Rd} = y_1 t_w f_{yd},\ N_{w2,Rd} = (h_w - y_1)t_w f_{yd}$$

$$M_{o,Rd} = N_{Rd}(t_f + h_t - \frac{\alpha}{2}) + N_{f,Rd}(\frac{t_f}{2}) - N_{w1,Rd}(\frac{y_1}{2})$$
$$+ N_{w2,Rd}(\frac{h_w + y_1}{2}) + N_{f,Rd}(h_w + \frac{t_f}{2}) - N_{o,Rd}(\frac{h_w}{2})$$

Case III: Partial shear connection, ($N_{c,Rd} > N_{a,Rd} > N_{sh,Rd}$ or $N_{a,Rd} > N_{c,Rd} > N_{sh,Rd}$)

Same as case II, except that $N_{Rd} = N_{sh,Rd}$

Step 3: Evaluate the shear resistances of the perforated section

a) Shear resistances of steel beam:

$$V_{f,Rd} = \frac{A_{vf} f_{yd}}{\sqrt{3}}, \quad V_{w,Rd} = \frac{A_{vw} f_{yd}}{\sqrt{3}}, \quad V_{a,Rd} = 2(V_{f,Rd} + V_{w,Rd})$$

where:

$V_{f,Rd}$ is the shear resistance of the flange of a tee-section and the shear area, $A_{vf} = (0.75t_f + t_w)t_f$

$V_{w,Rd}$ is the shear resistance of the web of a tee-section and the shear area, $A_{vw} = d_1 t_w$

$V_{a,Rd}$ is the shear resistance of the steel perforated section

b) Shear resistance of concrete slab, $V_{c,Rd}$

The expression for the design shear strength, v_c, of reinforced concrete members without shear reinforcement recommended by Eurocode 2 is:

$$v_c = \tau_{rd} k(1.2 + 40\rho_l)$$

where

τ_{rd} is the basic design shear strength. The value of τ_{rd} should be taken as 25 per cent of a conservatively low value for the tensile strength of the concrete, that is $\tau_{rd} = 0.25 f_{ct,0.05}/\gamma_c$ where $\gamma_c = 1.5$ and $f_{ct,0.05}$ is the tensile strength with a 5 per cent probability of not being exceed. This is given in EC2 as:

$$f_{ct,0.05} = 0.21 f_{ck}^{2/3}$$

Thus, the shear resistance of the concrete slab is given by:

$$V_{c,Rd} = v_c b_w d = \tau_{rd} k(1.2 + 40\rho_l) b_w d$$

where

ρ_l is the lesser of the longitudinal tension reinforcement ratio, $A_s/b_w d$, and 0.02

d is the effective depth of the concrete slab to resist shear force

k is the greater of (1.6-d) and 1

c) Total shear resistance for perforated section, $V_{o,Rd}$

$$V_{o,Rd} = V_{c,Rd} + V_{a,Rd}$$

Step 4: Check flexural and shear failures of perforated section

$$V_{o,Rd} \geq V_{Sd} \quad \text{and} \quad M_{o,Rd} \geq M_{Sd}$$

If either of the inequalities is not satisfied, then another steel section should be selected.

Step 5: Evaluate the shear force resisted by the flange and the web of both the top and the bottom tee-sections

It is assumed that the applied shear force is first resisted by the concrete slab until its shear resistance is fully utilized. Any remaining applied shear force is then assumed to be resisted by the top tee-section; that is, $V_{at,Sd} = V_{Sd} - V_{cSd}$. Then the shear force is assumed to be distributed between the flange and the web of the top tee-section according to the following formulas:

$$V_{f,Sd} = \frac{V_{f,Rd}}{V_{T,Rd}}(V_{at,Sd}) \quad \text{and} \quad V_{w,Sd} = \frac{V_{w,Rd}}{V_{T,Rd}}(V_{at,Sd})$$

where $V_{T,Rd}$ is the shear resistance of a tee-section. If $V_{at,Sd} > V_{T,Rd}$, then the bottom tee-section must also carry part of the shear force according to formulas similar to above.

Step 6: Evaluate the reduced bending strengths of the tee-sections under high shear force

The bending strengths of the shear areas of both the web and the flange of the top steel tee-section are reduced due to the shear forces they carry according to von Mises' yielding criterion as follows:

$$f_{vw} = \sqrt{f_{yd}^{\ 2} - 3\tau_w^{\ 2}} \quad \text{and} \quad f_{vf1} = \sqrt{f_{yd}^{\ 2} - 3\tau_f^{\ 2}}$$

where $\tau_w = \frac{V_{w,Sd}}{A_{vw}}$ and $\tau_f = \frac{V_{f,Sd}}{A_{vf}}$. The average reduced bending strength of the entire flange, f_{vf}, can then be calculated as follows:

$$f_{vf} = \frac{f_{vf1} A_{vf} + f_y (A_f - A_{vf})}{A_f}$$

where A_f is the area of the flange.

Step 7: Determine the position of the plastic axial centroid and the moment resistance of the top composite tee-section at HMS

a) Plastic axial centroid, y_{pcth}
This is a point at which the axial force arising from the global bending action is assumed to pass through at the HMS. Its distance from the top of the top tee-section is given as:

$$y_{pcth} = \frac{N_{Rd}(\frac{\alpha}{2}) + N_{f,V,Rd}(\frac{t_f}{2} + h_t) + N_{w,V,Rd}(h_t + t_f + \frac{d_1}{2})}{N_{Rd} + N_{f,V,Rd} + N_{w,V,Rd}}$$

where $N_{f,V,Rd} = b_f t_f f_{vf}$ and $N_{w,V,Rd} = d_1 t_w f_{vw}$, $N_{a,V,Rd} = N_{f,V,Rd} + N_{w,V,Rd}$, $N_{sh,Rd} = n_H P_{Rd}$, $N_{Rd} = MIN(N_{c,Rd}, N_{sh,Rd})$

b) Plastic moment resistance, $M_{Tth,V,Rd}$
Depending on the relative strengths of the top steel tee-section, the concrete slab, and the shear connectors, the nominal PNA may locate within the concrete slab, the steel flange, or the steel web. Table 6.2 summarizes the relevant geometrical parameters required to calculate the position of the nominal PNA. Various design formulas for the nominal moment resistance of the tee-section, $M_{Th,V,Rd}$, are also presented.

Step 8: Determine the position of the plastic axial centroid and the moment resistance of the top composite tee-section at LMS

a) Plastic axial centroid, y_{pctl}
This is a point at which the axial force arising from the global bending action is assumed to pass through at the LMS. Its distance from the top of the top tee-

section is given as:

$$y_{pctl} = \frac{N_{Rd}(d_e - \frac{\alpha}{2}) + N_{f,V,Rd}(\frac{t_f}{2} + h_t) + N_{w,V,Rd}(h_t + t_f + \frac{d_1}{2})}{N_{Rd} + N_{f,V,Rd} + N_{w,V,Rd}}$$

where $N_{sh,Rd} = n_L P_{Rd}$, $N_{Rd} = MIN(N_{c,Rd}, N_{sh,Rd})$

b) Plastic moment resistance, $M_{Ttl,V,Rd}$
Depending on the relative strengths of the top steel tee-section, the concrete slab, and the shear connectors, the nominal PNA may locate within the concrete slab, the steel flange, or the steel web. Table 6.3 summarizes the relevant geometrical parameters required to calculate the position of the nominal PNA. Various design formulas for the nominal moment resistance of the tee-section, $M_{T,tl,V,Rd}$, are also presented.

Step 9: Determine the position of the plastic axial centroid and the moment resistance of the bottom tee-sections

a) Plastic axial centroid (PC)
This is a point at which the axial force arising from the global bending action is assumed to pass through. Its distance from the top of a tee-section, y_{pc}, is given as follows:

$$y_{pcb} = \frac{N_{f,V,Rd}(\frac{t_f}{2}) + N_{w,V,Rd}(\frac{d_1}{2} + t_f)}{N_{f,V,Rd} + N_{w,V,Rd}}$$

b) Plastic moment resistance, $M_{T,V,Rd}$
In practice, the plastic neutral axis is always located within the flange. Its distance from the top of the flange is given as:

$$y_{po} = t_f(\frac{N_{f,V,Rd} + N_{w,V,Rd}}{2N_{f,v,Rd}})$$

The moment resistance of the tee-section may be obtained by summing moments of the forces about the PNA as follows:

$$M_{T,V,Rd} = N_{f,V,Rd}[\frac{y_{po}^2 + (t_f - y_{po})^2}{2t_f}] + N_{w,V,Rd}[\frac{d_1}{2} + t_f - y_{po}]$$

Step 10: Evaluate the applied axial force on the tee-sections

The axial force, $N_{T,Sd}$, arising from the global bending action is assumed to act at the plastic axial centroid and is given by:

$$N_{T,Sd} = \frac{2M_{Sd} - (M_{Tbt,N,Rd} + M_{Tbb,N,Rd} - M_{Tt,N,Rd} - M_{Tb,N,Rd})}{z_{tt} + z_{tb}}$$

where $z_H (= h_t + h - y_{pcth} - y_{pcb})$ and $z_L (= h_t + h - y_{pctl} - y_{pcb})$ are the lever arms between the axial forces acting at the HMS and the LMS of the perforated section, respectively. $M_{Tth,VN,Rd}$ and $M_{Ttl,VN,Rd}$ are the modified moment resistances of the top composite tee cross-sections at the HMS and the LMS of the web opening, respectively. $M_{Tbh,VN,Rd}$ and $M_{Tbl,VN,Rd}$ are the modified moment resistances of the bottom steel tee cross-sections at the HMS and the LMS of the perforated section, respectively. Since the modified bending resistances are calculated in the Steps 12 and 13, a first trial calculation of $N_{T,Sd}$ is given as follows:

$$N_{T,Sd} = \frac{2M_{Sd}}{z_H + z_L}$$

Step 11: Evaluate the modified moment resistances of the bottom tee-sections

a) Bottom tee-section at LMS
The modified moment resistance, $M_{Tbl,VN,Rd}$ is given by:

$$M_{Ttl,VN,Rd} = M_{T,V,Rd} - N_{f,Sd}\beta_f$$

where $\beta_f = y_{pcb} - (y_{po} - \frac{\alpha_f}{2})$, $N_{f,Sd} = 2\alpha_f b_f f_{vf}$, and $\alpha_f = \frac{N_{T,Sd}}{2b_f f_{vf}}$.

b) Bottom tee-section at HMS
The modified moment resistance, $M_{Tbh,VN,Rd}$ is given by:

$$M_{Tth,VN,Rd} = M_{T,V,Rd} + N_{f,Sd}\beta_f + N_{w,Sd}\beta_w$$

where $\beta_f = y_{pcb} - (y_{po} + \frac{\alpha_f}{2})$, $\beta_w = y_{pcb} - (y_{po} + \alpha_f + \frac{\alpha_w}{2})$,
$N_{w,Sd} = 2\alpha_w t_w f_{vw}$. If $N_{T,Sd}$ is larger than the residual strength of the flange, $2(t_f - y_{po})b_f f_{vf}$, then $\alpha_f = t_f - y_{po}$.

Step 12: Evaluate the modified moment resistances of the composite tee-sections

a) Composite tee-section at HMS
The modified moment resistance of the composite tee-section at the HMS may be found using the following equation:

$$M_{Tth,VN,Rd} = M_{Tth,V,Rd} + N_{c,Sd}\beta_c + N_{f,Sd}\beta_f + N_{w,Sd}\beta_w$$

where $N_{c,Sd} = 0.85\alpha_c b_e f_{ck}$, $N_{f,Sd} = 2\alpha_f b_f f_{vf}$, $N_{w,Sd} = 2\alpha_w t_w f_{vw}$. β_c, β_f, and β_w are given in Table 6.4.

b) Composite tee-section at LMS
The modified moment resistance of the composite tee-section at the LMS may

be found using the following equation:

$$M_{Ttl,VN,Rd} = M_{Ttl,V,Rd} - N_{c,Sd}\beta_c - N_{f,Sd}\beta_f - N_{w,Sd}\beta_w$$

where $N_{c,Sd} = 0.85\alpha_c b_e f_{ck}$, $N_{f,Sd} = 2\alpha_f b_f f_{vf}$, $N_{w,Sd} = 2\alpha_w t_w f_{vw}$. β_c, β_f, and β_w are given in Table 6.5. Steps 10 through 12 may be repeated until the value of $N_{T,Sd}$ converges.

Step 13: Check Vierendeel failure

The Vierendeel failure has to be considered separately for the top and the bottom tee-sections, respectively, as follows (until a true equilibrium is achieved):

Top composite tee-section:

$$M_{Ttl,VN,Rd} + M_{Tth,VN,Rd} + N_{T,Sd}(z_H - z_L) \geq (V_{at,Sd} + V_{c,Sd})a_o$$

Bottom steel tee-section:

$$M_{Tbl,VN,Rd} + M_{Tbh,VN,Rd} \geq V_{ab,Sd}a_o$$

If either of the above inequalities does not hold, then more shear force should be distributed to the other tee-section. Iterations should be performed from Step 5 through Step 13 until both inequalities are satisfied, which implies that the perforated section fails with flexural failures at both ends of the top and the bottom tee-sections. The proposed design method is illustrated with a fully worked design example in Section 6.5.

6.5 Design Example 2 – A Composite Beam with Two Rectangular Web Openings

Consider the composite beam with two rectangular web openings shown below:

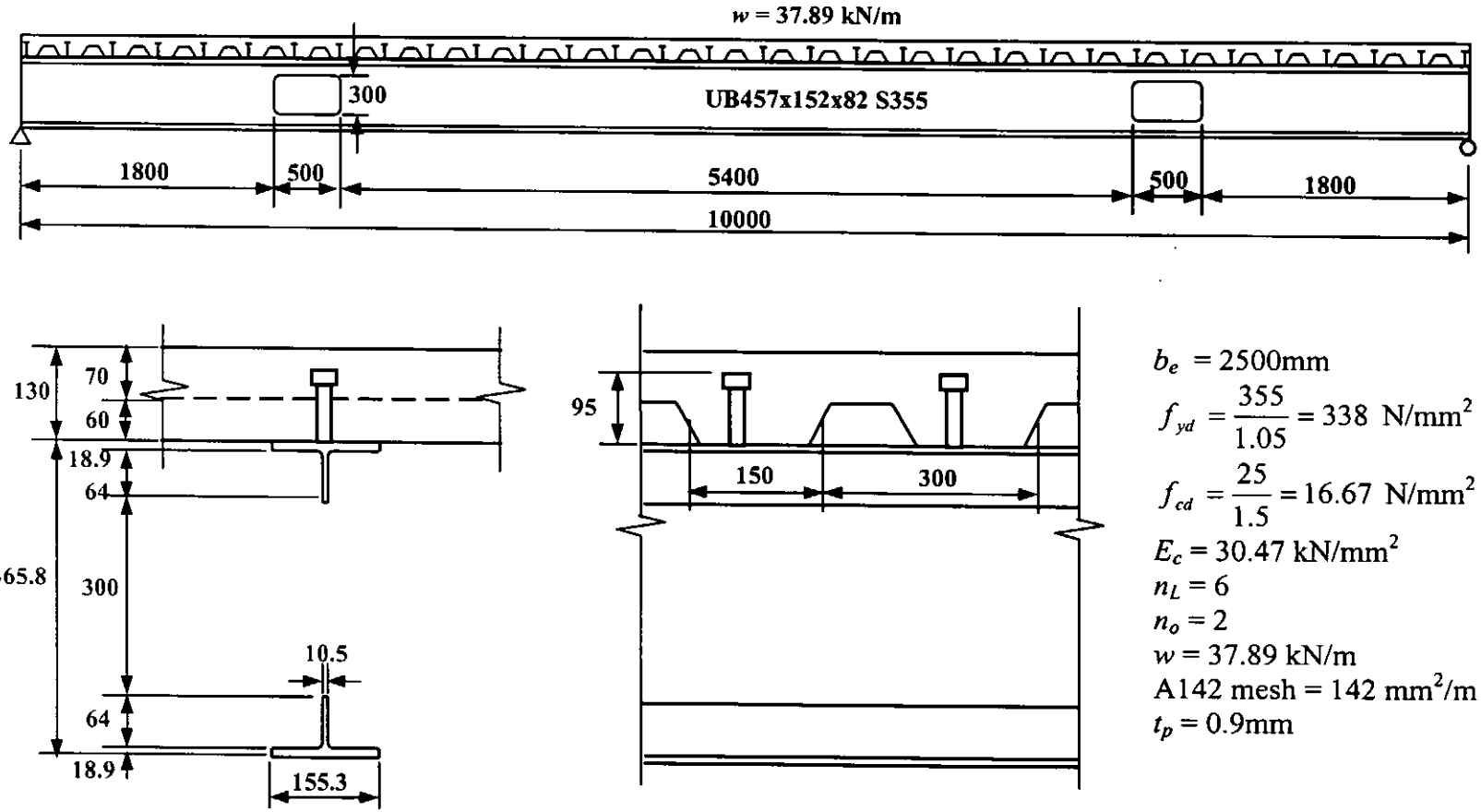

b_e = 2500mm

$f_{yd} = \frac{355}{1.05} = 338$ N/mm^2

$f_{cd} = \frac{25}{1.5} = 16.67$ N/mm^2

E_c = 30.47 kN/mm^2

n_L = 6

n_o = 2

w = 37.89 kN/m

A142 mesh = 142 mm^2/m

t_p = 0.9mm

Check the structural adequacy of the beam in according with the proposed design method.

Step 1: Evaluate the applied forces at the perforated section

Ultimate design shear force, $V_{Sd} = \frac{wL}{2} - wx_o = \frac{37.89 \times 10000}{2 \times 1000} - 37.89 \times \frac{2050}{1000}$

$= 111.78$ kN

Ultimate design moment, $M_{Sd} = \frac{w}{2}(x_o L - x_o^2)$

$= \frac{37.89(2050 \times 10000 - 2050^2)}{2 \times 1000000}$

$= 308.76$ kNm

Steps 2 & 4: Evaluate the moment resistance of the perforated section and check flexural failure

a) Axial resistance of concrete slab:

$$N_{c,Rd} = \frac{0.85 f_{ck} b_e d_e}{\gamma_c} = \frac{0.85 \times 25 \times 2500 \times 70}{1000 \times 1.5} = 2479 \text{ kN}$$

b) Axial resistances of steel tee-section

$$N_{f,Rd} = t_f b_f f_{yd} = \frac{18.9 \times 155.3 \times 338}{1000} = 992 \text{ kN}$$

$$N_{w,Rd} = h_w t_w f_{yd} = \frac{428 \times 10.5 \times 338}{1000} = 1519 \text{ kN}$$

c) Resistance of shear connectors

$$\lambda = 0.2(\frac{h_v}{d_v} + 1) = 0.2(\frac{95}{19} + 1) = 1.2 > 1.0$$

$$P_{Rd1} = \frac{0.29 \lambda d_v^2 \sqrt{f_{ck} E_c}}{\gamma_v} = \frac{0.29 \times 1.0 \times 19^2 \sqrt{\frac{25 \times 30.47}{1000}}}{1.25} = 73.1 \text{ kN}$$

$$P_{Rd2} = \frac{0.8 f_{uv} \pi d_v^2}{4 \gamma_v} = \frac{0.8(450)(\pi)(19^2)}{4 \times 1.25 \times 1000} = 81.7 \text{ kN}$$

$$k_t = \frac{0.7}{\sqrt{N_r}}(\frac{b_o}{h_p})(\frac{h_v}{h_p} - 1) = \frac{0.7}{\sqrt{1}}(\frac{150}{60})(\frac{95}{60} - 1) = 1.02 \Rightarrow 1.0$$

So, there is no reduction due to the decking profile, and $P_{Rd} = 73.1$ kN

$$N_{sh,Rd} = n_L P_{Rd} = 6 \times 73.1 = 438.6 \text{ kN}$$

d) Others

$$N_{o,Rd} = h_w t_w f_y = \frac{300 \times 10.5 \times 338}{1000} = 1065 \text{ kN}$$

$$N_{a,Rd} = 2N_{f,Rd} + N_{w,Rd} - N_{o,Rd} = 2x992 + 1519 - 1065 = 2438 \text{ kN}$$

N_{Rd} = minimum of ($N_{c,Rd}$, $N_{sh,Rd}$, $N_{a,Rd}$) = 438.6 kN

$$\alpha = \frac{N_{Rd}}{N_{cRd}} d_e = \frac{438.6}{2479}(70) = 12.38 \text{ mm}$$

Since $N_{c,Rd} > N_{a,Rd} > N_{sh,Rd}$, so there is partial shear connection and $N_{Rd} + N_{f,Rd} < N_{a,Rd} - N_{f,Rd}$, so the PNA is located within the steel web:

$$y_1 = d_w(\frac{N_{w,Rd} - N_{Rd} - N_{o,Rd}}{2N_{w,Rd}}) = 428(\frac{1519 - 438.6 - 1065}{2 \times 1519}) = 2.17 \text{ mm}$$

$$N_{w1,Rd} = y_1 t_w f_{yd} = \frac{2.17 \times 10.5 \times 338}{1000} = 7.7 \text{ kN}$$

$$N_{w2,Rd} = (h_w - y_1) t_w f_{yd} = \frac{(428 - 2.17) \times 10.5 \times 338}{1000} = 1511.3 \text{ kN}$$

$$M_{o,Rd} = N_{Rd}(t_f + h_t - \frac{\alpha}{2}) + N_{f,Rd}(\frac{t_f}{2}) - N_{w1,Rd}(\frac{y_1}{2})$$
$$+ N_{w2,Rd}(\frac{h_w + y_1}{2}) + N_{f,Rd}(h_w + \frac{t_f}{2}) - N_{o,Rd}(\frac{h_w}{2})$$
$$= [438.6(18.9 + 130 - \frac{12.38}{2}) + 992(\frac{18.9}{2}) - 7.7(\frac{2.17}{2})$$
$$+ 1511.3(\frac{428 + 2.17}{2}) + 992(428 + \frac{18.9}{2}) - 1065(\frac{428}{2})][\frac{1}{1000}]$$

$= 603.06 \text{ kNm} > M_{Sd} = 308.76 \text{ kNm}$ **(OK)**

Steps 3 & 4: Evaluate the shear resistance of the perforated section and check shear failure

a) Shear resistances of the perforated steel section:

$$A_{vf} = (0.75t_f + t_w)t_f = (0.75 \times 18.9 + 10.5) \times 18.9 = 466.36 \text{ mm}^2$$

$$A_{vw} = d_1 t_w = 64 \times 10.5 = 672 \text{ mm}^2$$

$$V_{f,Rd} = \frac{A_{vf} f_{yd}}{\sqrt{3}} = \frac{466.36 \times 338}{1000 \times \sqrt{3}} = 91.0 \text{ kN}$$

$$V_{w,Rd} = \frac{A_{vw} f_{yd}}{\sqrt{3}} = \frac{672 \times 338}{1000 \times \sqrt{3}} = 131.1 \text{ kN}$$

$$V_{a,Rd} = 2(V_{f,Rd} + V_{w,Rd}) = 2(91.0 + 131.1) = 444.2 \text{ kN}$$

b) Shear resistance of the concrete slab:

$$d = (h_c + \frac{h_p}{2}) = 70 + \frac{60}{2} = 100 \text{ mm} = 0.1 \text{ m}$$

$$k = \max(1, 1.6 - d) = \max(1, 1.6 - 0.1) = 1.5$$

$$\tau_{rd} = \frac{0.25 \times 0.21 f_{ck}^{\frac{2}{3}}}{\gamma_c} = \frac{0.25 \times 0.21 (25)^{\frac{2}{3}}}{1.5} = 0.30 \text{ N/mm}^2$$

Area of mesh = 142 x 0.3 = 42.6 mm^2

Area of deck = 0.9 x 300 = 270 mm^2

$$\rho_l = \frac{270 + 42.6}{300 \times 100} = 0.01 < 0.02$$

$$b_w = 3(h_c + \frac{h_p}{2}) = 3(70 + \frac{60}{2}) = 300 \text{ mm}$$

$$V_{c,Rd} = \tau_{rd} k (1.2 + 40\rho_l) b_w d = 0.3 \times 1.5 \times (1.2 + 40 \times 0.01) \times 300 \times 0.1 = 21.6 \text{ kN}$$

c) Total shear resistance:

$V_{o,Rd} = V_{c,Rd} + V_{a,Rd} = 21.6 + 444.2 = 465.8 \text{ kN} > V_{Sd}$ **(OK)**

Step 5: Evaluate the shear force resisted by the steel flanges and the steel webs of both the top and the bottom tee-sections

$$V_{c,Sd} = V_{c,Rd} = 21.6 \text{ kN}$$

$$V_{at,Sd} = V_{Sd} - V_{c,Sd} = 111.78 - 21.6 = 90.18 \text{ kN} < V_{at,Rd} \Rightarrow V_{ab,Sd} = 0 \text{ kN}$$

$$V_{f,Sd} = \frac{V_{f,Rd}}{V_{T,Rd}}(V_{at,Sd}) = \frac{91}{222.1}(90.18) = 36.95 \text{ kN}$$

$$V_{w,Sd} = \frac{V_{w,Rd}}{V_{T,Rd}}(V_{at,Sd}) = \frac{131.1}{222.1}(90.18) = 53.23 \text{ kN}$$

Step 6: Evaluate the reduced bending strengths of the tee-sections under high shear force

a) Top tee-section:

$$\tau_w = \frac{V_{w,Sd}}{A_{vw}} = \frac{53.23 \times 1000}{672} = 79.2 \text{ N/mm}^2$$

$$\tau_f = \frac{V_{f,Sd}}{A_{vf}} = \frac{36.95 \times 1000}{466.36} = 79.2 \text{ N/mm}^2$$

$$f_{vw} = \sqrt{f_{yd}^2 - 3\tau_w^2} = \sqrt{338^2 - 3(79.2)^2} = 308.9 \text{ N/mm}^2$$

$$f_{vf1} = \sqrt{f_{yd}^2 - 3\tau_f^2} = \sqrt{338^2 - 3(79.2)^2} = 308.9 \text{ N/mm}^2$$

$$f_{vf} = \frac{f_{vf1} A_{vf} + f_y (A_f - A_{vf})}{A_f} = \frac{308.9(466.36) + 338(2935.17 - 466.36)}{2935.17}$$

$= 333.4 \text{ N/mm}^2$

b) Bottom tee-section

Since $V_{ab,Sd} = 0$, so $f_{vw} = f_{vf} = 338 \text{ N/mm}^2$

Step 7: Determine the position of the plastic axial centroid and the moment resistance of the top composite tee-section at HMS

$$N_{sh,Rd} = n_H P_{Rd} = 8(73.1) = 584.8 \text{ kN}$$

$$N_{f,V,Rd} = b_f t_f f_{vf} = \frac{155.3 \times 18.9 \times 333.4}{1000} = 978.6 \text{ kN}$$

$$N_{w,V,Rd} = d_1 t_w f_{vw} = \frac{64 \times 10.5 \times 308.9}{1000} = 207.6 \text{ kN}$$

$$N_{a,V,Rd} = N_{f,V,Rd} + N_{w,V,Rd} = 978.6 + 207.6 = 1186.2 \text{ kN}$$

a) Position of the plastic axial centroid, y_{pcth}

N_{Rd} = minimum of ($N_{c,Rd}$, $N_{sh,Rd}$) = 584.8 kN

$$\alpha = \frac{N_{Rd}}{N_{c,Rd}} d_e = \frac{584.8}{2479}(70) = 16.51 \text{ mm}$$

$$y_{pcth} = \frac{N_{Rd}(\frac{\alpha}{2}) + N_{f,V,Rd}(\frac{t_f}{2} + h_t) + N_{w,V,Rd}(h_t + t_f + \frac{d_1}{2})}{N_{Rd} + N_{f,V,Rd} + N_{w,V,Rd}}$$

$$= \frac{584.8(\frac{16.51}{2}) + 978.6(\frac{18.9}{2} + 130) + 207.6(130 + 18.9 + \frac{64}{2})}{584.8 + 978.6 + 207.6}$$

$$= 101.0 \text{ mm}$$

b) Plastic moment resistance, $M_{Tth,V,Rd}$

With reference to Table 6.2, there is partial shear connection.
As $N_{shRd} + N_{f,V,Rd} > N_{w,V,Rd}$, the nominal PNA is located within the steel flange.

$$y_H = \frac{N_{f,V,Rd} + N_{Rd} - N_{w,V,Rd}}{2 b_f f_{vf}} = \frac{978.6 + 584.8 - 207.6}{2 \times 155.3 \times 333.4} \times 1000 = 13.09 \text{ mm}$$

$$y_{po} = h_t + t_f - y_H = 130 + 18.9 - 13.09 = 135.81 \text{ mm}$$

$$N_{f1,Rd} = (t_f - y_H) b_f f_{vf} = \frac{(18.9 - 13.09) \times 155.3 \times 333.4}{1000} = 300.8 \text{ kN}$$

$$N_{f2,Rd} = y_H b_f f_{vf} = \frac{13.09 \times 155.3 \times 333.4}{1000} = 677.8 \text{ kN}$$

$$M_{Tth,V,Rd} = N_{Rd}(t_f + h_t - \frac{\alpha}{2}) + N_{f1,Rd}(\frac{t_f + y_H}{2}) - N_{f2,Rd}(\frac{y_H}{2}) + N_{w,V,Rd}(\frac{d_1}{2})$$

=

$$[584.8(18.9 + 130 - \frac{16.51}{2}) + 300.8(\frac{18.9 + 13.09}{2}) - 677.8(\frac{13.09}{2}) + 207.6(\frac{64}{2})][10^{-3}]$$

= 89.27 kNm

Step 8: Determine the position of the plastic axial centroid and the moment resistance of the composite tee-section at LMS

$$N_{sh,Rd} = n_L P_{Rd} = 6(73.1) = 438.6 \text{ kN}$$

N_{Rd} = minimum of ($N_{c,Rd}$, $N_{sh,Rd}$) = 438.6 kN

$$\alpha = \frac{N_{Rd}}{N_{c,Rd}} d_e = \frac{438.6}{2479}(70) = 12.38 \text{ mm}$$

a) Position of the plastic axial centroid, y_{pctl}

$$y_{pctl} = \frac{N_{Rd}(t_e - \frac{\alpha}{2}) + N_{f,V,Rd}(\frac{t_f}{2} + h_t) + N_{w,V,Rd}(h_t + t_f + \frac{d_1}{2})}{N_{Rd} + N_{f,V,Rd} + N_{w,V,Rd}}$$

$$= \frac{438.6(70 - \frac{12.38}{2}) + 978.6(\frac{18.9}{2} + 130) + 207.6(130 + 18.9 + \frac{64}{2})}{438.6 + 978.6 + 207.6}$$

= 124.3 mm

b) Plastic moment resistance, $M_{Ttl,V,Rd}$

With reference to Table 6.3, there is partial shear connection.
As $N_{sh,Rd} + N_{w,V,Rd} < N_{f,V,Rd}$, the nominal PNA is located within the steel flange.

$$y_L = \frac{N_{f,V,Rd} - N_{Rd} - N_{w,V,Rd}}{2b_f f_{vf}} = \frac{978.6 - 438.6 - 207.6}{2 \times 155.3 \times 333.4} \times 1000 = 3.21 \text{ mm}$$

$$N_{f1,Rd} = (t_f - y_L) b_f f_{vf} = \frac{(18.9 - 3.21) \times 155.3 \times 333.4}{1000} = 812.4 \text{ kN}$$

$$N_{f2,Rd} = y_L b_f f_{vf} = \frac{3.21 \times 155.3 \times 333.4}{1000} = 166.2 \text{ kN}$$

$$M_{Ttl,V,Rd} = -N_{Rd}(t_f + h_p + \frac{\alpha}{2}) + N_{f1,Rd}(\frac{t_f + y_L}{2}) - N_{f2,Rd}(\frac{y_L}{2}) + N_{w,V,Rd}(\frac{d_1}{2})$$

=

$$[-438.6(18.9 + 60 + \frac{12.38}{2}) + 812.4(\frac{18.9 + 3.21}{2}) - 166.2(\frac{3.21}{2}) + 207.6(\frac{64}{2})][10^{-3}]$$

= -21.96 kNm

Step 9: Determine the position of the plastic axial centroid and the moment resistance of the bottom tee-section

$$N_{w,V,Rd} = d_1 t_w f_{vw} = \frac{64 \times 10.5 \times 338}{1000} = 227.2 \text{ kN}$$

$$y_{pcb} = \frac{N_{f,V,Rd}(\frac{t_f}{2}) + N_{w,V,Rd}(\frac{d_1}{2} + t_f)}{N_{f,V,Rd} + N_{w,V,Rd}} = \frac{992(\frac{18.9}{2}) + 227.2(\frac{64}{2} + 18.9)}{992 + 227.2}$$

= 17.17 mm

$$y_{pw} = t_f[\frac{N_{f,V,Rd} + N_{w,V,Rd}}{2N_{f,V,Rd}}] = 18.9[\frac{992 + 227.2}{2 \times 992}] = 11.61 \text{ mm}$$

$$M_{T,V,Rd} = N_{f,V,Rd}[\frac{y_{po}{}^2 + (t_f - y_{po})^2}{2t_f}] + N_{w,V,Rd}[\frac{d_1}{2} + t_f - y_{po}]$$

$$= \{992[\frac{11.61^2 + (18.9-11.61)^2}{2\times 18.9}] + 227.2[\frac{64}{2} + 18.9 - 11.61]\}(10^{-3})$$

$$= 13.86 \text{ kNm}$$

Step 10: Evaluate the applied axial force on the tee-sections

$$z_H = h_t + h - y_{pcth} - y_{pcb} = 130 + 465.8 - 101.0 - 17.17 = 477.63 \text{ mm}$$

$$z_L = h_t + h - y_{pctl} - y_{pcb} = 130 + 465.8 - 124.3 - 17.17 = 454.33 \text{ mm}$$

$$N_{T,Sd} = \frac{2M_{Sd}}{z_H + z_L} = \frac{2\times 308.76}{477.63 + 454.33} \times 1000 = 662.6 \text{ kN}$$

Step 11: Evaluate the modified moment resistances of the bottom steel tee-sections

a) Moment resistance at LMS

$$\alpha_f = \frac{N_{T,Sd}}{2b_f f_{vf}} = \frac{662.6\times 1000}{2\times 155.3\times 338} = 6.31 \text{ mm}$$

$$\beta_f = y_{pcb} - (y_{po} - \frac{\alpha_f}{2}) = 17.17 - (11.61 - \frac{6.31}{2}) = 8.715 \text{ mm}$$

$$N_{f,Sd} = 2\alpha_f b_f f_{vf} = N_{T,Sd} = 662.6 \text{ kN}$$

$$M_{Tbl,VN,Rd} = M_{T,V,Rd} - N_{f,Sd}\beta_f = 13.86 - \frac{662.6\times 8.715}{1000} = 8.08 \text{ kNm}$$

b) Moment resistance at HMS

$$2(t_f - y_{po})b_f f_{vf} = \frac{2(18.9-11.61)\times 155.3\times 338}{1000} = 765.3 \text{ kN} > N_{T,Sd}, \text{ so}$$

$$\alpha_f = \frac{N_{T,Sd}}{2b_f f_{vf}} = 6.31 \text{ mm}$$

$$\beta_f = y_{pcb} - (y_{po} + \frac{\alpha_f}{2}) = 17.17 - (11.61 + \frac{6.31}{2}) = 2.405 \text{ mm}$$

$$N_{f,Sd} = 2\alpha_f b_f f_{vf} = N_{T,Sd} = 662.6 \text{ kN}$$

$$M_{Tbh,VN,Rd} = M_{T,V,Rd} + N_{f,Sd}\beta_f + N_{w,Sd}\beta_w = 13.86 + \frac{662.6\times 2.405}{1000}$$

$$= 15.45 \text{ kNm}$$

Step 12: Evaluate the modified moment resistances of the top composite tee-sections

a) Moment resistance at HMS

The nominal PNA is located within the steel flange, and

$C_2 = 2y_H b_f f_{vf} = \frac{2\times 13.09\times 155.3\times 333.4}{1000} = 1355.5$ kN > $N_{T,Sd}$, so the PNA is remained in the steel flange.

$$\alpha_f = \frac{N_{T,Sd}}{2b_f f_{vf}} = \frac{662.6\times 1000}{2\times 155.3\times 333.4} = 6.4 \text{ mm}$$

$$\beta_f = y_{pcth} - (y_{po} + \frac{\alpha_f}{2}) = 101.0 - (135.81 + \frac{6.4}{2}) = -38.01 \text{ mm}$$

$$M_{Tth,VN,Rd} = M_{T,V,Rd} + N_{c,Sd}\beta_c + N_{f,Sd}\beta_f + N_{w,Sd}\beta_w$$
$$= 89.27 + \frac{662.6(-38.01)}{1000}$$
$$= 64.08 \text{ kNm}$$

b) Moment resistance at LMS

The nominal PNA is located within the steel flange, and

$C_5 = 2(t_f - y_L)b_f f_{vf} = \frac{2(18.9-3.21)\times 155.3\times 333.4}{1000} = 1624.8$ kN > $N_{T,Sd}$, so the PNA is remained in the steel flange.

$$\alpha_f = \frac{N_{T,Sd}}{2b_f f_{vf}} = 6.4\text{mm}$$

$$\beta_f = y_{pctl} - (h_t + \frac{\alpha_f}{2}) = 124.3 - (130 + \frac{6.4}{2}) = -8.9 \text{ mm}$$

$$M_{Ttl,VN,Rd} = M_{T,V,Rd} - N_{c,Sd}\beta_c - N_{f,Sd}\beta_f - N_{w,Sd}\beta_w$$
$$= -21.56 - \frac{662.6(-8.9)}{1000}$$
$$= -16.06 \text{ kNm}$$

Step 14: Check Vierendeel failure

a) Top tee-section

$$M_{Ttl,VN,Rd} + M_{Tth,VN,Rd} + N_{T,Sd}(z_H - z_L)$$
$$= -16.06 + 64.08 + \frac{662.6(477.63 - 454.33)}{1000}$$
$$= 63.46 \text{ kNm} > V_{t,Sd}a_o = (90.18+21.6)(0.5) = 55.89 \text{ kNm}$$

b) Bottom tee-section

$M_{Tbl,VN,Rd} + M_{Tbh,VN,Rd} = 8.08 + 15.45 = 23.53$ kNm > $V_{ab,Sd}a_o = 0$ **(OK)**

Since both the top and the bottom tee-sections do not exhibit Vierendeel failure, the beam is safe to carry the design load; there is no need to perform iterations.

Comments:

(1) If iterations are performed to evaluate an accurate applied axial forces acting

on the tee-sections for the same design load, the following results are obtained:

a) Top tee-section:
$M_{Tll,VN,Rd}$ = -17.22 kNm
$M_{Tlh,VN,Rd}$ = 68.08 kNm
$N_{T,Sd}$ = 564.35 kN

$$M_{Tll,VN,Rd} + M_{Tlh,VN,Rd} + N_{T,Sd}(z_H - z_L)$$
$$= -17.22 + 68.08 + \frac{564.35(477.63 - 454.33)}{1000}$$

= 64.03 kNm larger than 63.46 kNm by 1%

b) Bottom tee-section:
$M_{Tbl,VN,Rd}$ = 9.21 kNm
$M_{Tbh,VN,Rd}$ = 15.48 kNm
$M_{Tbl,VN,Rd} + M_{Tbh,VN,Rd}$ = 9.21 + 15.48 = 24.69 kNm larger than 23.53 kNm by 5%

(2) For illustration purpose, a detailed analysis has been performed to determine the load capacity of the beam. The beam is found to fail under a uniformly disturbed load of 55.16 kN/m, which is about 46.7% higher than the current loading. The force distributions around the web opening at failure are shown in Figure 6.4. At failure, the tee-sections are subjected to different shear force ratios. Also, the moment resistances of the top composite tee-sections at the LMS and the HMS are different. Axial-moment interaction curves for the tee-sections are plotted in Figure 6.5. The plastic moment resistances of the four tee-sections are also marked on the interaction curve for comparison.

(3) A global moment-shear interaction curve for the perforated section in the example at failure is shown in Figure 6.6. Under the current design load, the perforated section is subjected to low global moment and low shear force, which is also indicated as a point below the curve.

6.6 The Specialist Computer Program

A computer program is developed specifically for back-analysis and calibration of the proposed design method against test data. The program is capable of running analysis for both steel beams and composite beams with un-reinforced concentric web openings of the following variations:

a) Steel beams with web openings

Opening shapes: Circular and rectangular

b) Composite beams with web openings

Opening shapes: Rectangular
Concrete slab: No decking,
With profiled steel decking placed parallel to steel beam
With profiled steel decking placed transversely to steel beam

The computer program basically consists of three procedures when performing the calibration exercises. They are: data input, run analysis, and output results.

Procedure I: Data input

At the start of the program, the user is required to choose the types of beams, the opening shapes, and also the types of concrete slabs. Then the program will automatically retrieve the relevant test data from the database for back-analysis in Procedure II.

Procedure II: Run Analysis

Depending on the types of the test data chosen, the program will follow either the procedures in Section 6.2 for the analysis of steel beams with web openings or the procedures in Section 6.4 for the analysis of composite beams with web openings. In either case, the analysis consists of the following eight steps:

Step 1: Determine the global shear force and bending moment at the centerline of the web openings

Step 2: Evaluate the shear and the moment resistances of the perforated section and check the shear and the flexural failures of the perforated section

Step 3: Determine the reduced bending strengths of the flange and the web of the steel tee-sections under shear force

Step 4: Evaluate the basic resistances of the tee-sections

Step 5: Evaluate the axial force acting on the tee-sections

Step 6: Determine the moment resistances of the tee-sections under the axial force and repeat Steps 5 and 6 until a converged axial force is found

Step 7: Check Vierendeel failure of the perforated section

Step 8: Repeat all above steps until the beam fails

Procedure III: Output results

Once a beam is found to fail in a particular mode, the load capacity of the beam together with other information obtained from the back-analysis are output to a spreadsheet for easy interpretation.

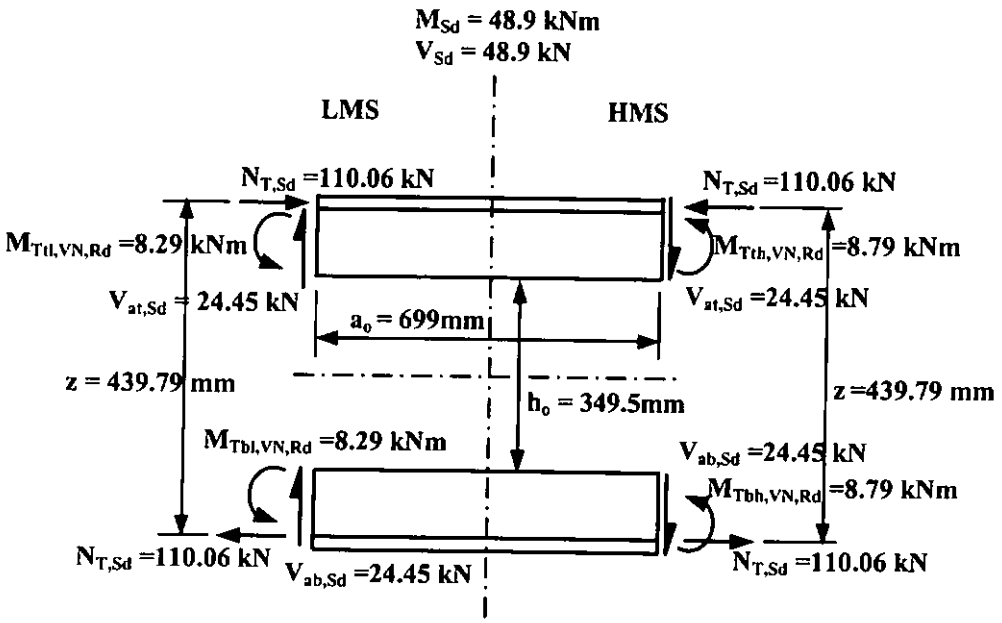

Figure 6.1 Local force distributions at steel perforated section (Design example 1)

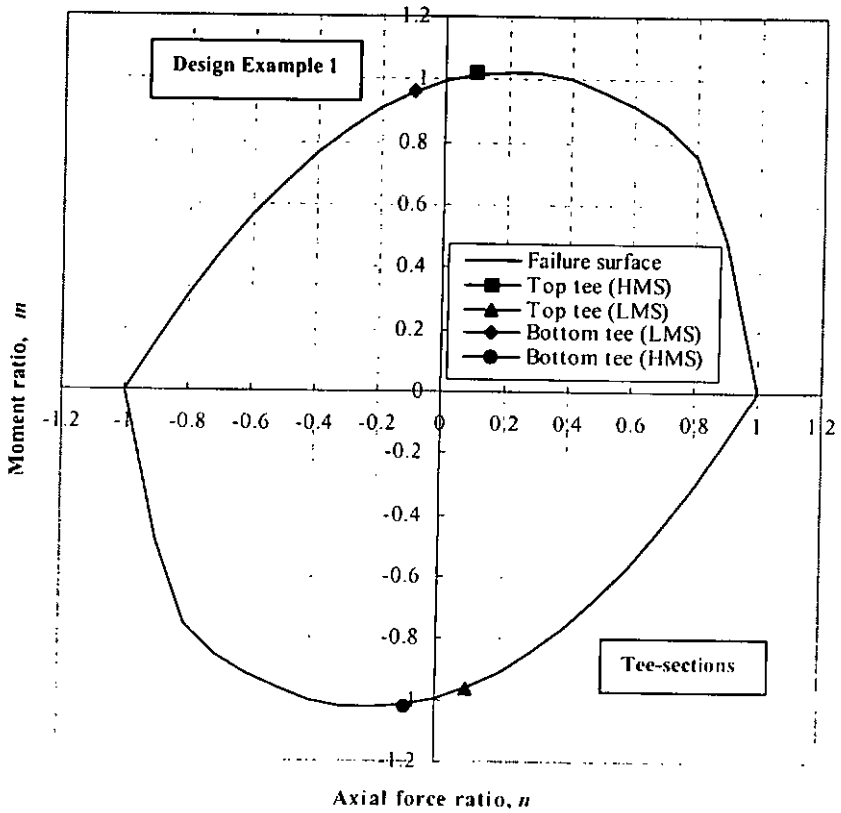

Figure 6.2 Axial-moment interaction curves of steel tee-sections under a shear force ratio of 0.14 (Design example 1)

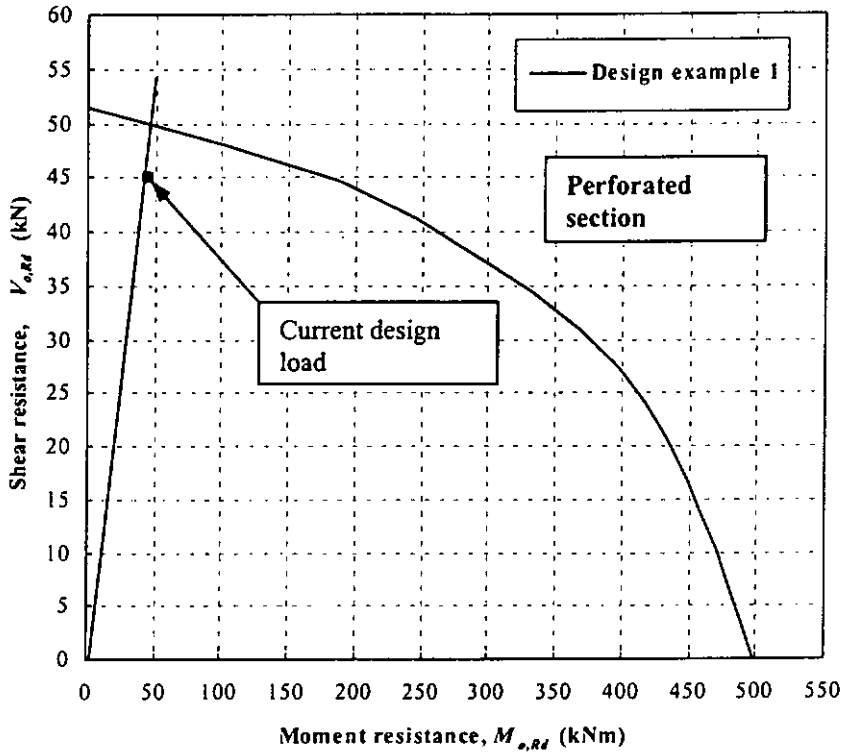

Figure 6.3 Moment-shear interaction curve of perforated steel beam (Design example 1)

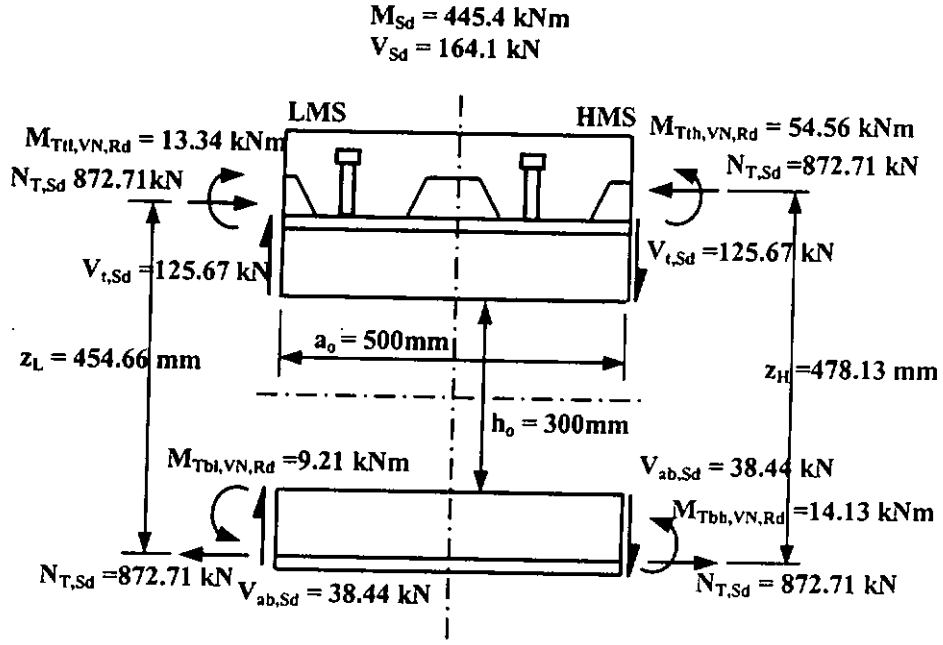

Figure 6.4 Local force distributions at composite perforated section (Design example 2)

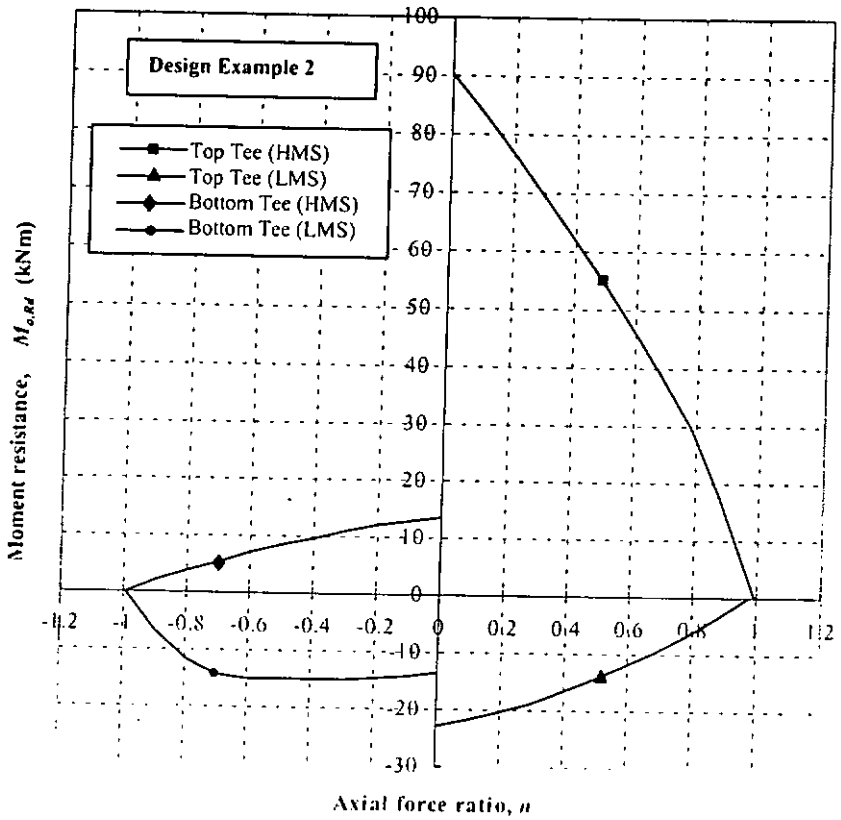

Figure 6.5 Axial-moment interaction curves of tee-sections (Design example 2)

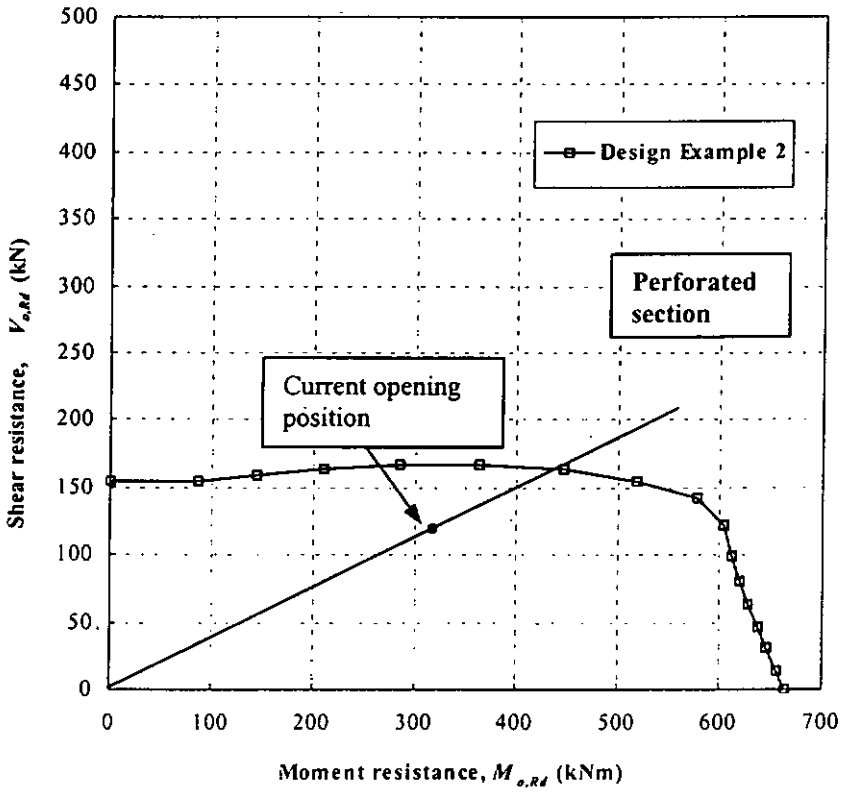

Figure 6.6 Moment-shear interaction curve of perforated composite beam (Design example 2)

Table 6.1 Parameters in determining moment resistance of steel tee-section under axial force

	Nominal PNA_0	Shifted PNA	Criteria	α_f	α_w	β_f	β_w
HMS	Flange	Flange	$N_{TSd} - C_1 \le 0$	$\frac{N_{TSd}}{2b_f f_{vf}}$	0	$y_{pc} - (y_{po} + \frac{\alpha_f}{2})$	0
		Web	$N_{TSd} - C_1 \le C_2$	$t_f - y_{po}$	$\frac{N_{TSd} - N_{fSd}}{2t_w f_{vw}}$	$y_{pc} - (y_{po} + \frac{\alpha_f}{2})$	$y_{pc} - (y_{po} + \alpha_f + \frac{\alpha_w}{2})$
LMS	Flange	Flange	$N_{TSd} - C_3 \le 0$	$\frac{N_{TSd}}{2b_f f_{vf}}$	0	$y_{pc} - (y_{po} - \frac{\alpha_f}{2})$	0

Notes:

$C_1 = 2(t_f - y_{po})b_f f_{vf}$

$C_2 = 2d_1 t_w f_{vw}$

$C_3 = 2y_{po} b_f f_{vf}$

$N_{f,Sd} = 2\alpha_f b_f f_{vf}$

$N_{w,Sd} = 2\alpha_w t_w f_{vw}$

Table 6.2 Formulas in determining nominal moment resistance of composite tee-section at HMS

		Nominal PNA	y_H	y_{po}	$M_{Tth,V,Rd}$
Full shear connection	$N_{shRd} > N_{cRd} > N_{a,V,Rd}$ or $N_{cRd} > N_{shRd} > N_{a,V,Rd}$	**Concrete**	t_f	$h_t + t_f - y_H$	$N_{Rd}(t_f + h_t - \frac{\alpha}{2}) - N_{f,V,Rd}(\frac{t_f}{2}) + N_{w,V,Rd}(\frac{d_1}{2})$
	$N_{shRd} > N_{a,V,Rd} > N_{cRd}$ or $N_{a,V,Rd} > N_{shRd} > N_{cRd}$	**Flange** $N_{Rd} + N_{f,V,Rd} \geq N_{w,V,Rd}$	$\frac{N_{f,V,Rd} + N_{Rd} - N_{w,V,Rd}}{2b_f f_{vf}}$	$h_t + t_f - y_H$	$N_{Rd}(t_f + h_t - \frac{\alpha}{2}) + N_{f1,Rd}(\frac{t_f + y_H}{2}) - N_{f2,Rd}(\frac{y_H}{2}) + N_{w,V,Rd}(\frac{d_1}{2})$
		Web $N_{Rd} + N_{f,V,Rd} < N_{w,V,Rd}$	$\frac{N_{w,V,Rd} - N_{Rd} - N_{f,V,Rd}}{2t_w f_{vw}}$	$h_t + t_f + y_H$	$N_{Rd}(t_f + h_t - \frac{\alpha}{2}) + N_{f,V,Rd}(\frac{t_f}{2}) - N_{w1,Rd}(\frac{y_H}{2}) + N_{w2,Rd}(\frac{d_1 + y_H}{2})$
Partial shear connection	$N_{a,V,Rd} > N_{cRd} > N_{shRd}$ or $N_{cRd} > N_{a,V,Rd} > N_{shRd}$	**Flange** $N_{Rd} + N_{f,V,Rd} \geq N_{w,V,Rd}$	$\frac{N_{f,V,Rd} + N_{Rd} - N_{w,V,Rd}}{2b_f f_{vf}}$	$h_t + t_f - y_H$	$N_{Rd}(t_f + h_t - \frac{\alpha}{2}) + N_{f1,Rd}(\frac{t_f + y_H}{2}) - N_{f2,Rd}(\frac{y_H}{2}) + N_{w,V,Rd}(\frac{d_1}{2})$
		Web $N_{Rd} + N_{f,V,Rd} < N_{w,V,Rd}$	$\frac{N_{w,V,Rd} - N_{Rd} - N_{f,V,Rd}}{2t_w f_{vw}}$	$h_t + t_f + y_H$	$N_{Rd}(t_f + h_t - \frac{\alpha}{2}) + N_{f,V,Rd}(\frac{t_f}{2}) - N_{w1,Rd}(\frac{y_H}{2}) + N_{w2,Rd}(\frac{d_1 + y_H}{2})$

Notes:

$N_{f1,Rd} = (t_f - y_H) b_f f_{vf}$

$N_{f2,Rd} = y_H b_f f_{vf}$

$N_{w1,Rd} = y_H t_w f_{vw}$

$N_{w2,Rd} = (d_1 - y_H) t_w f_{vw}$

$N_{Rd} = MIN(N_{ShRd}, N_{cRd}, N_{a,V,Rd})$

$\alpha = \frac{N_{Rd}}{N_{c,Rd}}(d_c)$

$d_c = h_t$ for solid slab

$d_c = h_c$ for profiled steel decking placed transversely to steel beam

$d_c = h_c + \frac{h_p}{2}$ for profiled steel decking placed parallel to steel beam

Table 6.3 Formulas in determining nominal moment resistance of composite tee-section at LMS

		Nominal PNA	y_L	y_{po}	$M_{Tll,V,Rd}$
Full shear connection	$N_{shRd} > N_{cRd} > N_{a,V,Rd}$ or $N_{cRd} > N_{shRd} > N_{a,V,Rd}$	**Concrete**	t_f	$h_t + t_f - y_L$	$-N_{Rd}(t_f + h_p + \frac{\alpha}{2}) + N_{f,V,Rd}(\frac{t_f}{2}) - N_{w,V,Rd}(\frac{d_1}{2})$
	$N_{shRd} > N_{a,V,Rd} > N_{cRd}$ or $N_{a,V,Rd} > N_{shRd} > N_{cRd}$	**Flange** $N_{Rd} + N_{w,V,Rd} < N_{f,V,Rd}$	$\frac{N_{f,V,Rd} - N_{Rd} - N_{w,V,Rd}}{2b_f f_{vf}}$	$h_t + t_f - y_L$	$-N_{Rd}(t_f + h_p + \frac{\alpha}{2}) + N_{f1,Rd}(\frac{t_f + y_L}{2}) - N_{f2,Rd}(\frac{y_L}{2}) + N_{w,V,Rd}(\frac{d_1}{2})$
		Web $N_{Rd} + N_{w,V,Rd} \geq N_{f,V,Rd}$	$\frac{N_{w,V,Rd} + N_{Rd} - N_{f,V,Rd}}{2t_w f_{vw}}$	$h_t + t_f + y_L$	$-N_{Rd}(t_f + h_p + \frac{\alpha}{2}) + N_{f,V,Rd}(\frac{t_f}{2}) - N_{w1,Rd}(\frac{y_L}{2}) + N_{w2,Rd}(\frac{d_1 + y_L}{2})$
Partial shear	$N_{a,V,Rd} > N_{cRd} > N_{shRd}$ or $N_{cRd} > N_{a,V,Rd} > N_{shRd}$	**Flange** $N_{Rd} + N_{w,V,Rd} < N_{f,V,Rd}$	$\frac{N_{f,V,Rd} - N_{Rd} - N_{w,V,Rd}}{2b_f f_{vf}}$	$h_t + t_f - y_L$	$-N_{Rd}(t_f + h_p + \frac{\alpha}{2}) + N_{f1,Rd}(\frac{t_f + y_L}{2}) - N_{f2,Rd}(\frac{y_L}{2}) + N_{w,V,Rd}(\frac{d_1}{2})$
		Web $N_{Rd} + N_{w,V,Rd} \geq N_{f,V,Rd}$	$\frac{N_{w,V,Rd} + N_{Rd} - N_{f,V,Rd}}{2t_w f_{vw}}$	$h_t + t_f + y_L$	$-N_{Rd}(t_f + h_p + \frac{\alpha}{2}) + N_{f,V,Rd}(\frac{t_f}{2}) - N_{w1,Rd}(\frac{y_L}{2}) + N_{w2,Rd}(\frac{d_1 + y_L}{2})$

Notes:

$N_{f1,Rd} = (t_f - y_L) b_f f_{vf}$

$N_{f2,Rd} = y_L b_f f_{vf}$

$N_{w1,Rd} = y_L t_w f_{vw}$

$N_{w2,Rd} = (d_1 - y_L) t_w f_{vw}$

$N_{Rd} = MIN(N_{ShRd}, N_{cRd}, N_{a,V,Rd})$

$\alpha = \frac{N_{Rd}}{N_{c,Rd}}(d_c)$

$d_c = h_t$ for solid slab

$d_c = h_c$ for profiled steel decking placed transversely to steel beam

$d_c = h_c + \frac{h_p}{2}$ for profiled steel decking placed parallel to steel beam

Table 6.4 Parameters in determining moment resistance of composite tee-section at HMS under axial force

Nominal PNA	Shifted PNA	Criteria	α_c	α_f	α_w	β_c	β_f	β_w
Concrete	Concrete	$N_{TSd} - C_1 \le 0$	$\frac{N_{TSd}}{0.85 b_e f_{ck}}$	0	0	$y_{pcth} - (\alpha + \frac{\alpha_c}{2})$	0	0
	Flange	$N_{TSd} - C_1 \le C_2$	$\frac{C_1}{0.85 b_e f_{ck}}$	$\frac{N_{TSd} - N_{cSd}}{2 b_f f_{vf}}$	0	$y_{pcth} - (\alpha + \frac{\alpha_c}{2})$	$y_{pcth} - (y_{po} + \frac{\alpha_f}{2})$	0
	Web	$N_{TSd} - C_1 - C_2 \le C_3$	$\frac{C_1}{0.85 b_e f_{ck}}$	y_H	$\frac{N_{TSd} - N_{cSd} - N_{fSd}}{2 t_w f_{vw}}$	$y_{pcth} - (\alpha + \frac{\alpha_c}{2})$	$y_{pcth} - (y_{po} + \frac{\alpha_f}{2})$	$y_{pcth} - (y_{po} + a_f + \frac{\alpha_w}{2})$
Flange	Flange	$N_{TSd} - C_2 \le 0$	0	$\frac{N_{TSd} - N_{cSd}}{2 b_f f_{vf}}$	0	0	$y_{pcth} - (y_{po} + \frac{\alpha_f}{2})$	0
	Web	$N_{TSd} - C_2 \le C_3$	0	y_H	$\frac{N_{TSd} - N_{cSd} - N_{fSd}}{2 t_w f_{vw}}$	0	$y_{pcth} - (y_{po} + \frac{\alpha_f}{2})$	$y_{pcth} - (y_{po} + a_f + \frac{\alpha_w}{2})$
Web	Web	$N_{TSd} - C_4 \le 0$	0	0	$\frac{N_{TSd} - N_{cSd} - N_{fSd}}{2 t_w f_{vw}}$	0	0	$y_{pcth} - (y_{po} + a_f + \frac{\alpha_w}{2})$

Notes:

$C_1 = MIN(N_{c.Rd}, N_{sh.Rd}) - N_{a.V.Rd}$

$C_2 = 2 y_H b_f f_{vf}$

$C_3 = 2 d_1 t_w f_{vw}$

$C_4 = 2(d_1 - y_H) t_w f_{vw}$

$N_{c.Sd} = 0.85 \alpha_c b_e f_{ck}$

$N_{f.Sd} = 2 \alpha_f b_f f_{vf}$

$N_{w.Sd} = 2 \alpha_w t_w f_{vw}$

$M_{Th.VN.Rd} = M_{Th.V.Rd} + N_{c.Sd} \beta_c + N_{f.Sd} \beta_f + N_{w.Sd} \beta_w$

Refer to Table 6.2 for value of y_H

Table 6.5 Parameters in determining moment resistance of composite tee-section at LMS under axial force

Nominal PNA	Shifted PNA	Criteria	α_c	α_f	α_w	β_c	β_f	β_w
Concrete	Concrete	$N_{TSd} - C_1 \le 0$	$\frac{N_{TSd}}{0.85 b_e f_{ck}}$	0	0	$y_{pctl} - (t_e - \alpha - \frac{\alpha_c}{2})$	0	0
	Flange	$N_{TSd} - C_1 \le C_2$	$\frac{C_1}{0.85 b_e f_{ck}}$	$\frac{N_{TSd} - N_{cSd}}{2 b_f f_{vf}}$	0	$y_{pctl} - (t_e - \alpha - \frac{\alpha_c}{2})$	$y_{pctl} - (h_t + \frac{\alpha_f}{2})$	0
	Web	$N_{TSd} - C_1 - C_2 \le C_3$	$\frac{C_1}{0.85 b_e f_{ck}}$	t_f	$\frac{N_{TSd} - N_{cSd} - N_{fSd}}{2 t_w f_{vw}}$	$y_{pctl} - (t_e - \alpha - \frac{\alpha_c}{2})$	$y_{pctl} - (h_t + \frac{\alpha_f}{2})$	$y_{pctl} - (h_t + a_f + \frac{\alpha_w}{2})$
Web	Flange	$N_{TSd} - C_2 \le 0$	0	$\frac{N_{TSd} - N_{cSd}}{2 b_f f_{vf}}$	0	0	$y_{pctl} - (h_t + \frac{\alpha_f}{2})$	0
	Web	$N_{TSd} - C_2 \le C_4$	0	t_f	$\frac{N_{TSd} - N_{cSd} - N_{fSd}}{2 t_w f_{vw}}$	0	$y_{pctl} - (h_t + \frac{\alpha_f}{2})$	$y_{pctl} - (h_t + a_f + \frac{\alpha_w}{2})$
Flange	Flange	$N_{TSd} - C_5 \le 0$	0	$\frac{N_{TSd} - N_{cSd}}{2 b_f f_{vf}}$	0	0	$y_{pctl} - (h_t + \frac{\alpha_f}{2})$	0

Notes:

$C_1 = MIN(N_{c,Rd}, N_{sh,Rd}) - N_{a,V,Rd}$

$C_2 = 2 t_f b_f f_{vf}$

$C_3 = 2 d_1 t_w f_{vw}$

$C_4 = 2(d_1 - y_L) t_w f_{vw}$

$C_5 = 2(t_f - y_L) b_f f_{vf}$

$N_{c,Sd} = 0.85 \alpha_c b_c f_{ck}$

$N_{f,Sd} = 2 \alpha_f b_f f_{vf}$

$N_{w,Sd} = 2 \alpha_w t_w f_{vw}$

$M_{Tld,VN,Rd} = M_{Tld,V,Rd} - N_{c,Sd} \beta_c - N_{f,Sd} \beta_f - N_{w,Sd} \beta_w$

Refer to Table 6.3 for value of y_L

CHAPTER 7

CONCLUSIONS

A unified design method is developed to provide harmonized design of steel beams and composite beams with web openings of various sizes and shapes. Based on the study of the tee-sections and the perforated sections of steel beams and composite beams with web openings, the following conclusions can be made:

1) Design formulas for the axial resistances, the shear resistances, and the nominal plastic moment resistances of both steel and composite tee-sections are derived based on structural design principles and plastic stress blocks. Due to global moment at the perforated section and different degrees of shear connection at different locations along a composite beam, two different nominal plastic moment resistances are determined for the composite tee-sections at the LMS and the HMS of the web opening to allow for the different stress blocks. The axial forces arising from global bending action are assumed to act at the plastic axial centroids of the tee-sections above and below the web openings. For composite beams, the axial forces do not coincide at the ends of the top composite tee-section.

2) Simple design formulas for tee-sections based on plastic stress blocks are derived analytically to allow for interaction of axial force and bending moment. It is found that the plastic moment resistance of a steel tee-section can either be increased or decreased, depending on the signs and the magnitudes of both the bending moment and the axial force acting on the steel tee-section. The plastic moment resistances of the steel tee-sections at the LMS are always reduced while those of the steel tee-sections at the HMS are increased for low

values of axial force, but are decreased for high values of axial force. In general, the current empirical interaction formulas with different power indices are conservative as they do not allow any increase in the moment resistance of the tee-section in the presence of low axial force

3) The plastic moment resistances of composite tee-sections at both the LMS and the HMS of the web openings are always modified in the presence of axial force. In the case of full shear connection, the plastic moment resistances of the composite tee-sections are always increased under low axial force. However, there is always reduction in the plastic moment resistances of the composite tee-sections in the presence of axial force when there is partial shear connection. The moment resistance of the composite tee-section at the HMS is always higher than that of the composite tee-section at the LMS.

4) A modified formula is used to evaluate the flange shear area in order to incorporate the effect of the flange thickness. Shear effect on the plastic moment resistance of a tee-section is allowed for through the reduction of the bending strengths of both the web and the flange based on von Mises' yielding criterion. The concrete slab is allowed to carry shear force. A complete axial-moment interaction curve for a steel tee-section under different values of shear force is developed successfully. It is found that low shear force often has a smaller effect on the plastic moment resistance of a tee-section than the axial force. However, a high shear force can cause significant reduction in the plastic moment resistance even when the co-existing axial force is low. A high axial force can cause significant reduction in the plastic moment resistance for all values of applied shear force.

5) Axial-moment interaction curves for composite tee-sections at both the LMS and the HMS of the web opening under different values of shear force are also developed. It is found that the effect of shear force on the plastic moment resistance of a composite tee-section is not as significant as the axial force.

6) In order to assess the load capacities of beams with web openings, the design formulas for tee-section analysis are extended for analysis of perforated section by considering the equilibrium of forces around the perforated section. For steel beams with rectangular web openings, the proposed design method is used to generate moment-shear $(M\text{-}V)_o$ interaction curves for a number of beams, which are compared with those obtained from finite element analysis. The results indicated that the proposed design method is accurate and conservative. For composite beams with rectangular web openings, similar $(M\text{-}V)_o$ interaction curves are also generated and the results are presented.

7) For steel beams with circular web openings, a transformation expression requiring the conversion of the opening into an equivalent octagonal web opening is suggested for use with the proposed design method. Moment-shear interaction curves for these beams have also been generated and compared with results obtained from finite element study and other design methods. The results indicated the proposed design method is both accurate and conservative.

8) Over a hundred test data have been collected from various sources and a comprehensive database is established. Test data using compact steel sections without instability problems are used for the calibration of the proposed design method with a specifically developed computer program. Fourteen test data are selected from the database to calibrate the proposed design method for steel beams with rectangular web openings. The calibration results indicate that the

proposed design method has an improvement of about 8% on the model factors over the current SCI design method. For calibration of steel beams with circular web openings, nine test data are retrieved. The performance of the proposed design method for this kind of beams is also satisfactory.

9) Forty test data of composite beams with rectangular web openings are selected from the established database for the calibration of the proposed design method. It is demonstrated that the proposed design method is able to provide improvement over the SCI design method, especially for composite beams with rectangular web openings utilizing solid slabs and slabs with profiled steel decking placed transversely to the steel beams.

10) The design procedures for both steel and composite beams with web openings are presented in accordance with the proposed design method. Two fully worked design examples are also presented.

11) The proposed unified design method is considered to be straightforward and easy to understand with a high degree of structural accuracy and economy. It is considered to have great potential in practical design with the aid of computer software.

12) The formulation of the proposed design method allows it to be extended readily to cover beams with multiple web openings of various shapes and sizes and steel sections with different cross-section geometries such as symmetric or asymmetric and un-reinforced or reinforced.

CHAPTER 8

FURTHER RESEARCH

Given the complexity and difficulty of the topic in beams with web openings, the proposed unified design method is not able to cover every aspect. It is thus suggested further researches on the topic be carried out and they are briefly discussed in the followings.

1) Local buckling of flange and web

   Beams with web openings with non-compact steel sections may fail prematurely due to local buckling of the flange or the web before the plastic moment resistance of the perforated section is achieved. Thus, more investigations are needed if the proposed design method is to be extended to cover more slender sections.

2) Web post buckling

   In beams with multiple web openings, the width between adjacent openings maybe so narrow that web post buckling could be a problem, which will reduce the load capacity of the beams. The proposed design method currently does not take into account the problem of web post buckling and thus it is only applicable to beams with single web openings.

3) Deflection

   Although additional deflection due to individual web opening represents only a few percents of the total deflection, it could be a problem if there are many openings along the beam, especially when the openings are spaced very closely.

4) Relative positions of deck trough and opening

It is suggested that the strength of the composite perforated section does not depend solely on the number of shear connectors over the opening, but also on the relative positions of deck trough and opening. However, the exact stress distribution around the composite perforated section is still largely unknown. It is envisaged that finite element analysis can provide a better understanding and clarification on this aspect.

5) Various opening shapes

Beams with rectangular web openings often have well-defined tee-sections above and below the openings. Although an equivalent octagonal web opening has been proposed for beams with circular web openings, its application to other opening shapes requires further investigation.

6) Reinforcement for single web opening

Although reinforcement is seldom used around web opening, it is sometimes used in remedial work or when a higher resistance is needed at some particular perforated sections. Some attention could be paid to this subject.

REFERENCES

1. Aglan, A. A. and Qaqish, S. "Plastic behavior of beams with mid-depth web openings". *AISC Engineering Journal*, Vol. 19, No.1, pp. 20-26 (1982)

2. Aglan, A. A. and Redwood, R G. "Web buckling in castellated beams". *Proceedings of the Institution of Civil Engineering (London)*, Vol. 57, Part 2, pp. 307-320 (1974)

3. American Society of Civil Engineers. "Suggested design guides for beams with web holes". By the Subcommittee on Beams with Web Openings of the Task Committee on Flexure Members of the Structural Division, John E. Bower, Chairman, *Journal of the Structural Division, Proceedings of the ASCE*, Vol. 97, No. ST11, pp. 2707-2728 (1971)

4. Bayramoglu, G. " Behaviour of steel I-beams with rectangular web openings". *Proceedings of the 6th International Conference on STEEL & SPACE STRUCTURES*, Singapore, 2-3 September, 1999, pp. 371-377 (1999)

5. Benitez, M. A., Darwin, D., and Donahey, R. C. "Deflections of composite beams with web openings". *SL Report No. 90-3*, University Kansas Center for Research, Lawrence, Kansas, USA, 62pp (1990)

6. Benitez, M. A., Darwin, D., and Donahey, R. C. "Deflections of composite beams with web openings". *Journal of Structural Engineering*, ASCE, Vol. 124, No. 10, pp. 1139-1147 (1998)

7. Bode, H. and Odenbreit, C. "Long-span and high-rise structures". *IABSE reports*, IABSE Symposium, Kobe, Vol. 79, pp. 755-760 (1998)

8. Bode, H., Stengel, J. and Zhou, D. "Composite beam test for a new high-rise building in Frankfurt". *AISC Conference on Composite Construction in Steel and Concrete*, Irsee/Germany, June 14-19 (1996)

9. Bower, J. E. "Elastic stresses around holes in wide-flange beams". *Journal of the Structural Division, Proceedings of the ASCE*, Vol. 92, No. ST2, pp. 85-101 (1966)

10. Bower, J. E. "Design of beams with web openings". *Journal of the Structural Division, Proceedings of the ASCE*, Vol. 94 No. ST3, pp. 783-803 (1968a)

11. Bower, J. E. "Ultimate strength of beams with rectangular holes". *Journal of the Structural Division, Proceedings of the ASCE*, Vol. 94, No. ST6, pp. 1315-1337 (1968b)

12. Bower, J. E. "Recommended design procedures for beams with web openings". *AISC Engineering Journal*, Vol. 8, No. 4, pp. 132-137 (1971)

13. Boyer, J. P. "Castellated beams - new developments". *AISC Engineering Journal*, Vol. 1, No. 3, pp. 104-108 (1964)

14. British Standards Institution. DD ENV 1994-1-1. *Eurocode 4: Design of composite steel and concrete structures, Part 1.1: General rules and rules for buildings (together with United Kingdom National Application Document)*, BSI, 1994, London (1994)

15. British Standards Institution. DD ENV 1993-1-1. *Eurocode 3: Design of steel structures, Part 1.1 General Rules and Rules for Buildings*, BSI, 1992, London (1992)

16. British Standards Institution. ENV 1993-1-1: 1992/A2: 1998. *Amendment A2 of Eurocode 3: Annex N – Openings in webs*, BSI, 1998, London (1998)

17. Chan, P. W. and Redwood, R. G. "Stresses in beams with circular eccentric web holes". *Journal of the Structural Division, Proceedings of the ASCE*, Vol. 100, No. ST1, pp. 231-248 (1974)

18. Chick, C. G., Dayawansa, P. H. and Patrick, M. "Design of composite beams with large steel web penetrations". *The Mechanics of Structures and Materials*, pp.159-164 (1997)

19. Cho, S. H. *Slab behaviour in composite beams at web openings*, PhD thesis, McGill University, Montreal, Quebec, Canada, 162 (1990)

20. Cho, S. H. and Redwood, R. G. "Slab behavior in composite beams at openings I: Analysis". *Journal of Structural Engineering*, ASCE, Vol. 118, ST9, pp. 2287-2303 (1992a)

21. Cho, S. H. and Redwood, R. G. "Slab behavior in composite beams at openings II: Tests and verifications". *Journal of Structural Engineering*, ASCE, Vol. 118, ST9, pp. 2304-2322 (1992b)

22. Chung, K. F. "Structural performance of cold formed sections with single and multiple web openings. Part I: Experimental investigation". *The Structural Engineer*, Vol. 73, No. 9, pp. 141-149 (1995)

23. Chung, K. F. "Structural performance of cold formed sections with single and multiple web openings. Part II: Design rules". *The Structural Engineer*, Vol. 73, No. 14, pp. 223-228 (1995)

24. Chung, K. F. and Chan W. M. "Practical design of composite beams integrated with building services". *Proceedings of the Fifth International Conference on Tall Buildings*, Hong Kong, December 1998, pp. 496-501 (1998)

25. Chung, K. F. and Lawson, R. M. "Simplified design of composite beams with large web openings to Eurocode 4". *Journal of Constructional Steel Research*, Vol. 57, No. 2, pp. 135-163 (2001)

26. Chung, K. F., Liu, T. C. H., and Ko, A. C. H. "Investigation on Vierendeel mechanism in steel beams with circular web openings". *Journal of Constructional Steel Research*, Vol. 57, pp. 467-490 (2001)

27. Chung, K. F. and Liu, T. C. H., and Ko, A. C. H. "Steel beams with large web openings of various shapes and sizes: An empirical design method using a generalized moment-shear interaction curve". (To be published)

28. Clawson, W. C. and Darwin, D. *Composite beams with web openings*, SM Report No. 4, University of Kansas Center for Research, Lawrence, Kansas, 209pp (1980)

29. Clawson, W. C. and Darwin, D. "Strength of composite beams with web openings". *Journal of the Structural Division, Proceedings of the ASCE*, Vol. 108, ST3, pp. 623-641 (1982a)

30. Clawson, W. C. and Darwin, D. "Tests of composite beams with web openings". *Journal of the Structural Division, Proceedings of the ASCE*, Vol. 108, ST1, pp. 145-162 (1982b)

31. Congdon, J. G. and Redwood, R. G. "Plastic behavior of beams with reinforced holes". *Journal of the Structural Division, Proceedings of the ASCE*, Vol. 96, No. ST9, pp. 1933-1956 (1970)

32. Cooper, P. B. and Snell, R. R. "Tests on beams with reinforced web openings". *Journal of the Structural Division, Proceedings of the ASCE*, Vol. 98, No. ST3, pp. 611-632 (1972)

33. Cooper, P. B., Snell, R. R. and Knostman, H. D. "Failure tests on beams with eccentric web holes". *Journal of the Structural Division, Proceedings of the ASCE*, Vol. 103, No. ST9, pp. 1731-1737 (1977)

34. Darwin, David. "Composite beams with web openings". Proceedings of the *AISC National Engineering Conference, Florida*, USA, March 28-30, 1984; also *ASCE Journal of the Boston Society of Civil Engineers Section 71*, No. 1 & 2, pp. 67-83 (1985)

35. Darwin, David. "Behavior and design of composite beams with web openings". In Narayanan, ed., *chapter 3 in Steel-Concrete Composite Structures: Stability and Strength*, Applied Science Publishers, London and New York, pp.53-78 (1988)

36. Darwin, David. *Steel and composite beams with web openings*, American Institute of Steel Construction, Steel Design Guide Series No. 2, Chicago, IL, USA, 63pp (1990)

37. Darwin, David. "Design of composite beams with web openings". *Progress in Structural Engineering and Materials*, Vol. 2, Issue 2, pp. 157-163 (2000)

38. Darwin, D. and Donahey, R. C. "LRFD for composite beams with unreinforced web openings". *Journal of Structural Engineering*, ASCE, Vol. 114, No. ST3, pp. 535-552 (1988)

39. Darwin, D. and Lucas, W. K. "LRFD for steel and composite beams with web openings". *Journal of Structural Engineering*, ASCE, Vol. 116, No. ST6, pp. 1579-1593 (1990)

40. Davies, M. W., Ward, J. K., and Greasley, D. I. "A new approach to the design of long-span floor beams using composite cellform beams". *Steel Construction Today*, Vol. 3, pp. 135-140 (1989)

41. Donoghue, M. "Composite beams with web openings: Design". *Journal of the Structural Division, Proceedings of the ASCE*, Vol. 108, No. ST12, pp. 2652-2667 (1982)

42. Donahey, R. C. and Darwin, D. *Performance and design of composite beams with web openings*, SM Report No. 18, University of Kansas Center for Research, Lawrence, Kansas, 267pp (1986)

43. Donahey, R. C. "Deflections of composite beams with web openings". In Sherman, D. R., ed., *Proceedings of Building Structures, ASCE Structures Congress*, Orlando, Florida, USA, August 1987, pp. 404-417 (1987)

44. Donahey, R. C. and Darwin, D. "Web openings in composite beams with ribbed slabs". *Journal of Structural Engineering*, ASCE, Vol. 114, No. ST3, pp. 518-534 (1988)

45. Dougherty, B. K. "Elastic deformation of beams with web openings". *Journal of the Structural Division, Proceedings of the ASCE*, Vol. 106, No. ST1, pp. 301-312 (1980)

46. Dougherty, B. K. "Buckling of web posts in perforated beams". *Journal of the Structural Division, Proceedings of the ASCE*, Vol. 107, No. ST3, pp. 507-519 (1981)

47. Douglas, T. R. and Gambrell, Jr. S. C. "Design of beams with off-center web openings". *Journal of the Structural Division, Proceedings of the ASCE*, Vol. 100, No. ST6, pp. 1189-1203 (1974)

48. Drucker, D. C. "The effect of shear on the plastic bending of beams". *Journal of Applied Mechanics*, Vol. 23, pp. 509-514 (1956)

49. Fahmy, E. H. "Analysis of composite beams with rectangular web openings". *Journal of Constructional Steel Research*, Vol. 37, No. 1, pp. 47-62 (1996)

50. Frost, R. W. and Leffler, R. E. "Fatigue tests of beams with rectangular web holes". *Journal of the Structural Division, Proceedings of the ASCE*, Vol. 97, No. ST2 (1971)

51. Gotoh, K. "The stresses in wide-flange beams with web holes". *Theoretical and Applied Mechanics*, Vol. 23, pp. 233-242 (1975)

52. Hallex, P. "Limit analysis of castellated steel beams". *Acier-Stahl-Steel*, Vol. 32, No. 3, pp. 133-144 (1967)

53. Hartono, W. and Chiew, S. P. "Composite behaviour of half castellated beam with concrete top slab". *Proceedings of the Fourth Pacific Structural Steel Conference*, Vol. 3, Singapore, pp. 69-76 (1995)

54. Chiew, S. P. and Hartono, W. "Experimental study of composite castellated steel beams". *Journal of Singapore Structural Steel Society*, Vol. 6, No, 1, pp. 31-35 (1995)

55. Heyman, J. and Dutton, V. L. "Plastic design of plate girders with unstiffened webs". *Welding and Metal Fabrication*, Vol. 22, pp. 265-271 (1954)

56. Hodge, P. G. "Interaction curves for shear and bending of plastic beams". *Journal of Applied Mechanics*, Vol. 24, pp. 453-456 (1957)

57. Hope, B. B. and Sheikh, M. A. "The design of castellated beams". *The Engineering Journal, Transaction of the Engineering Institute of Canada*, Vol. 12, No. A-8, pp. 1-9 (1969)

58. Horne, M. R. "The full plastic moments of sections subjected to shear force and axial load". *British Welding Journal*, Vol. 5, pp.170-178 (1958)

59. Hrabok, M. M. and Hosain, M. U. "Castellated beam deflections using substructuring". *Journal of the Structural Division, Proceedings of the ASCE*, Vol. 103, No. ST1, pp. 265-269 (1977)

60. Ito, M., Fujiwara, K., and Okazaki, K. "Ultimate strength of beams with U-shaped hole in top of web". *Journal of Structural Engineering*, ASCE, Vol. 117, No. 7, pp. 1929-1945 (1991)

61. Johnson R. P. and Anderson, D. *Designers' Handbook to Eurocode 4, Part 1.1: Design of Composite Steel and Concrete Structures*, Thomas Telford Services Ltd, London (1993)

62. Johnson R. P. and Yuan, H. "Models and design rules for stud shear connectors in troughs of profiled sheeting". *Proceedings of the Institution of Civil Engineers: Structures and Buildings*, Vol. 128, No. 8, pp. 252-263 (1998)

63. Kerdal, D. and Nethercot, D. A. "Failure modes for castellated beams". *Journal of Constructional Steel Research*, Vol. 4, pp. 295-315 (1984)

64. Kitipornchai, S., Zhu, L., Xiang, Y., and Al-Bermani, F. G. A. "Single-equation yield surfaces for monosymmetric and asymmetric sections". Engineering Structures, Vol. 13, pp. 366-370 (1991)

65. Ko, C. H. and Chung, K. F. "A comparative study on existing design rules of steel beams with circular web openings". In Yang, Y. B., Leu, L. L., and Hsieh, S. H., eds., *Proceedings of the First International Conference on Structural Stability and Dynamics*, Taipei, Taiwan, December 2000, pp. 733-738 (2000)

66. Kong, F. K. and Evans, R. H. *Reinforced and prestressed concrete*, EL BS with Chapman & Hall, U.K., 508pp (1987)

67. Knowles, P. R. "Castellated beams". *Proceedings of the Institute of Civil Engineering*, Vol. 90, Part 1, pp. 521-536 (1991)

68. Kussman, R. L. and Cooper, P. B. "Design example for beams with web openings." *AISC Engineering Journal*, Vol.13, No. 2, pp. 48-56 (1976)

69. Knostman, H. D., Cooper, P. B., and Snell, R. R. "Shear force distribution at eccentric web openings". *Journal of the Structural Division, Proceedings of the ASCE*, Vol. 103, No. ST6, pp. 1207-1221 (1977)

70. Larnach, W. J. and Park, R. "The behaviour under load of six castellated composite T-beams". *Civil Engineering and Public Works Review*, Vol. 59, No. 692, pp. 339-343, (1964)

71. Lawson, R. M. *Design for openings in the webs of composite beams*, CIRIA Special Publication and SCI Publication 068, CIRIA/The Steel Construction Institute, UK, 44pp (1987)

72. Lawson, R. M., Chung K. F., and Price, A. M. "Tests on composite beams with large web openings to justify existing design methods". *The Structural Engineer*, Vol. 70, No. 1, pp. 1-7 (1992)

73. Liu, T. C. H. and Chung, K. F. "Steel beams with large web openings of various shapes and sizes: Finite element investigation". (To be published)

74. Liu, T. C. H., Chung, K. F., and Ko, A. C. H. "Finite element modeling on Vierendeel mechanism in steel beams with large circular web openings". *Proceedings of the International Conference on Structural Engineering, Mechanics and Computation*, Cape Town, South Africa, April 2001, pp. 1567-1574 (2001)

75. Low, E. F. and Chang, W. F. "Stress concentrations around shaped holes". *Journal of the Engineering Mechanics Division, Proceedings of the ASCE*, Vol. 93, EM3, pp. 33-44 (1967)

76. Lu, F. and Sherbourne, A. N. "Strain hardening beams under shear, bending, and axial forces". *Journal of Engineering Mechanics*, ASCE, Vol. 119, No. 11, pp. 2174-2193 (1993)

77. Lucas, W. K. and Darwin, D. *Steel and composite beams with web openings*, SM Report No. 23, University of Kansas Center for Research, Lawrence, Kansas, 188pp (1990)

78. Lupien, R. *Web openings in steel beams reinforced on one side*, Master of Engineering Thesis, McGill University, Montreal, Quebec, Canada, 167pp (1977)

79. Lupien, R. and Redwood, R. G. "Steel beams with web openings reinforced on one side". *Canadian Journal of Civil Engineering*, Vol. 5, No. 4, pp. 451-461 (1978)

80. MacGinley, T. J. and Choo, B. S. *Reinforced concrete: Design theory and Examples*, Chapman & Hall, U.K., 520pp (1990)

81. McCutcheon, J. O., So, W. C., and Gersovitz, B. "A study of the effects of large circular openings in the webs of wide flange beams". *Applied Mechanics Series Report No. 2*, Structures Laboratory, Department of Civil Engineering and Applied Mechanics, McGill University, Montreal, Canada, 12pp (1963)

82. Neal, B. G. "The effect of shear and normal forces on the fully plastic moment of a beam of rectangular cross section". *Journal of Applied Mechanics*, Vol. 28, pp. 269-274 (1961b)

83. Neal, B. G. "Effect of shear force on the fully plastic moment of an I-beam", *Journal of Mechanical Engineering Science*, Vol. 3, No. 3, pp. 258-266 (1961a)

84. Neal, B. G. "Effect of shear and normal forces on the fully plastic moment of a beam of an I-beam". *Journal of Mechanical Engineering Science*, Vol. 3, No. 3, pp. 279-285 (1961c)

85. Nethercot, D. A. and Rockey, K. C. "A unified approach to the elastic lateral buckling of beams". *The Structural Engineer*, Vol. 49, No. 7, pp. 321-330 (1971)

86. Oehlers, D. J. and Bradford, M. A. *Composite steel and concrete structural members: Fundamental behaviour*, Oxford: Pergamon Press (1995)

87. Olander, H. C. "A method of calculating stress in rigid frame corners". *Journal of the Structural Division, Proceedings of the ASCE*, August (1953)

88. Oostrom, J. Van. *Plastic analysis of the castellated beam*, Master of Applied Science in Civil Engineering Thesis, University of Waterloo, USA, 172pp (1969)

89. Patrick, M. and Tse, D. "Composite beam web penetration design methods – putting theory into practice". *Paper Supplement at the Pacific Structural Steel Conference 1989*, Australian Institute of Steel Construction, Queensland, Australia, 28-21 May, 1989, pp. 1-48 (1989)

90. Poumbouras, George. *Modification of a theory predicting the shear strength of hollow composite beams with large web openings*, Project Report No. U83-20, Department of Civil Engineering and Applied Mechanics, McGill University, Montreal, Quebec, Canada, 109pp (1983)

91. Price, A. M. *Tests on composite beams with web openings*, Department of Engineering, University of Warwick (1990)

92. Redwood, R. G. "Plastic behavior and design of beams with web openings". *Proceedings of the First Canadian Structural Engineering Conference*, Canadian Steel Industries Construction Council, Toronto, Canada, February, 1968, pp. 127-138 (1968)

93. Redwood, R. G. "The strength of steel beams with unreinforced web holes". *Civil Engineering and Public Works Review*, Vol. 64, No. 755, pp. 559-562 (1969)

94. Redwood, R. G. "Simplified plastic analysis for reinforced web holes". *AISC Engineering Journal*, No. 8, No. 3, pp. 128-131 (1971)

95. Redwood, R. G. "Tables for plastic design of beams with rectangular holes". *AISC Engineering Journal*, Vol. 9, No. 1, pp. 2-19 (1972)

96. Redwood, R. G. *Design of beams with web holes*. Canadian Steel Industries Construction Council, Canada, 45pp (1973)

97. Redwood, R. G. "Design of I-beams with web perforations". In Narayanan, R., ed., *Chapter 4 in Beams and Beam Columns: Stability and Strength*, Applied Science Publishers, London and New York, pp. 95-133 (1983)

98. Redwood, R. G. "The design of composite beams with web openings". *Proceedings of the First Pacific Structural Steel Conference*, Auckland, New Zealand, pp. 169-185 (1986)

99. Redwood, R. G. "Behaviour of composite castellated beams". *Progress in Structural Engineering and Materials*, Vol. 2, Issue 2, pp. 164-168 (2000)

100. Redwood, R. G. and Chan, P. W. "Design aids for beams with circular eccentric web holes". *Journal of the Structural Division, Proceedings of the ASCE*, Vol. 100, No. ST2, pp. 297-303 (1974)

101. Redwood, R. G. and Cho, S. H. "Design tools for steel beams with web openings". *In Composite Steel Structures*, Elsevier Applied Science, London, pp. 75-83 (1987)

102. Redwood, R. G. and Cho, S. H. "Design of steel and composite beams with web openings". *Journal of Constructional Steel Research*, Vol. 25, pp. 231-248 (1993)

103. Redwood, R. G. and McCutcheon, J. O. "Beam tests with unreinforced web openings". *Journal of the Structural Division, Proceedings of the ASCE*, Vol. 94, No. ST1, pp. 1-17 (1968)

104. Redwood, R. G. and Poumbouras, G. "Tests of composite beams with web openings". *Canadian Journal of Civil Engineering*, Vol. 10, No. 4, pp. 713-721 (1983)

105. Redwood, R. G. and Poumbouras, G. "Analysis of composite beams with web openings". *Journal of Structural Engineering*, ASCE, Vol. 110, No. ST9, pp. 1949-1958 (1984)

106. Redwood, R. G. and Shrivastava, S. C. "Design recommendations for steel beams with web holes". *Canadian Journal of Civil Engineering*, Vol. 7, No. 4, pp. 642-650 (1980)

107. Redwood, R. G. and Uenoya, M. "Critical loads for webs with holes". *Journal of the Structural Division, Proceedings of the ASCE*, Vol. 105, No. ST10, pp. 2053-2067 (1979)

108. Redwood, R. G. and Wong, P. K. "Web holes in composite beams with steel deck". *Proceedings of the Eighth Canadian Structural Engineering Conference*. Canadian Steel Construction Council, Willowdale, Ontario, Canada, February 1982, 41pp (1982)

109. Redwood, R. G., Baranda, H. and Daly, M. J. "Tests of thin-webbed beams with unreinforced holes". *Journal of the Structural Division, Proceedings of the ASCE*, Vol. 104, ST3, pp. 577-595 (1978)

110. Robbie, J. N. "Structural applications of cellular beams". In Lee, ed., *Structures in the New Millennium*, Balkema, Rotterdam, pp. 303-310 (1997)

111. Sahmel, P. "Konstruktive Ausbildung and Näherungsberechnung geschweisster Biegeträger und Torsionssäbe mit grossen Stegausnehmungen (The design, construction and approximate calculation of welded transverse beams and torsion bars having pronounced web clearance)". *Schweissen und Schneiden*, Vol. 21, No. 3, pp. 116-122 (1969)

112. Segner, E. P. "Reinforcement requirements for girder web openings". *Journal of the Structural Division, Proceedings of the ASCE*, Vol. 90, No. ST3, pp. 147-164 (1964)

113. Shan, M. Y., LaBoube, R. A., and Yu, W. W. "Bending and shear behavior of web elements with openings". *Journal of Structural Engineering*, ASCE, Vol. 122, No. 8, pp. 854-859 (1996)

114. Shan, M. Y., Batson, K. D., LaBoube, R. A., and Yu, W. W. "Local buckling flexural strength of webs with openings". *Engineering Structures*, Vol. 16, No. 5, pp. 317-323 (1994)

115. Sherbourne, A. N. and Oostrom, J. V. "Plastic analysis of castellated beams I: Interaction of moment, shear and axial force". *Computers and Structures*, Vol. 2, pp. 79-109 (1972a)

116. Sherbourne, A. N. and Oostrom, J. V. "Plastic analysis of castellated beams II: Analysis and tests". *Computers and Structures*, Vol. 2, pp. 111-140 (1972b)

117. Shrivastava, S. C. and Redwood R. G. "Web instability near reinforced rectangular holes". *IABSE Proceedings*, No. P-6, pp. 1-15 (1977)

118. Shrivastava, S. C. and Redwood, R. G. "Shear carried by flanges at unreinforced web holes". *Journal of the Structural Division, Proceedings of the ASCE*, Vol. 105, No. ST8, pp. 1706-1711 (1979)

119. Slutter, R. G. and Driscoll, G. C. "Flexural strength of steel-concrete composite beams". *Journal of the Structural Division, Proceedings of the ASCE*, Vol. 91, No. ST2, pp. 71-99 (1965)

120. Srimani, S. L. and Das, P. K. "Finite element analysis of castellated beams". *Computers and Structures*, Vol. 9, pp. 169-174 (1978)

121. Swartz, S. E. and Eliufoo, K. S. "Composite beams with web openings". *Journal of the Structural Division, Proceedings of the ASCE*, Vol. 106, No. ST5, pp. 1203-1208 (1980)

122. Thompson, P. J. and Ainsworth, I. "Composite beams with web penetrations: Grosvenor Place, Sydney". *Proceedings of the Third Conference on Steel Development*, Australian Institute of Steel Conference, Melbourne, Australia, pp. 11-18 (1985)

123. Todd, D. M. and Cooper, P. B. "Strength of composite beams with web openings". *Journal of the Structural Division, Proceedings of the ASCE*, Vol. 106, No. ST2, pp.431-444 (1980)

124. Tse, D. and Dayawansa, P. H. "Elastic deflection of steel and composite beams with web penetrations". *The Structural Engineer*, Vol. 70, No. 21, pp. 372-380 (1992)

125. Uenoya, M. and Redwood, R. G. "Buckling of webs with openings". *Computers and Structures*, Vol. 9, No. 2, pp. 191-199 (1978)

126. Wang, T. M., Snell, R. R. and Cooper, P. B. "Strength of beams with eccentric reinforced holes". *Journal of the Structural Division, Proceedings of the ASCE*, Vol. 101, No. ST9, pp. 1783-1799 (1975)

127. Ward, J. K. *Design of composite and non-composite cellular beams.* SCI Publication 100, The Steel Construction Institute, 49pp (1990)

APPENDIX A

SUMMARY OF EXPERIMENTAL TEST DATA

A.1 TESTS FOR STEEL BEAMS WITH WEB OPENINGS

A.1.1 Bower (1968b)
A.1.2 Clawson and Darwin (1980)
A.1.3 Congdon and Redwood (1970)
A.1.4 Cooper and Snell (1972)
A.1.5 Cooper, Snell, and Knostman (1977)
A.1.6 Redwood and McCutcheon (1968)
A.1.7 Lupien and Redwood (1978)
A.1.8 Redwood, Baranda, and Daly (1978)
A.1.9 Shrivastava and Redwood (1977)

A.2 TESTS FOR COMPOSITE BEAMS WITH WEB OPENINGS

A.2.1 Cho and Redwood (1992b)
A.2.2 Clawson and Darwin (1980)
A.2.3 Donahey and Darwin (1986)
A.2.4 Lawson, Chung, and Price (1992)
A.2.5 Redwood and Poumbouras (1983)
A.2.6 Redwood and Wong (1982)

A.1.1 Bower (1968b)

1 General

1.1	Number of beams (tests):	4(4)
1.2	Beam spans:	3 m
1.3	Steel beam sizes:	4-W16x36
1.4	Steel element yield strength:	232.4 – 303.4 N/mm^2
1.5	Steel beam depth:	401.3-404.8 mm
1.6	Span/depth ratio:	7.53-7.59

2 Opening Configurations

2.1	Shapes of web openings:	4-rectangular
2.2	Number of eccentric openings:	0
2.3	Number of reinforced openings:	0
2.4	Location of opening/span:	0.17-0.5 span
2.5	Length/height of openings:	1.01-1.26
2.6	Height of openings/depth of beam:	0.45-0.46
2.7	M/V ratio at centerline of opening:	0-1.02 m
2.8	Others:	

			Measured yield strength (N/mm^2)		
Tests	Failure loads, P (kN)	Modes of failure	Top flange	Bottom flange	Web
B11	419.0	Vierendeel	249.6	249.6	303.4
B21	378.2	Vierendeel	245.5	245.5	277.2
B31	442.2 + 221.1	Vierendeel	232.4	232.4	259.9
B41	444.8	Vierendeel	241.3	241.3	301.3

Beam B11

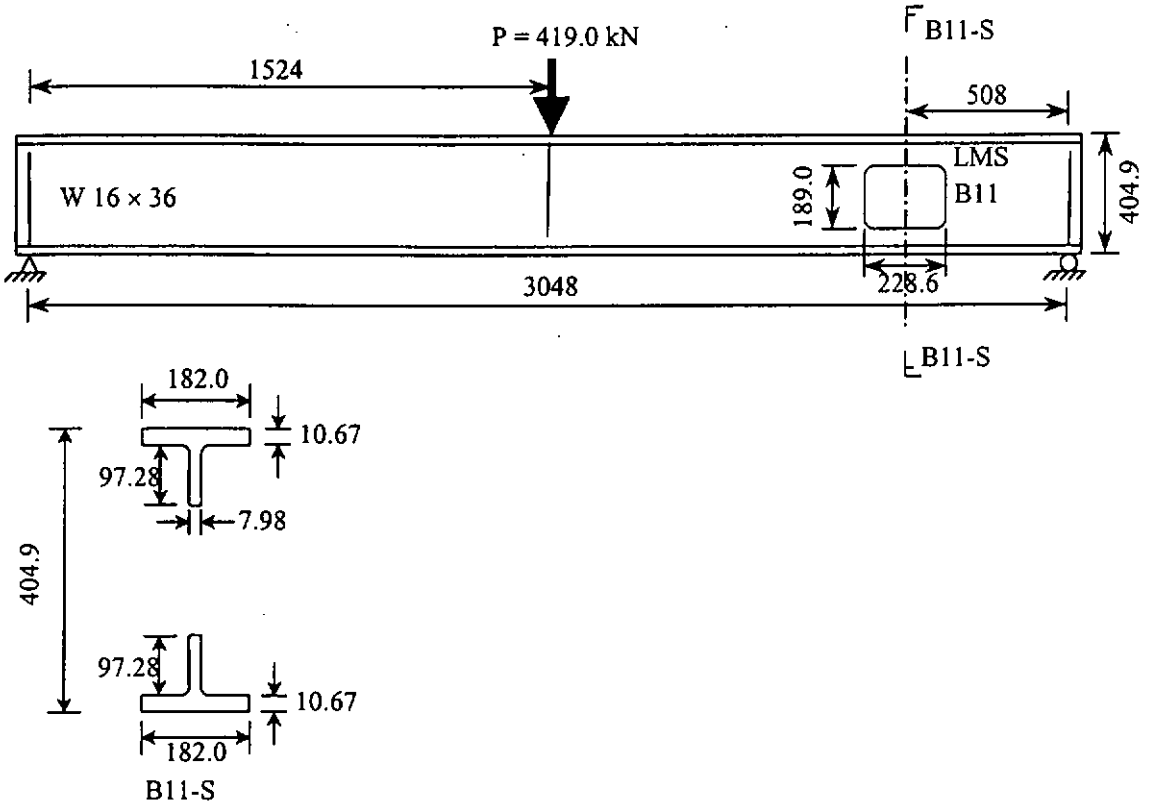

Beam B21

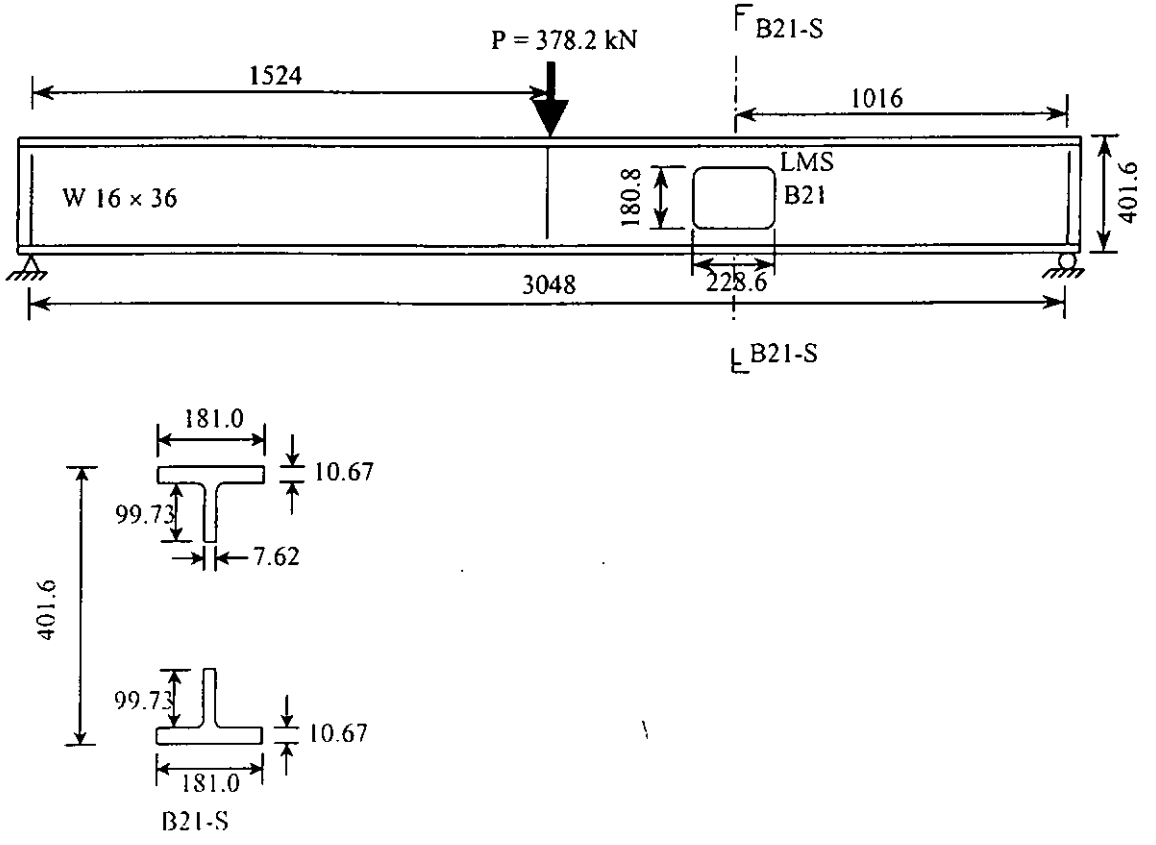

Beam B31

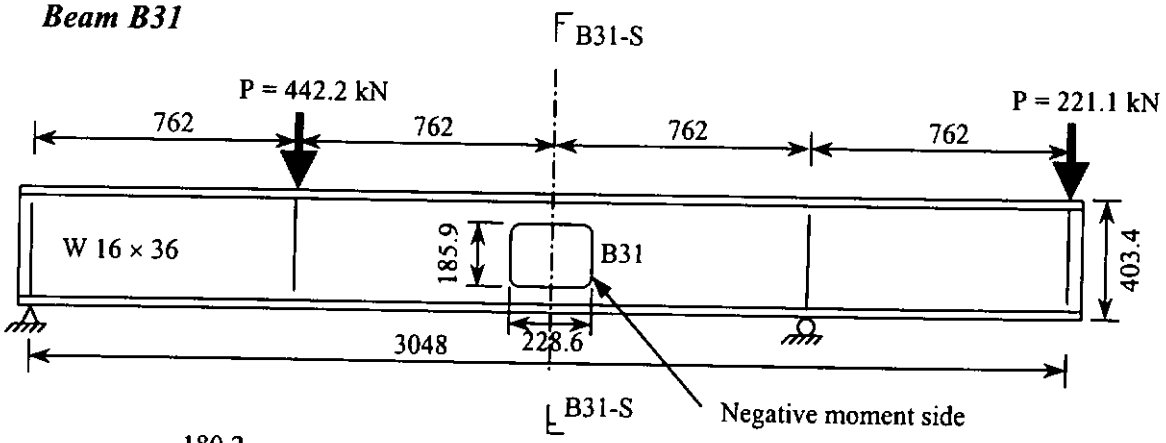

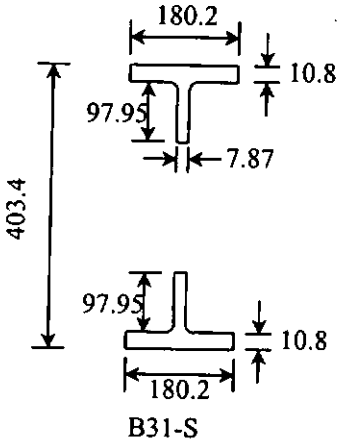

Beam B41

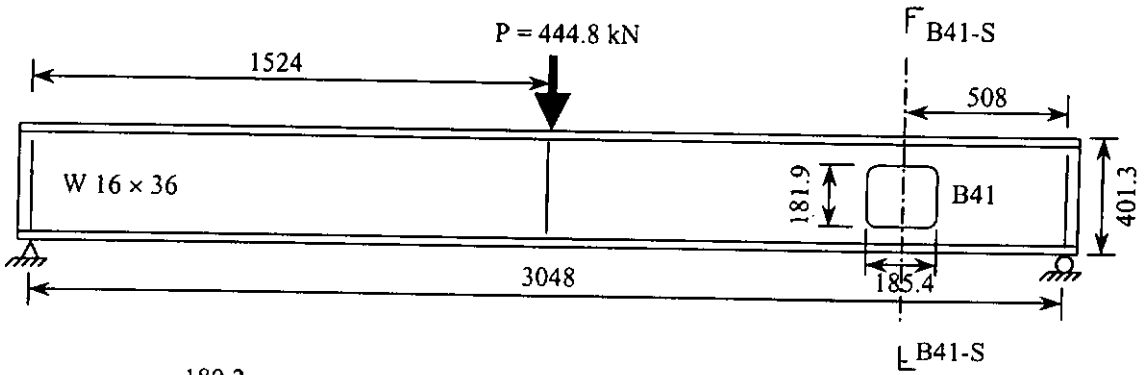

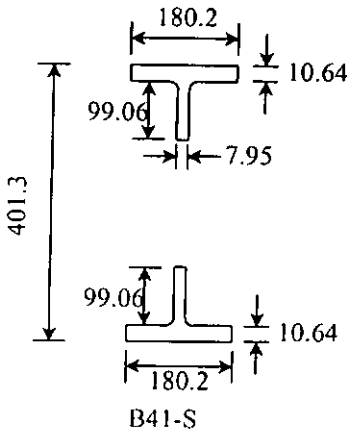

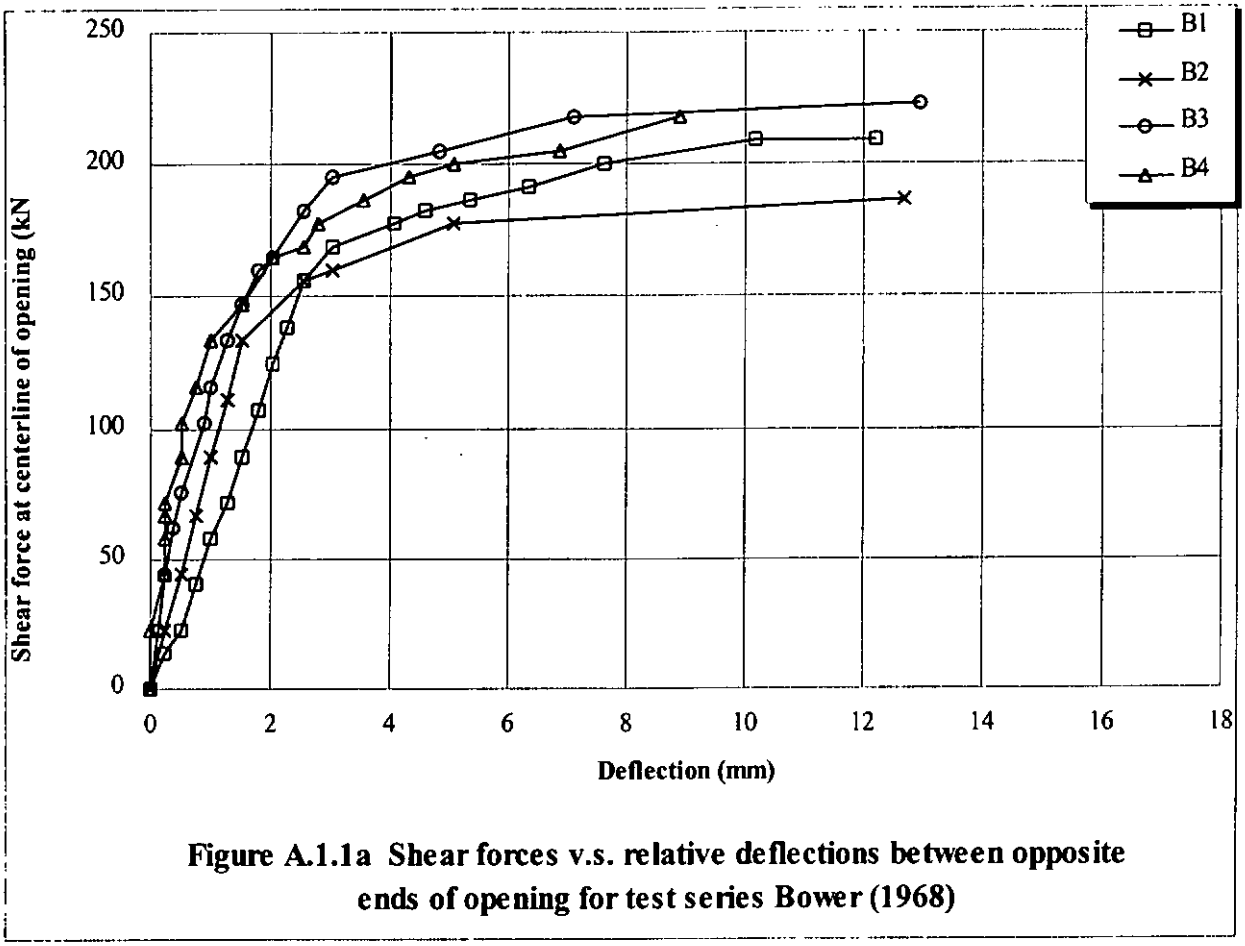

Figure A.1.1a Shear forces v.s. relative deflections between opposite ends of opening for test series Bower (1968)

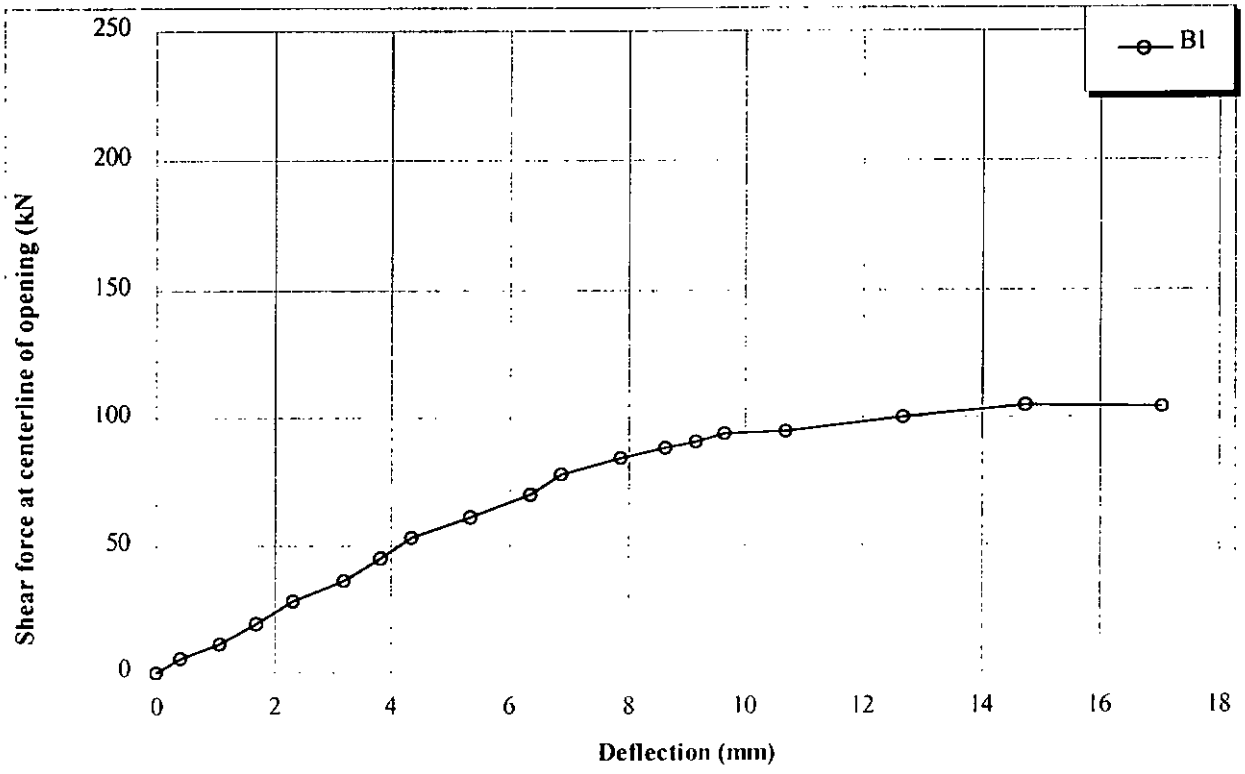

Figure A.1.1b Shear forces v.s. mid-span deflections for test series Bower (1968)

A.1.2 Clawson and Darwin (1980)

1 General

1.1	Number of beams (tests):	1(1)
1.2	Beam spans:	4.5 m
1.3	Steel beam sizes:	1-W18x45
1.4	Steel element yield strength:	309.5-358.5 N/mm^2
1.5	Steel beam depth:	454 mm
1.6	Span/depth ratio:	10

2 Opening Configurations

2.1	Shapes of web openings:	1-rectangular
2.2	Number of eccentric openings:	0
2.3	Number of reinforced openings:	0
2.4	Length/height of openings:	1.99
2.5	Height of openings/depth of beam:	0.6
2.6	Location of opening along beam:	0.2 span
2.7	M/V ratio at centerline of opening:	0.91 m
2.8	Others:	

			Measured yield strength (N/mm^2)		
Tests	Failure loads, P (kN)	Modes of failure	Top flange	Bottom flange	Web
CD4B	123.66 + 123.66	Vierendeel	319.85	309.51	358.53

Beam CD4B

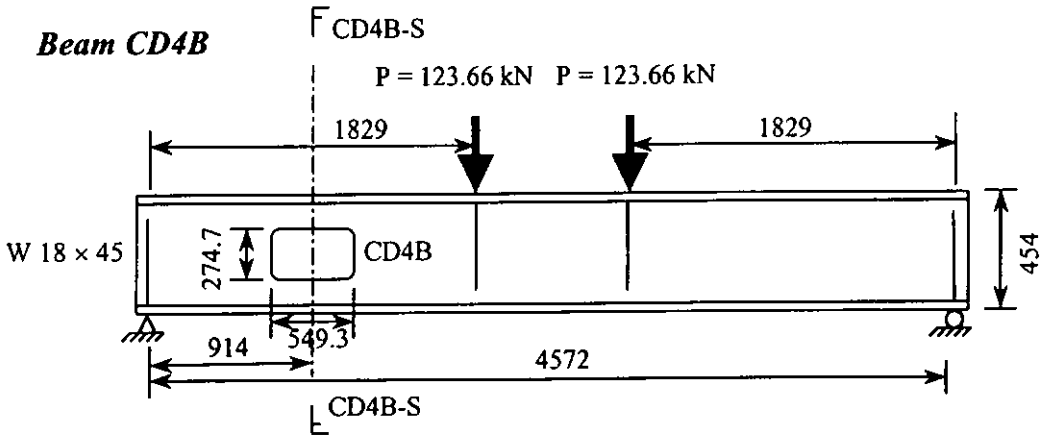
CD4B-S
P = 123.66 kN
P = 123.66 kN
1829
1829
W 18 × 45
274.7
CD4B
454
914
549.3
4572
CD4B-S

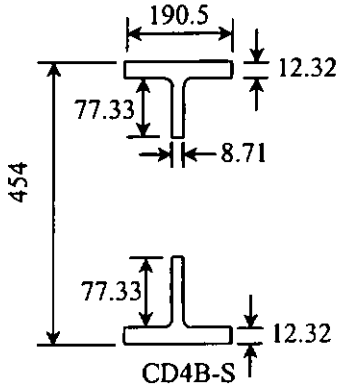
190.5
12.32
77.33
8.71
454
77.33
12.32
CD4B-S

A.1.3 Congdon and Redwood (1970)

1 General

1.1	Number of beams (tests):	13(13)
1.2	Beam spans:	2.2 m
1.3	Steel beam sizes:	1-W10x21, 12-W14x38
1.4	Steel beam grade:	274.4 – 395.1 N/mm^2
1.5	Steel beam depth:	251.2-362.4 mm
1.6	Span/depth ratio:	6.3-9.1

2 Opening Configurations

2.1	Shapes of web openings:	13-rectangular
2.2	Number of eccentric openings:	0
2.3	Number of reinforced openings:	2-one sided, 10-two sided
2.4	Location of opening/span:	0.19-0.50 span
2.5	Length/height of openings:	1.49-1.99
2.6	Height of openings/depth of beam:	0.49-0.63
2.7	M/V ratio at centerline of opening:	0.43-1.14 m
2.8	Others:	

			Measured yield strength (N/mm^2)			
Tests	Failure loads, P (kN)	Modes of failure	Top flange	Bottom flange	Web	Reinforcement
CJR1A	160.1	Vierendeel	297.2	297.2	395.1	255.1
CJR2A	473.3	Vierendeel	267.5	267.5	284.8	301.3
CJR2B	367.4	Vierendeel	267.5	267.5	284.8	301.3
CJR2C	487.5	Vierendeel	307.5	307.5	384.7	274.4
CJR2D	596.1	Vierendeel	307.5	307.5	384.7	274.4
CJR3A	511.5	Vierendeel	267.5	267.5	284.8	301.3
CJR3B	442.2	Vierendeel	307.5	307.5	384.7	228.2
CJR4A	508.9	Vierendeel	307.5	307.5	384.7	274.4
CJR4B	382.5	Vierendeel	307.5	307.5	384.7	274.4
CJR5A	395.9	Vierendeel	307.5	307.5	384.7	306.1
CJR6A	400.3	Vierendeel	307.5	307.5	384.7	-
CJR7B	379.0	Vierendeel	279.2	279.2	328.9	275.1
CJR7B	544.5	Vierendeel	279.2	279.2	328.9	275.1

Beam CR1A

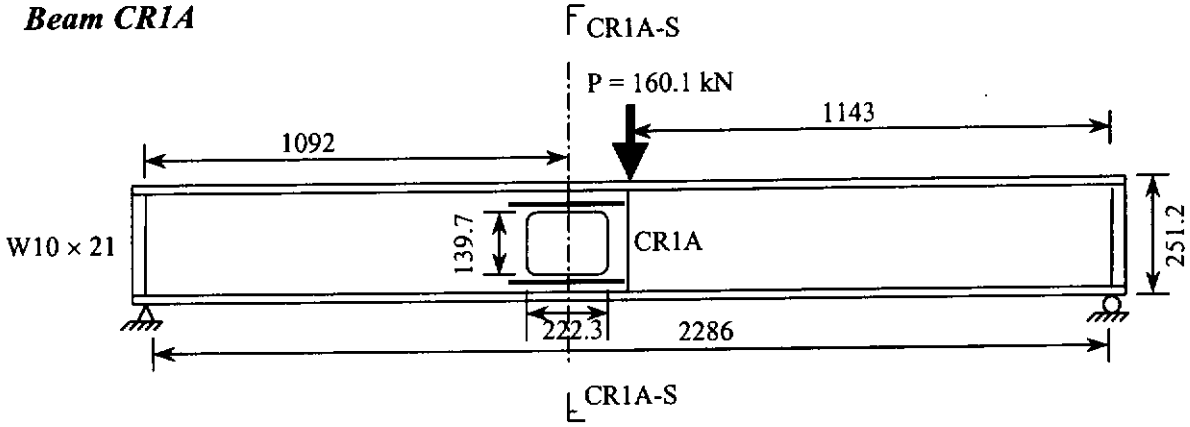

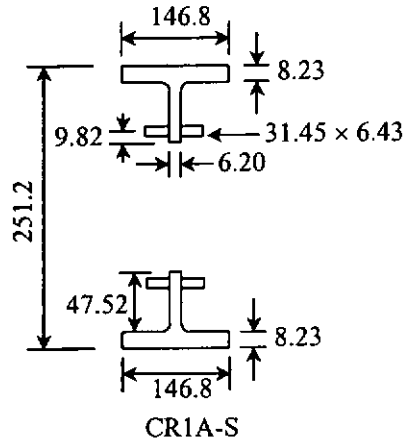

Beam CR2A

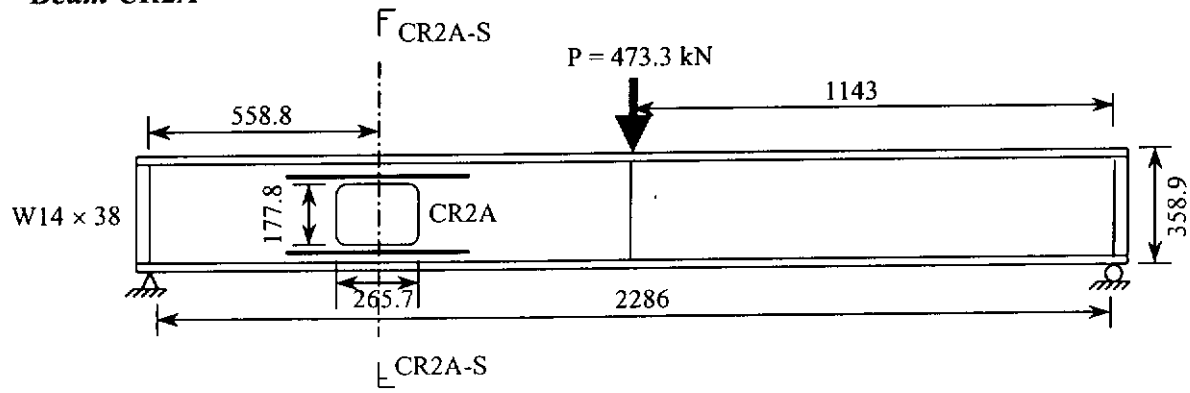

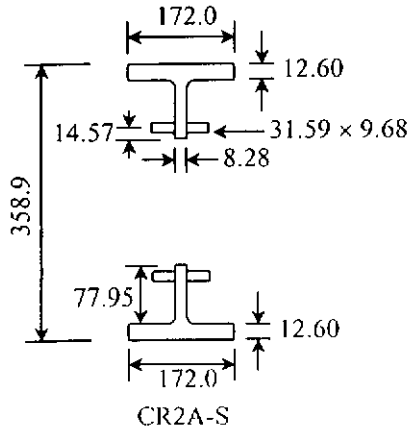

Beam CR2B

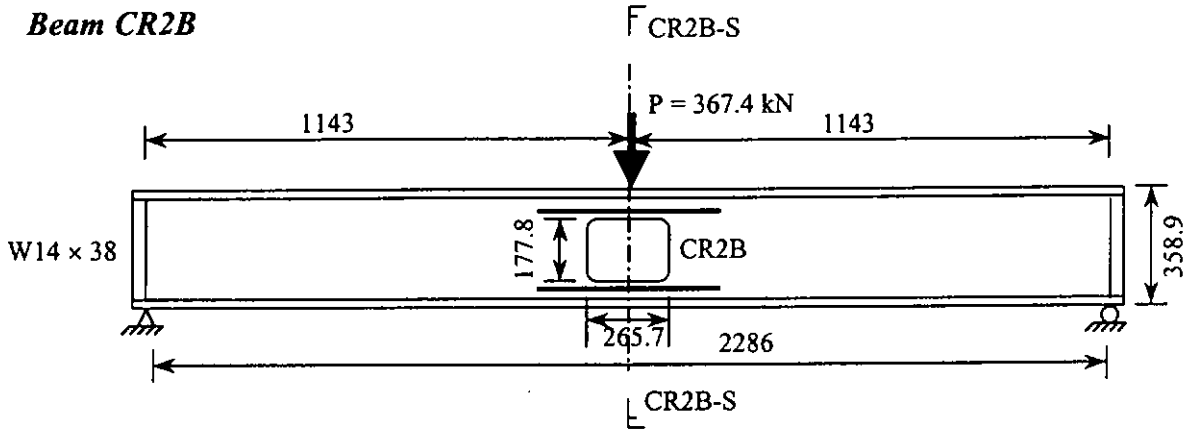

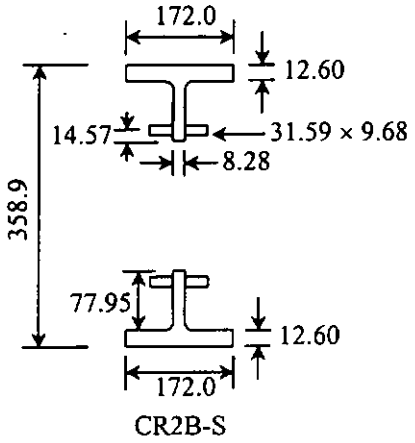

Beam CR2C

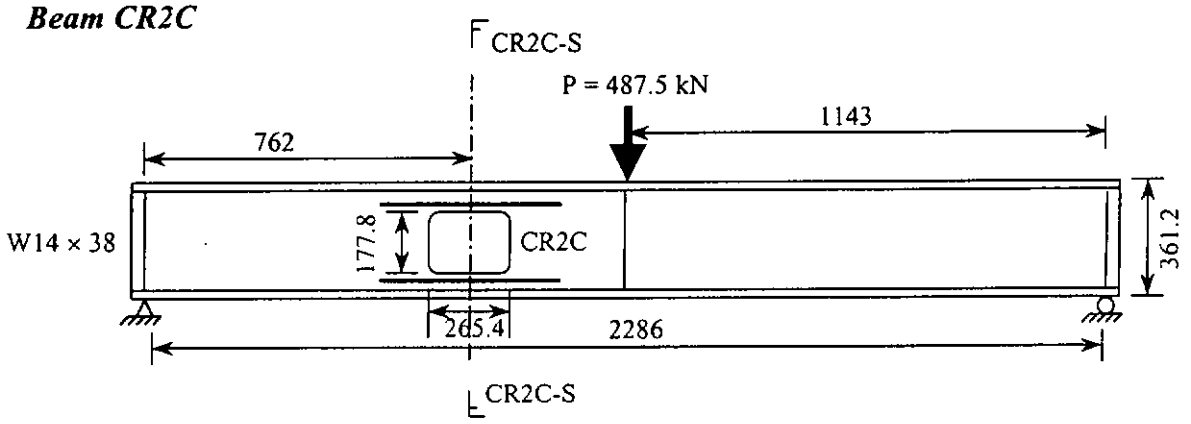

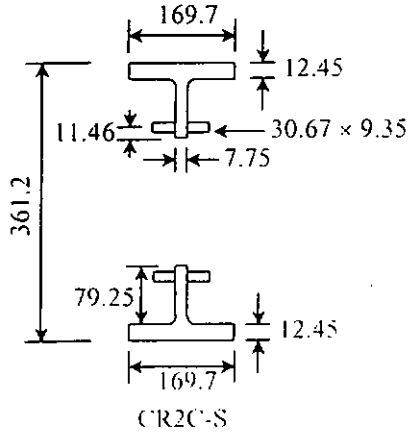

Beam CR2D

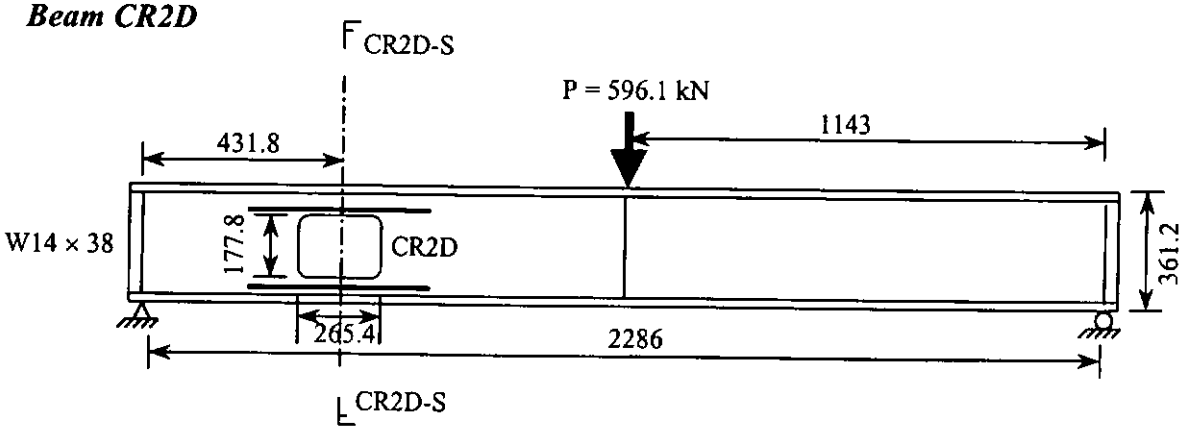

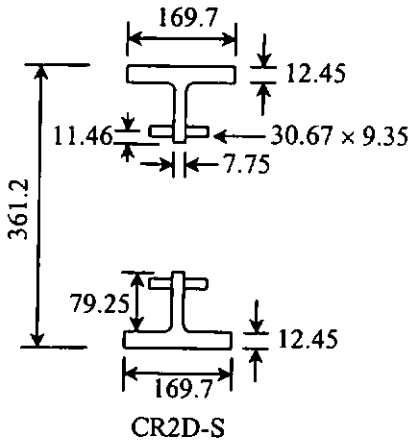

Beam CR3A

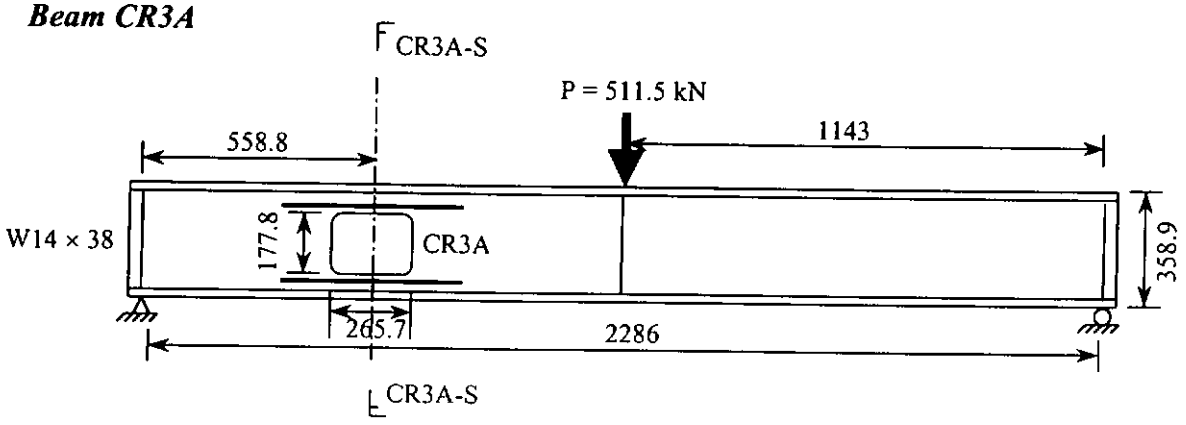

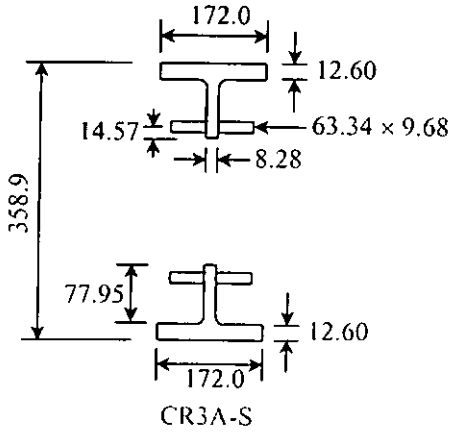

Beam CR3B

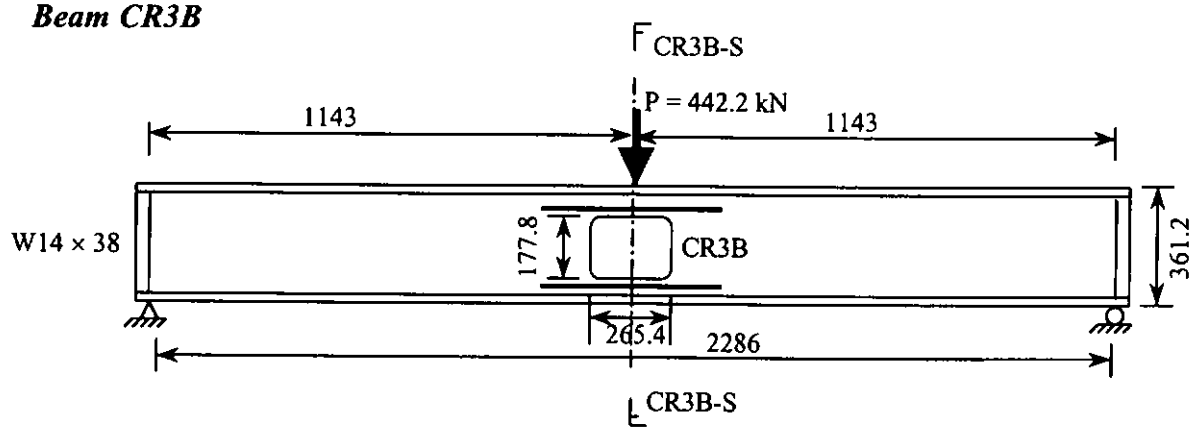

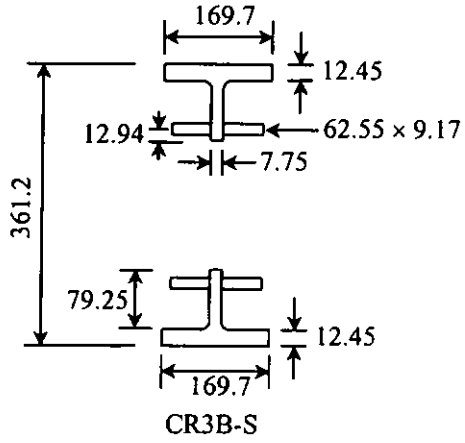

Beam CR4A

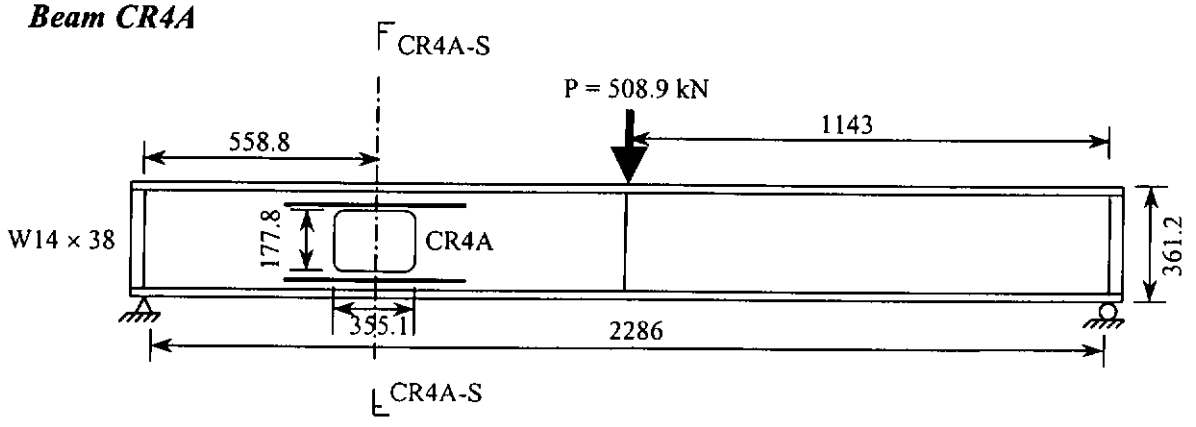

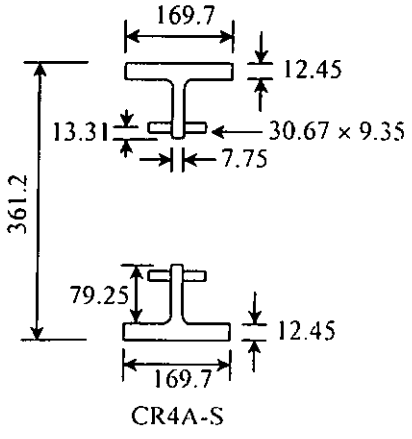

Beam CR4B

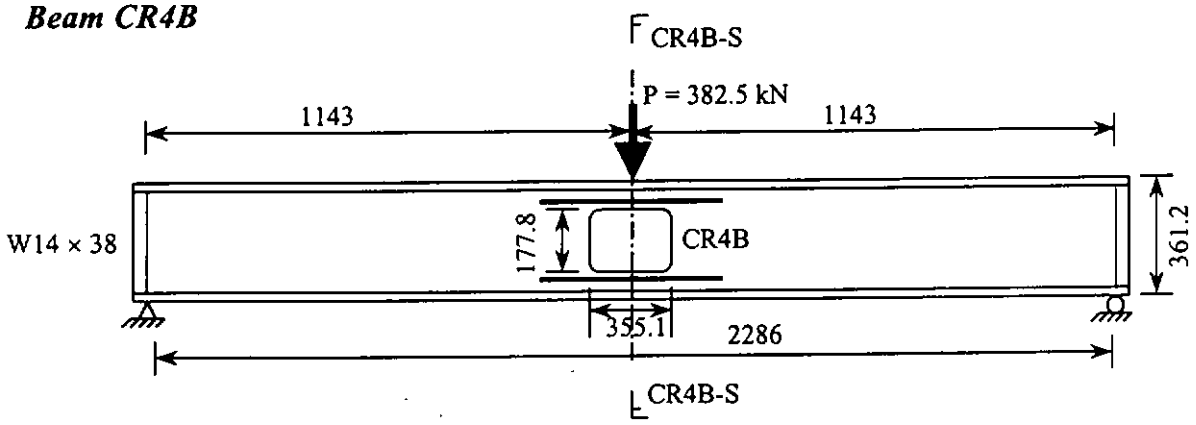

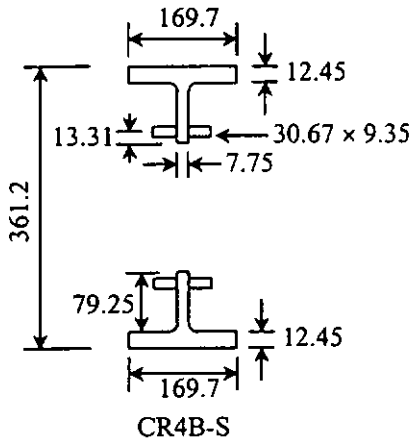

Beam CR5A

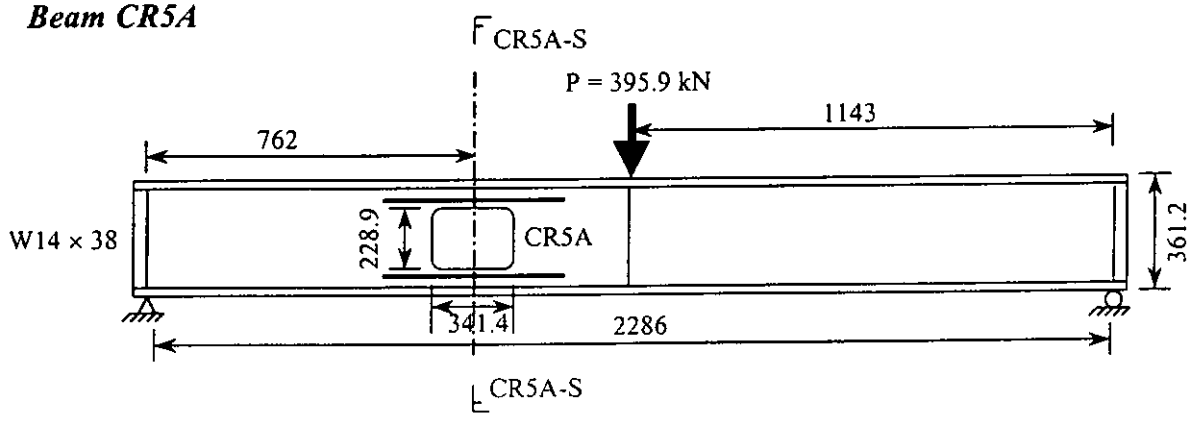

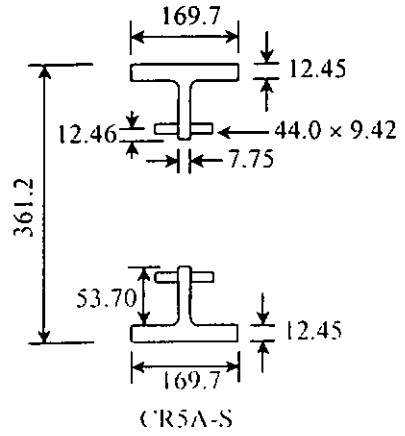

Beam CR6A

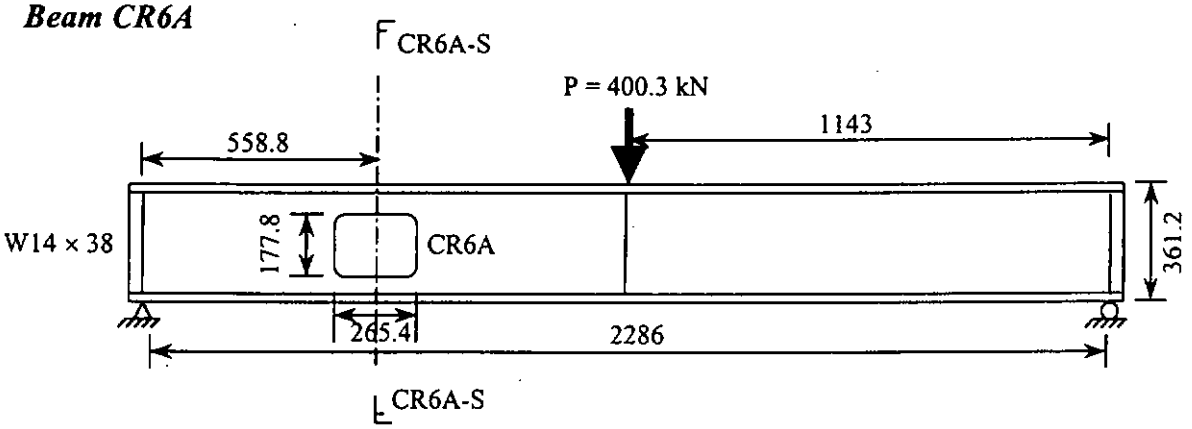

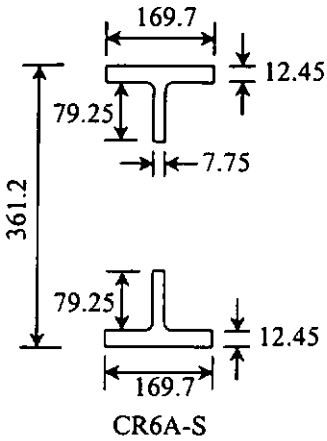

Beam CR7B

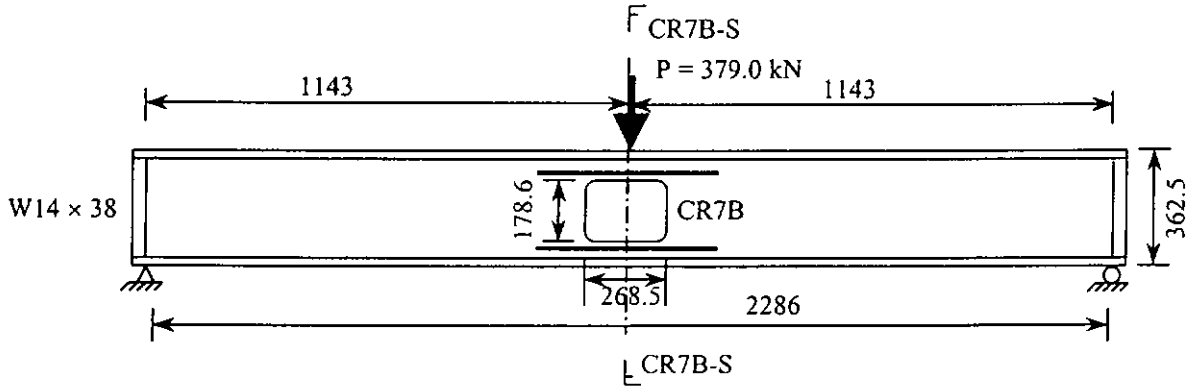

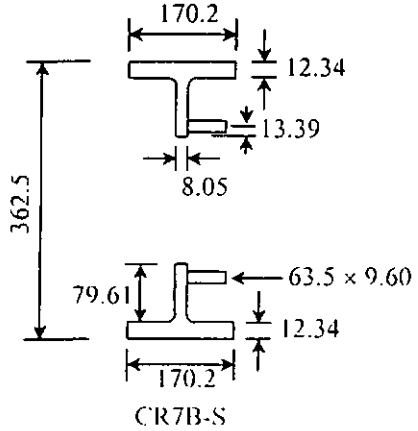

Beam CR7D

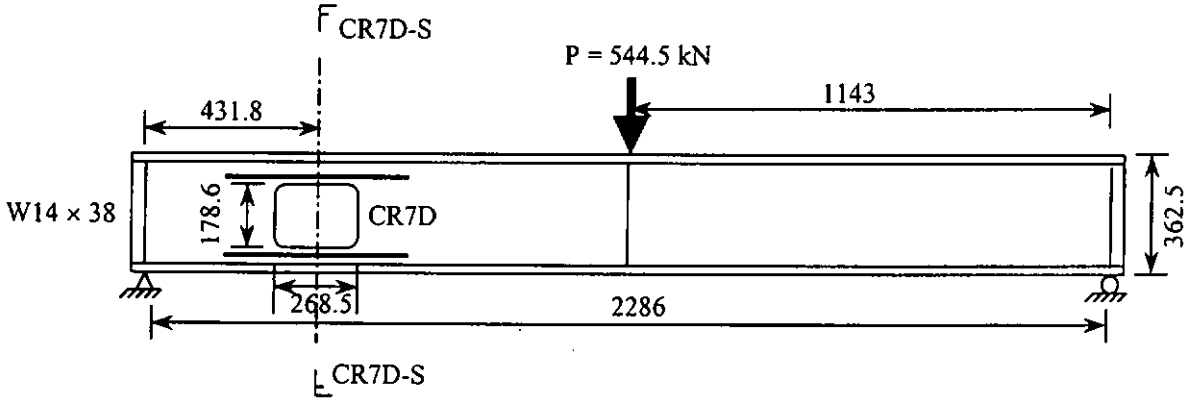
CR7D-S
P = 544.5 kN
431.8
1143
W14 × 38
178.6
CR7D
362.5
268.5
2286
CR7D-S

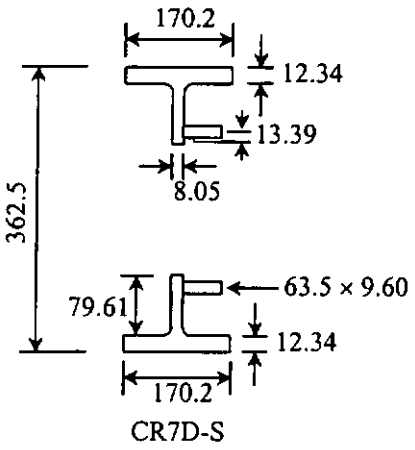
170.2
12.34
13.39
8.05
362.5
79.61
63.5 × 9.60
12.34
170.2
CR7D-S

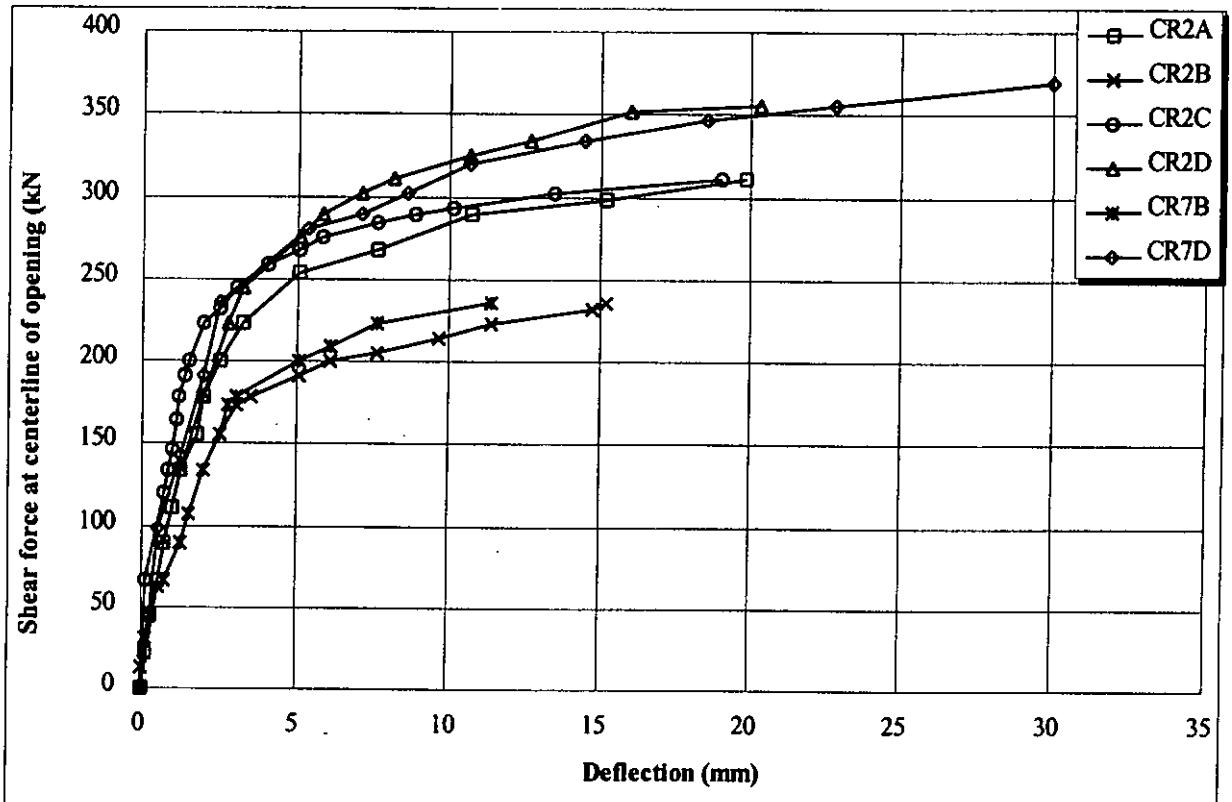

Figure A.1.3a Shear forces v.s. relative deflections between ends of opening for test series Congdon & Redwood (1970)

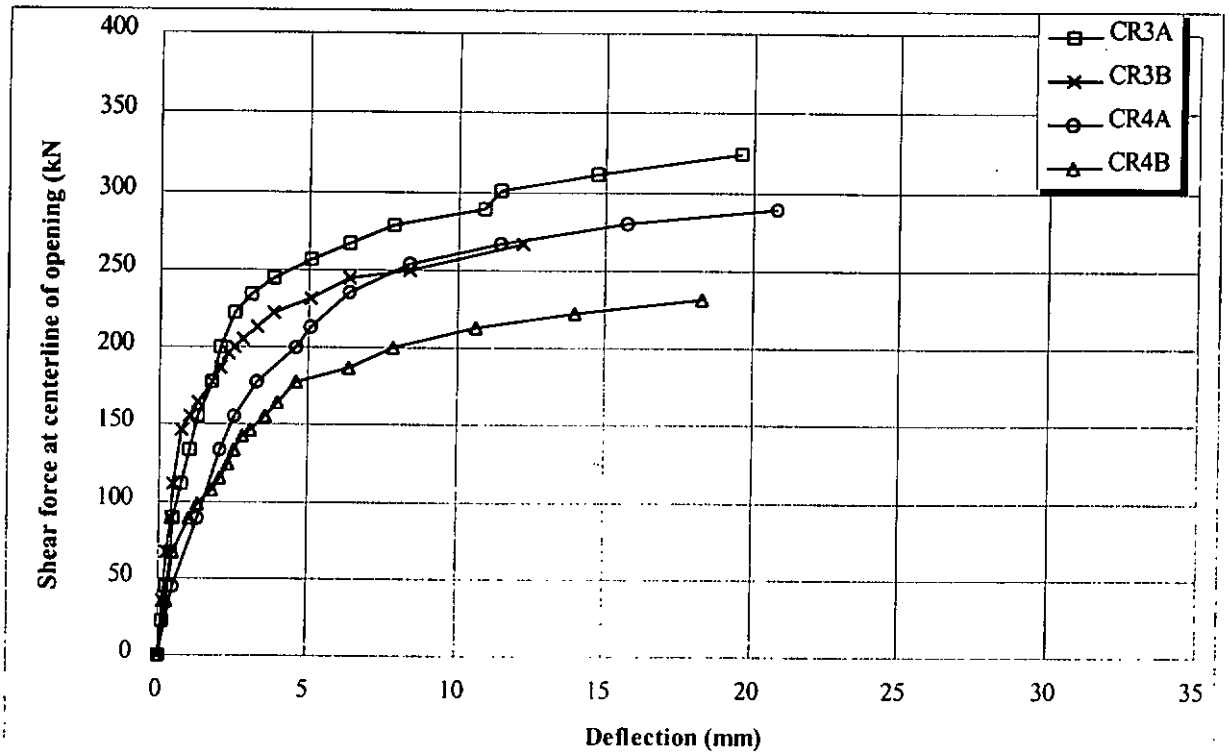

Figure A.1.3b Shear forces v.s. relative deflections between ends of opening for test series Congdon & Redwood (1970)

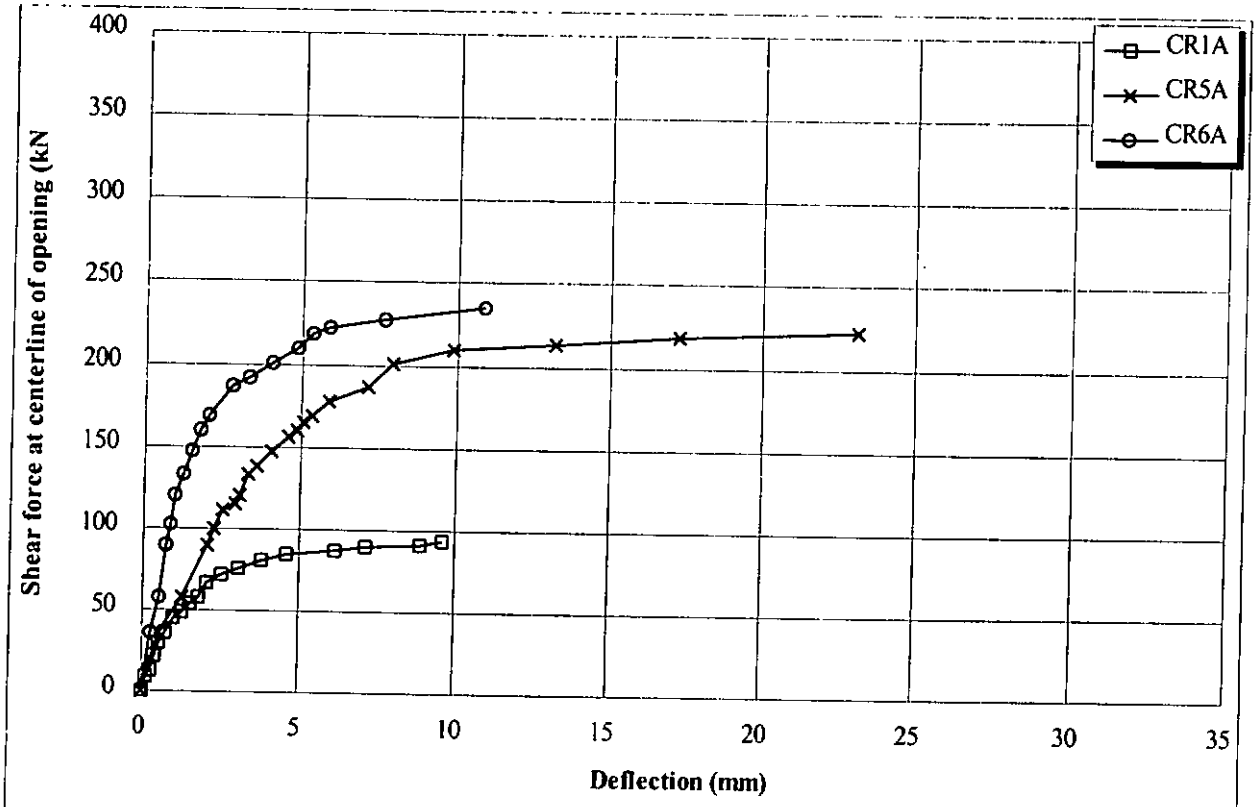

Figure A.1.3c Shear forces v.s. relative deflections between ends of opening for test series Congdon & Redwood (1970)

A.1.4 Cooper and Snell (1972)

1 General

1.1	Number of beams (tests):	3(3)
1.2	Beam spans:	3.0-4.0 m
1.3	Steel beam sizes:	3-W12x45
1.4	Steel yield strength:	222.0 – 258.6 N/mm^2
1.5	Steel beam depth:	306.3 mm
1.6	Span/depth ratio:	9.9-13.2

2 Opening Configurations

2.1	Shapes of web openings:	3-rectangular
2.2	Number of eccentric openings:	0
2.3	Number of reinforced openings:	1-one sided, 2-two sided
2.4	Location of opening/span:	0.33-0.38 span
2.5	Length/height of openings:	1.50
2.6	Height of openings/depth of beam:	0.49
2.7	M/V ratio at centerline of opening:	1.02-1.52 m
2.8	Others:	

			Measured yield strength (N/mm^2)			
Tests	Failure loads, P (kN)	Modes of failure	Top flange	Bottom flange	Web	Reinforcement
CS1	231	Flexure	227.5	227.5	258.6	239.2
CS2	233	Flexure	232.4	232.4	248.9	241.3
CS3	316	Vierendeel	222.0	222.0	257.9	228.2

Beam CS1

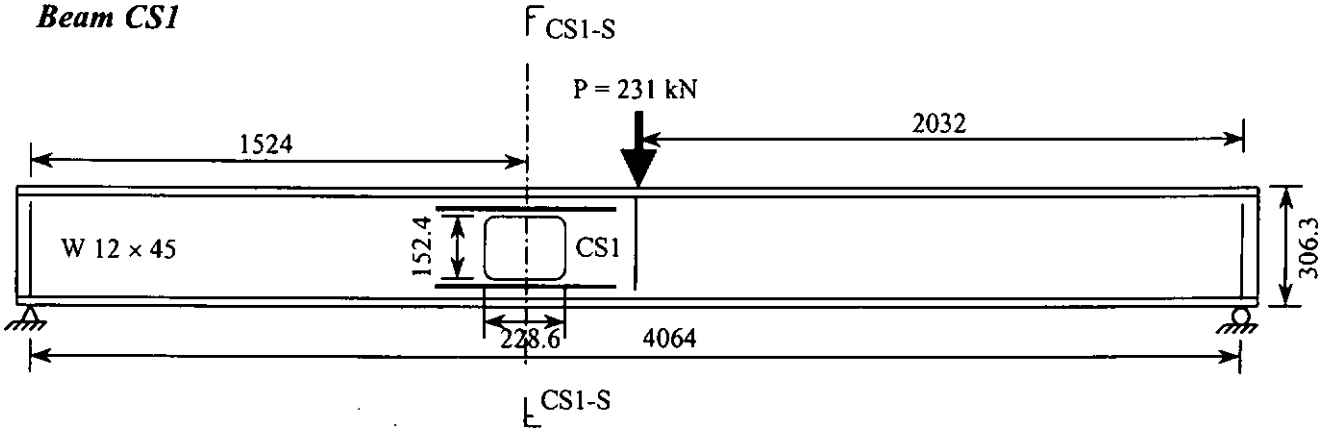

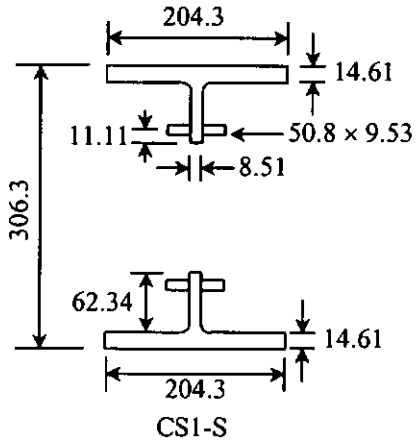

Beam CS2

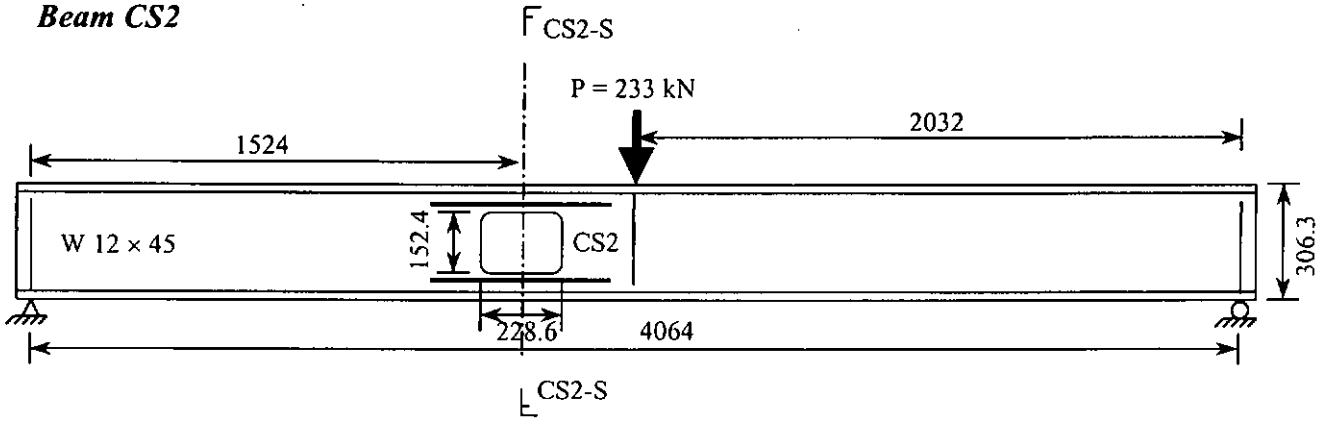

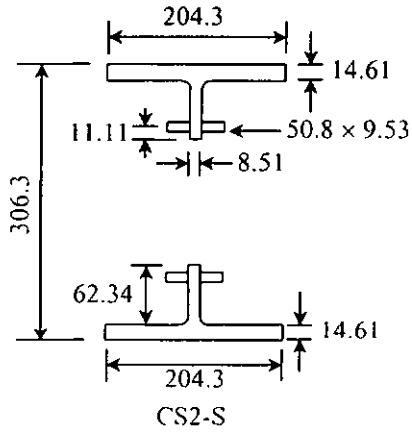

Beam CS3

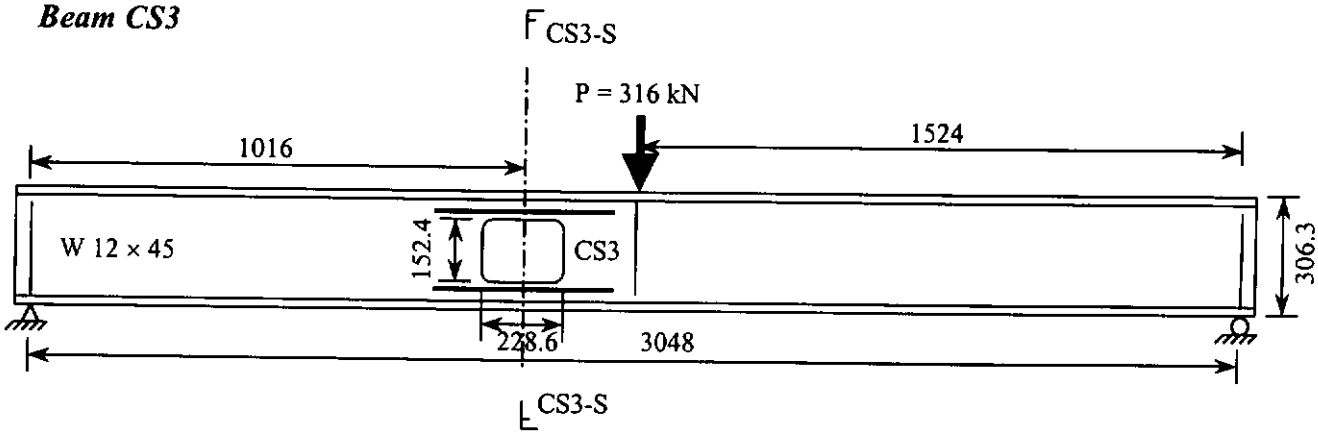
CS3-S
P = 316 kN
1016
1524
W 12 × 45
152.4
CS3
306.3
228.6
3048
CS3-S

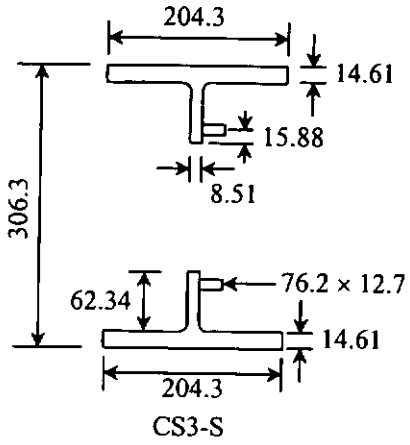
204.3
14.61
15.88
8.51
306.3
62.34
76.2 × 12.7
14.61
204.3
CS3-S

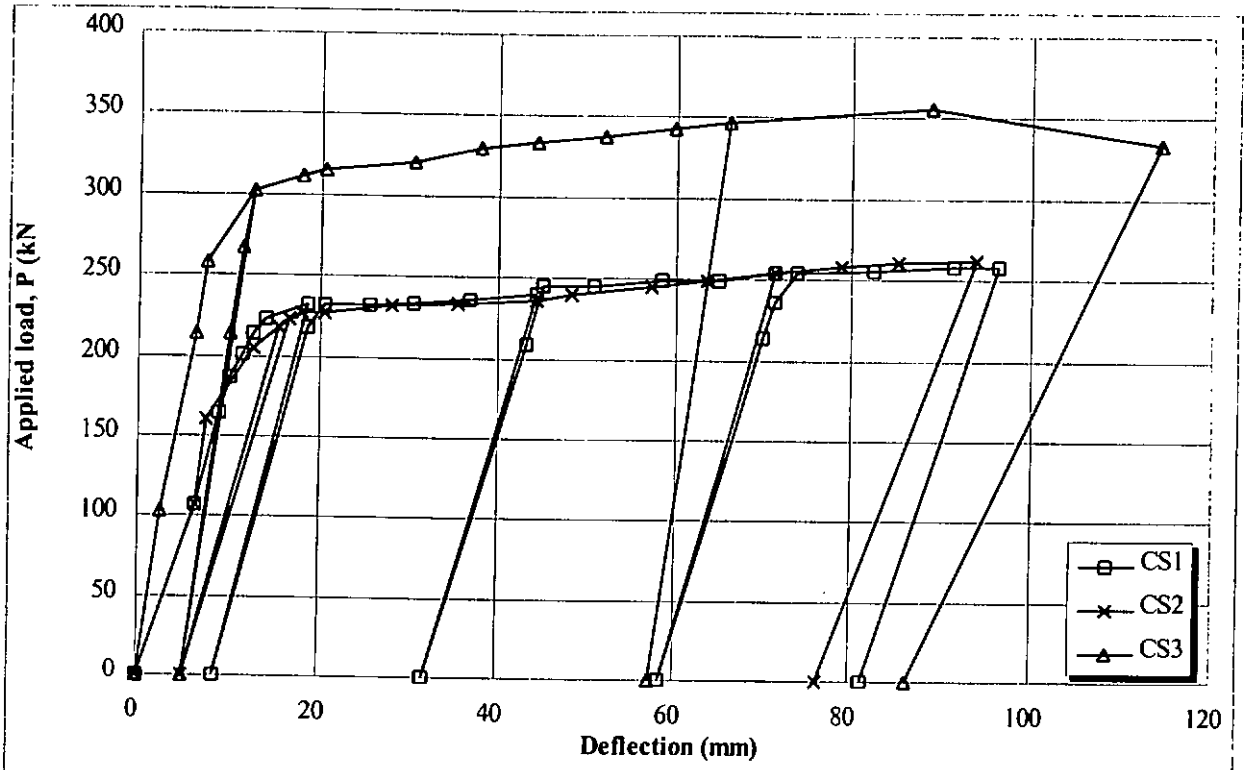

A.1.4 Applied load v.s. mid-span deflection for test series Cooper & Snell (1972)

A.1.5 Cooper, Snell, and Knostman (1977)

1 General

1.1	Number of beams (tests):	5(5)
1.2	Beam spans:	2.7-2.8 m
1.3	Steel beam sizes:	3-W16x40, 2-W16x45
1.4	Steel yield strength:	244.9 – 317.6 N/mm^2
1.5	Steel beam depth:	406.6-409.7 mm
1.6	Span/depth ratio:	6.6-6.9

2 Opening Configurations

2.1	Shapes of web openings:	5-rectangular
2.2	Number of eccentric openings:	3-upward, 2-downward
2.3	Number of reinforced openings:	3-one sided, 1-two sided
2.4	Location of opening/span:	0.27-0.28 span
2.5	Length/height of openings:	1.5-2.0
2.6	Height of openings/depth of beam:	0.37-0.49
2.7	M/V ratio at centerline of opening:	0.76 m
2.8	Others:	

			Measured yield strength (N/mm^2)			
Tests	Failure loads, P (kN)	Modes of failure	Top flange	Bottom flange	Web	Reinforcement
CSK1	605	Vierendeel	317.0	317.6	317.6	0.0
CSK2	689.5	Vierendeel	313.2	309.5	317.6	299.4
CSK5	511.6	Vierendeel	293.9	303.0	308.3	294.5
CSK6	373.7	Vierendeel	293.9	303.0	308.3	244.9
CSK7	449.3	Vierendeel	293.9	303.0	308.3	244.9

Beam CSK1

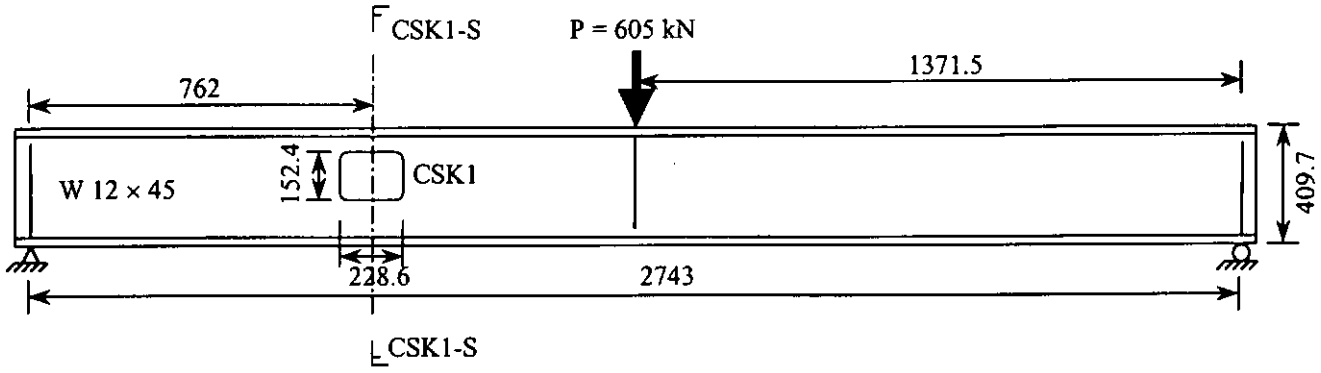

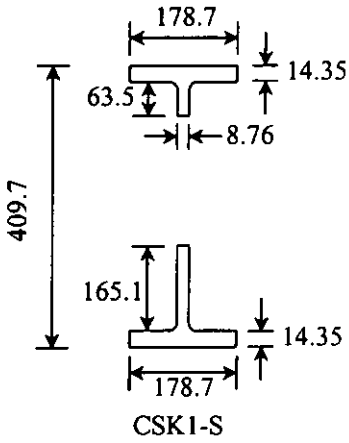

CSK1-S

Beam CSK2

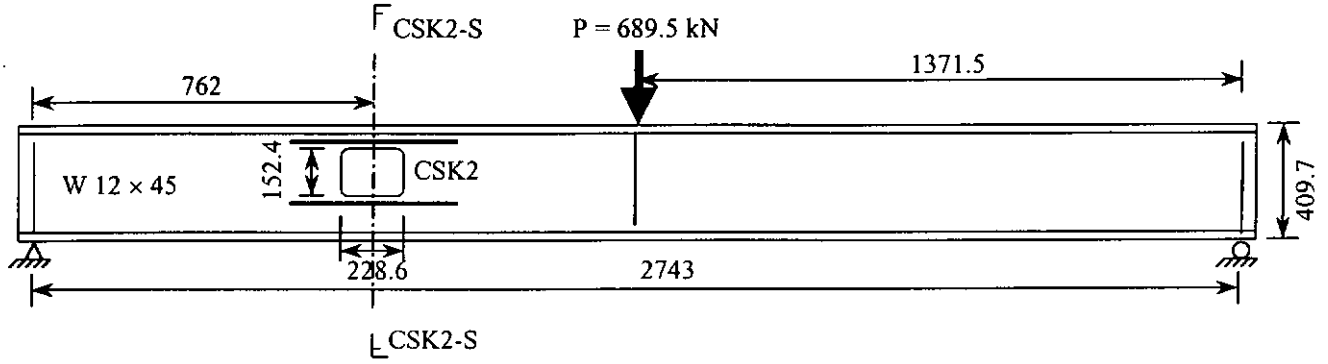

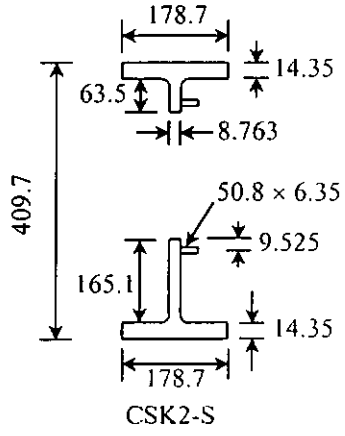

CSK2-S

Beam CSK5

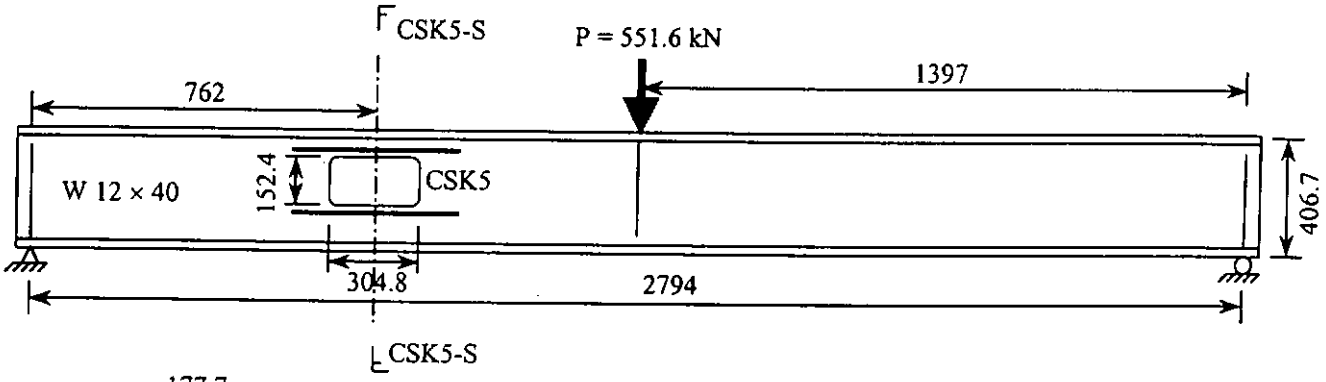

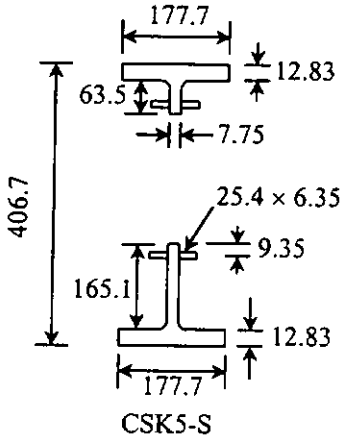

Beam CSK6

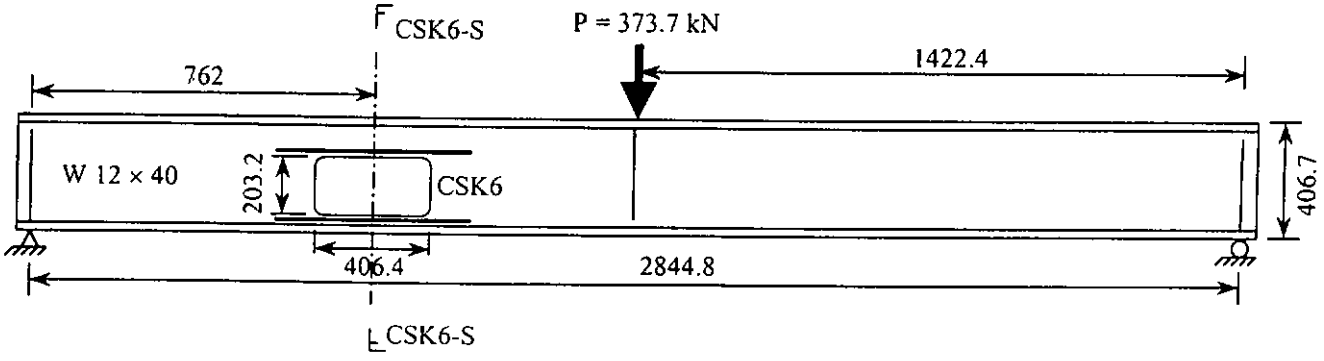

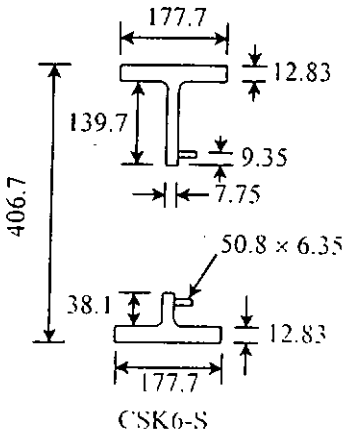

Beam CSK7

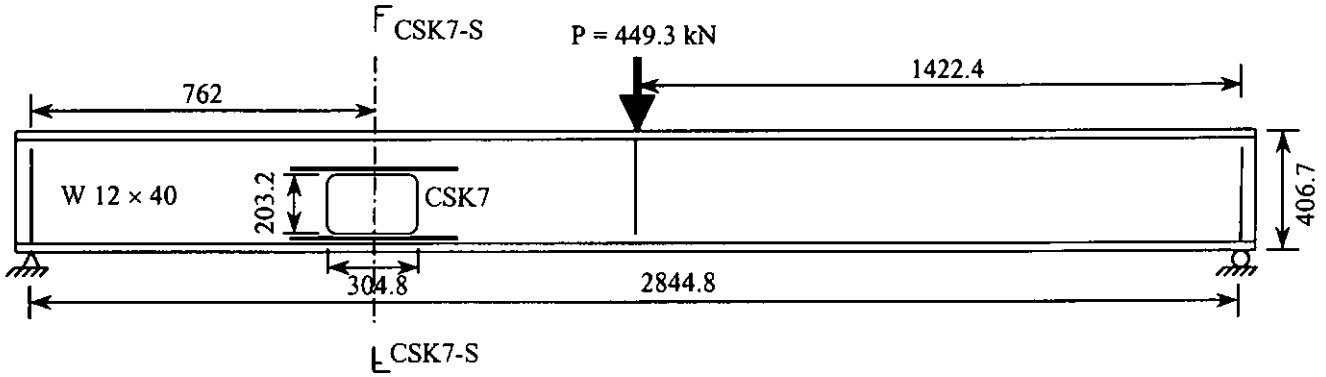
CSK7-S
P = 449.3 kN
762
1422.4
W 12 × 40
203.2
CSK7
406.7
304.8
2844.8
CSK7-S

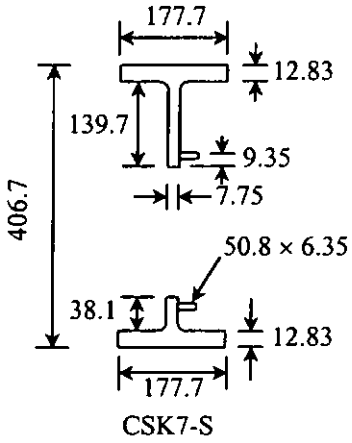
177.7
12.83
139.7
9.35
7.75
406.7
50.8 × 6.35
38.1
12.83
177.7
CSK7-S

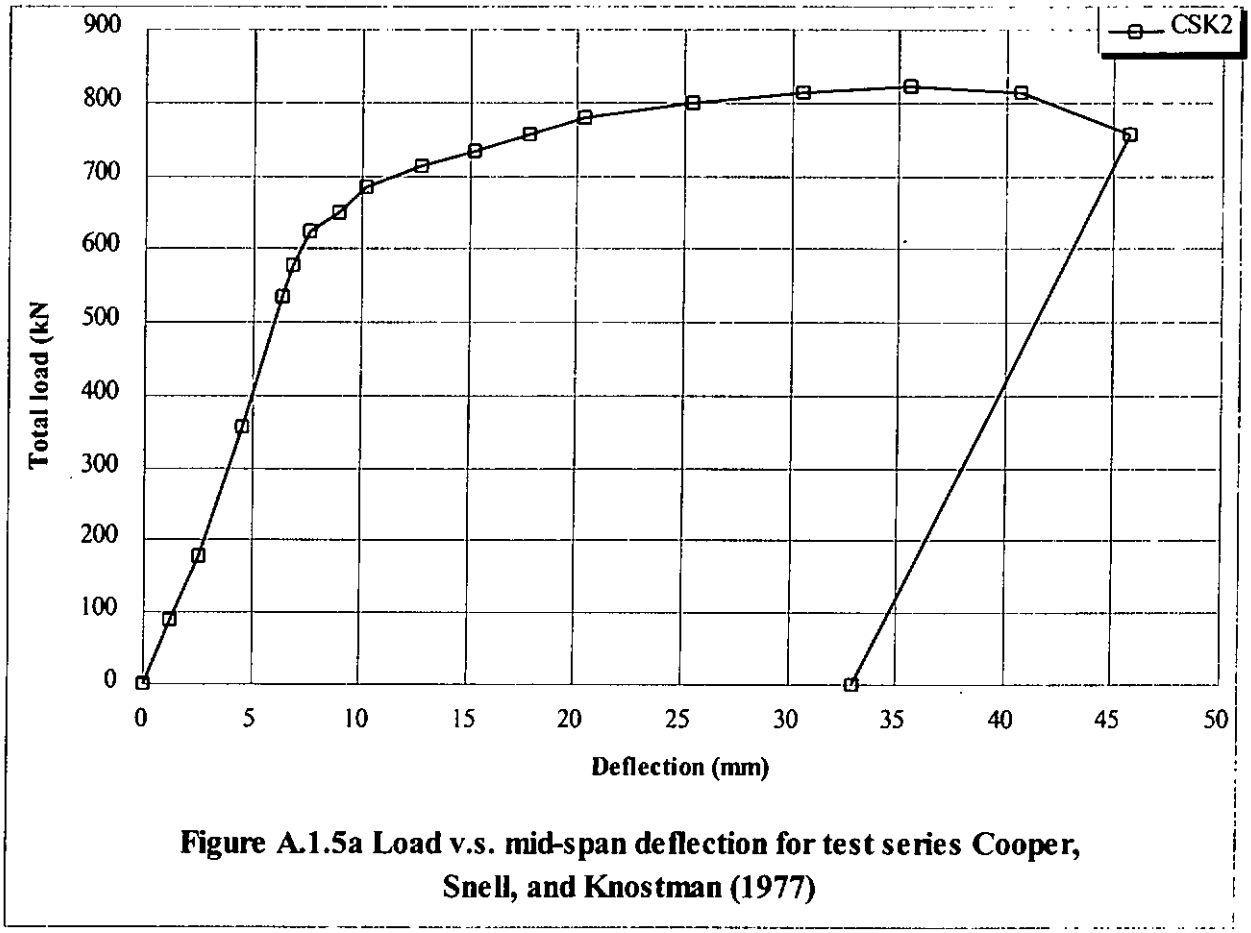

Figure A.1.5a Load v.s. mid-span deflection for test series Cooper, Snell, and Knostman (1977)

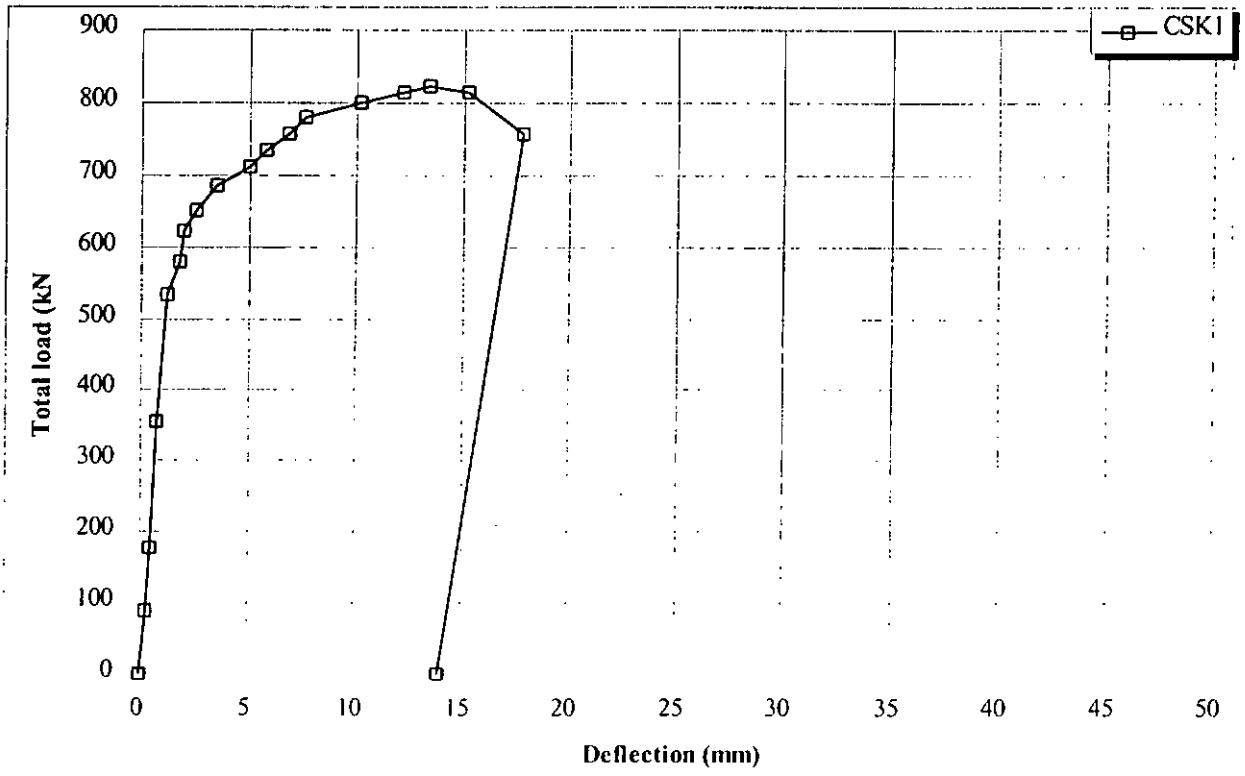

Figure A.1.5b Load v.s. relative deflection between opposite ends of opening for test series Cooper, Snell, and Knostman (1977)

A.1.6 Redwood and McCutcheon (1968)

1 General

1.1	Number of beams (tests):	19(19)
1.2	Beam spans:	1.5-2.5 m
1.3	Steel beam sizes:	19-W8x17
1.4	Steel element yield strength:	277.2 – 399.9 N/mm^2
1.5	Steel beam depth:	203.2-206.3 mm
1.6	Span/depth ratio	7.3-12.3

2 Opening Configurations

2.1	Shapes of web openings:	4-single circular, 5-multiple circular, 2-single rectangular 5-multiple rectangular, 3-extended rectangular
2.2	Number of eccentric openings:	0
2.3	Number of reinforced openings:	0
2.4	Location of opening/span:	0.3-0.5 span
2.5	Length/height of openings:	1.0-1.5
2.6	Height of openings/depth of beam:	0.27-0.56
2.7	M/V ratio at centerline of opening:	0.46-1.22 m, ∞
2.8	Others:	

			Measured yield strength (N/mm^2)		
Tests	Failure loads, P (kN)	Modes of failure	Top flange	Bottom flange	Web
RM1A	111.2 + 111.2	Flexure	313.7	313.7	354.4
RM1B	111.2 + 111.2	Flexure	309.6	309.6	355.8
RM1D	98.8 + 98.8	Flexure	318.5	318.5	342.0
RM11H	122.2 + 122.2	Flexure	311.0	311.0	386.8
RM2A	262.8	Vierendeel, web yielding	350.9	350.9	375.1
RM2B	104.3	Vierendeel	319.9	319.9	312.3
RM2C	230.3	Vierendeel	296.5	296.5	304.7
RM2D	246.1	Vierendeel	313.0	313.0	370.9
RM2F	136.0	Vierendeel	299.9	299.9	314.4
RM21G	93.9	Vierendeel	277.2	277.2	325.4
RM21H	122.2	Vierendeel	302.7	302.7	335.1
RM3A	145.6	Vierendeel, web yielding	310.3	310.3	359.9
RM4A	140.9	Web yielding	315.1	315.1	359.2
RM4B	118.2	Vierendeel	296.5	296.5	351.6
RM4C	146.6	Vierendeel	295.1	295.1	399.9
RM4D	154.6	Vierendeel	330.9	330.9	370.9
RM4F	125.2	Vierendeel	317.8	317.8	373.0
RM4G	120.1	Vierendeel	326.8	326.8	373.0
RM4H	106.6	Vierendeel	309.6	309.6	348.9

Beam RM1A

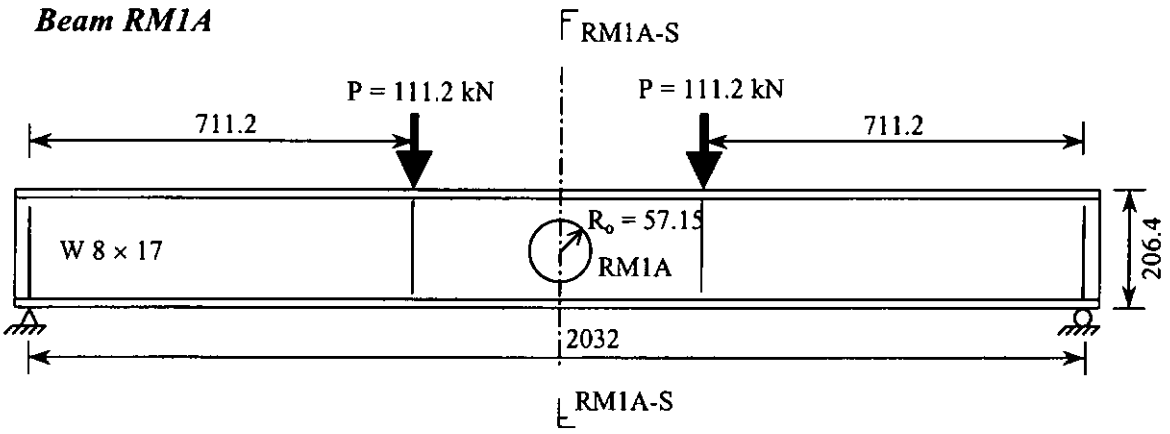

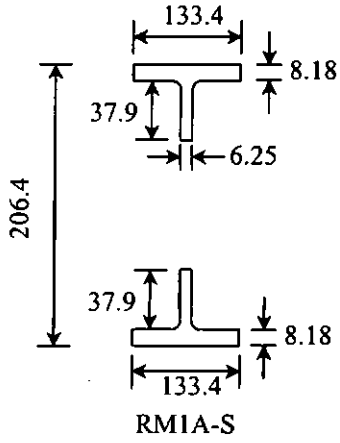

Beam RM1B

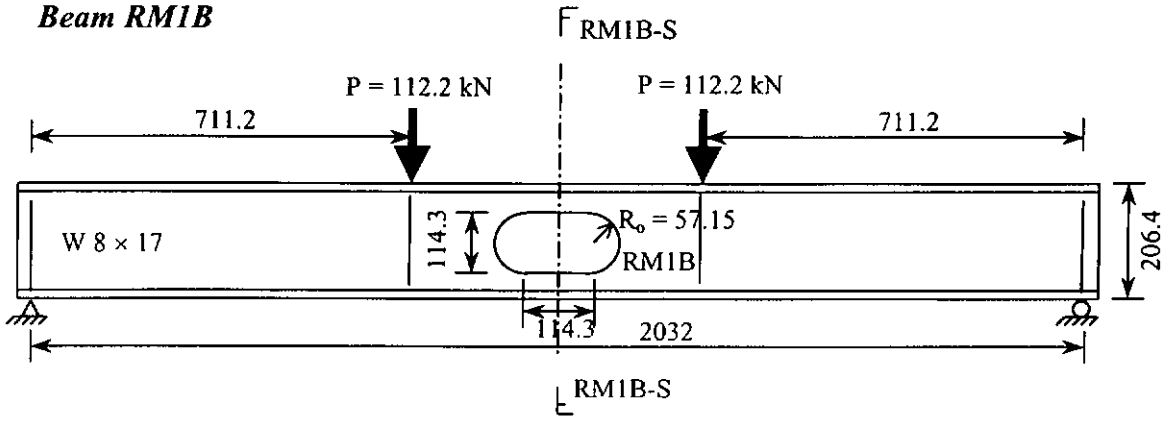

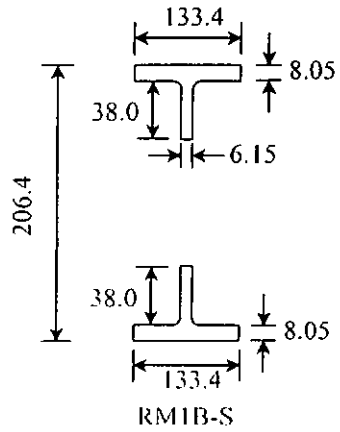

Beam RM1D

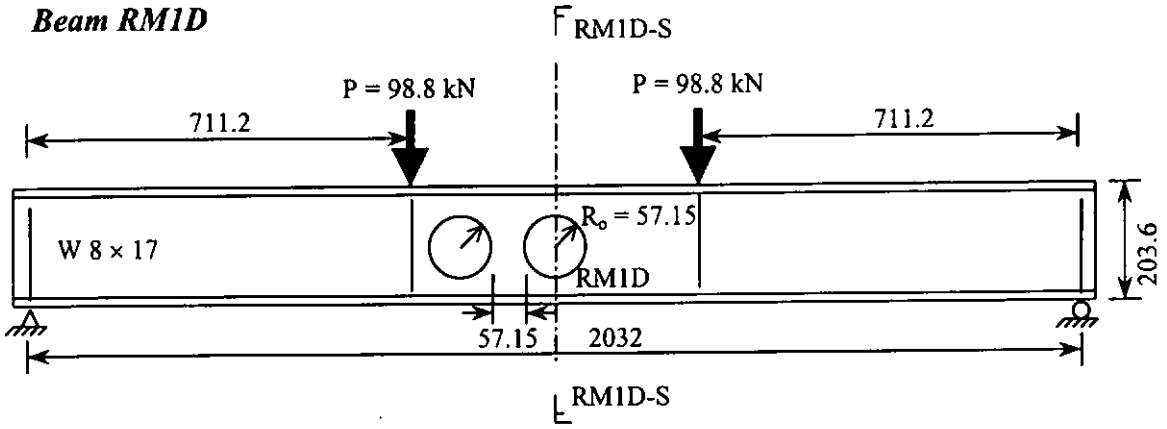

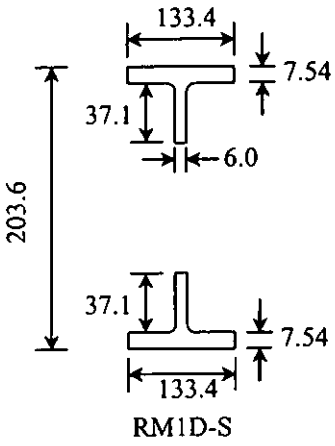

Beam RM11H

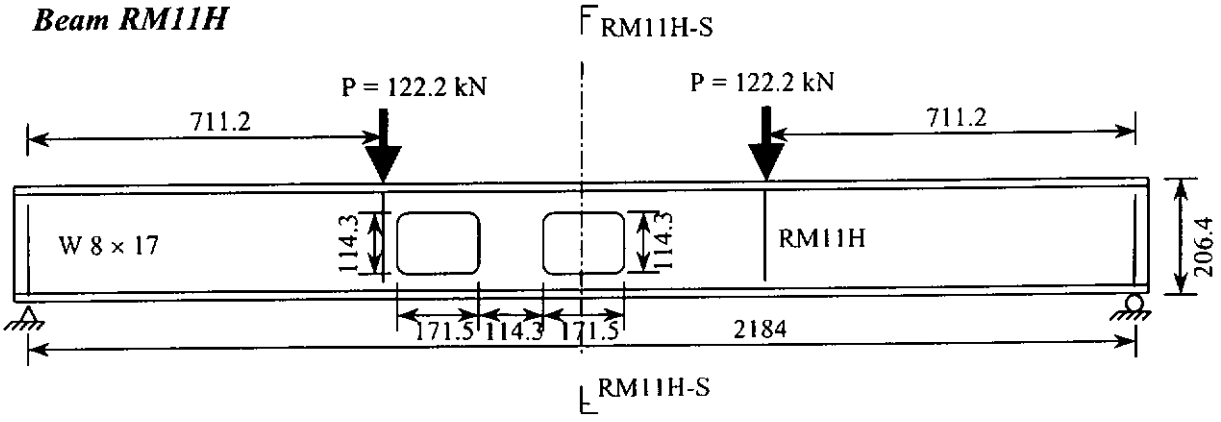

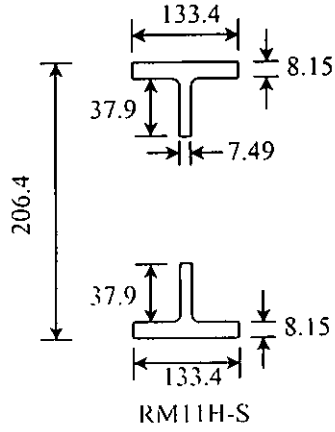

Beam RM2A

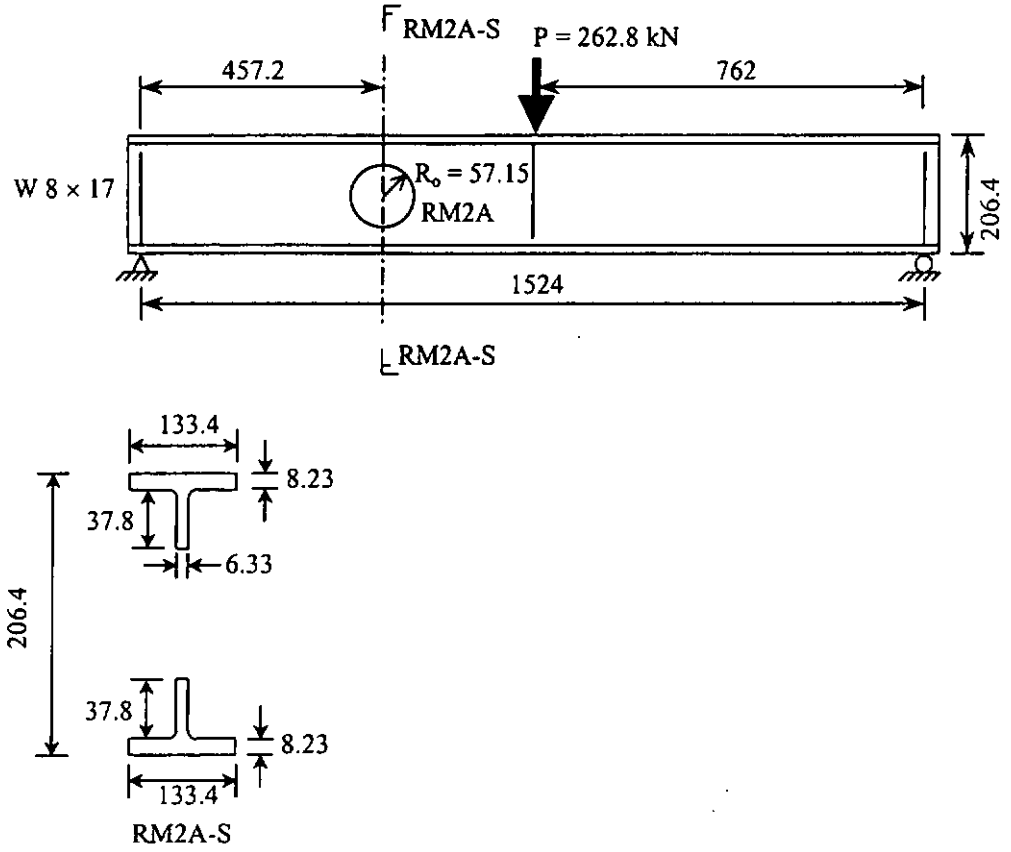

Beam RM2B

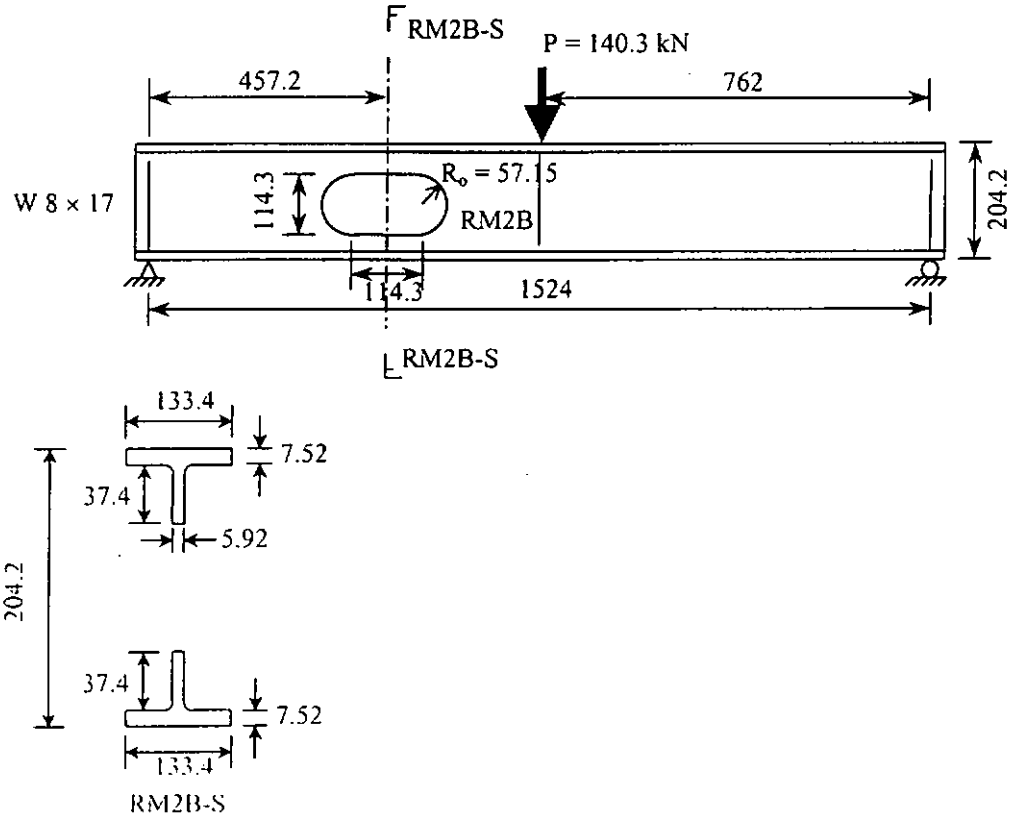

Beam RM2C

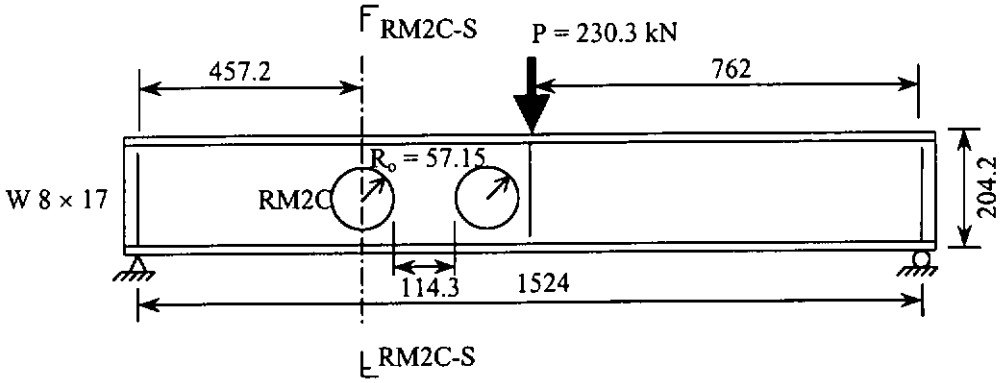

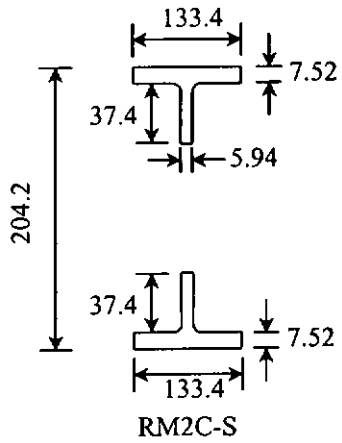

Beam RM2D

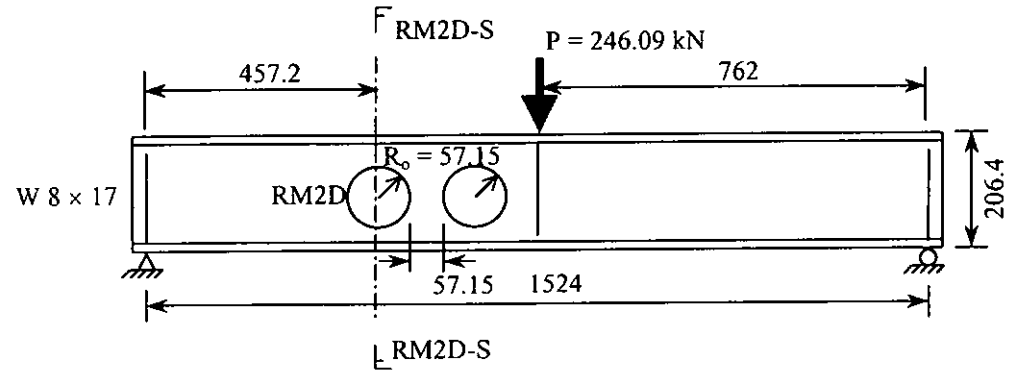

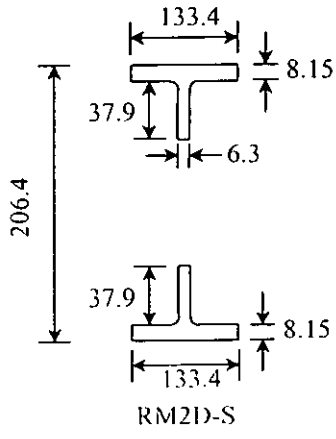

Beam RM2F

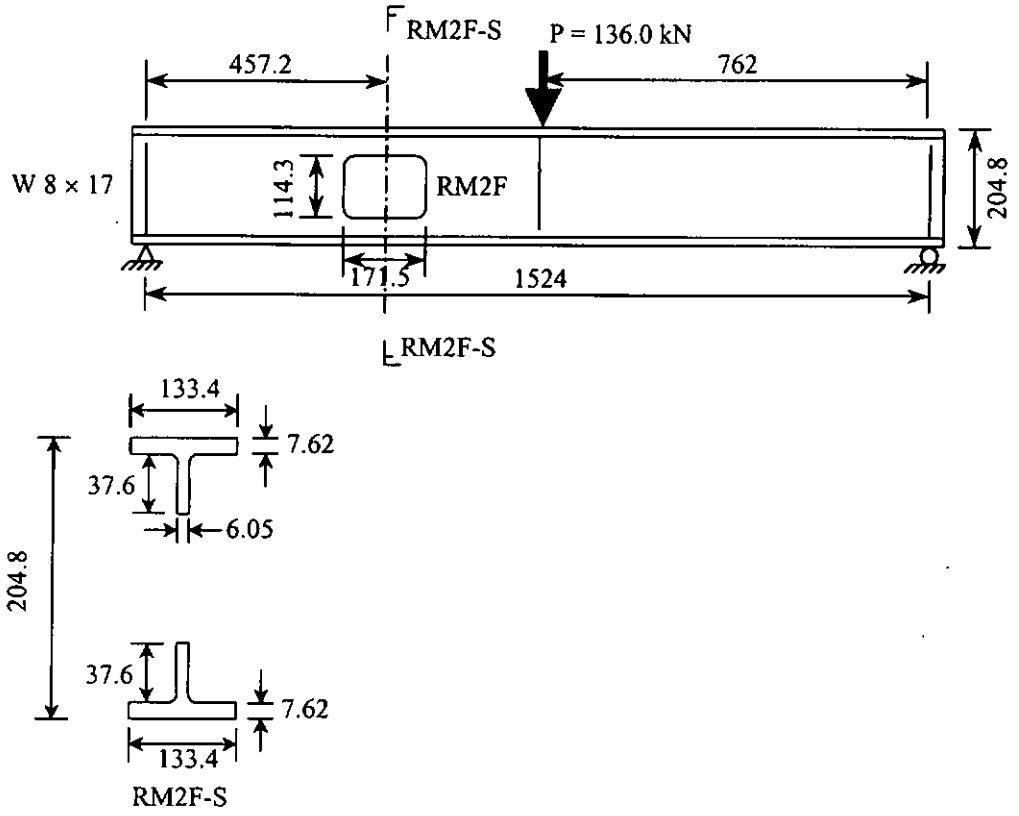

Beam RM21G

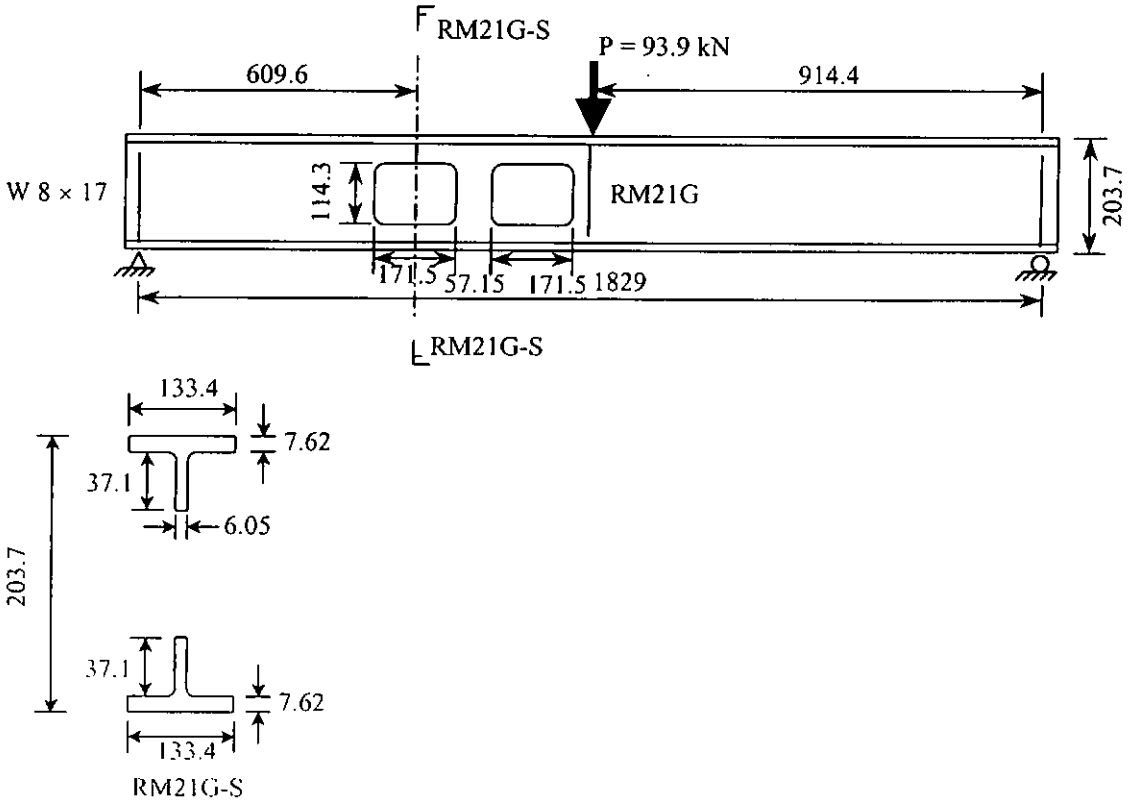

Beam RM21H

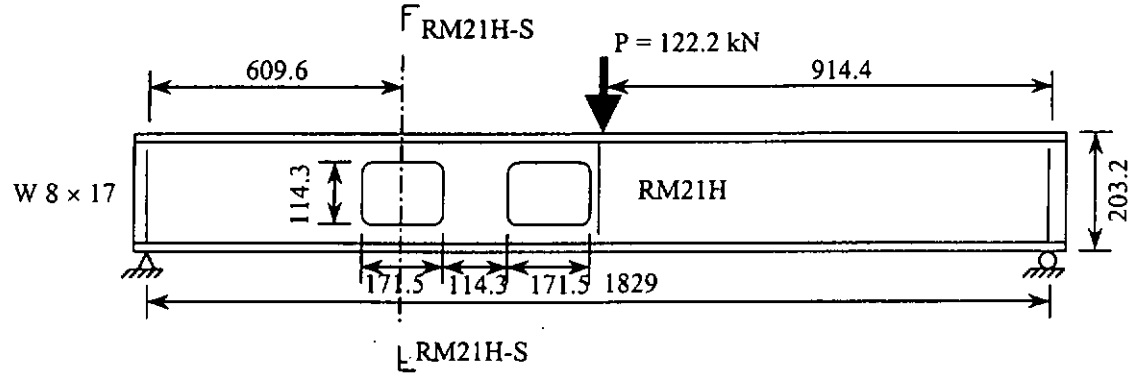

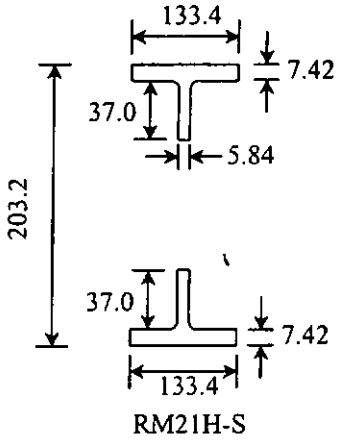

RM21H-S

Beam RM3A

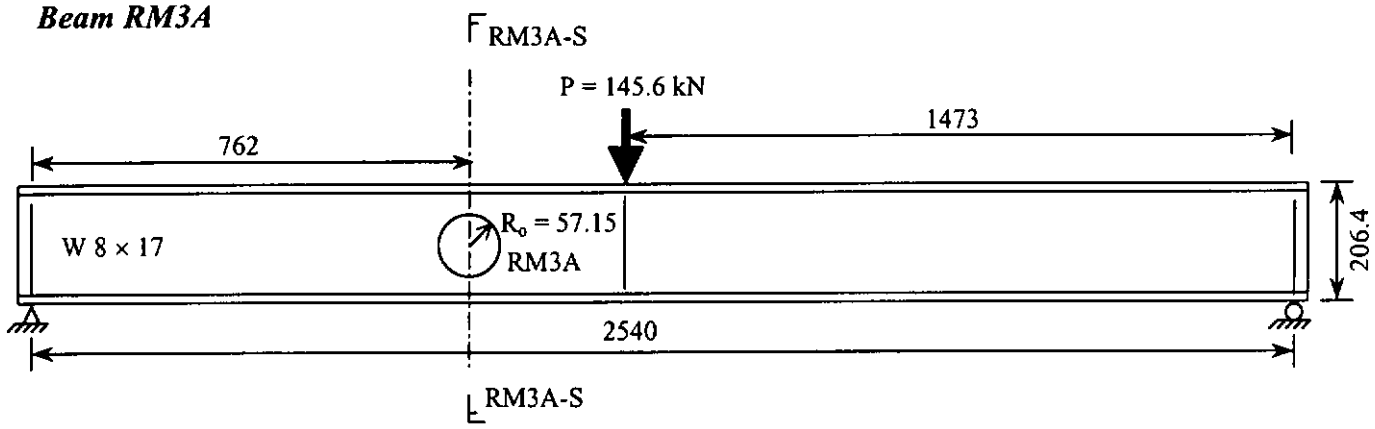

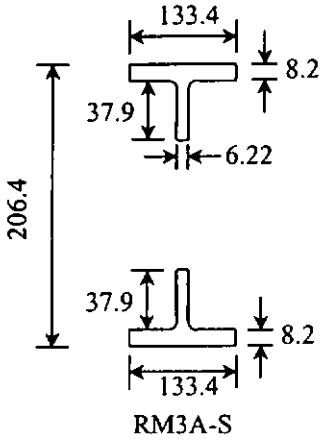

RM3A-S

Beam RM4A

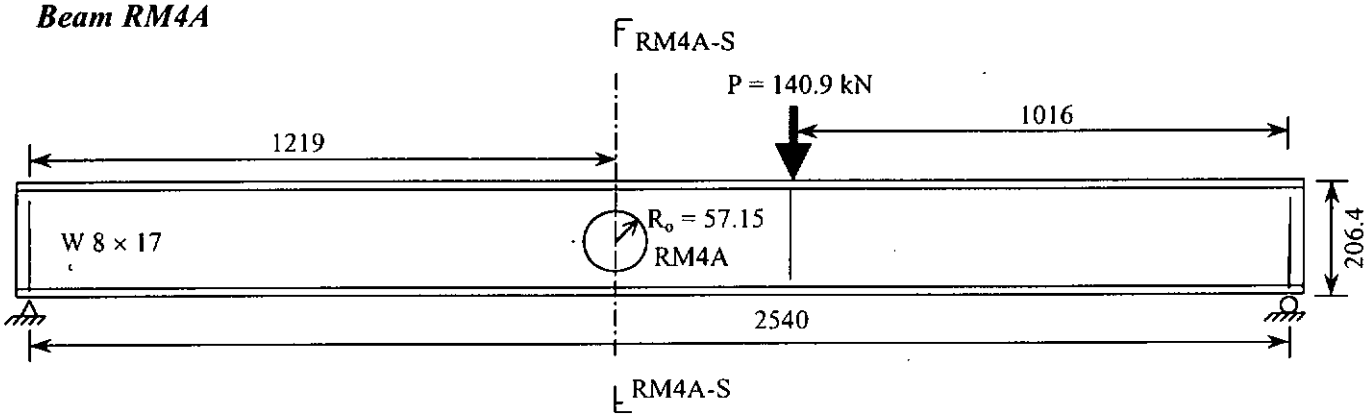

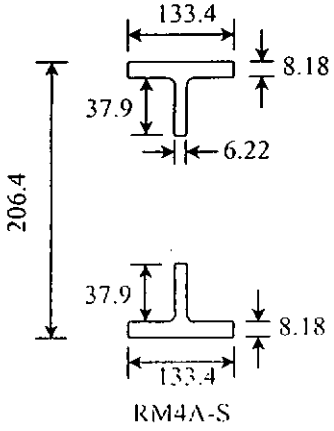

RM4A-S

Beam RM4B

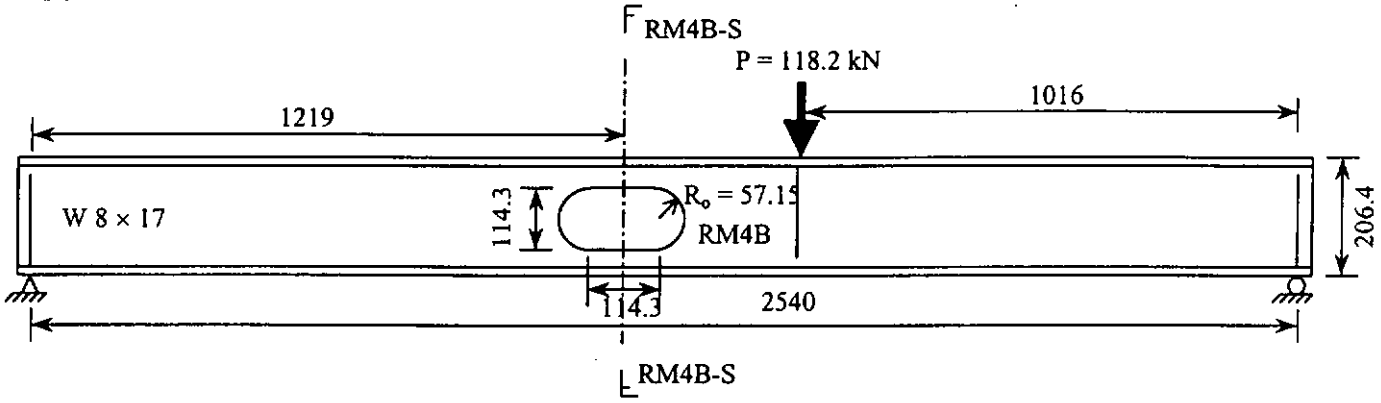

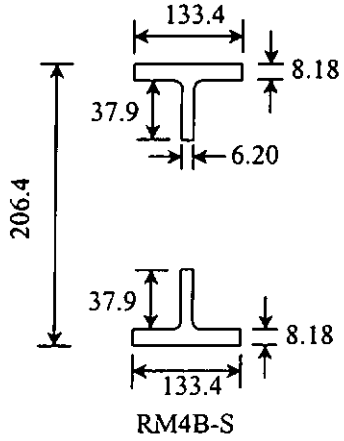

Beam RM4C

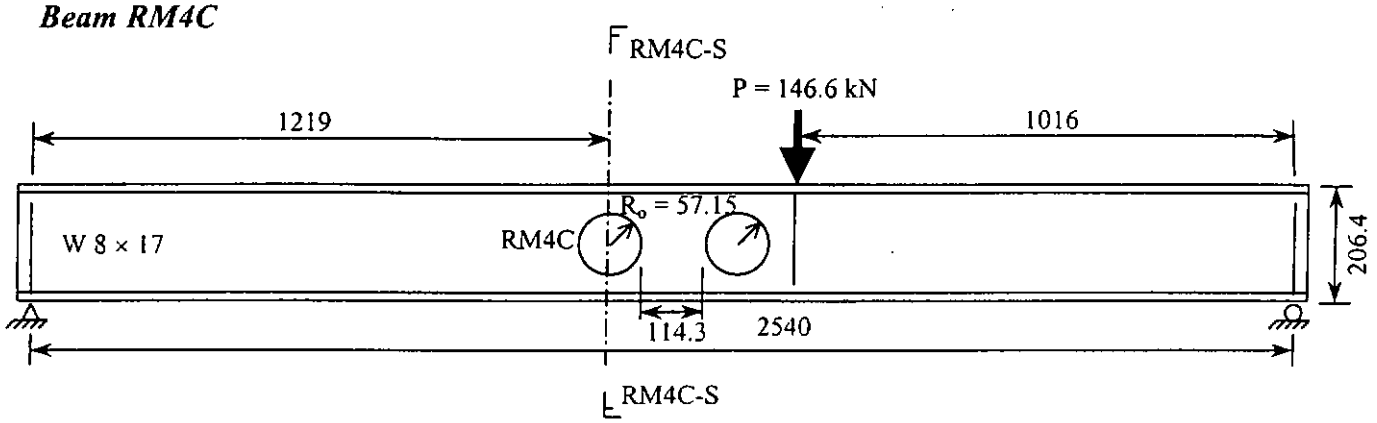

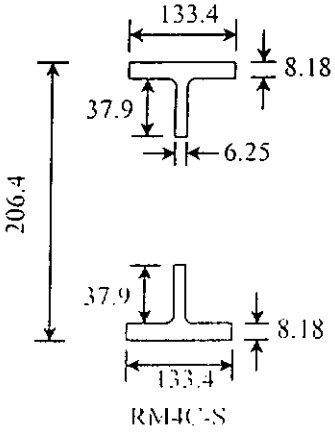

Beam RM4D

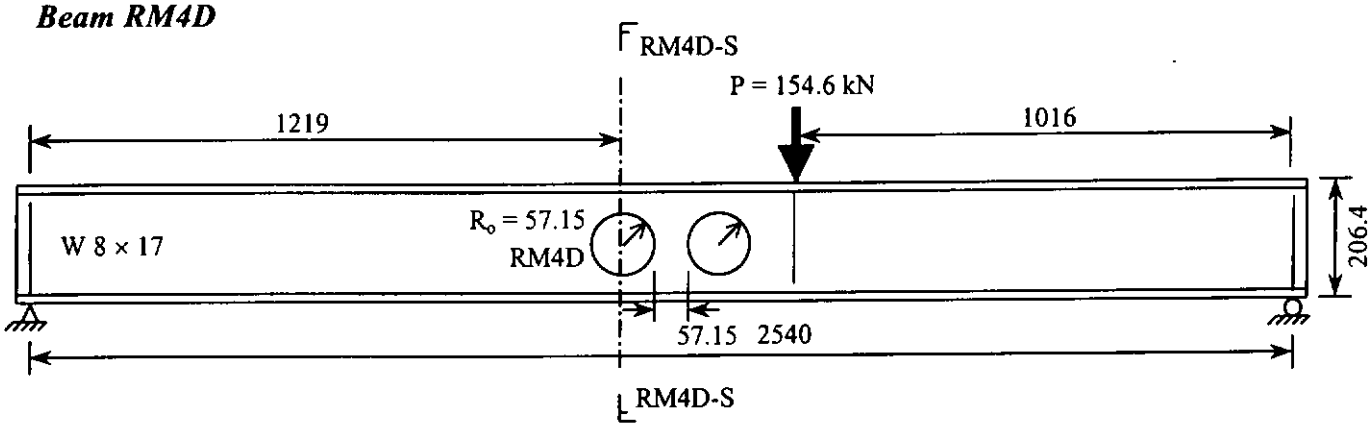

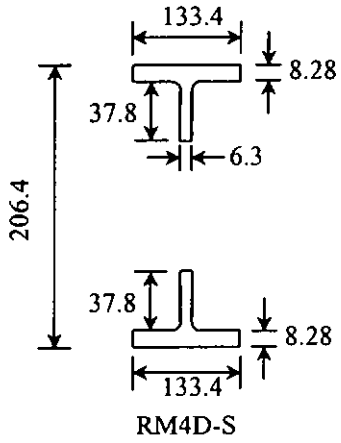

Beam RM4F

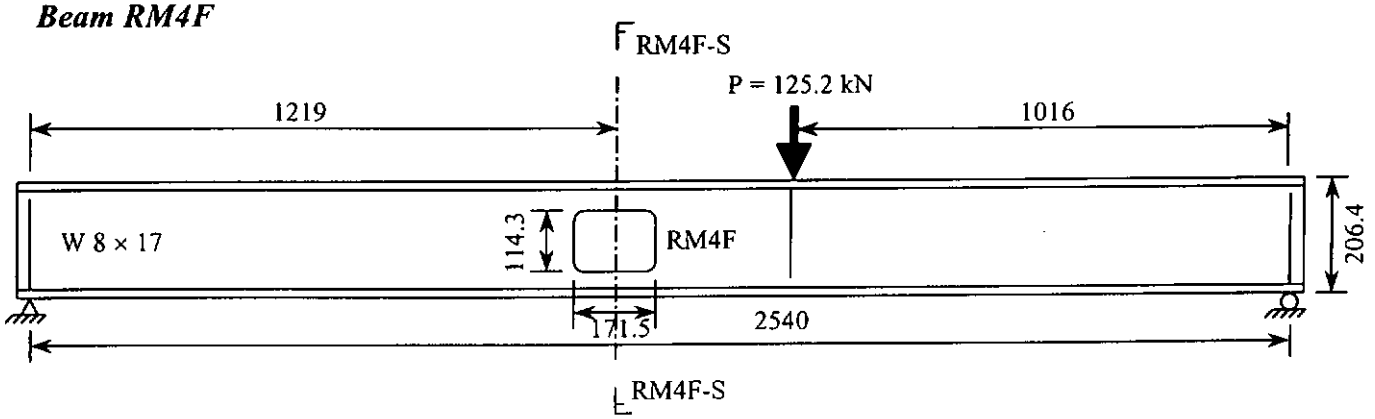

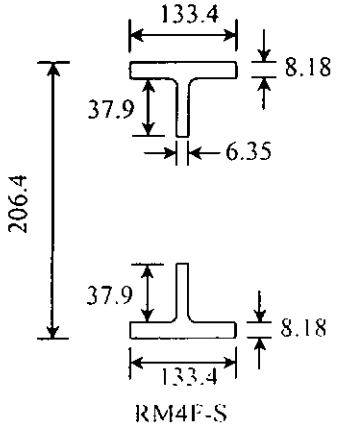

Beam RM4G

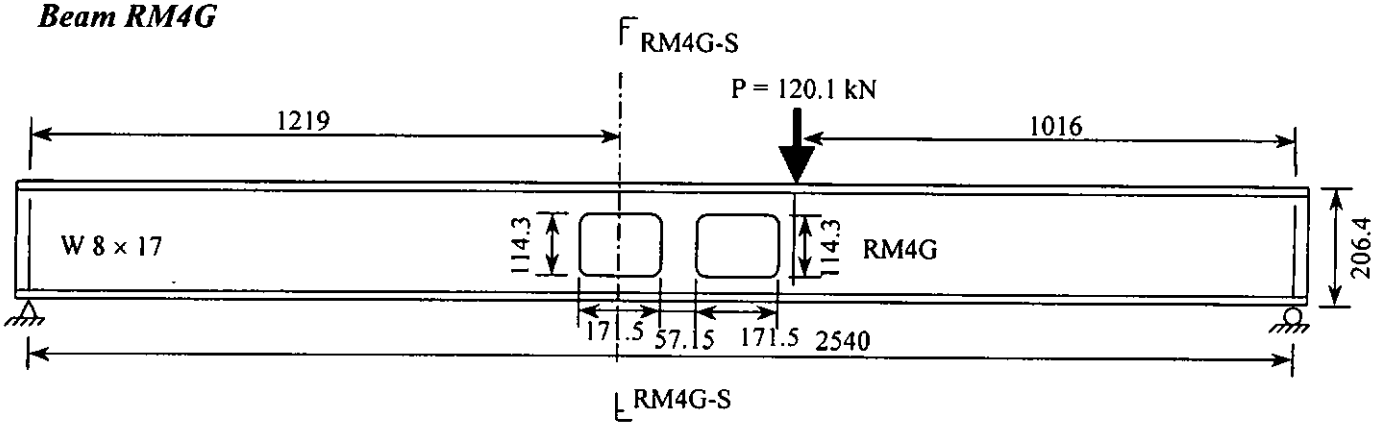

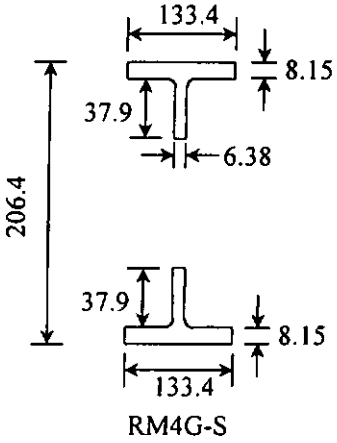

RM4G-S

Beam RM4H

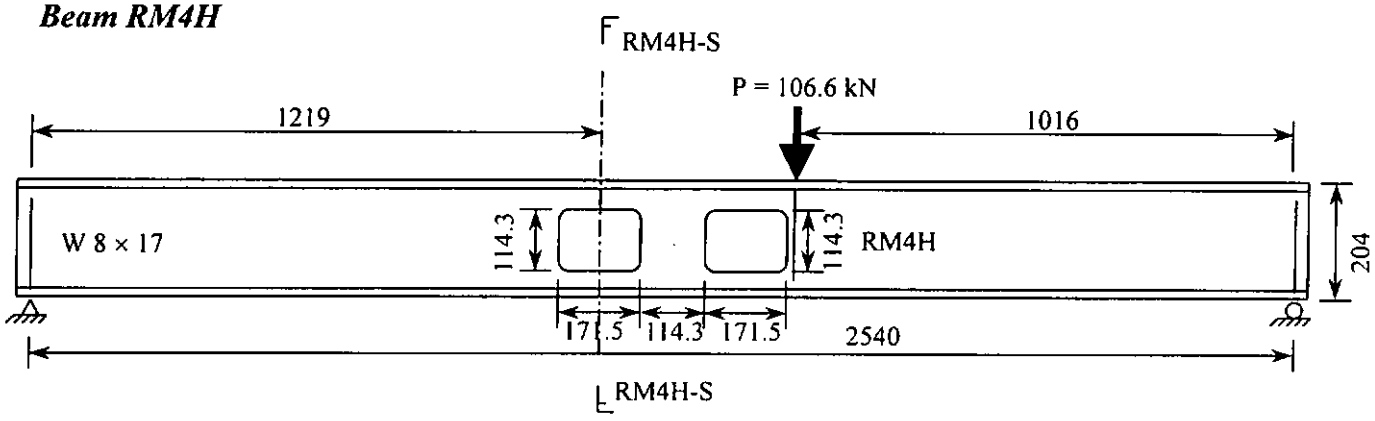

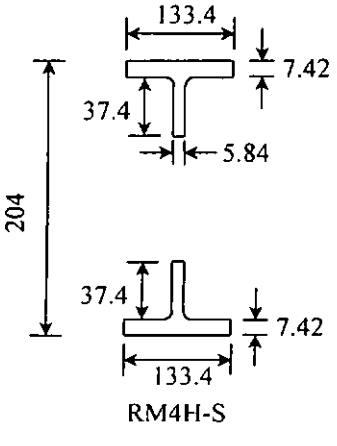

RM4H-S

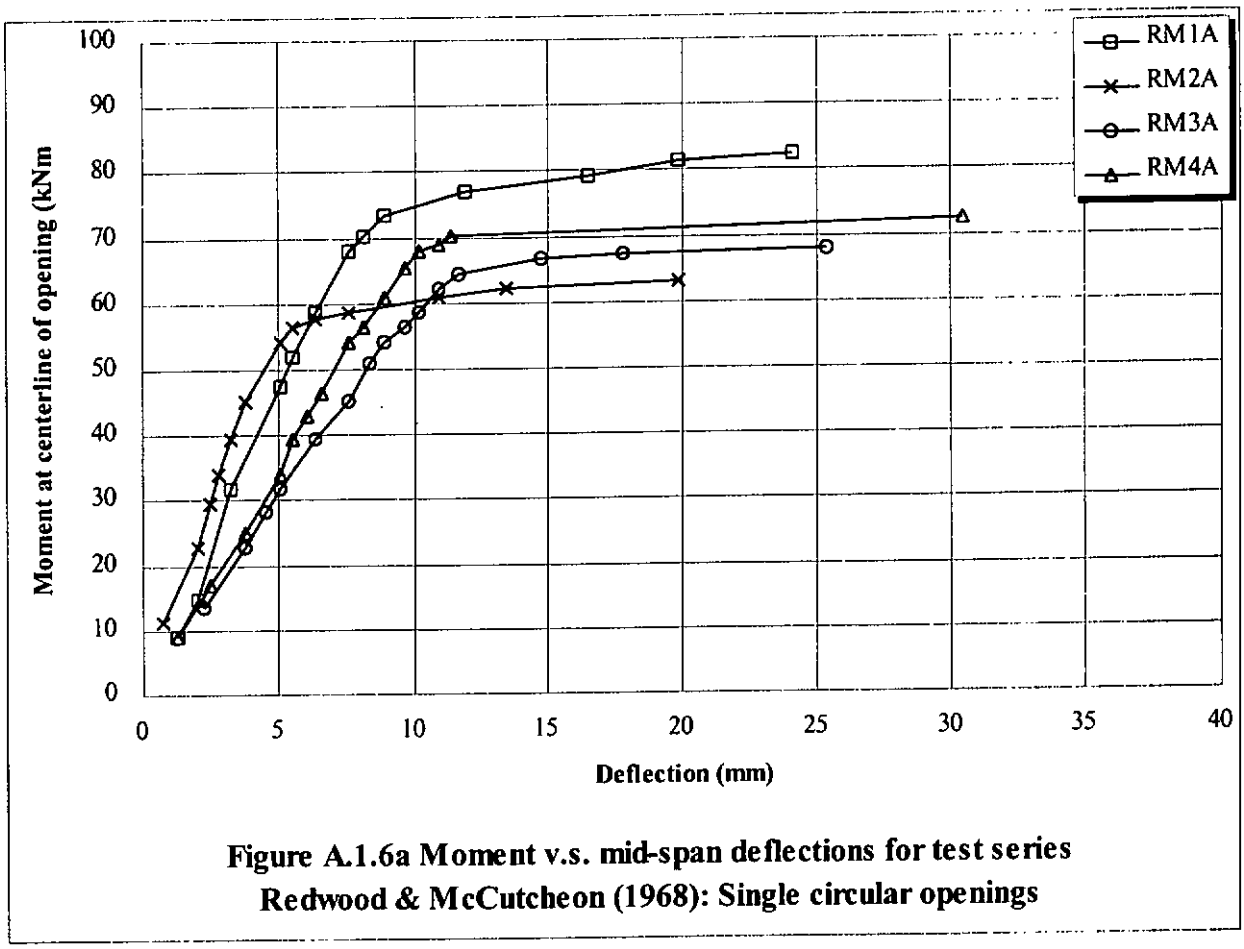

Figure A.1.6a Moment v.s. mid-span deflections for test series Redwood & McCutcheon (1968): Single circular openings

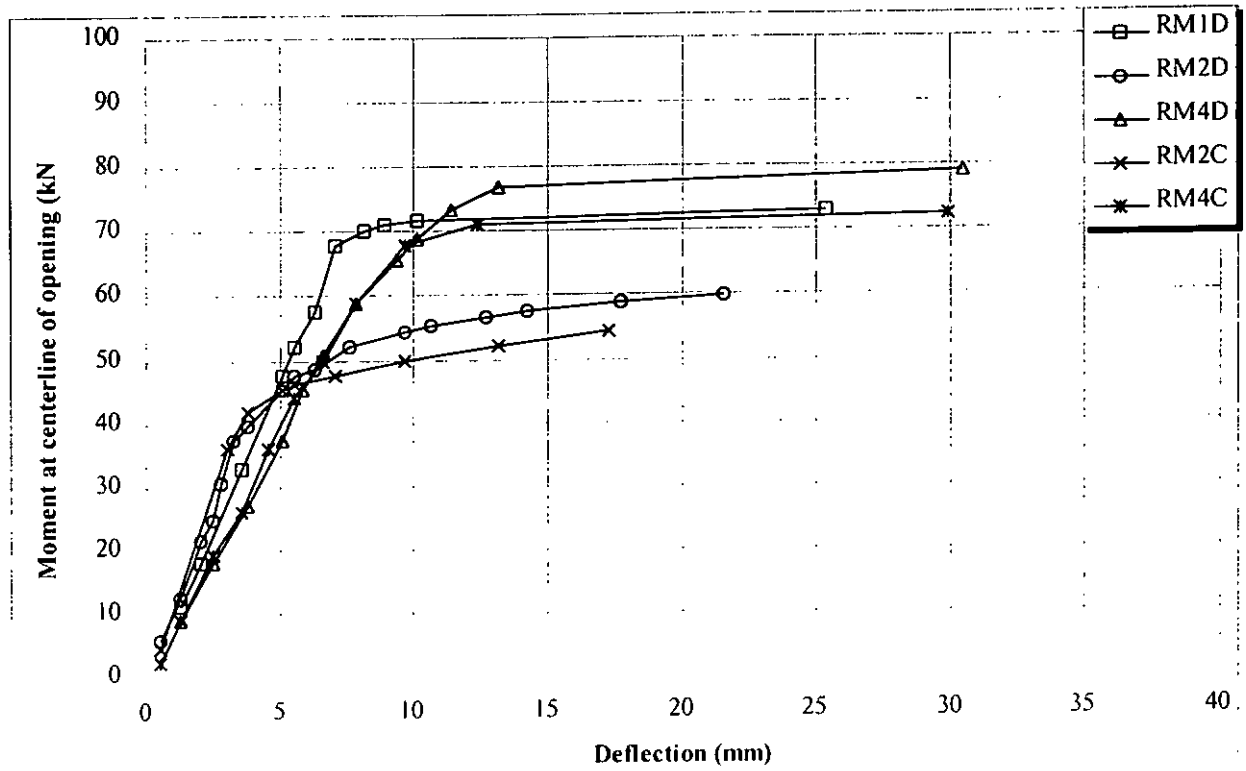

Figure A.1.6b Moment v.s. mid-span deflections of opening for test series Redwood & McCutcheon (1968): Two circular openings

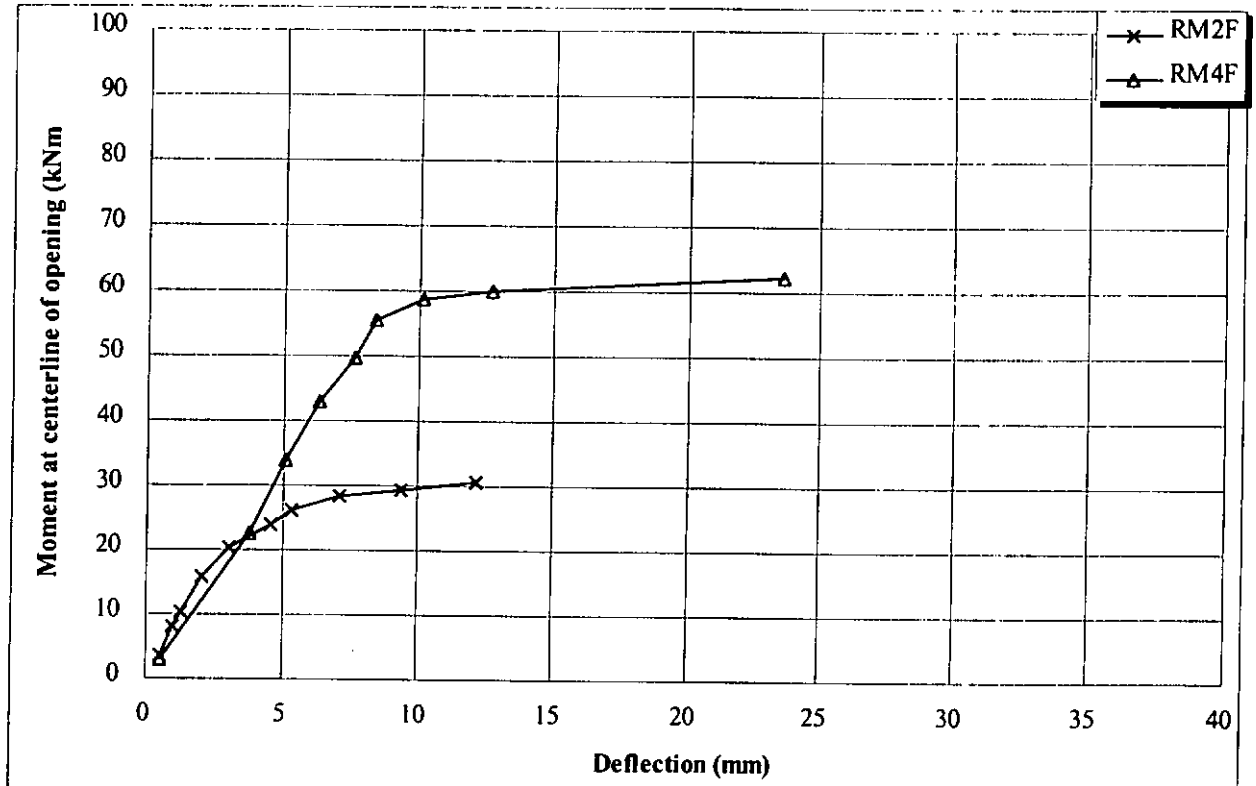

Figure A.1.6c Moment v.s. mid-span deflections of opening for test series Redwood & McCutcheon (1968): Single rectangular openings

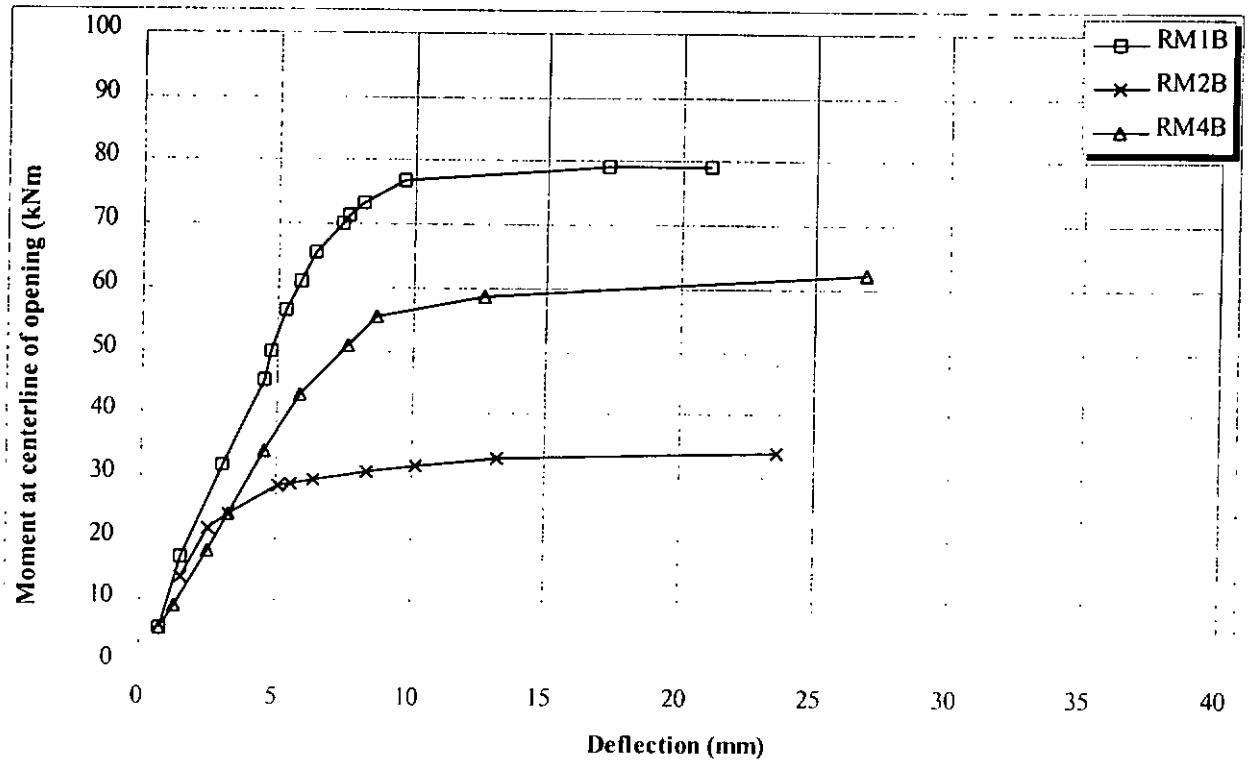

Figure A.1.6d Moment v.s. mid-span deflections of openings for test series Redwood & McCutcheon (1968): Extended rectangular openings

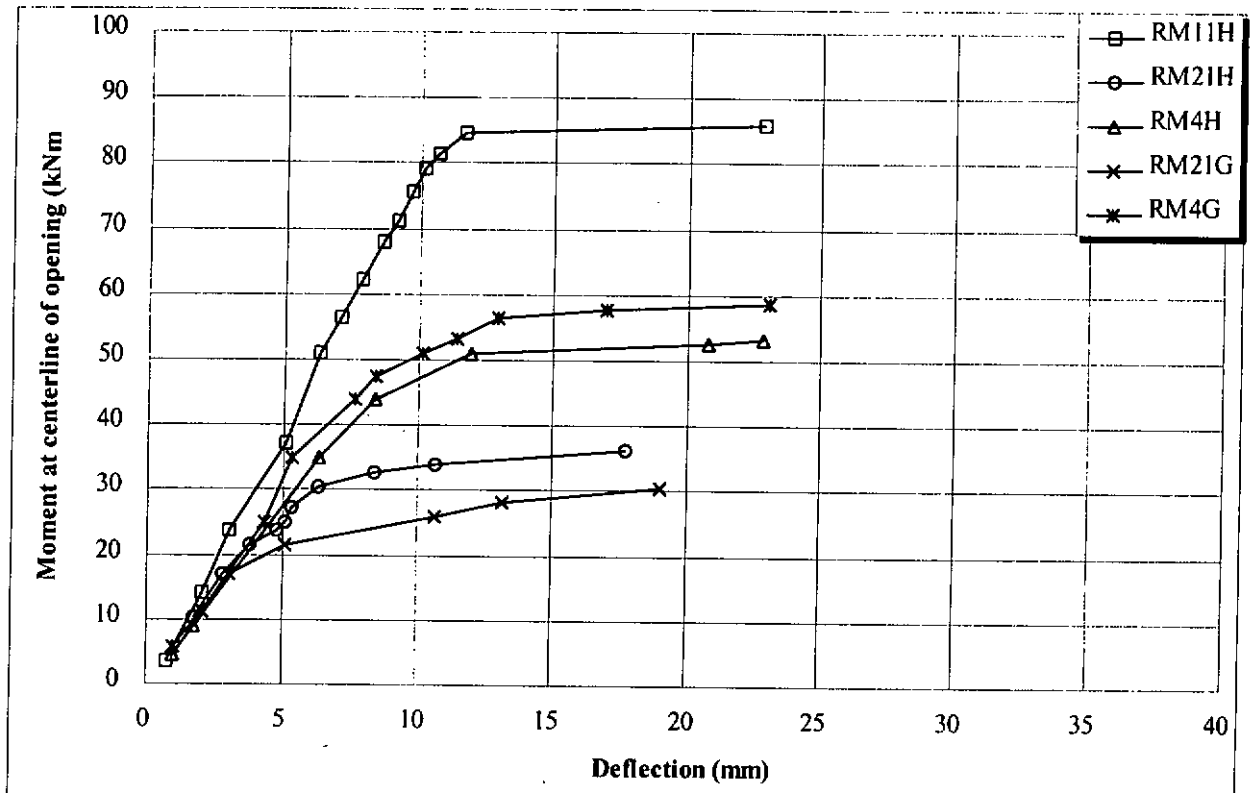

Figure A.1.6e Moment v.s. mid-span deflections of opening for test series Redwood & McCutcheon (1968): Two rectangular openings

A.1.7 Lupien and Redwood (1978)

1 General

1.1	Number of beams (tests):	6(6)
1.2	Beam spans:	2.3-3.9 m
1.3	Steel beam sizes:	1-W16x26, 5-welded I section
1.4	Steel element yield strength:	262.9 – 461.9 N/mm^2
1.5	Steel beam depth:	395.9-522.2 mm
1.6	Span/depth ratio:	6.0-8.4

2 Opening Configurations

2.1	Shapes of web openings:	6-rectangular
2.2	Number of eccentric openings:	0
2.3	Number of reinforced openings:	6-one sided
2.4	Location of opening/span:	0.25-0.5 span
2.5	Length/height of openings:	2.48-2.50
2.6	Height of openings/depth of beam:	0.43-0.65
2.7	M/V ratio at centerline of opening:	0.6-1.24 m, ∞
2.8	Others:	

			Measured yield strength (N/mm^2)			
Tests	Failure loads, P (kN)	Modes of failure	Top flange	Bottom flange	Web	Reinforcement
RL1	369.2 + 369.5	Lateral bracing	382.5	382.5	419.7	324.5
RL2	367.0 +367.0	Flange buckling	373.5	373.5	404.5	298.6
RL3	502.6	Web buckling	367.0	367.0	401.7	301.9
RL4	429.3	Flange buckling	368.5	368.5	461.9	324.5
RL5	290.2 + 290.2	Flexure	284.3	284.3	330.3	262.9
RL6	323.8	Flange buckling	278.1	278.1	344.5	308.5

Beam RL1

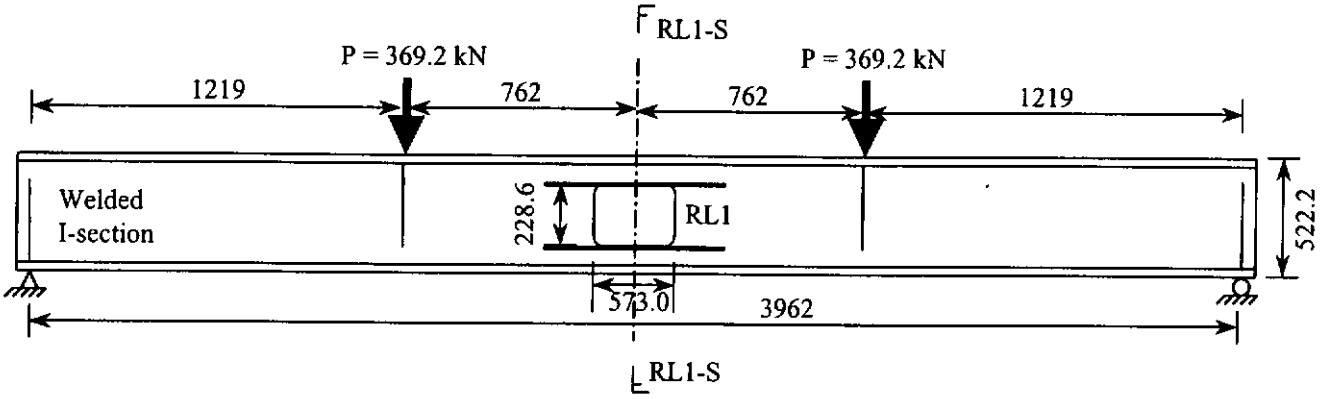

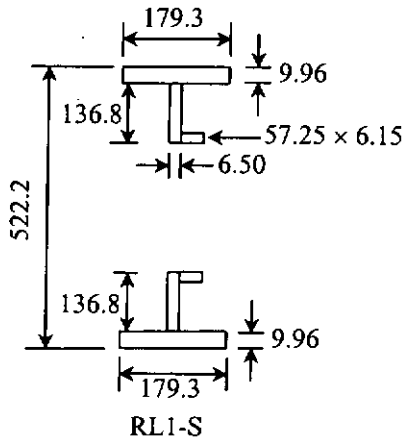

Beam RL2

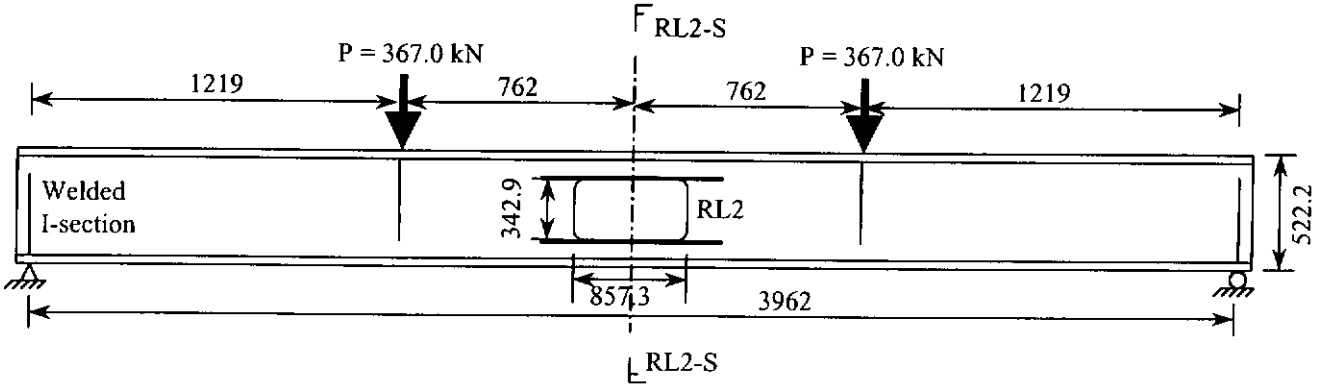

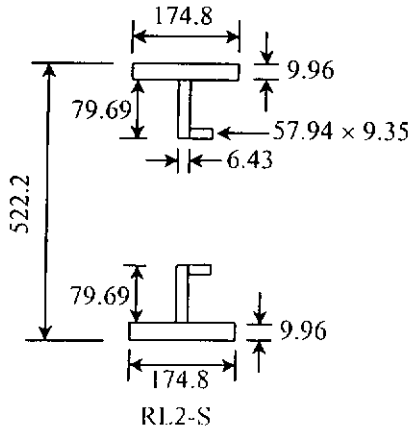

Beam RL3

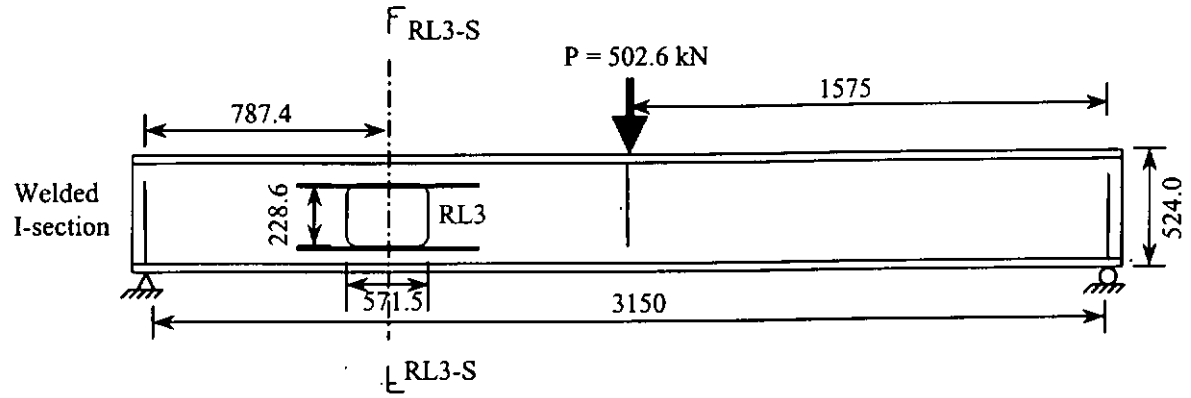

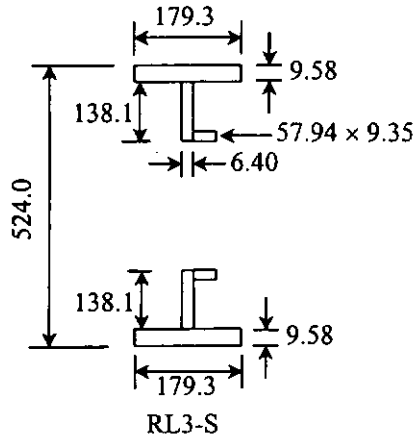

Beam RL4

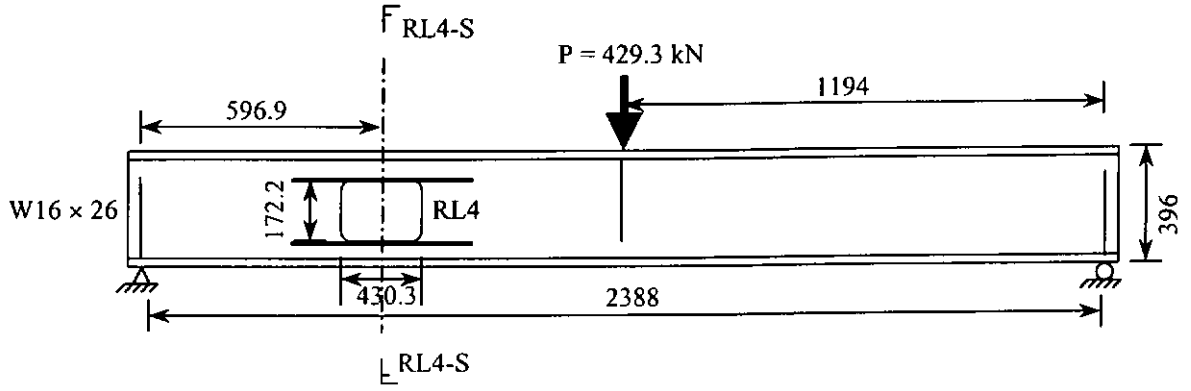

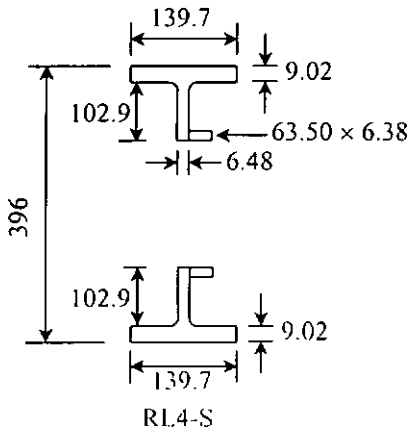

Beam RL5

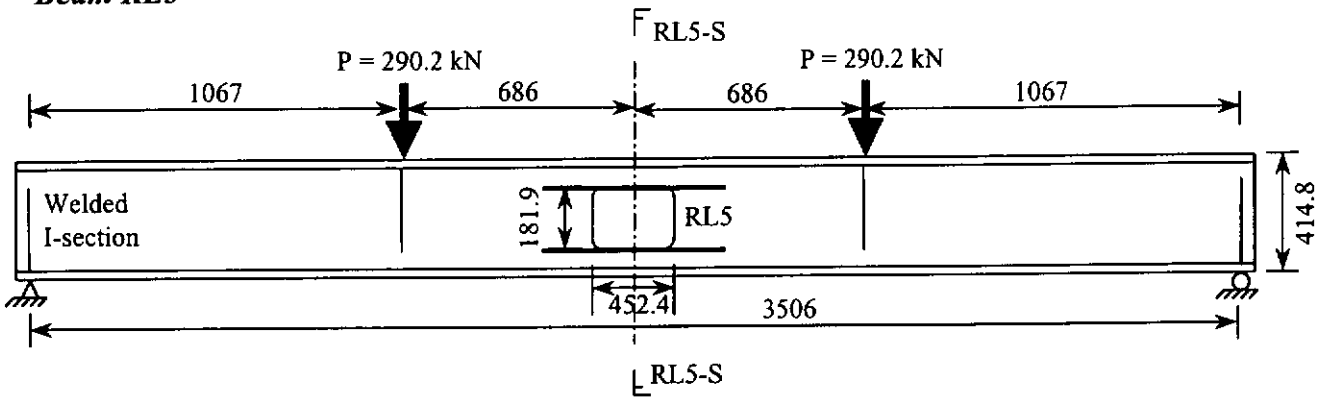

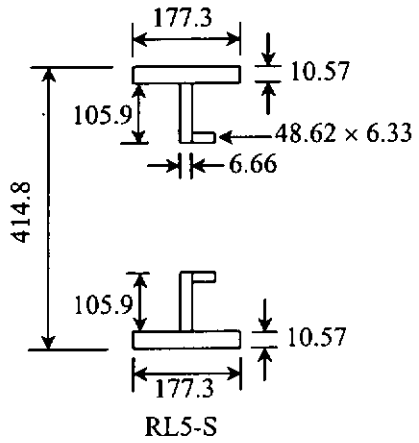

Beam RL6

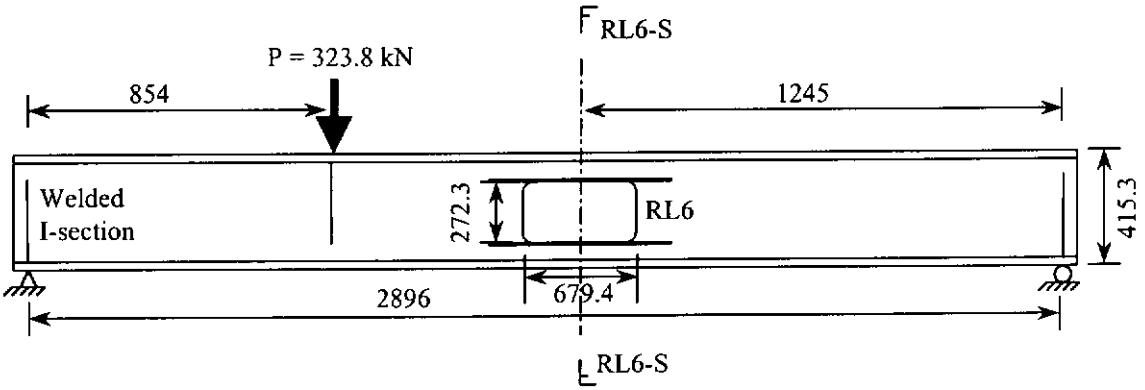

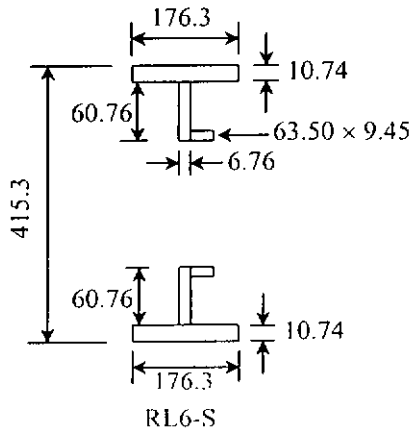

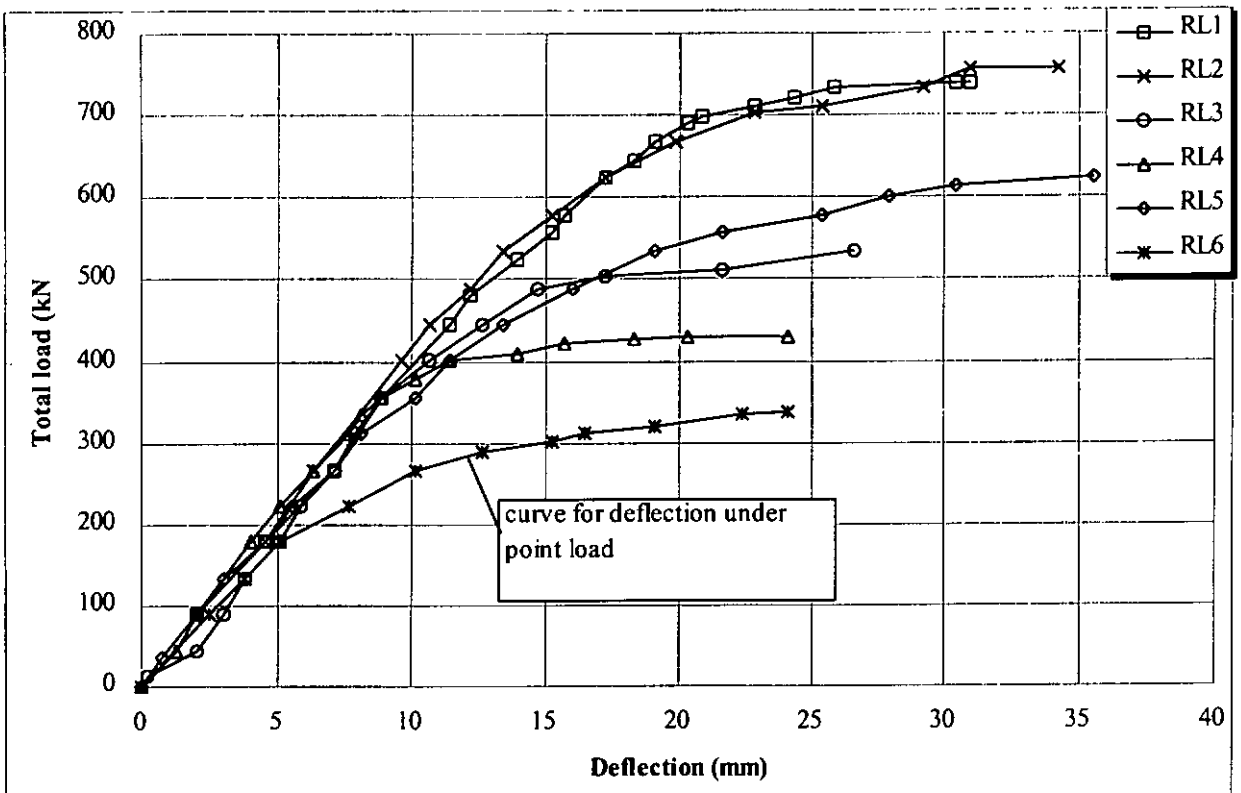

Figure A.1.7 Loads v.s. mid-span deflections for test series Lupien & Redwood (1977)

A.1.8 Redwood, Baranda, and Daly (1978)

1 General

1.1	Number of beams (tests):	11(15)
1.2	Beam spans:	2.0-4.2 m
1.3	Steel yield strength:	297.2 – 409.5 N/mm^2
1.4	Steel beam depth:	404.8-527.5 mm
1.5	Span/depth ratio:	4.6-10.5

2 Opening Configurations

2.1	Shapes of web openings:	10-rectangular, 5-circular
2.2	Number of eccentric openings:	1-downward
2.3	Number of reinforced openings:	0
2.4	Location of opening/span:	0.22-0.50 span
2.5	Length/height of openings:	1.00-3.00
2.6	Height of openings/depth of beam:	0.13-0.62
2.7	M/V ratio at centerline of opening:	0.54-10.54 m
2.8	Others:	

			Measured yield strength (N/mm^2)		
Tests	Failure loads, P (kN)	Modes of failure	Top flange	Bottom flange	Web
RBD-HB3	622.8	Vierendeel, flange buckling	297.9	297.9	315.1
RBD-HB4	216.7 + 327.1	Vierendeel, web buckling	297.9	297.9	315.1
RBD-HB3A	438.6	Vierendeel, flange buckling	297.9	297.9	315.1
RBD-R1B	711.7	Vierendeel, web buckling	299.2	299.2	320.6
RBD-EH1	422.6	Vierendeel	321.3	321.3	330.3
RBD-HB5A	478.6	Web buckling	384.7	384.7	397.1
RBD-HB5	265.1	Vierendeel, web buckling	384.7	384.7	397.1
RBD-R2	524.9	Vierendeel, web buckling	297.2	297.2	320.6
RBD-HB2	254.4	Vierendeel	297.9	297.9	315.1
RBD-HB1	183.2	Vierendeel, flange buckling	298.5	298.5	315.1
RBD-HB1A	633.5 + 522.7	Web buckling	298.5	298.5	315.1
RBD-C1	751.8	Vierendeel	297.2	297.2	320.6
RBD-UG2	578.3	Web buckling	373.0	373.0	399.9
RBD-UG3	689.7	Web and flange buckling	364.0	364.0	409.5
RBD-UG2A	456.4	Web buckling	373.0	373.0	399.9

Beam RBD-HB3

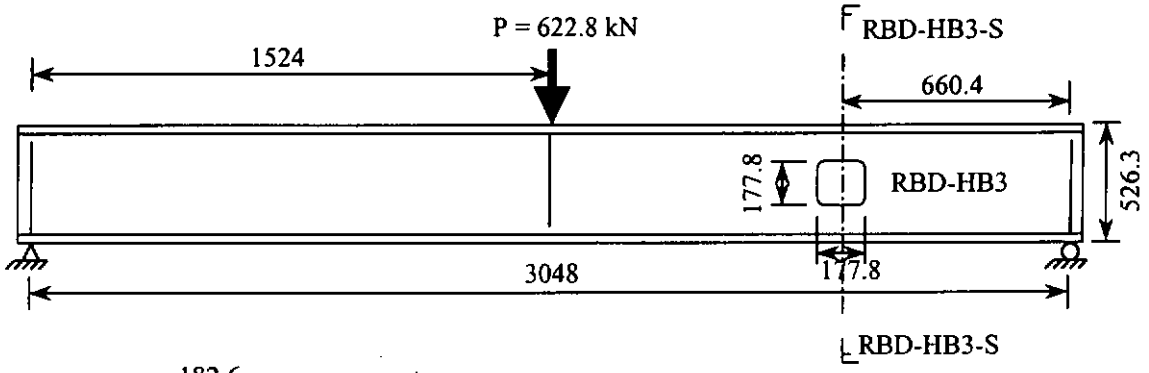

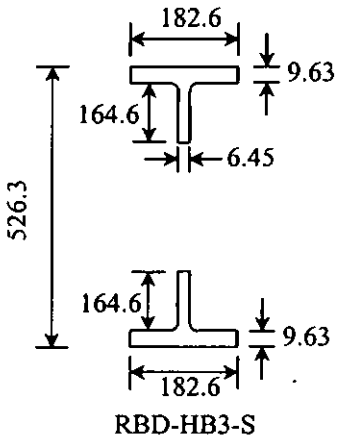

Beam RBD-HB4

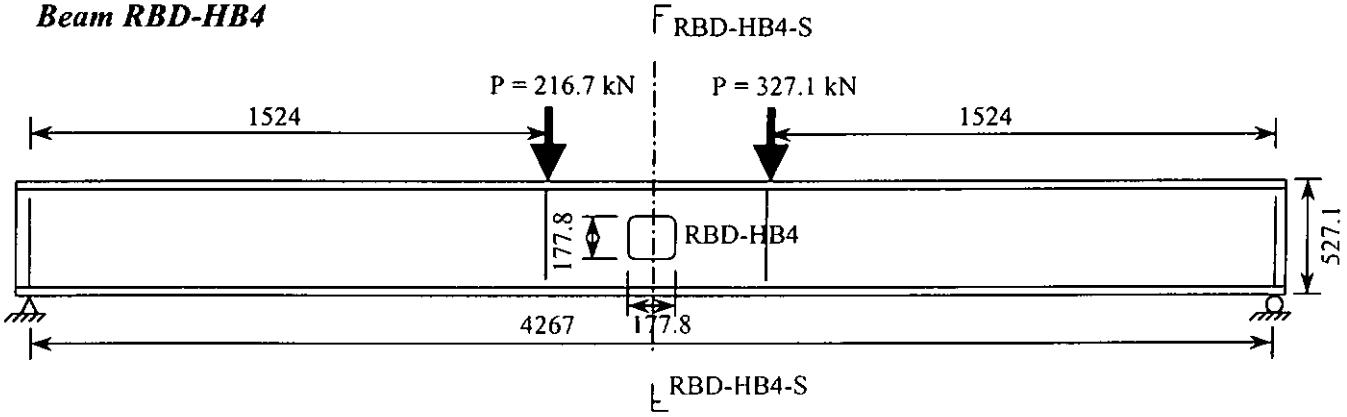

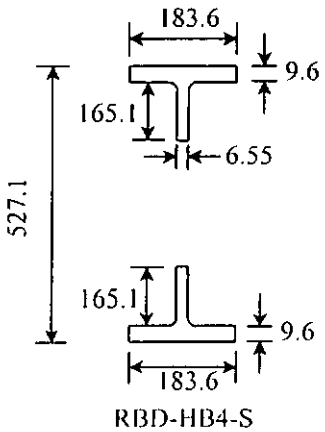

Beam RBD-HB3A

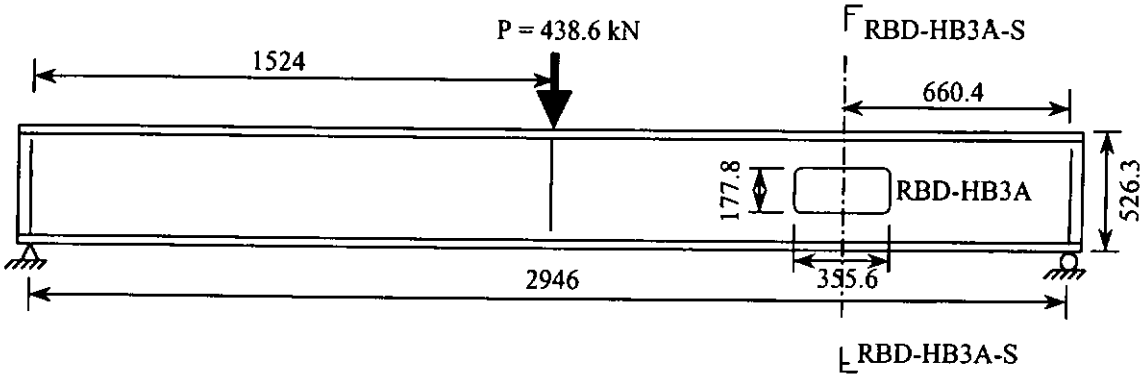

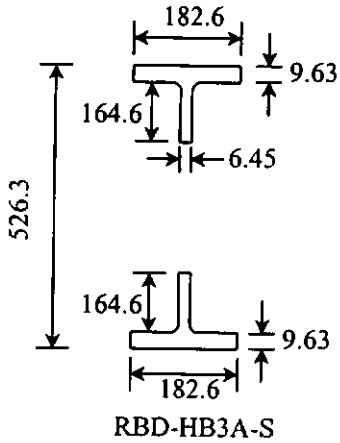

RBD-HB3A-S

Beam RBD-R1B

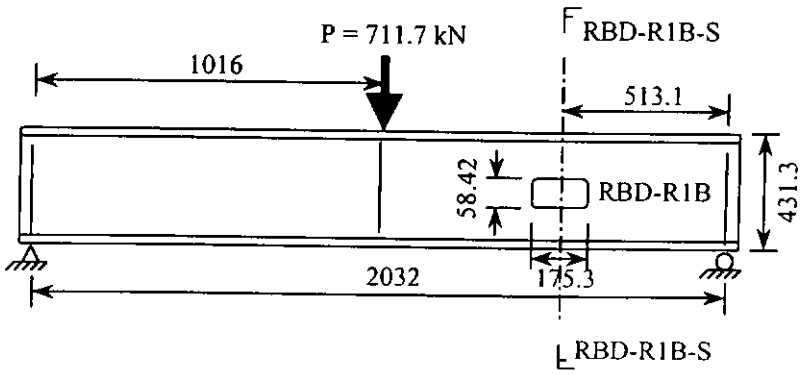

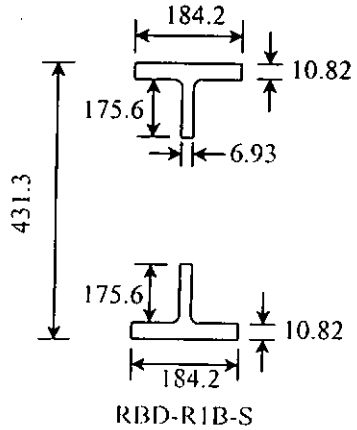

RBD-R1B-S

Beam RBD-EH1

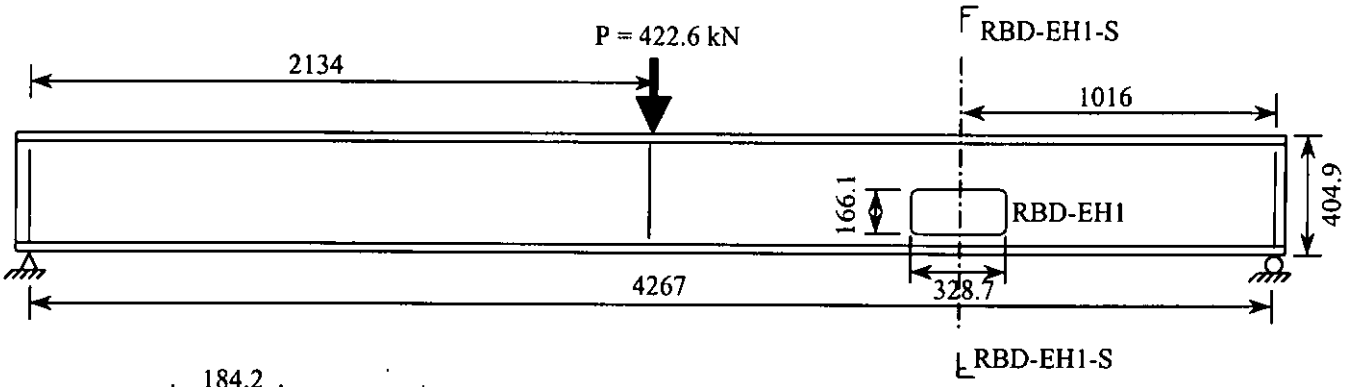

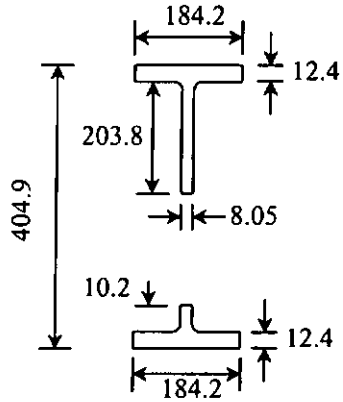

RBD-EH1-S

Beam RBD-HB5A

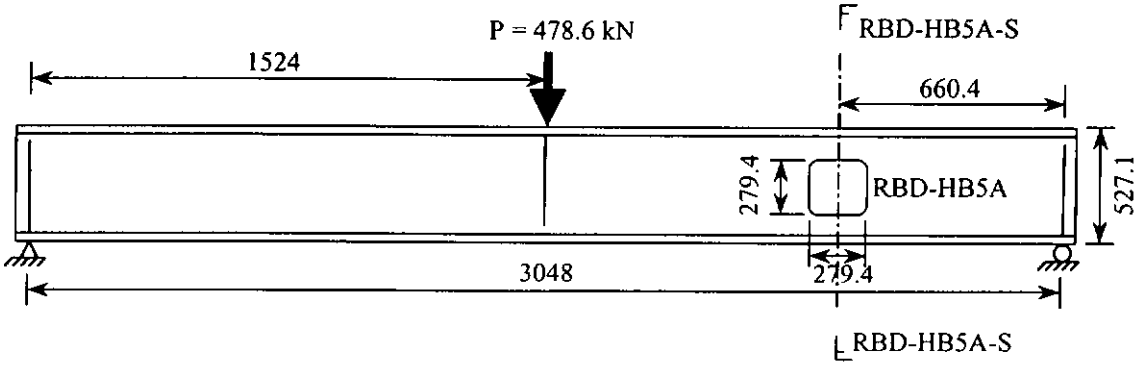

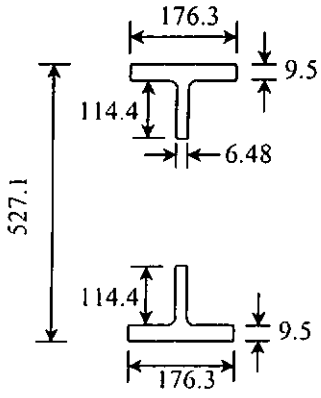

RBD-HB5A-S

Beam RBD-HB5

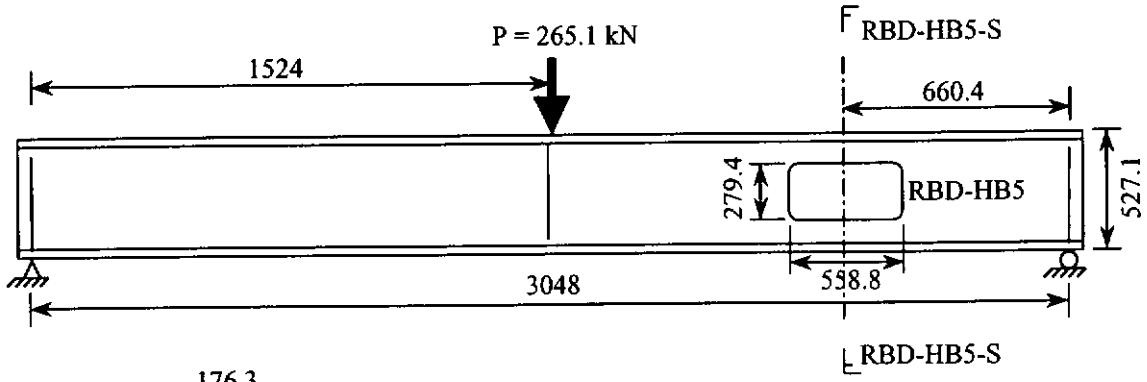

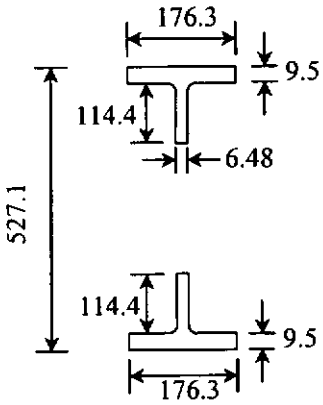

RBD-HB5-S

Beam RBD-R2

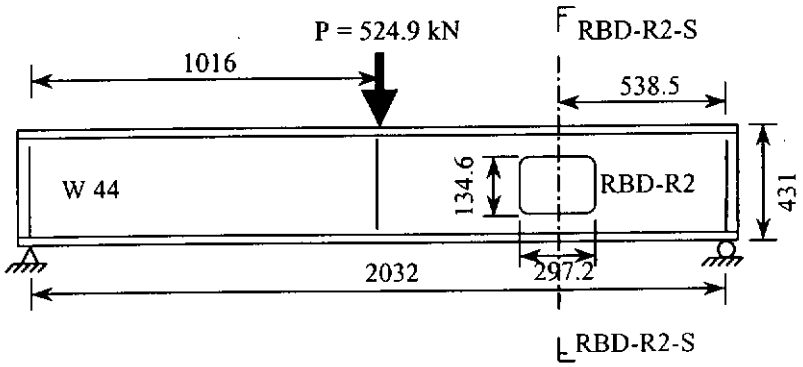

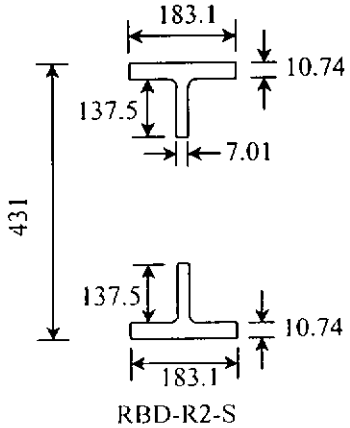

RBD-R2-S

Beam RBD-HB2

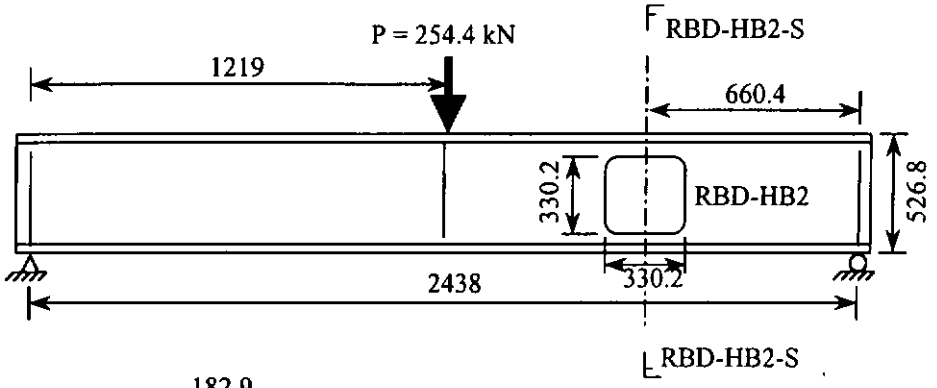

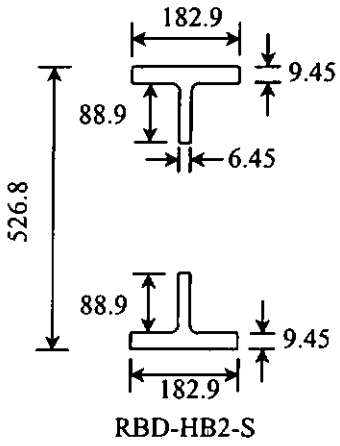

Beam RBD-HB1

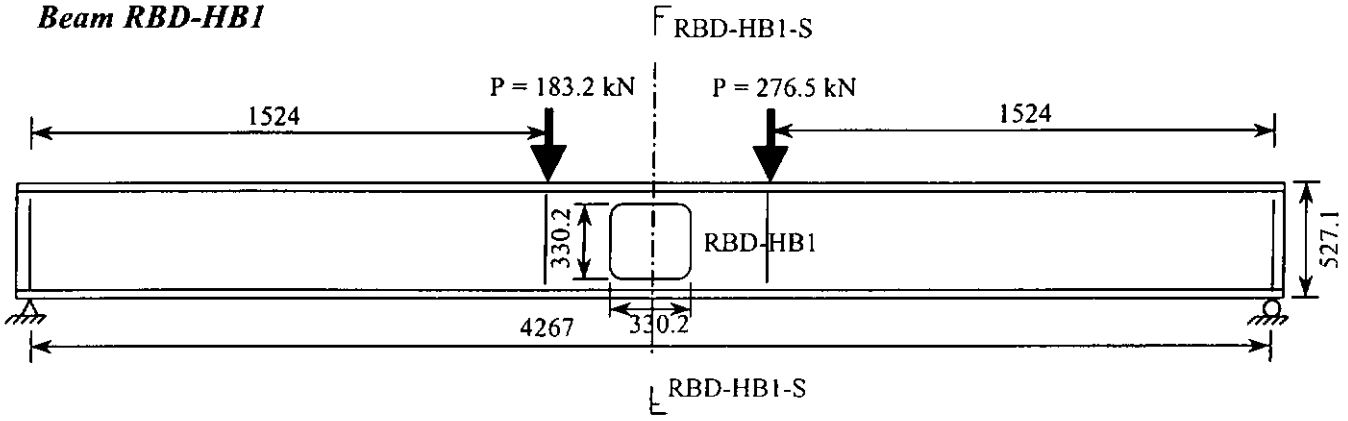

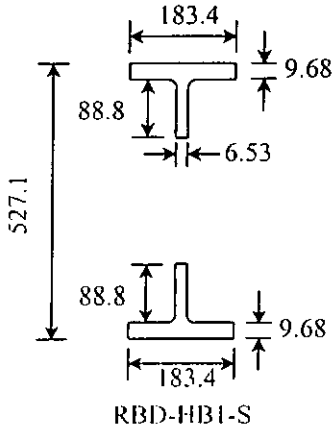

Beam RBD-HB1A

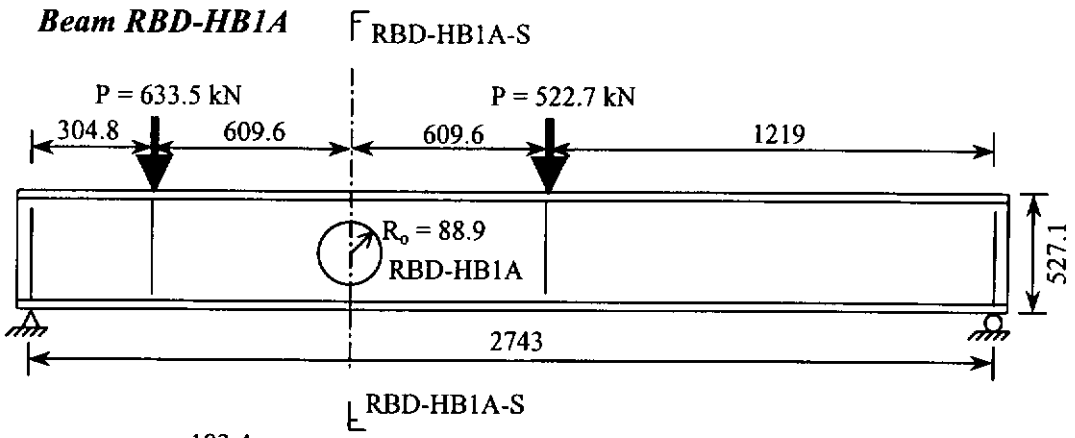

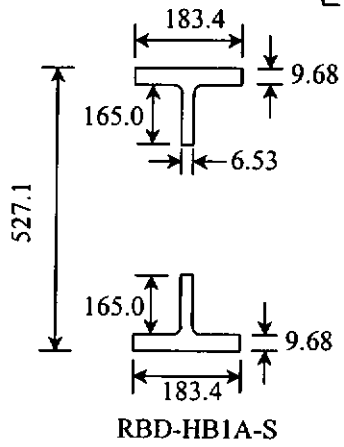

Beam RBD-C1

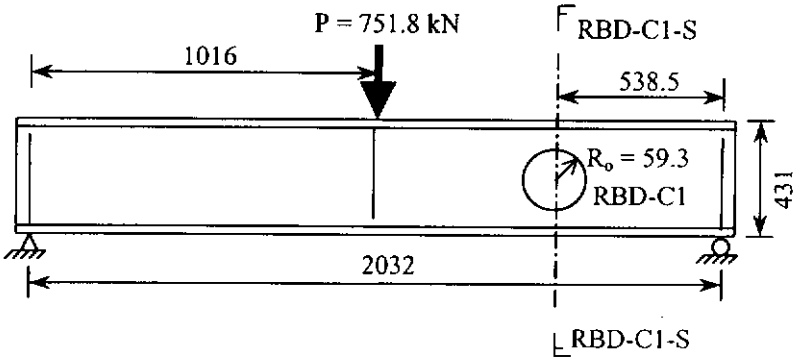

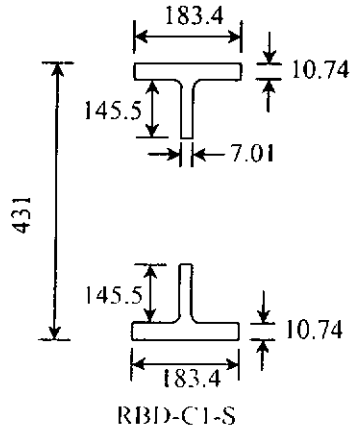

Beam RBD-UG2

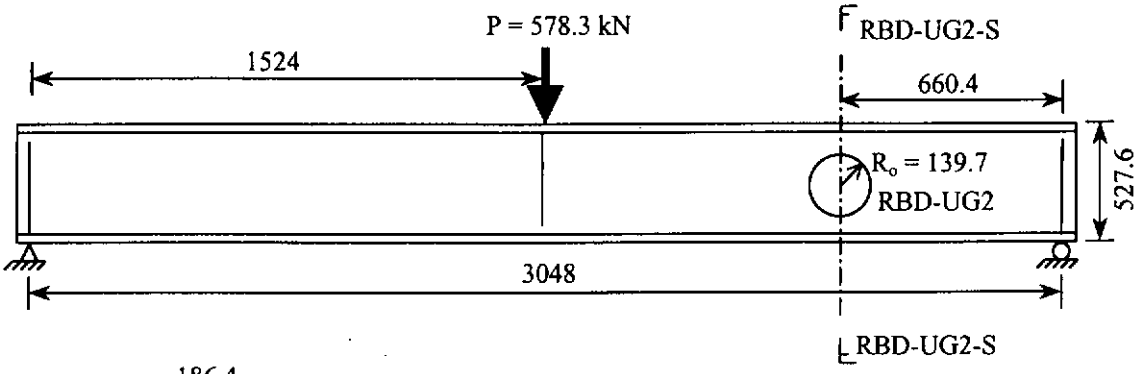

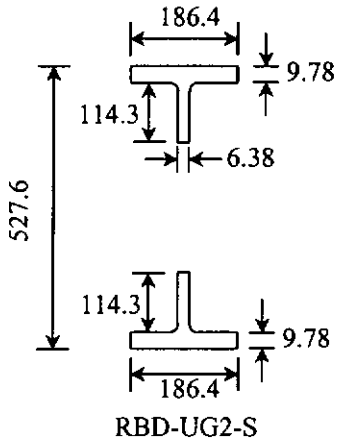

Beam RBD-UG3

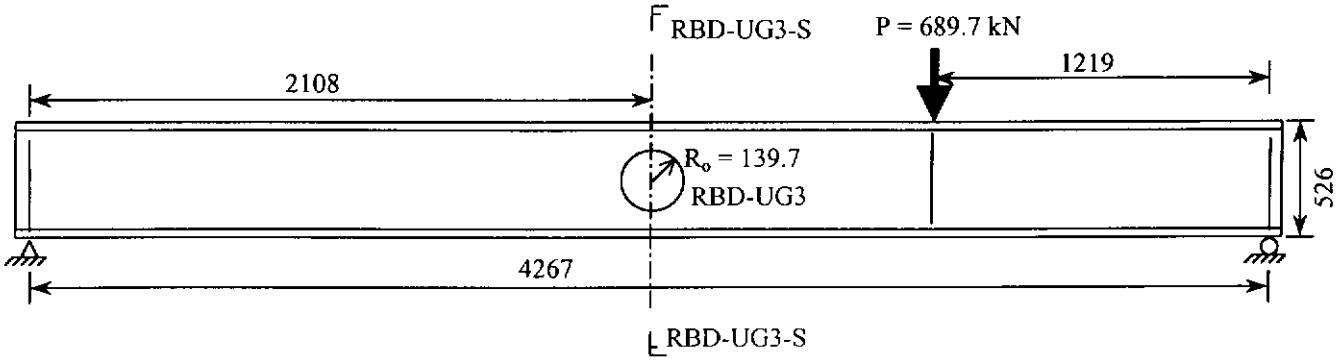

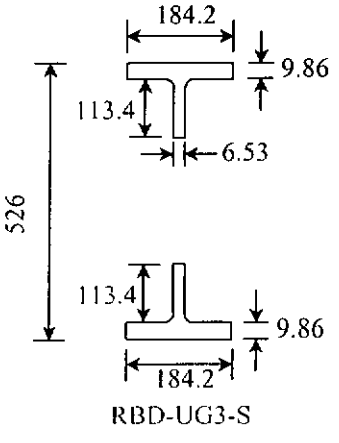

Beam RBD-UG2A

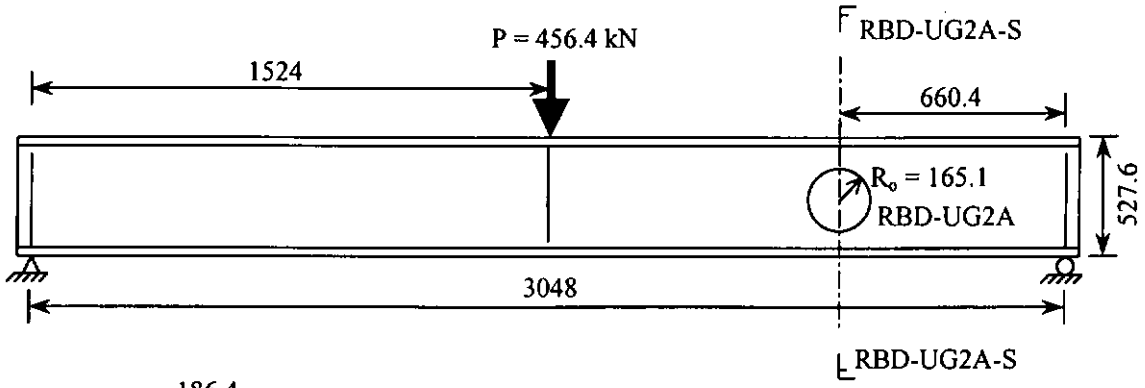

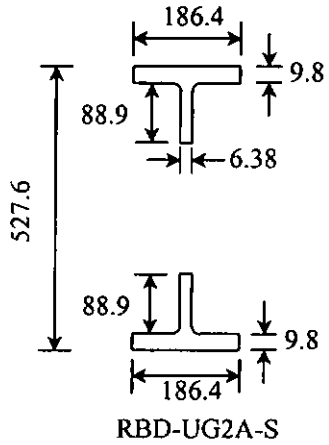

RBD-UG2A-S

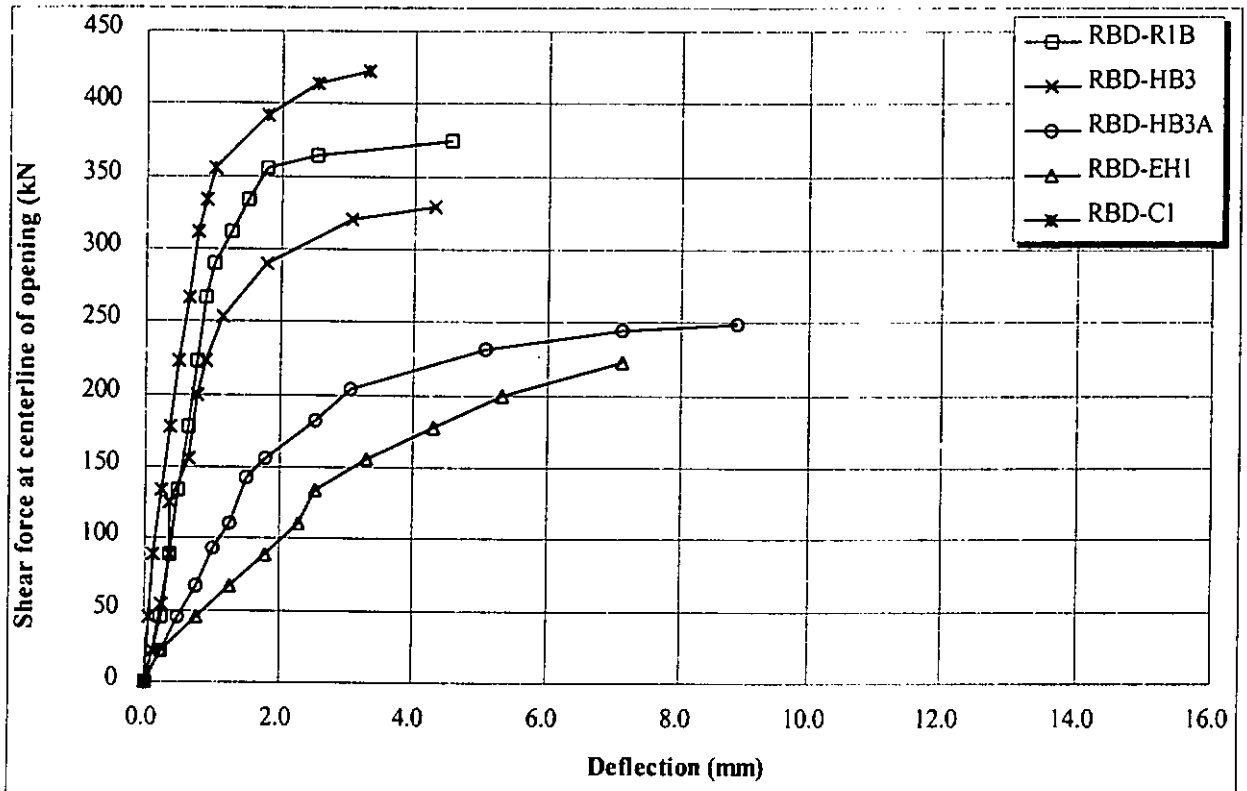

Figure A.1.8a Shear forces v.s. relative deflections between opposite ends of opening for test series Redwood, Baranda , and Daly (1978)

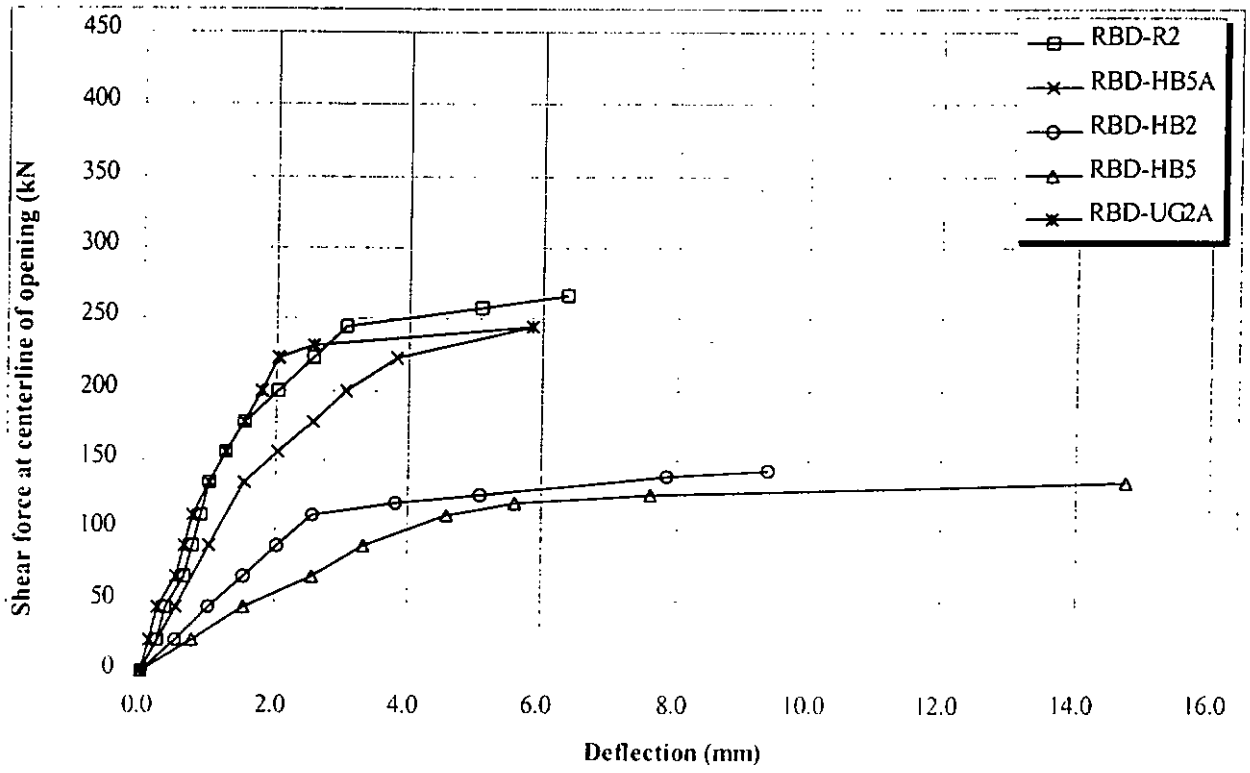

Figure A.1.8b Shear forces v.s. relative deflections between opposite ends of opening for tests series Redwood, Baranda, and Daly (1978)

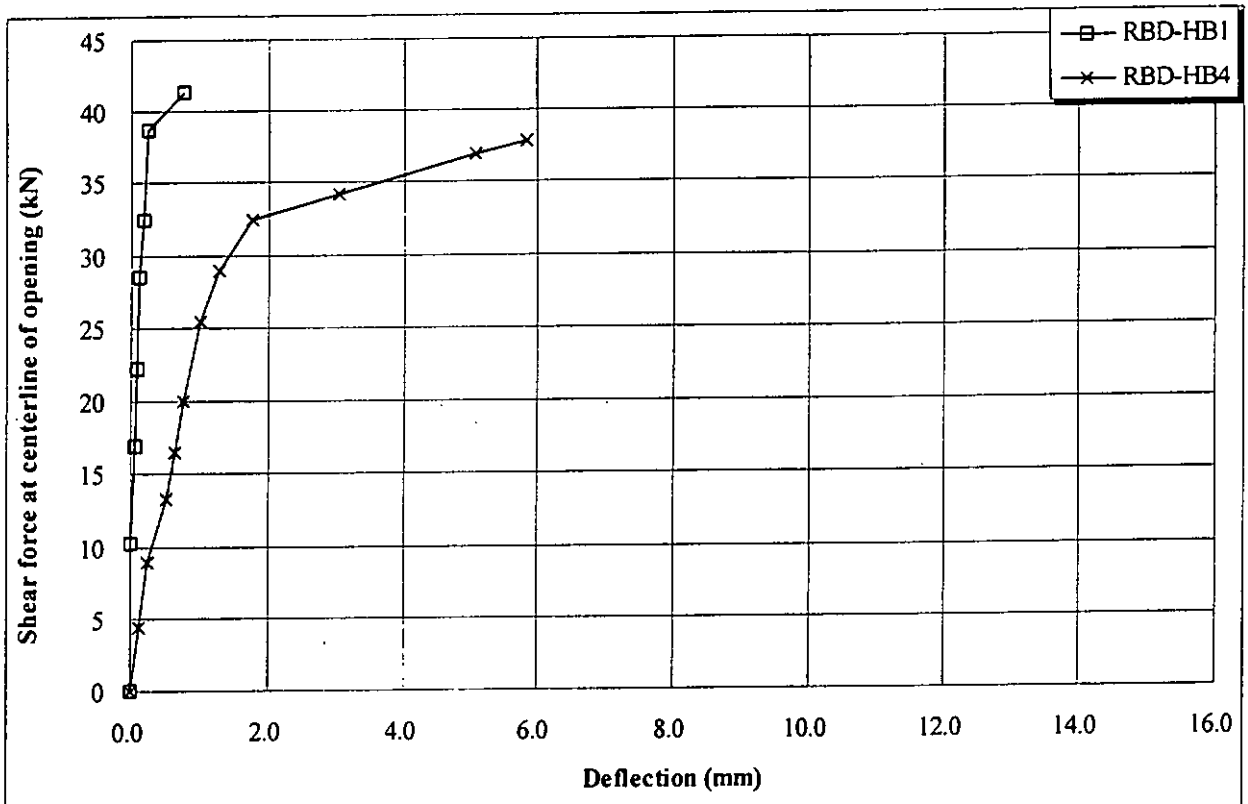

Figure A.1.8c Shear forces v.s. relative deflections between opposite ends of opening for test series Redwood, Baranda, and Daly (1978)

A.1.9 Shrivastava and Redwood (1977)

1 General

1.1	Number of beams (tests):	4(4)
1.2	Beam spans:	2.3-3.0 m
1.3	Steel beam sizes:	4-welded I sections
1.4	Steel element yield strength:	255.1 – 402.0 N/mm^2
1.5	Steel beam depth:	414.2-524.7 mm
1.6	Span/depth ratio:	5.5-6.9

2 Opening Configurations

2.1	Shapes of web openings:	4-rectangular
2.2	Number of eccentric openings:	0
2.3	Number of reinforced openings:	4-two sided
2.4	Location of opening/span:	0.22-0.26 span
2.5	Length/height of openings:	1.58-3.00
2.6	Height of openings/depth of beam:	0.29-0.67
2.7	M/V ratio at centerline of opening:	0.6-0.8 m
2.8	Others:	

			Measured yield strength (N/mm^2)			
Tests	Failure loads, P (kN)	Modes of failure	Top flange	Bottom flange	Web	Reinforcement
SR-UG1	633.9	Web buckling	372.3	372.3	393.0	303.4
SR-VB1	700.6	Web buckling	376.5	376.5	402.0	255.1
SR-VB2	295.8	Vierendeel	277.9	277.9	337.8	255.1
SR-VB3	633.9	Vierendeel	287.2	287.2	308.2	257.2

Beam SR-UG1

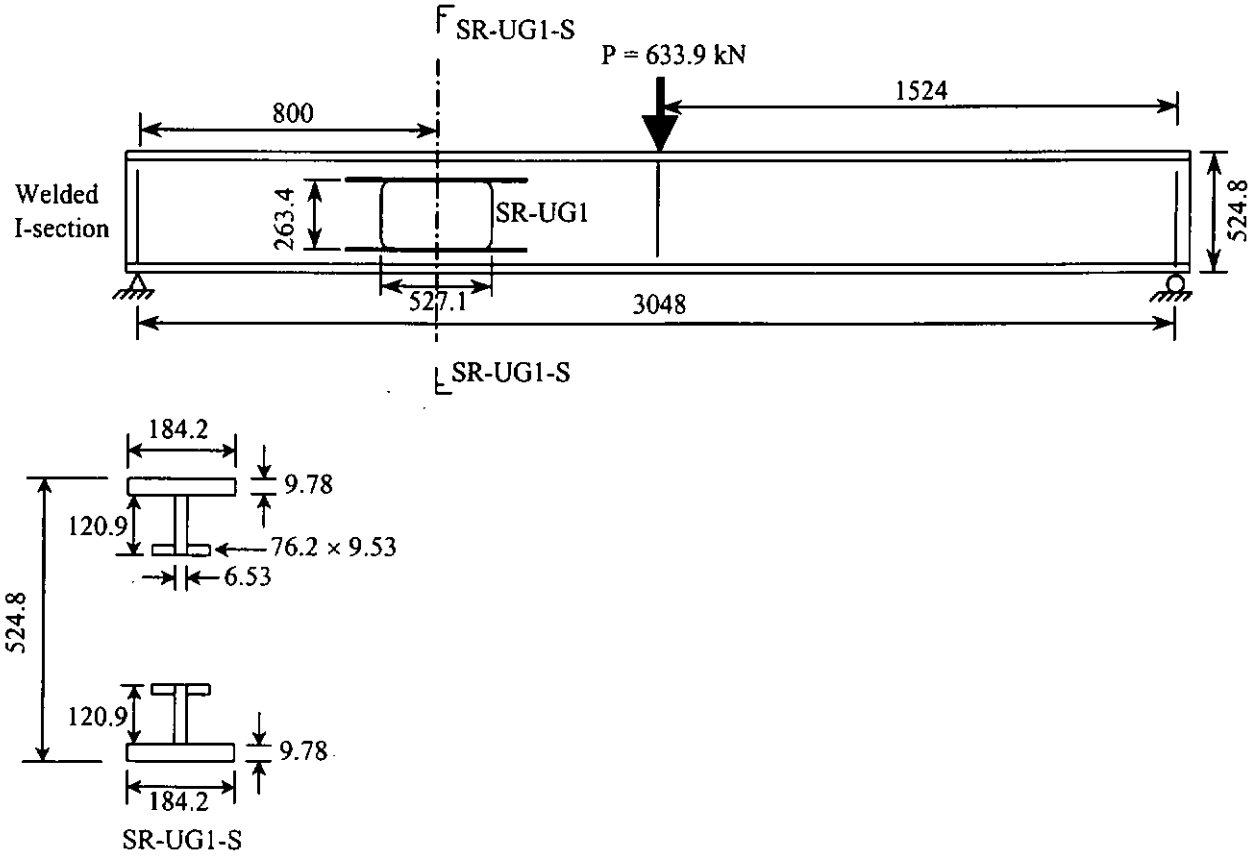

Beam SR-VB1

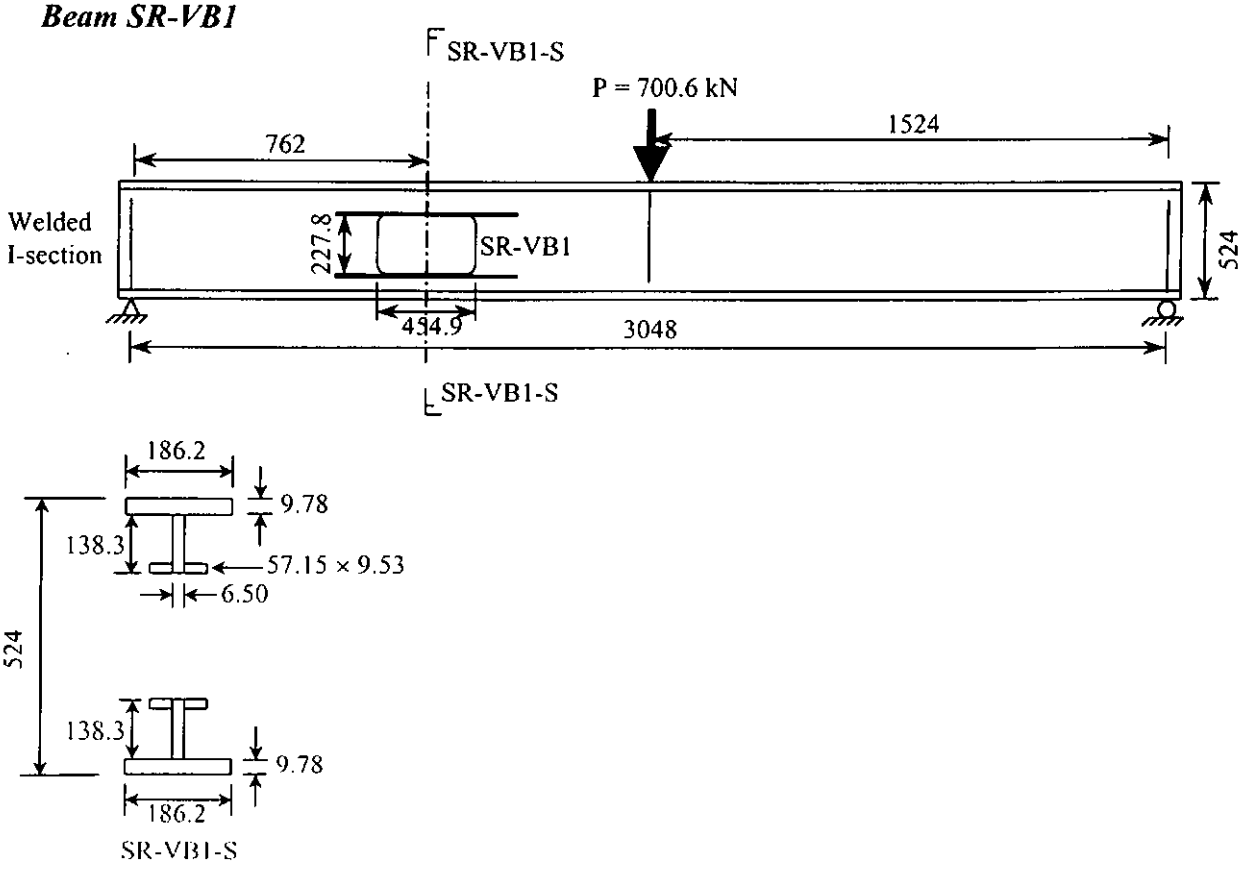

Beam SR-VB2

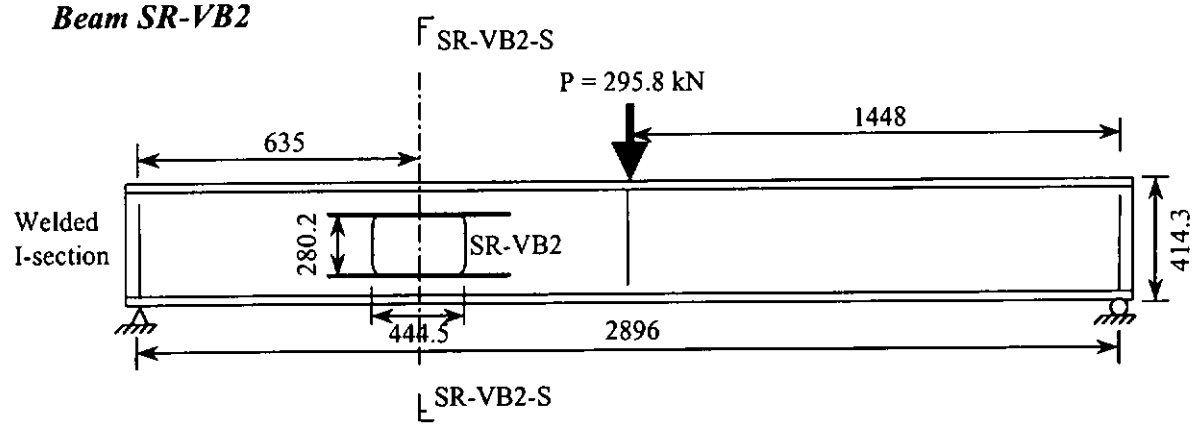

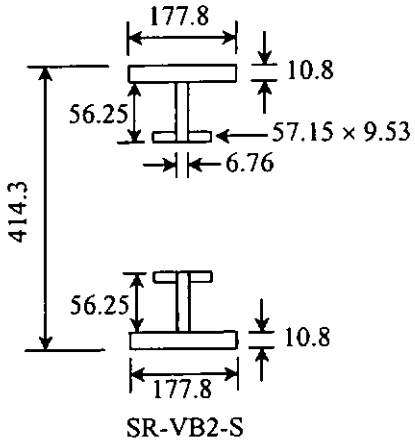

Beam SR-VB3

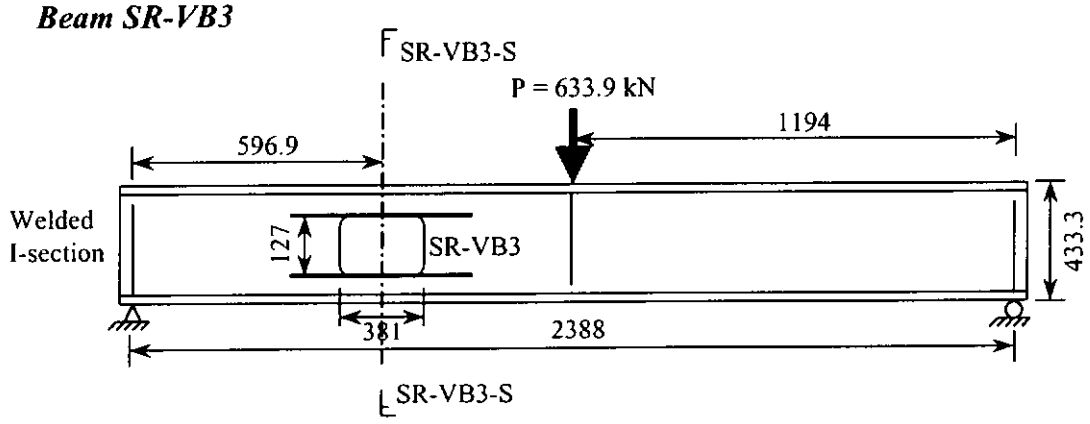

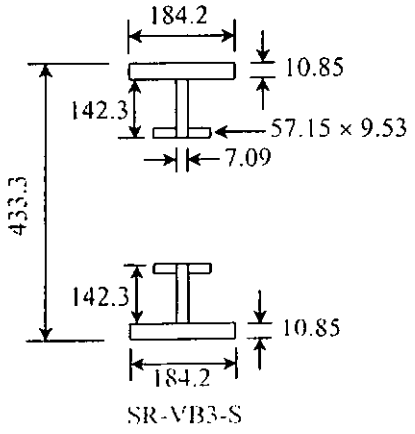

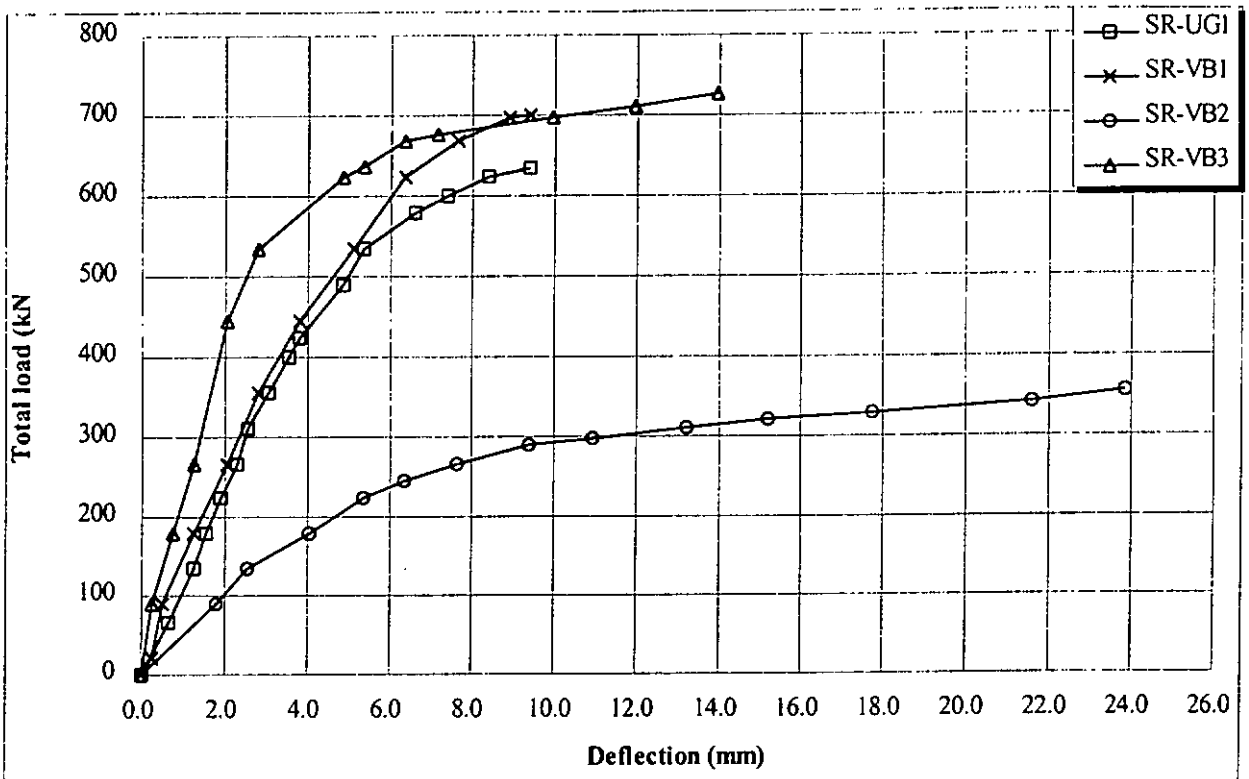

Figure A.1.9 Loads v.s. relative deflection between opposite ends of opening for test series Shrivastava & Redwood (1977)

A.2.1 Cho and Redwood (1992b)

1 General

1.1	Number of beams (tests):	6(9)
1.2	Beam spans:	4.0 m
1.3	Steel beam sizes:	6-W360x51
1.4	Steel beam grade:	301 – 347 N/mm^2
1.5	Steel beam depth:	357-359.5 mm
1.6	Profiled steel decking:	7-placed transversely to steel beams, 2-none
1.7	Span/depth ratio:	7.9-8.6

2 Opening Configurations

2.1	Shapes of web openings:	9-rectangular
2.2	Number of eccentric openings:	0
2.3	Number of reinforced openings:	0
2.4	Length/height of openings:	1.70-1.72
2.5	Height of openings/depth of beam:	0.68 – 0.69
2.6	Location of opening/span:	0.24-0.44
2.7	M/V ratio at centerline of opening:	0-1.05 m

3 Concrete Slabs

3.1	Type of concrete:	Normal weight
3.2	Slab width:	See table
3.3	Height of profiled steel decking:	76 mm
3.4	Trough spacing:	304.8 mm
3.5	Trough width (mean):	156 mm
3.6	Thickness of decking:	0.914 mm
3.7	Ultimate strength of shear connectors:	413 N/mm^2
3.8	Height of stud shear connectors:	114 mm (except CR66, CR69 = 76 mm)
3.9	Diameter of stud shear connectors:	19 mm
3.10	Welded position of shear connectors:	all favorable
3.11	Others:	

			Measured yield strength (N/mm^2)			Concrete slab		
Tests	Failure loads, P (kN)	Modes of failure	Top Flange	Bottom flange	Web	Cylinder strength (N/mm^2)	Height over decking (mm)	Width (mm)
CR11	143.1 + 71.6	Vierendeel	335.0	335.0	345.5	24.40	67.0	758
CR22	109.3 + 54.7	Vierendeel	301.5	301.5	347.5	24.60	69.0	750
CR33	106.2 + 53.1	Vierendeel	329.0	329.0	339.5	24.90	67.0	380
CR44	186.6	Vierendeel	312.5	312.5	331.0	22.70	68.0	1005
CR47	210.3	Vierendeel	312.5	312.5	331.0	22.70	68.0	1005
CR55	183.9	Vierendeel	303.5	303.5	334.0	22.20	67.0	1005
CR58	237.7	Vierendeel	303.5	303.5	334.0	22.20	67.0	1005
CR66	167.2	Vierendeel	306.5	306.5	332.0	23.80	104.0	510
CR69	191.2	Vierendeel	306.5	306.5	332.0	23.80	104.0	510

Beam CR1

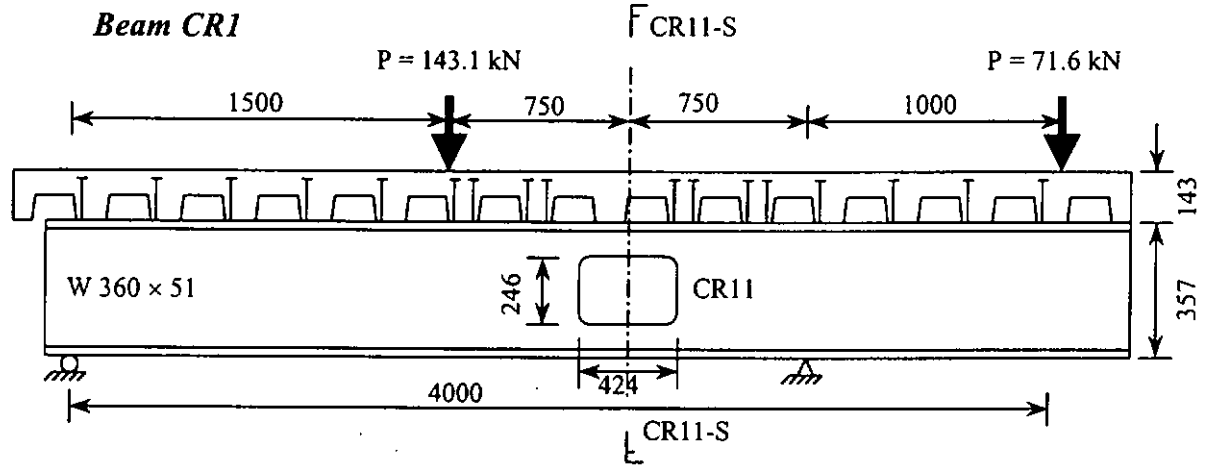

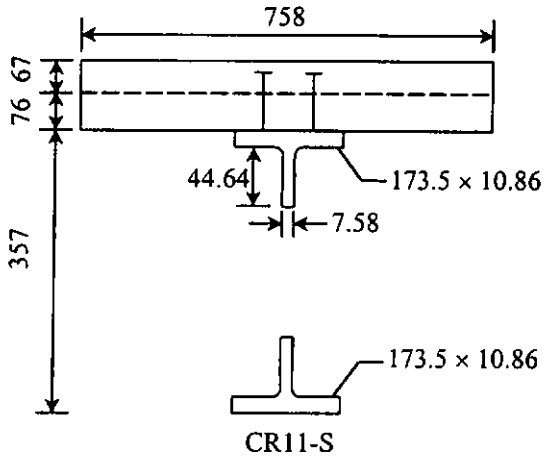

Beam CR2

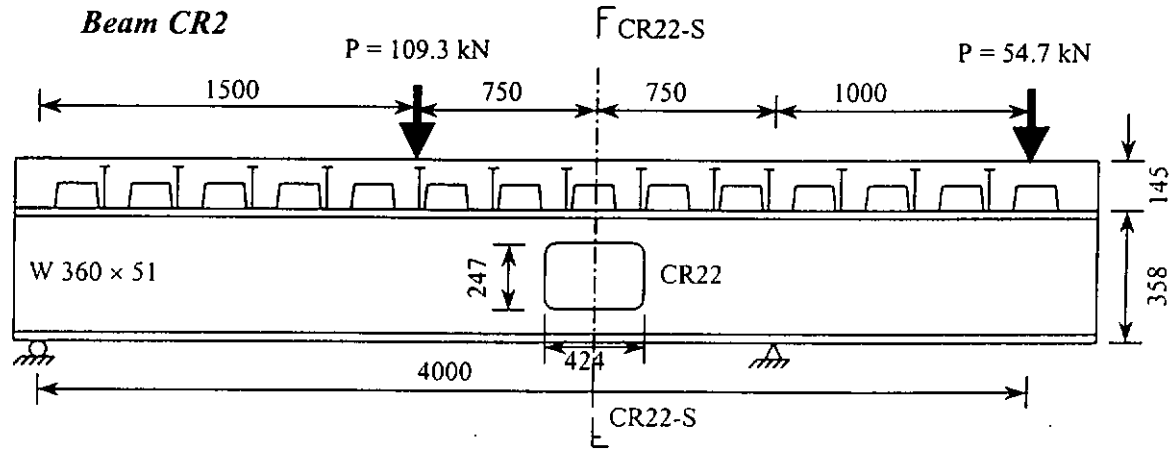

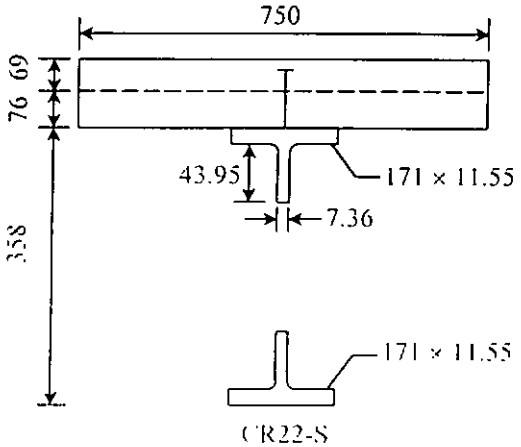

Beam CR3

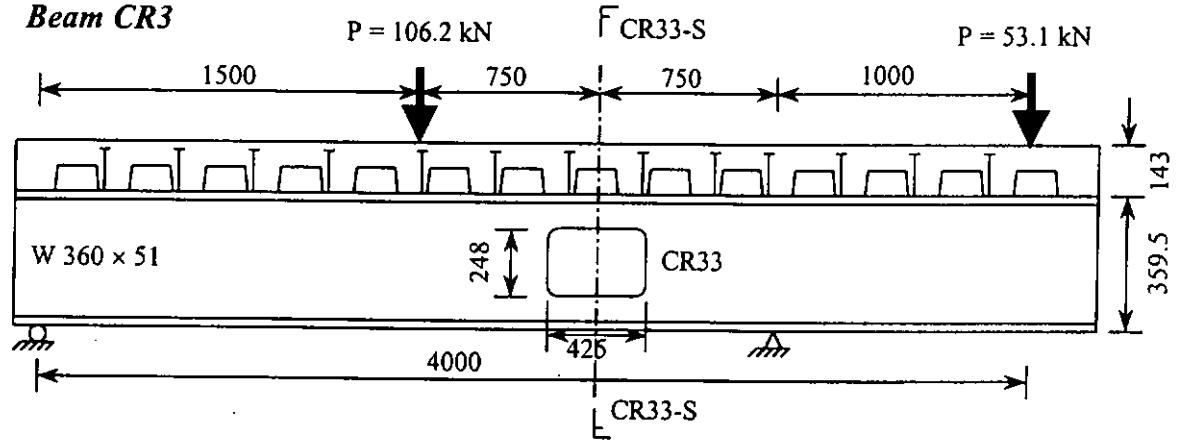

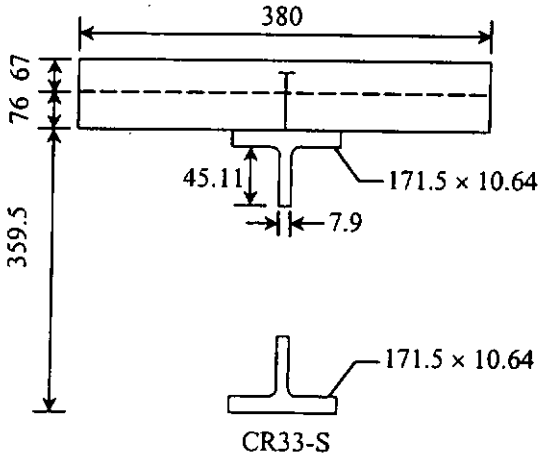

Beam CR4

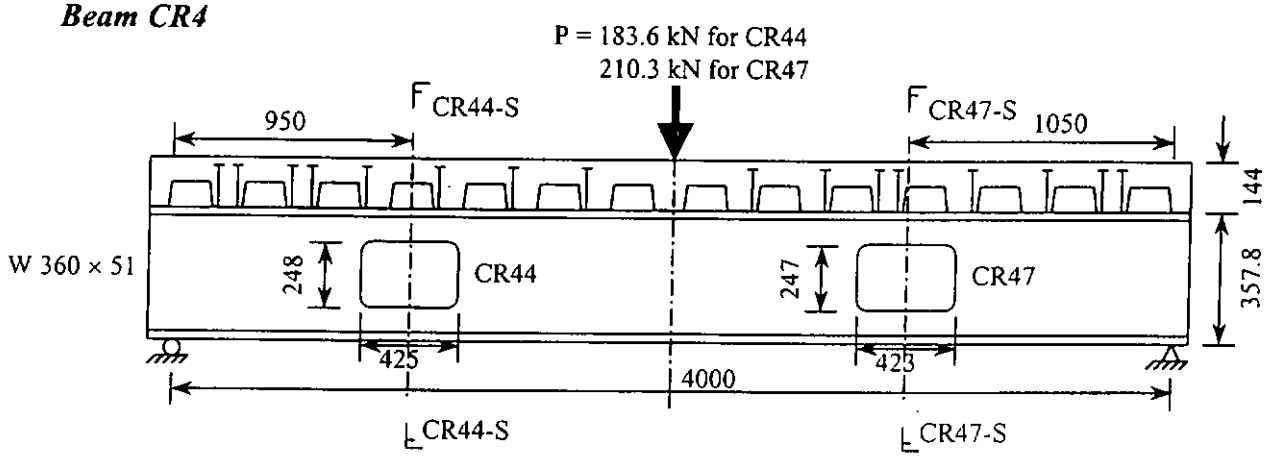

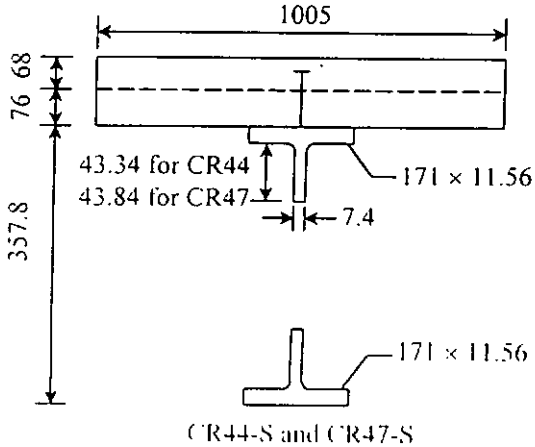

Beam CR5

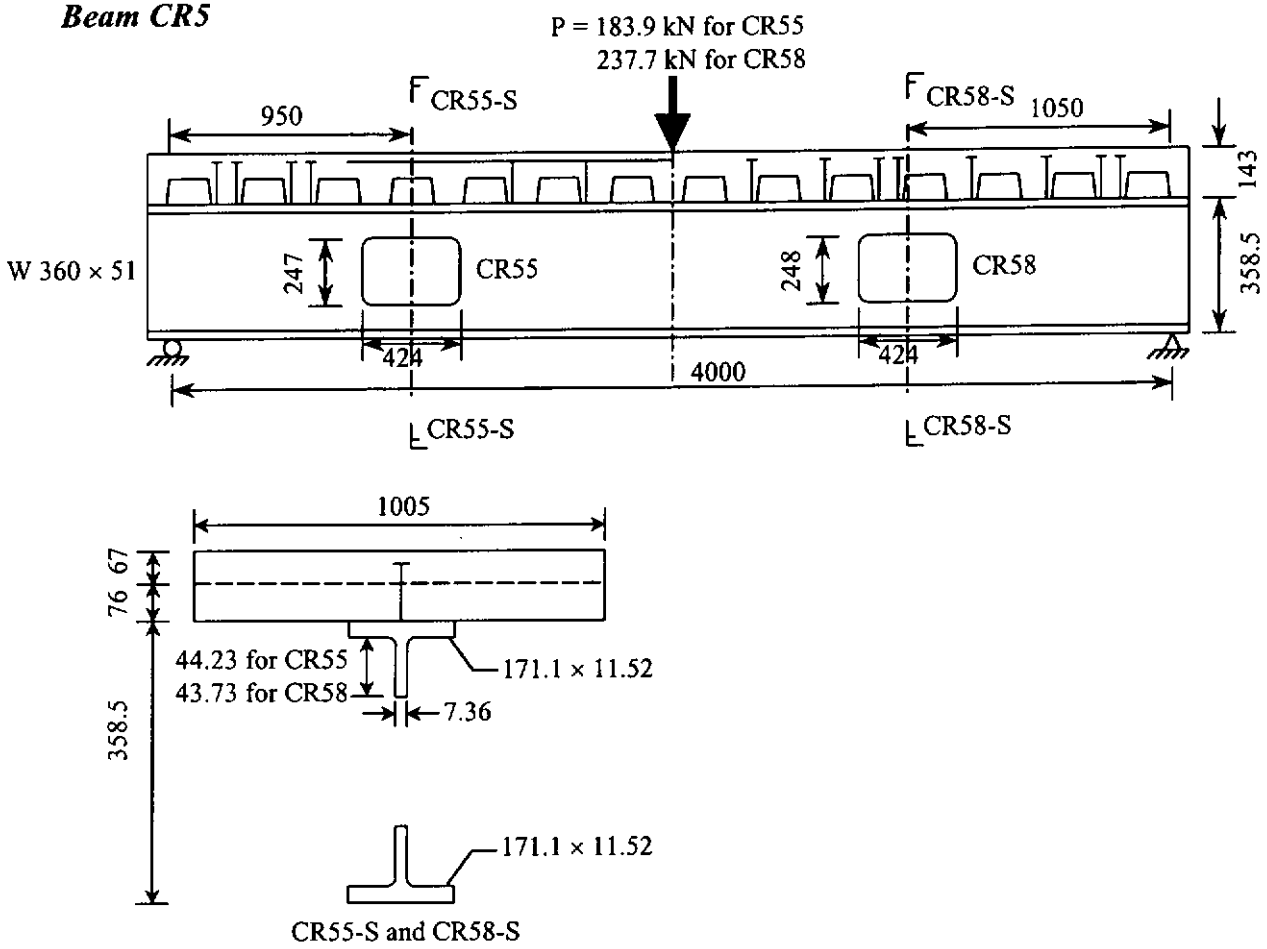

Beam CR6

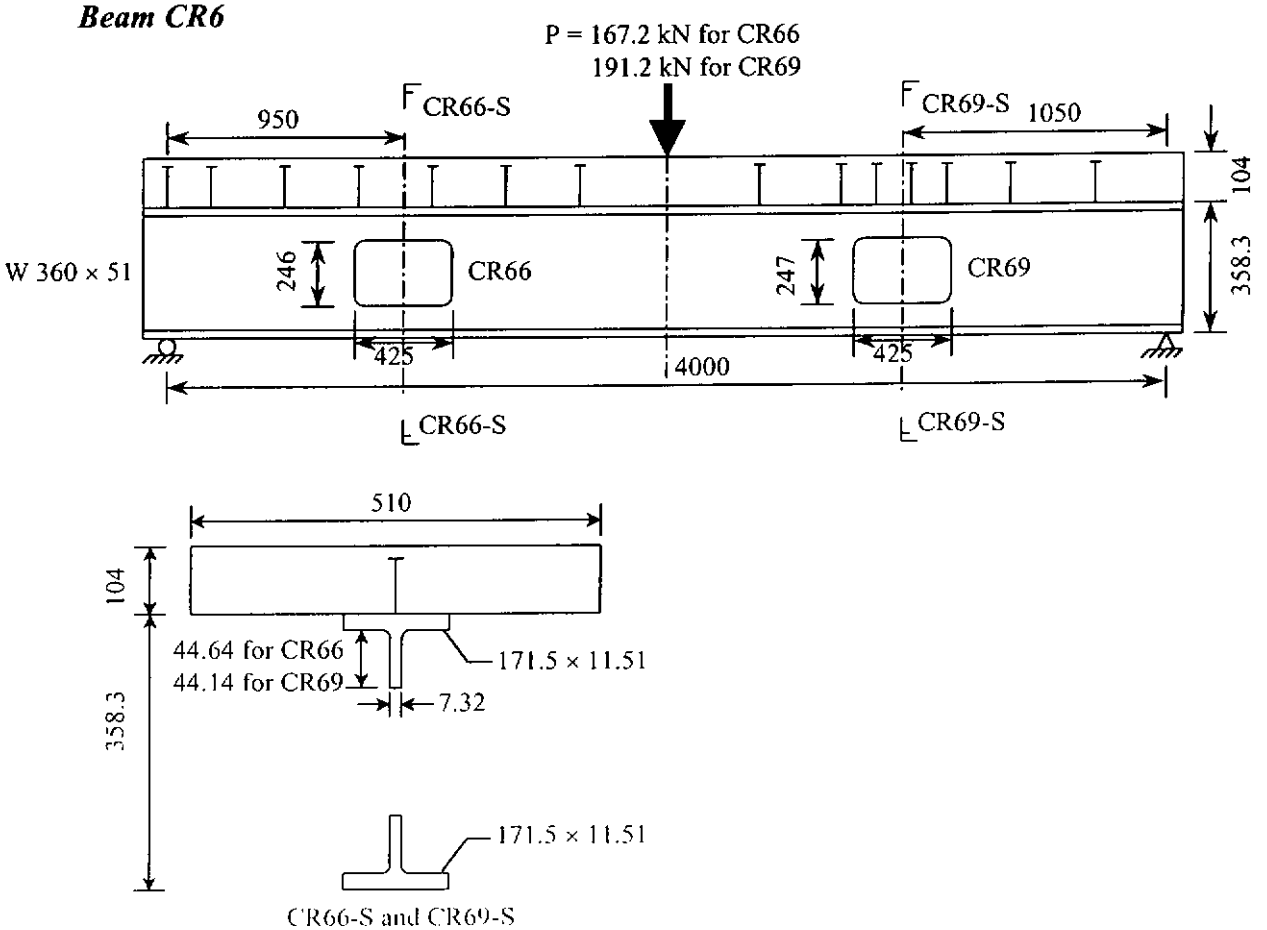

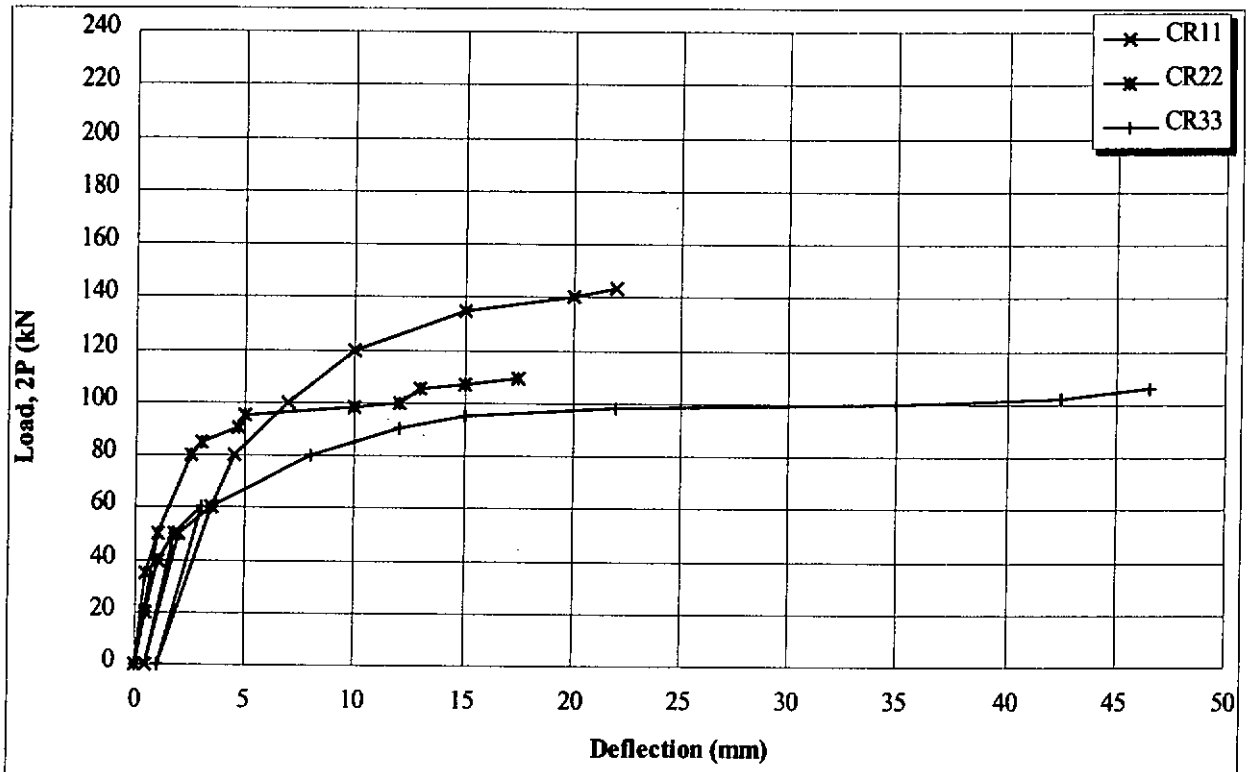

Figure A.2.1a Applied load v.s. relative deflections between opposite ends of opening for test series Cho & Redwood (1992)

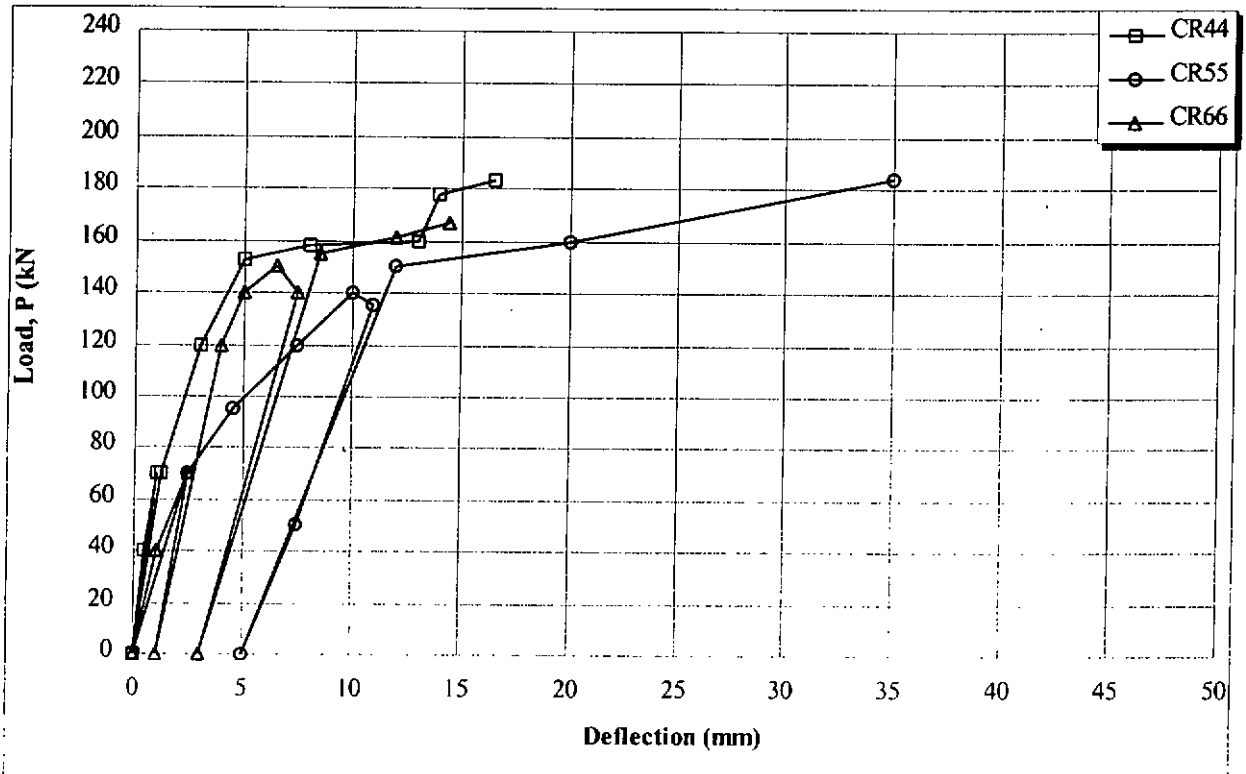

Figure A.2.1b Applied load v.s. relative deflections between opposite ends of openings for test series Cho & Redwood (1992)

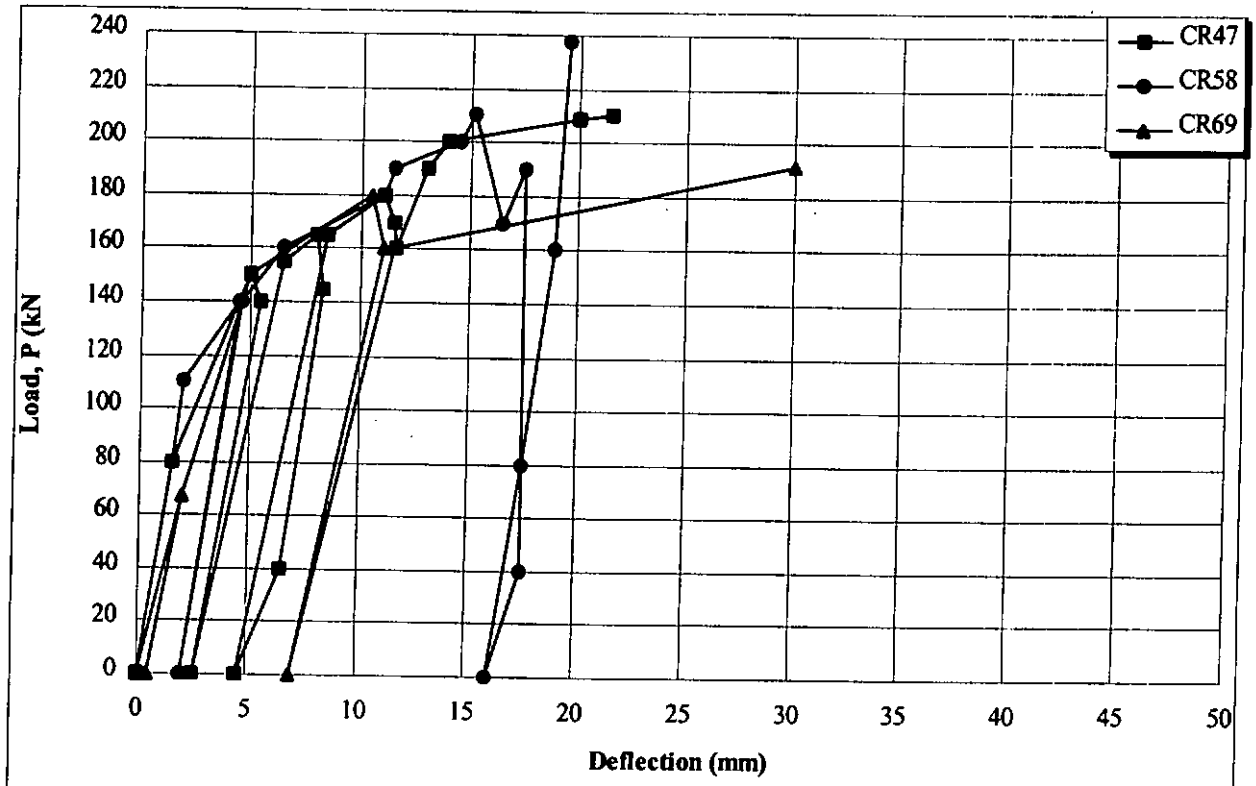

Figure A.2.1c Applied load v.s. relative deflections between opposite ends of openings for test series Cho & Redwood (1992)

A.2.2 Clawson and Darwin (1980)

1 General

1.1	Number of beams (tests):	6(6)
1.2	Beam spans:	4.5 - 7.3 m
1.3	Steel beam sizes:	2-W14x34, 3-W18x45, 1-W18x46
1.4	Steel beam grade:	247 – 335 N/mm^2
1.5	Steel beam depth:	338-458 mm
1.6	Profiled steel decking:	None
1.7	Span/depth ratio:	8.2-15.9

2 Opening Configurations

2.1	Shapes of web openings:	6-rectangular
2.2	Number of eccentric openings:	0
2.3	Number of reinforced openings:	0
2.4	Location of opening/span:	0.20 – 0.38
2.5	Length/height of openings:	2.0
2.6	Height of openings/depth of beam:	0.57 – 0.60
2.7	M/V ratio at centerline of opening:	0.9-9.9 m

3 Concrete Slabs

3.1	Type of concrete:	Normal weight
3.2	Slab width:	1219 mm
3.3	Slab height:	101.6 mm
3.4	As-welded height of shear connectors:	76.2 mm ?
3.5	Diameter of shear connectors:	19.05 mm
3.6	Others:	

			Measured yield strength (N/mm^2)			Concrete slab
Tests	Failure loads, P (kN)	Modes of failure	Top flange	Bottom flange	Web	Cylinder strength (N/mm^2)
CD1	143.5 + 143.5	Vierendeel	240.76	247.11	238.35	48.26
CD2	214 + 214	Vierendeel	268.07	268.69	279.79	28.96
CD3	236.9 + 236.9	Flexure	268.07	268.69	279.79	33.99
CD4	206.8 + 206.8	Vierendeel	305.99	284.34	335.84	30.75
CD5	209.1 + 209.1	Vierendeel	282.20	288.61	272.14	32.27
CD6	173 + 173	Vierendeel	271.93	272.83	301.71	27.72

Beam CD1

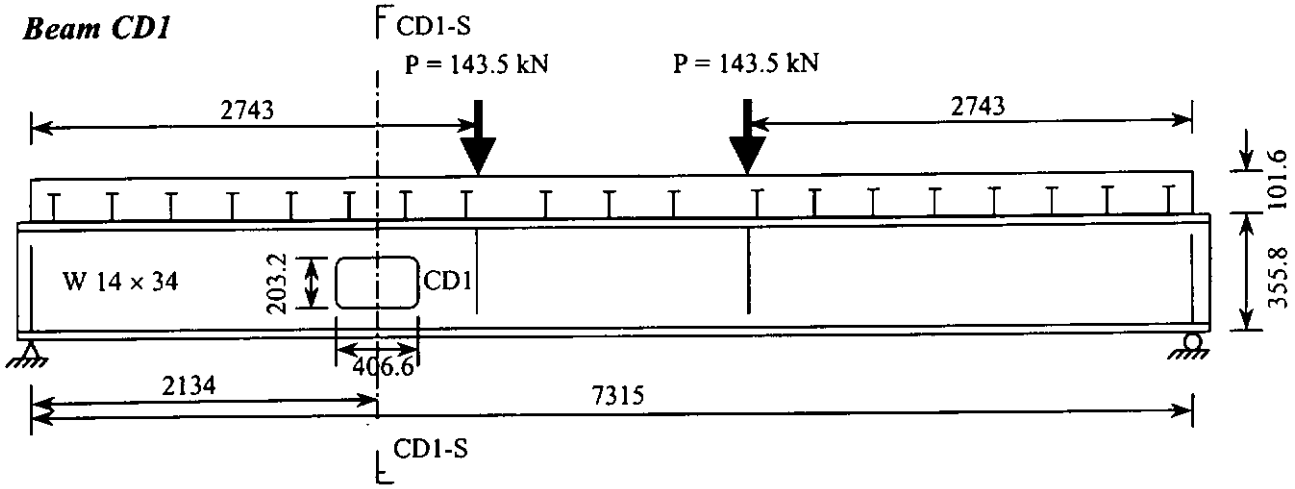

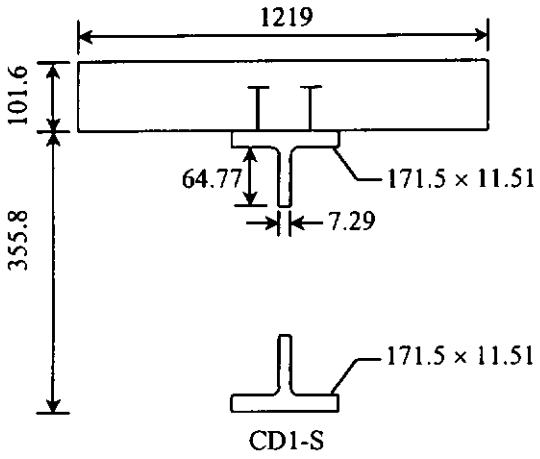

Beam CD2

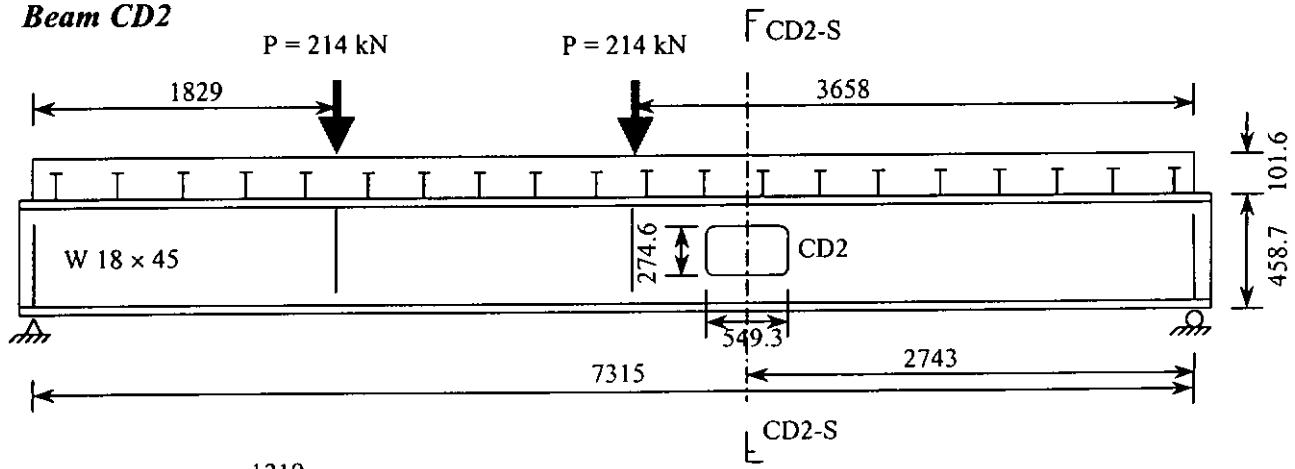

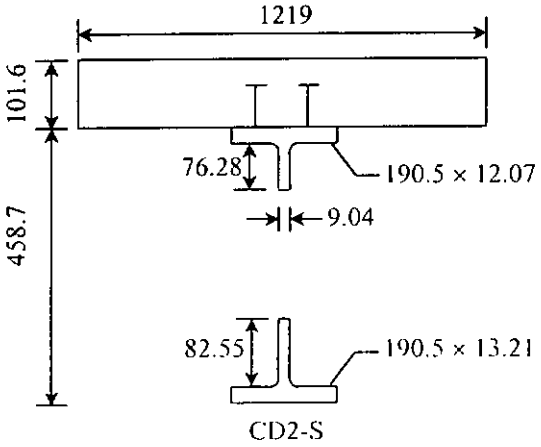

Beam CD3

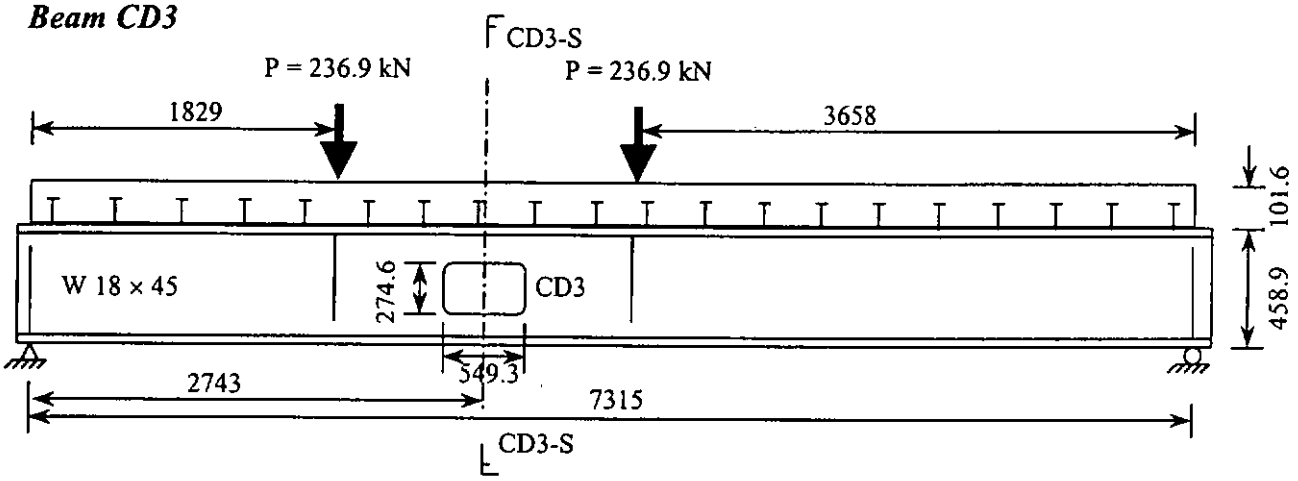

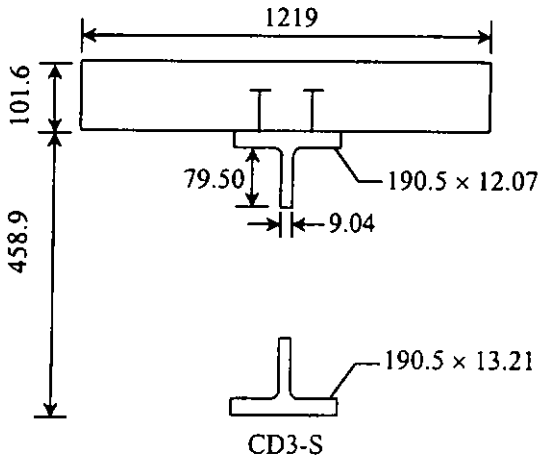

Beam CD4

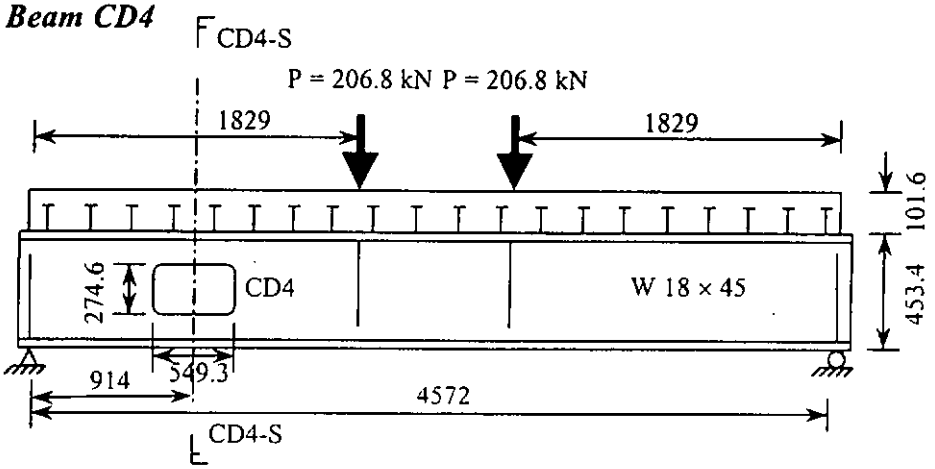

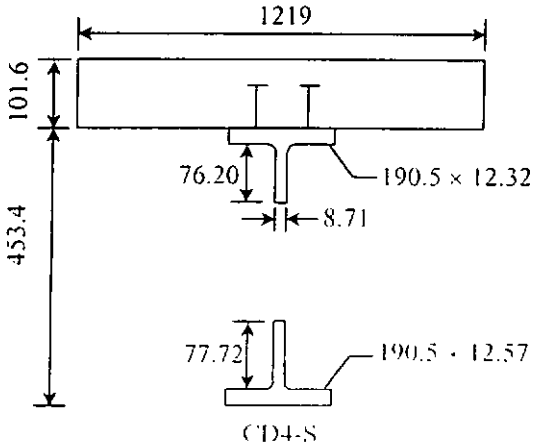

Beam CD5

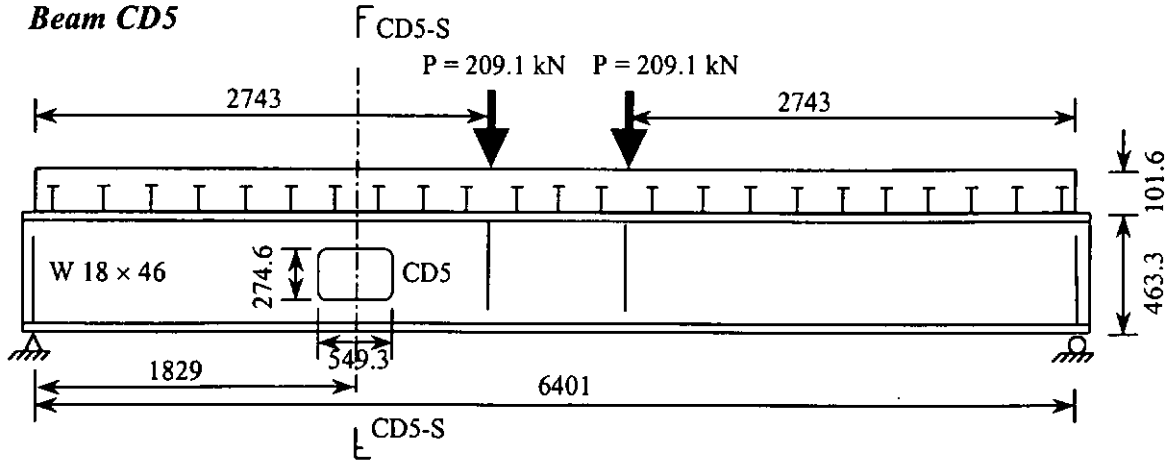

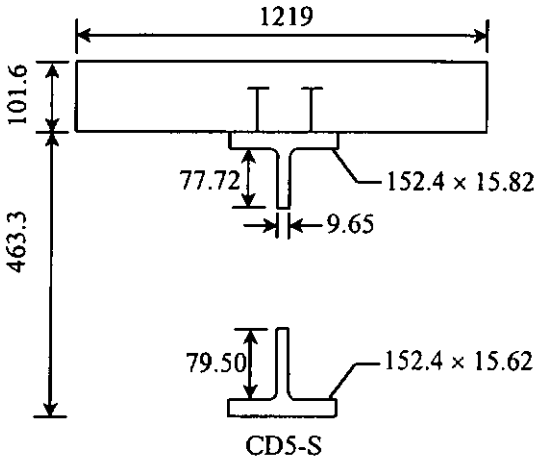

Beam CD6

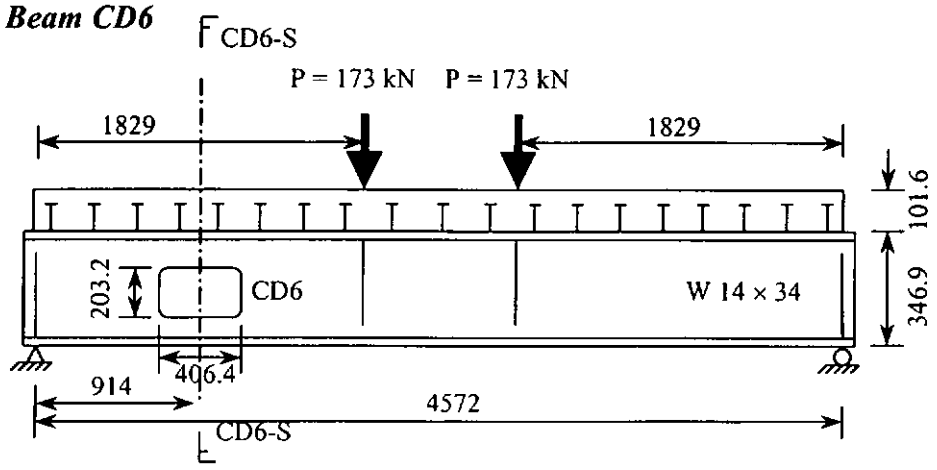

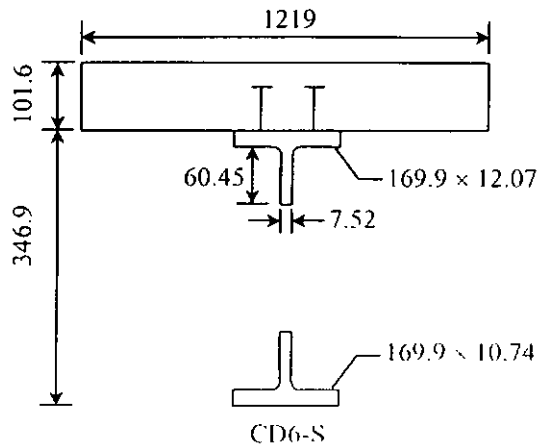

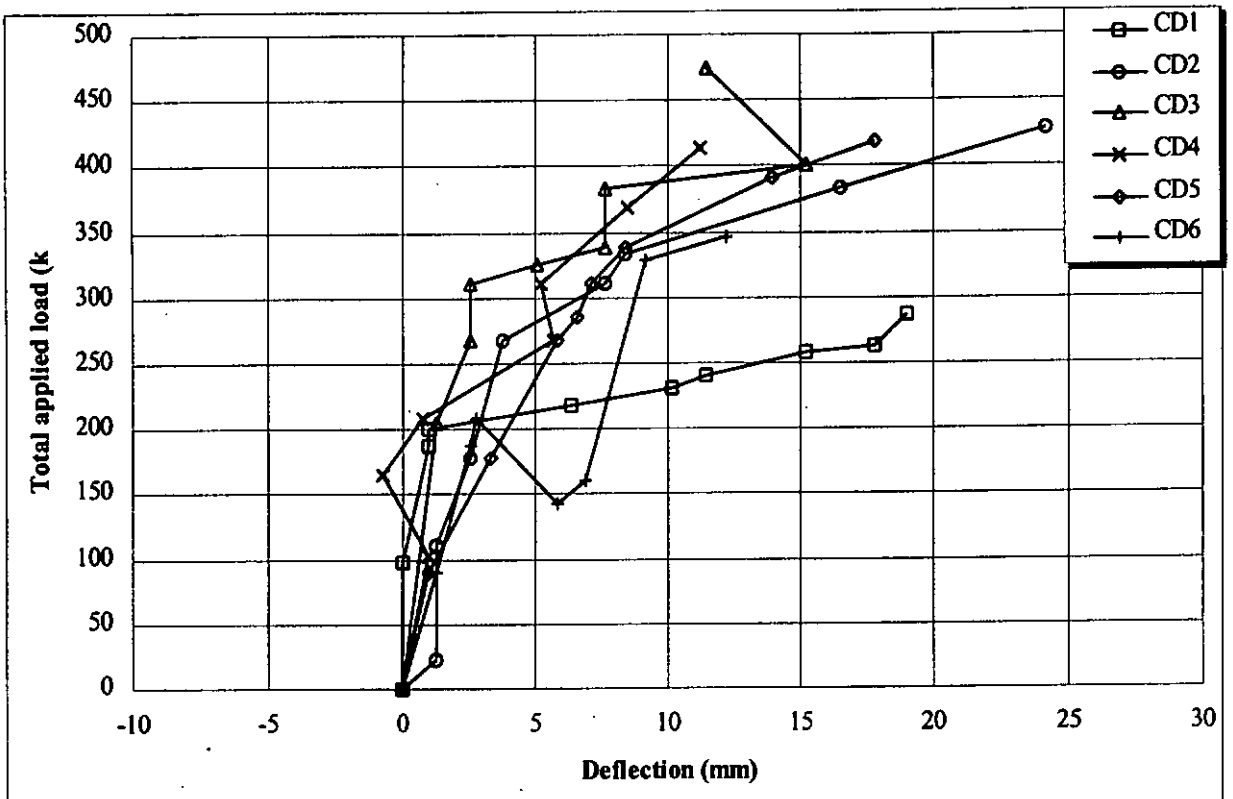

Figure A.2.2a Applied load v.s. relative deflections between opposite ends of openings for test series Clawson & Darwin (1980)

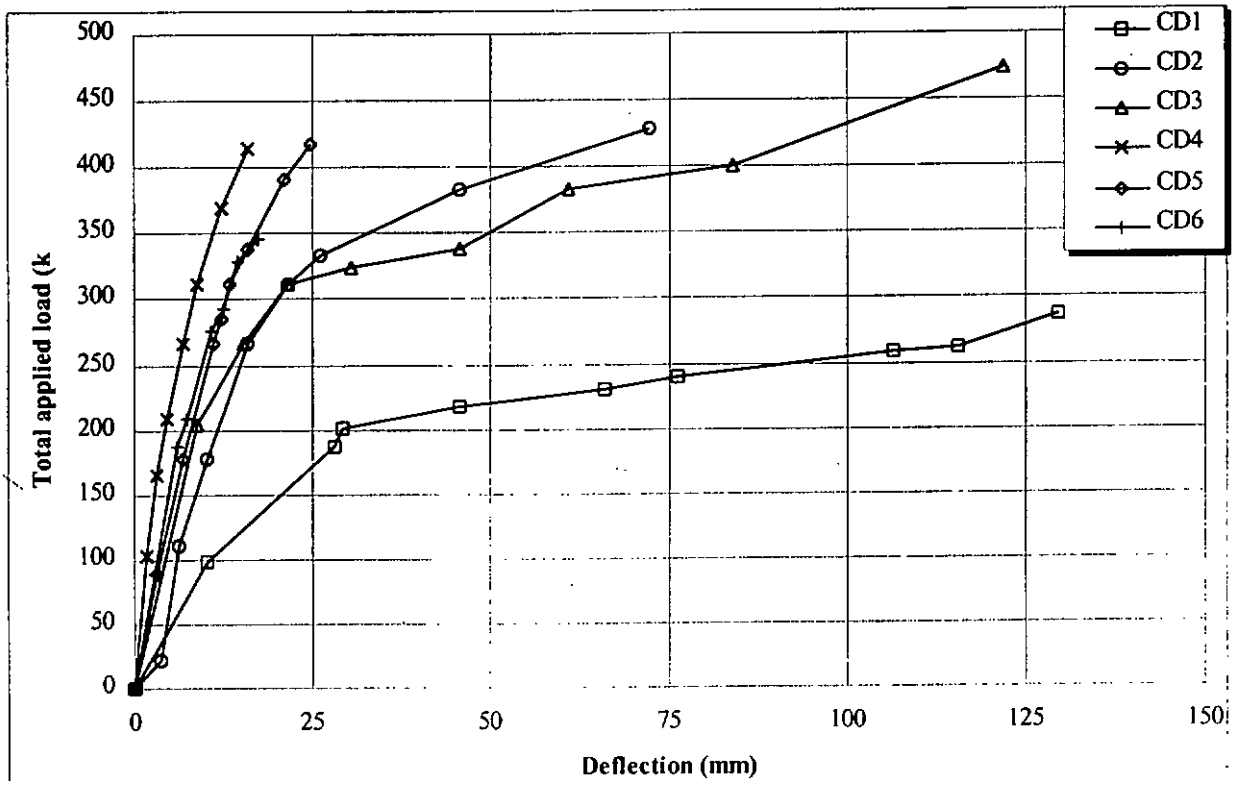

Figure A.2.2b Applied load v.s. mid-span deflections for test series Clawson & Darwin (1980)

A.2.3 Donahey and Darwin (1986)

1 General

1.1	Number of beams (tests):	9(15) (one test with cantilever)
1.2	Beam spans:	3.6-6.7 m
1.3	Steel beam sizes:	8-W21x44, 1-W10x15
1.4	Steel beam grade:	264 – 357 N/mm^2
1.5	Steel beam depth:	257-524 mm
1.6	Profiled steel decking:	12-transverse to steel beams, 3-longitudinal to steel beams
1.7	Span/depth ratio:	7.3-10.3

2 Opening Configurations

2.1	Shapes of web openings:	15-rectangular
2.2	Number of eccentric openings:	1-downwards
2.3	Number of reinforced openings:	0
2.4	Length/height of openings:	1.0-2.92
2.5	Height of openings/depth of beam:	0.58-0.71
2.6	Location of opening along beam:	0.16-0.46 span
2.7	M/V ratio at centerline of opening:	0-13.66 m

3 Concrete Slabs

3.1	Type of concrete:	Normal weight
3.2	Slab width:	1219 mm (except D8A, D8B = 1001mm)
3.3	Height of profiled steel decking:	76.2 mm
3.4	Trough spacing:	304.8 mm
3.5	Trough width (mean):	152.4 mm
3.6	Thickness of decking:	0.759 mm
3.7	Ultimate strength of shear connectors:	468 N/mm^2 (except D8A, D8B, D9A, D9B)
3.8	Height of stud shear connectors:	114.3 mm (except D8A, D8B, D9A, D9B)
3.9	Diameter of stud shear connectors:	19 mm (except D8A, D8B = 15.875 mm)
3.10	Welded position of shear connectors:	15 favorable
3.11	Others:	

			Measured yield strength (N/mm^2)			Concrete slab		Shear connector	
Tests	Failure loads, P (kN)	Modes of failure	Top flange	Bottom flange	Web	Cylinder strength (N/mm^2)	Height over decking (mm)	Ultimate strength (N/mm^2)	Height (mm)
DD1	207.3 + 207.3	Vierendeel	348.9	349.6	357.1	30.82	50.8	468	114.3
DD2	217.5 + 217.5	Vierendeel	339.2	336.5	349.6	33.44	50.8	468	114.3
DD3	322.7 + 322.7	Flexure	348.9	342.0	347.5	37.23	50.8	468	114.3
DD4A	282.0	Vierendeel	344.7	346.1	349.6	32.68	50.8	468	114.3
DD4B	338.5	Vierendeel	344.7	346.1	349.6	36.40	50.8	468	114.3
DD5A	299.4	Vierendeel	347.5	341.3	344.7	32.68	50.8	468	114.3
DD5B	278.5	Vierendeel	347.5	341.3	344.7	35.09	50.8	468	114.3
DD6A	304.0 + 304.0	Vierendeel	350.3	342.7	346.1	27.72	50.8	468	114.3
DD6B	329.6	Vierendeel	350.3	342.7	346.1	29.65	50.8	468	114.3
DD7A	167.0 + 167.0	Vierendeel	264.8	265.4	267.5	28.89	50.8	468	114.3
DD7B	203.3 + 203.3	Vierendeel	264.8	265.4	267.5	29.65	50.8	468	114.3
DD8A	141.9	Vierendeel	310.3	311.0	328.9	27.17	63.5	436	127.0
DD8B	102.8	Vierendeel	310.3	311.0	328.9	34.40	63.5	436	127.0
DD9A	290.5	Vierendeel	265.4	264.8	267.5	28.75	101.6	474	139.7
DD9B	403.0	Vierendeel	265.4	264.8	267.5	30.06	101.6	474	139.7

Beam DD1

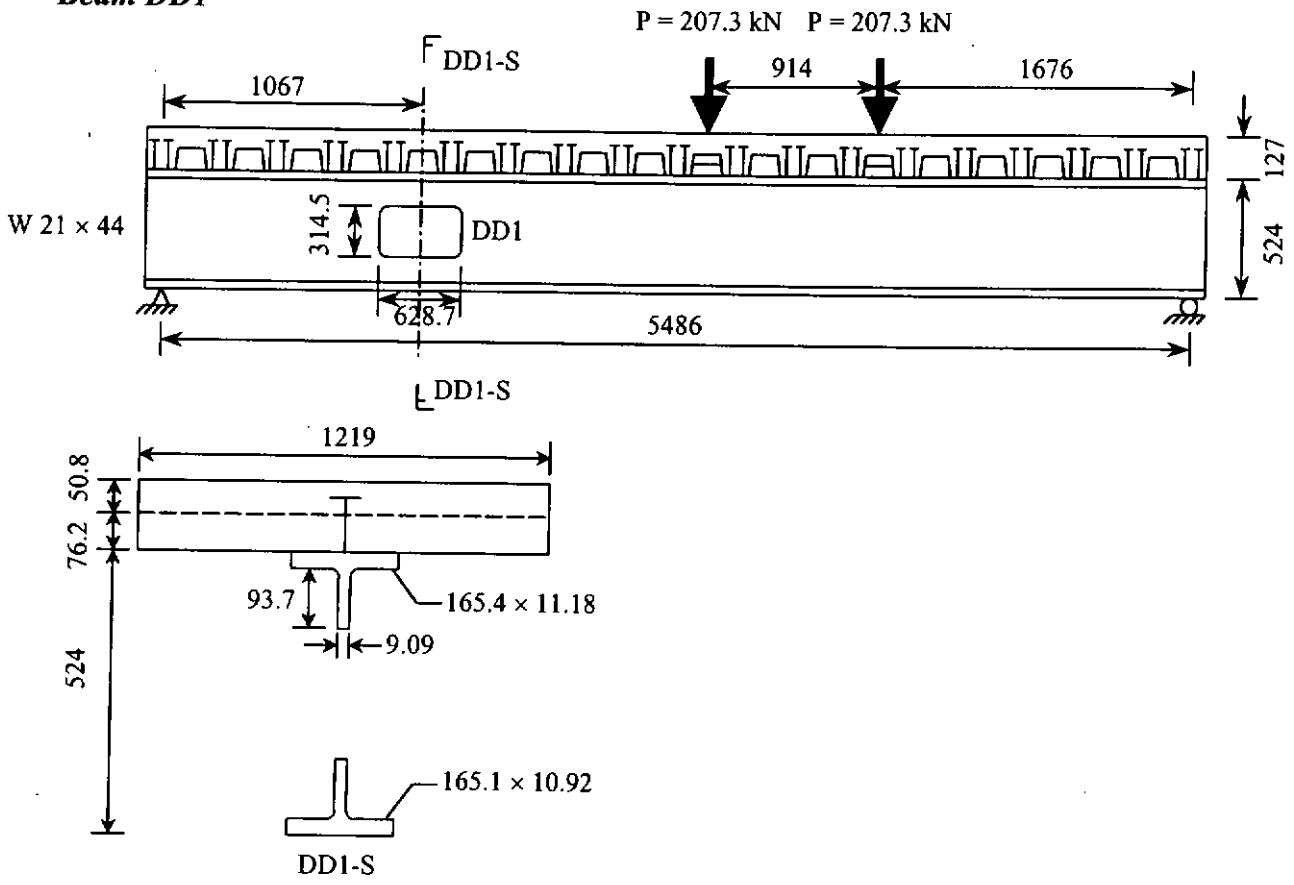

Beam DD2

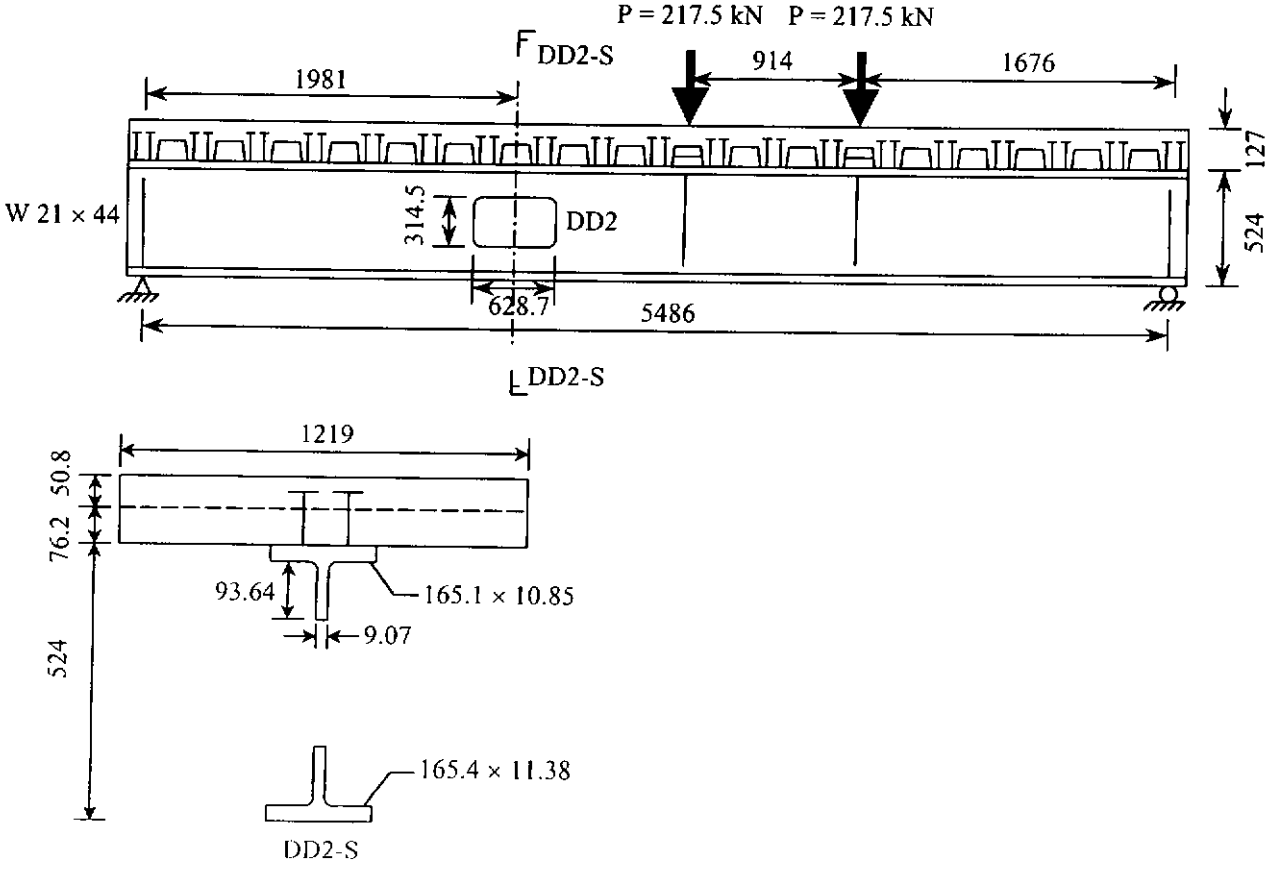

Beam DD3

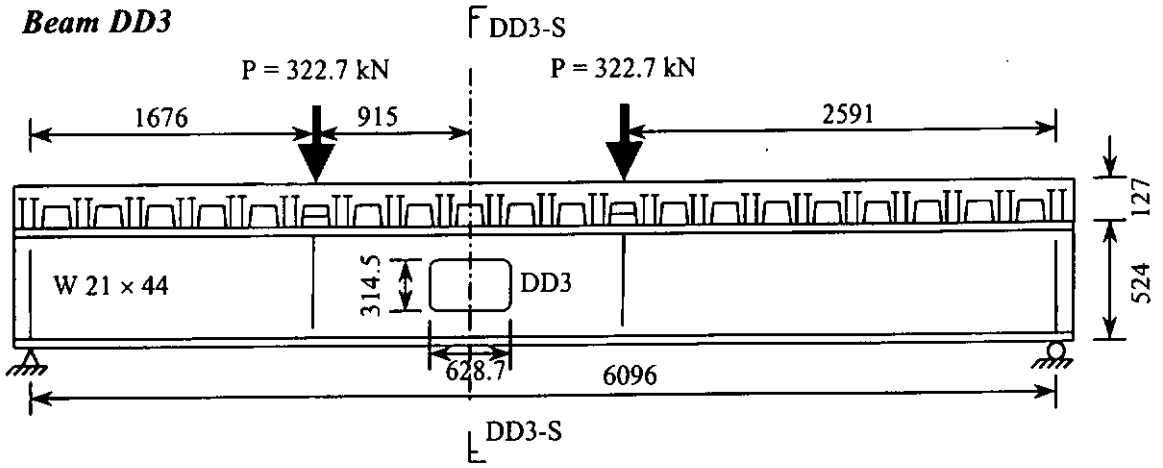

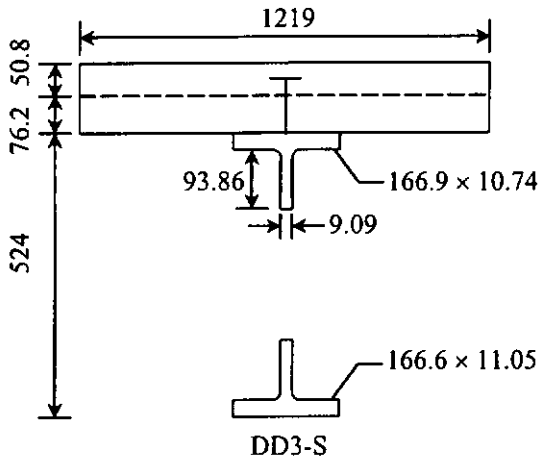

Beam DD4

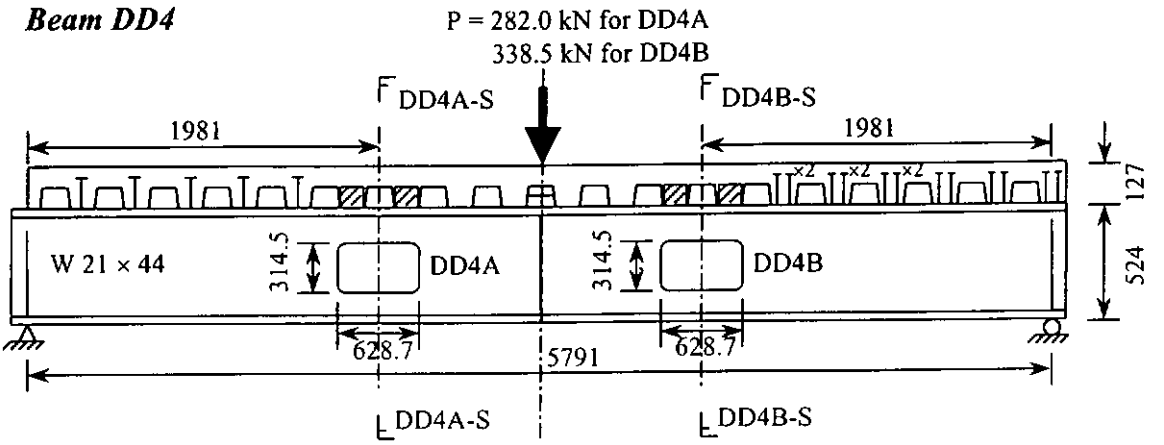

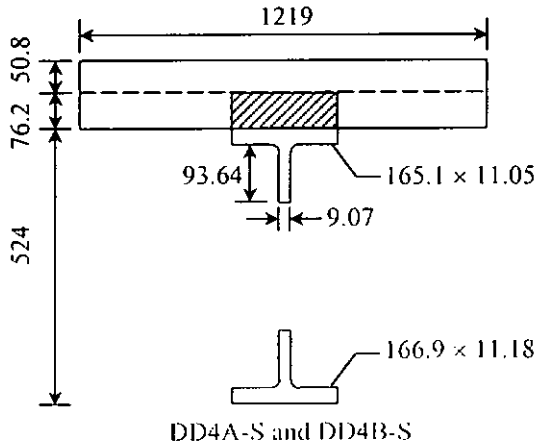

Note: Puddle weld was used over the openings

Beam DD5

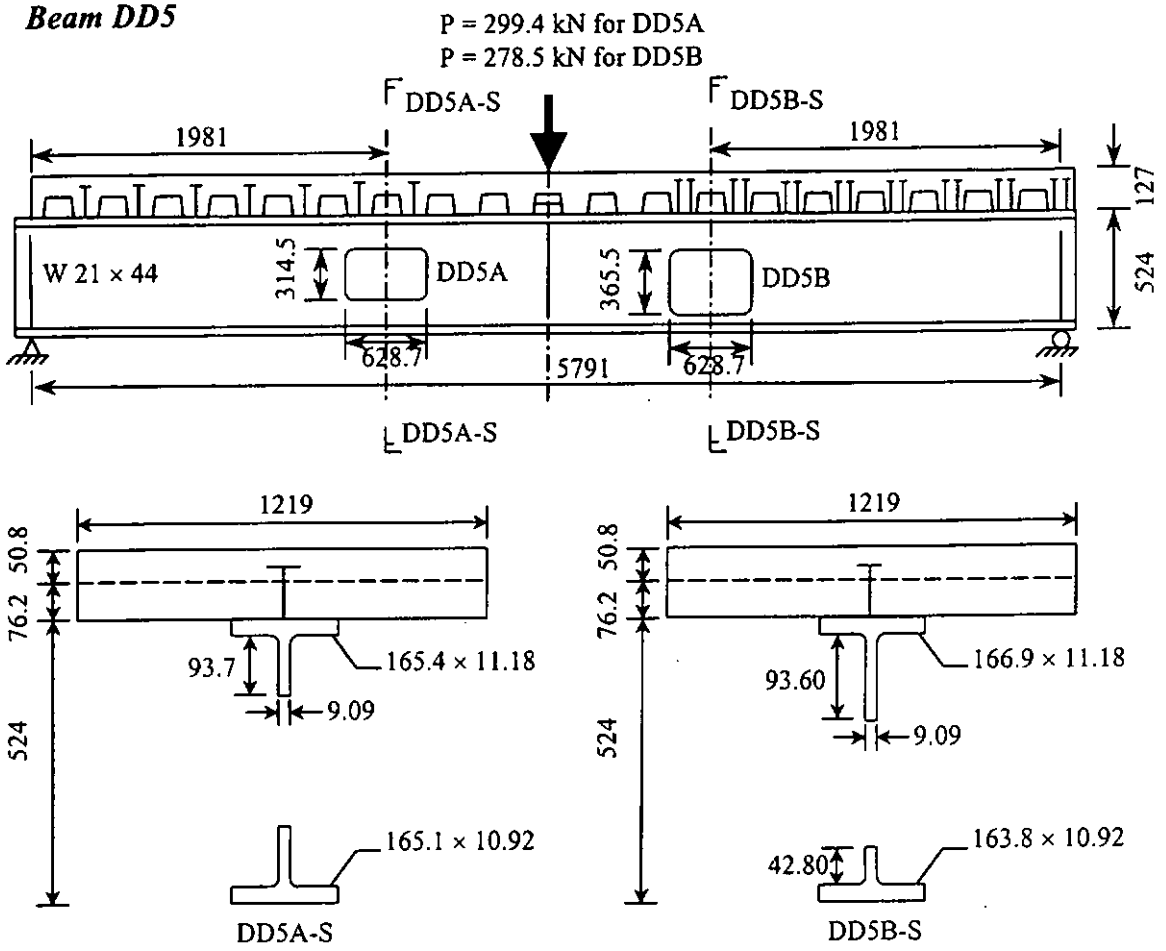
P = 299.4 kN for DD5A
P = 278.5 kN for DD5B
DD5A-S
DD5B-S
1981
1981
127
524
W 21 × 44
314.5
DD5A
365.5
DD5B
628.7
5791
628.7
DD5A-S
DD5B-S
1219
50.8
76.2
524
93.7
165.4 × 11.18
9.09
165.1 × 10.92
DD5A-S
1219
50.8
76.2
524
93.60
166.9 × 11.18
9.09
42.80
163.8 × 10.92
DD5B-S

Beam DD6

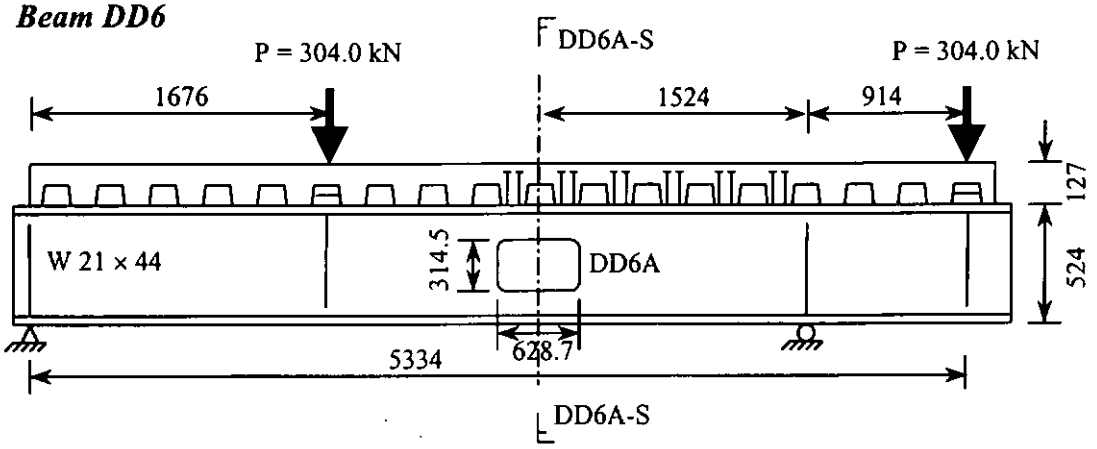

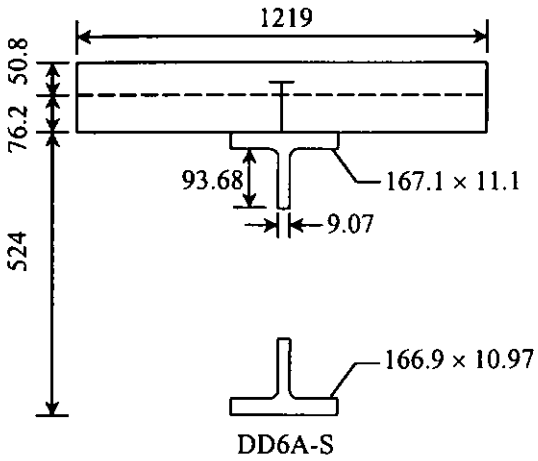

Beam DD6

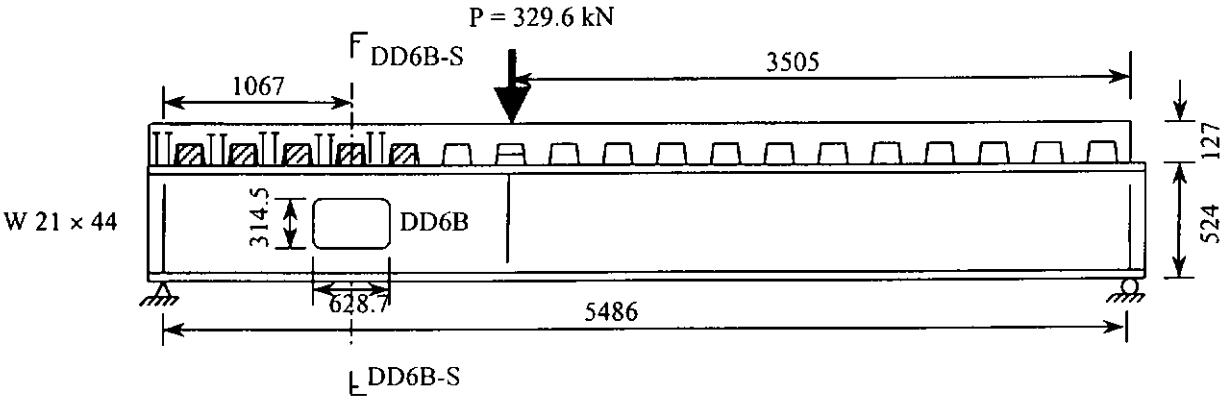

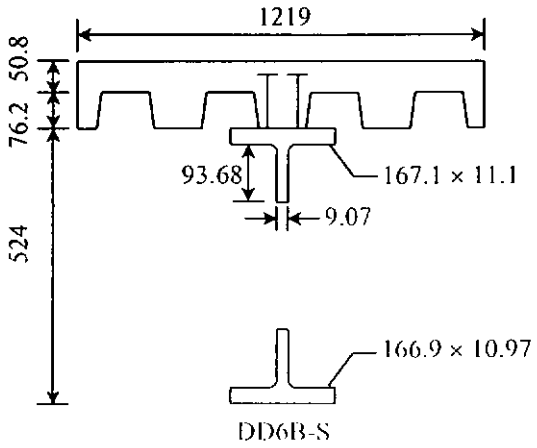

Note: Modified decking is used

Beam DD7

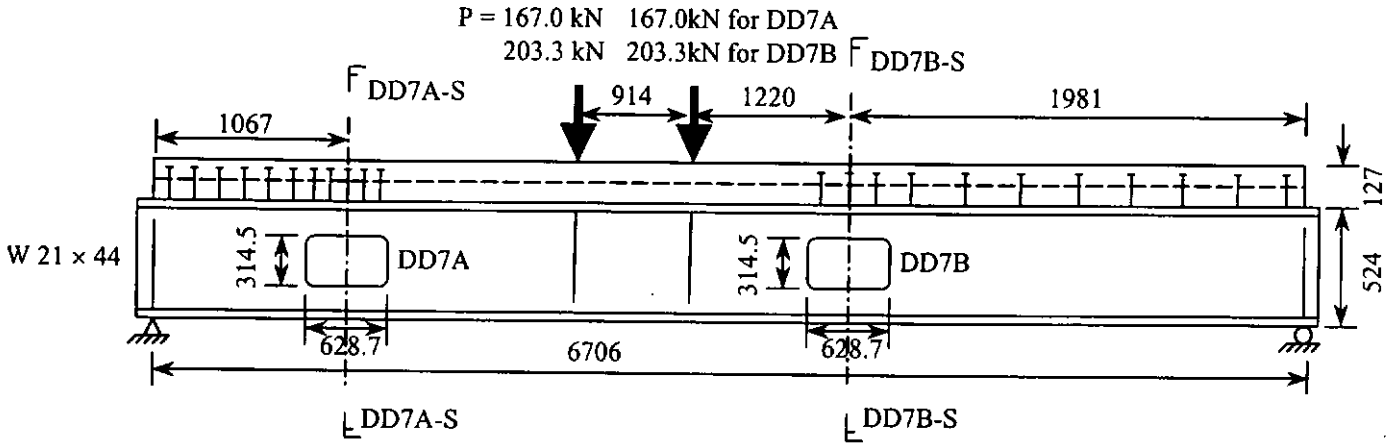

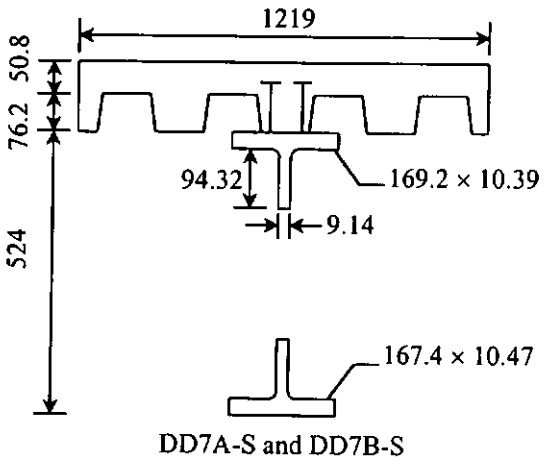

Beam DD8

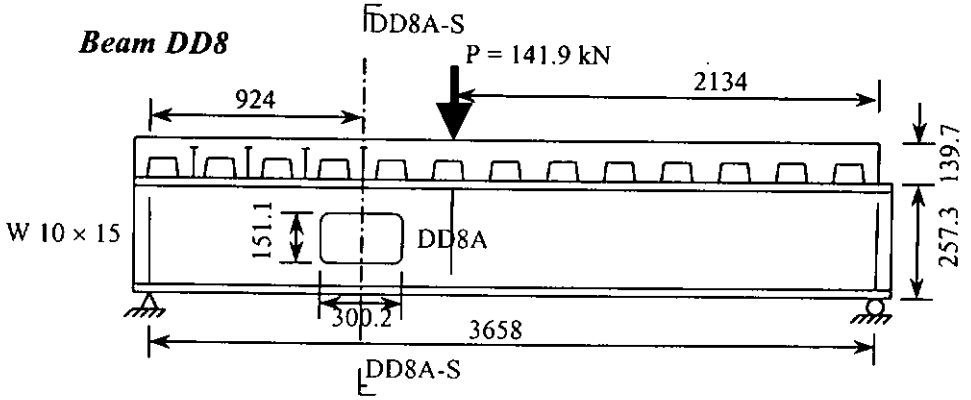

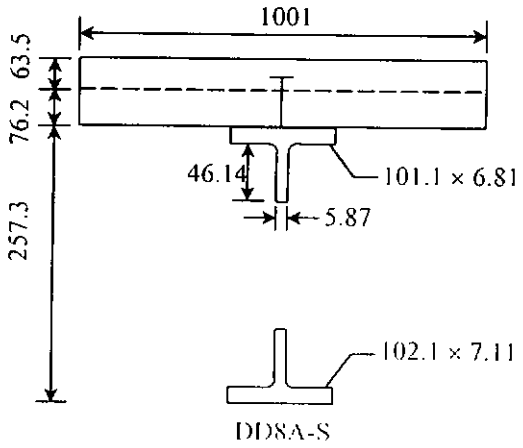

Beam DD8

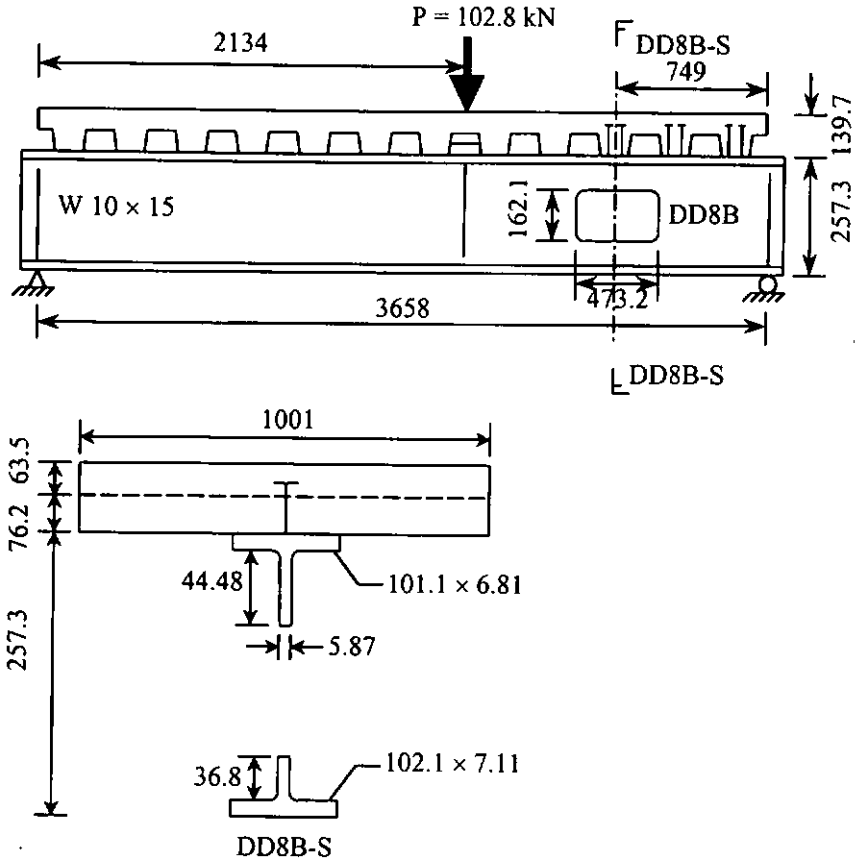

Beam DD9

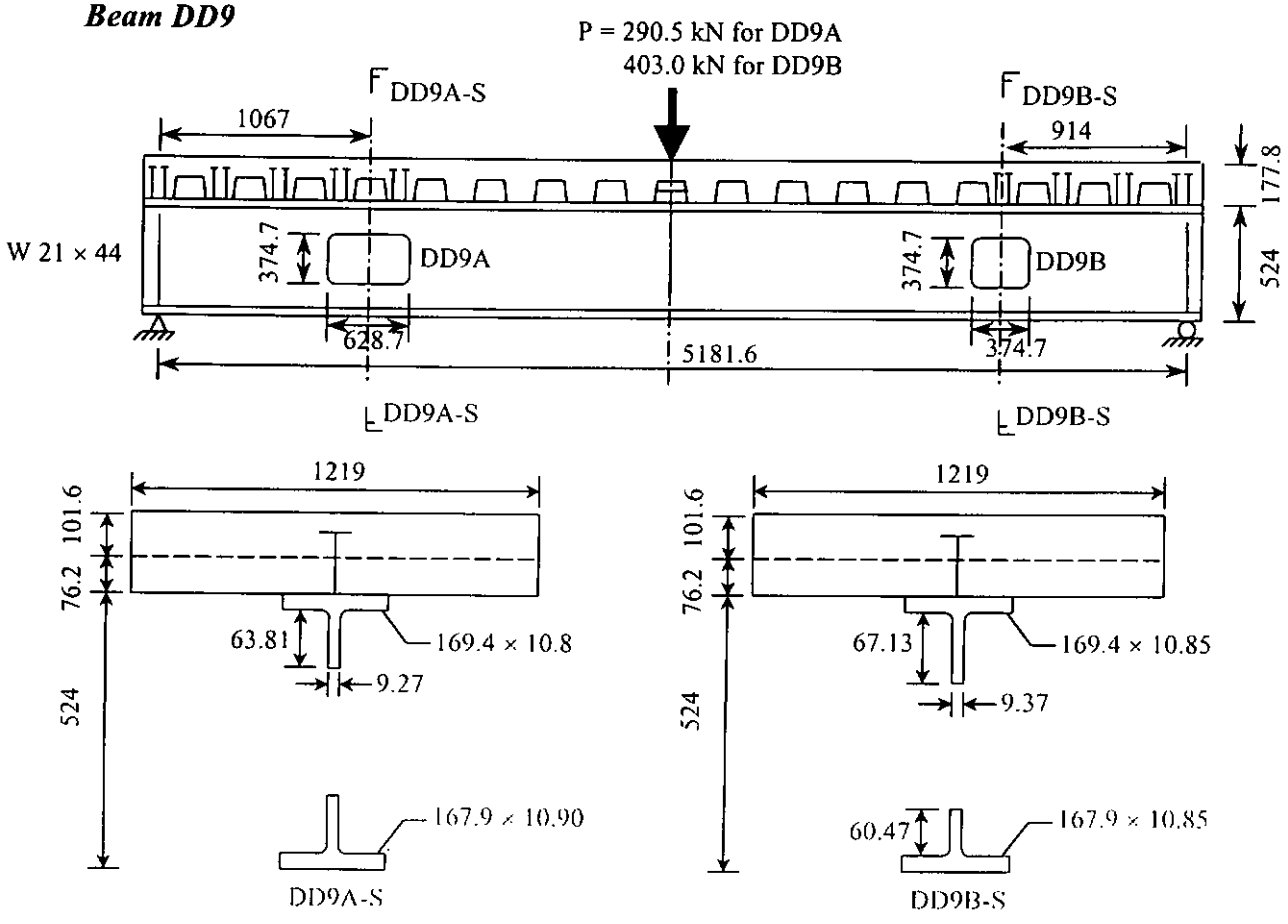

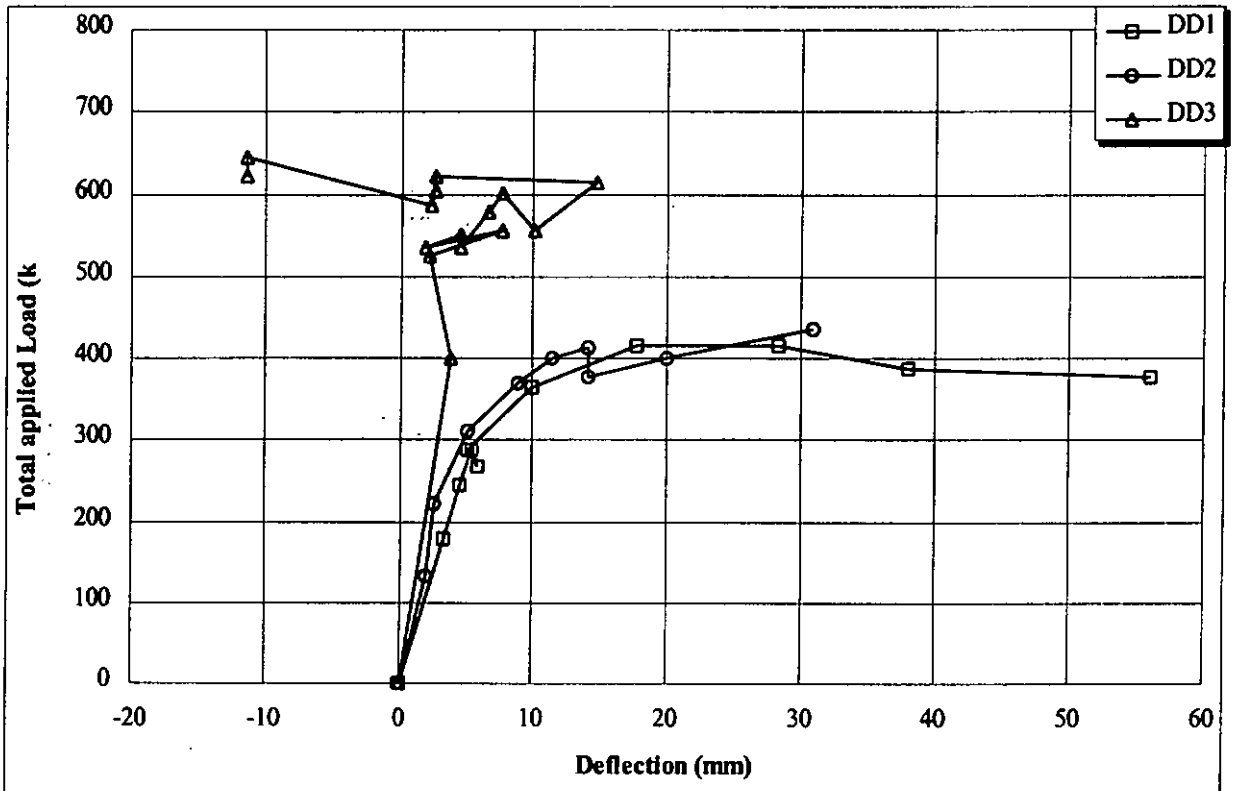

Figure A.2.3a Applied load v.s. relative deflections between opposite ends of openings for test series Donahey & Darwin (1986)

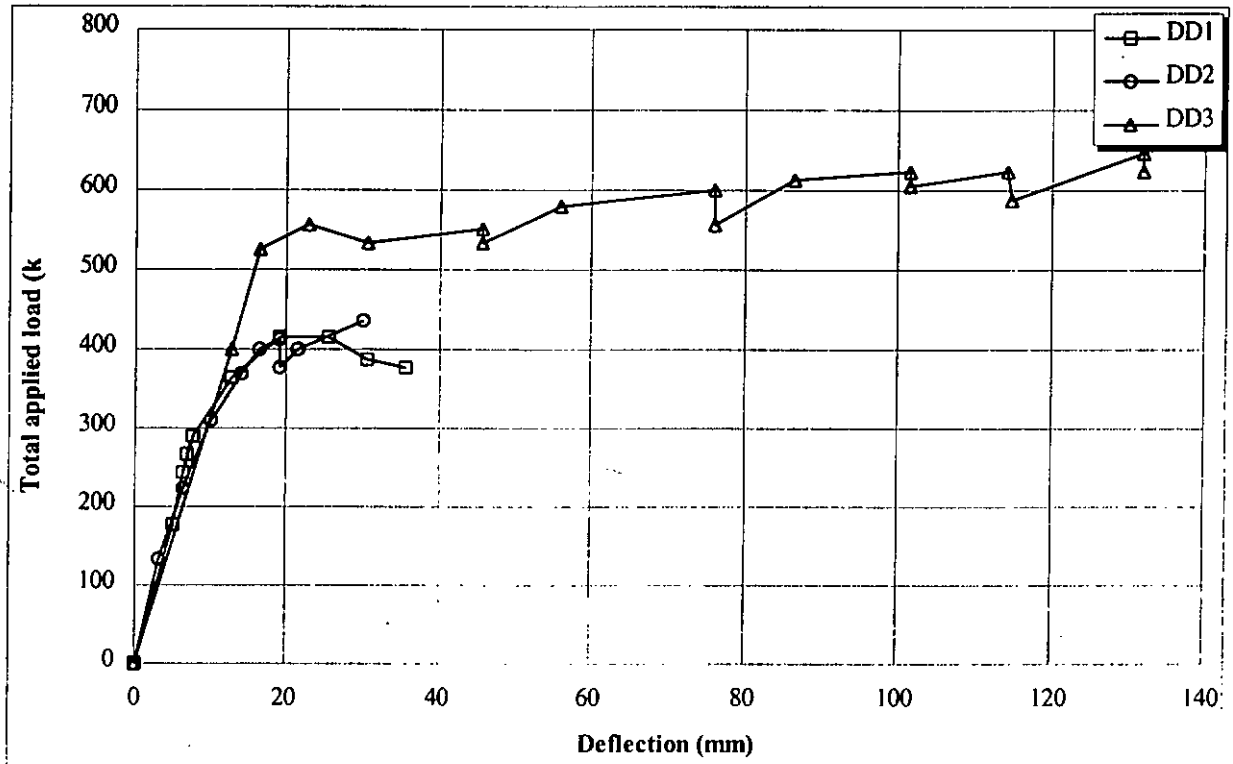

Figure A.2.3b Applied load v.s. deflections at point load near mid-span for test series Donahey & Darwin (1986)

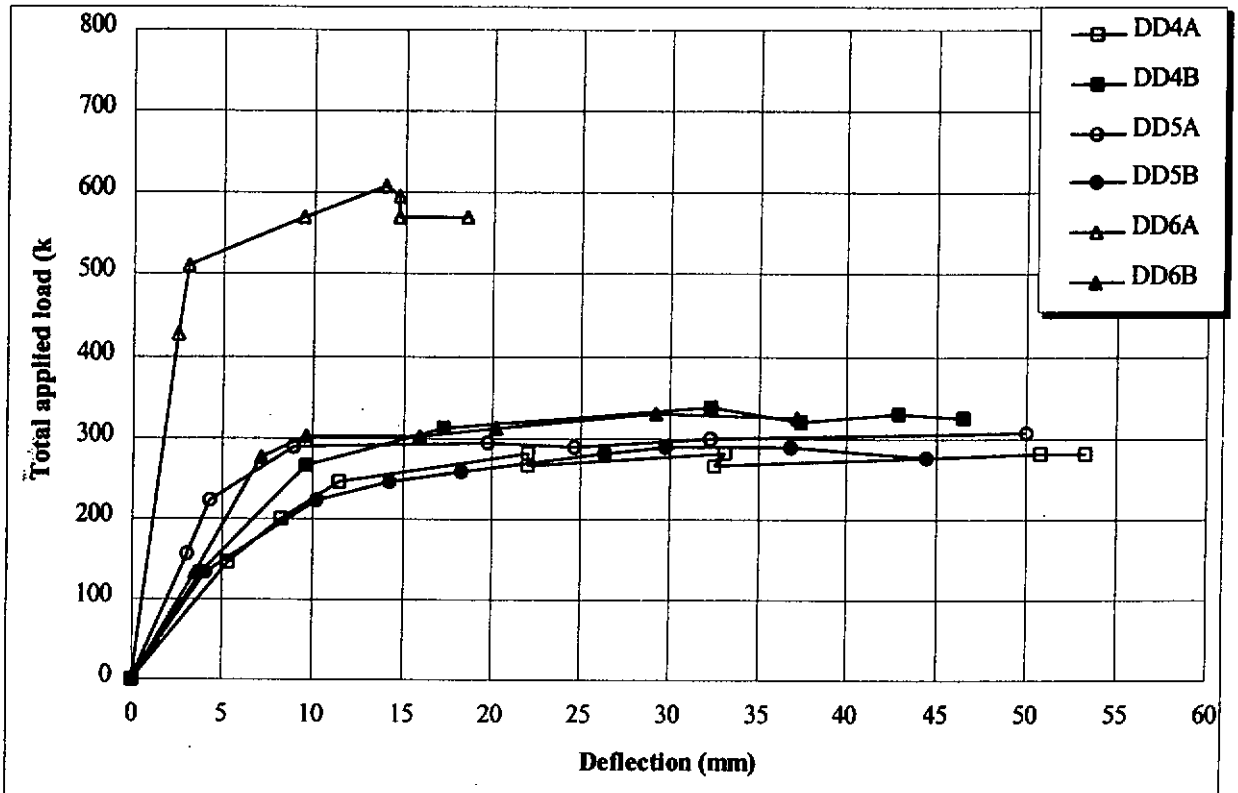

Figure A.2.3c Applied load v.s. relative deflections between opposite ends of openings for test series Donahey & Darwin (1968)

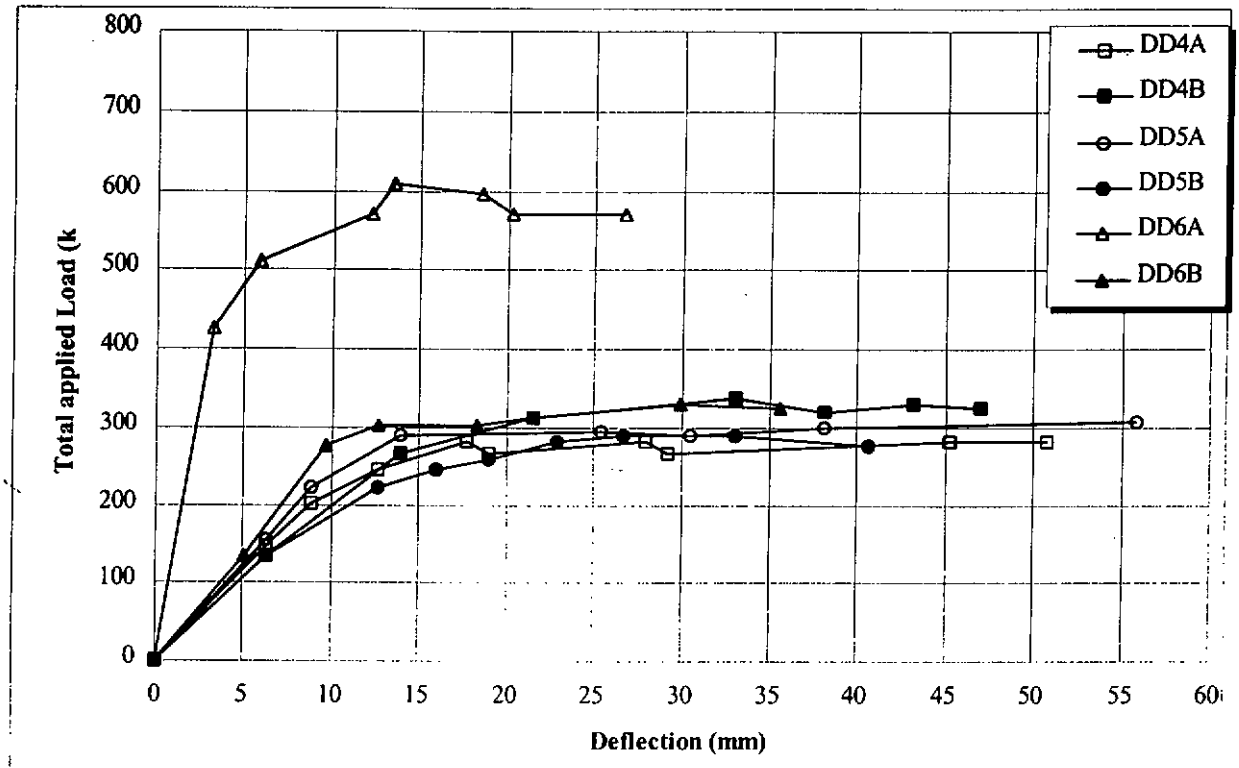

Figure A.2.3d Applied load v.s. deflections at point load near mid-span for test series Donahey & Darwin (1986)

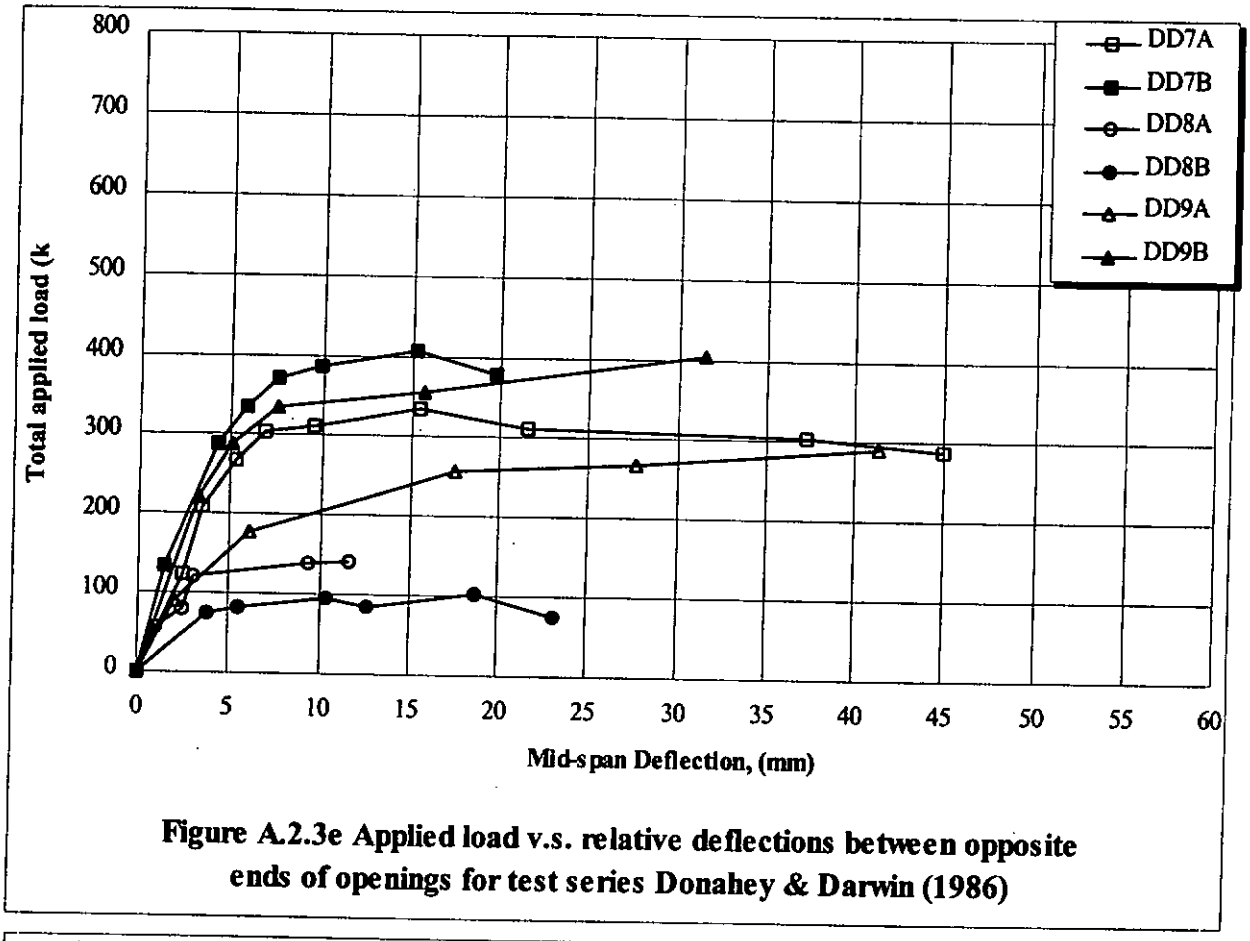

Figure A.2.3e Applied load v.s. relative deflections between opposite ends of openings for test series Donahey & Darwin (1986)

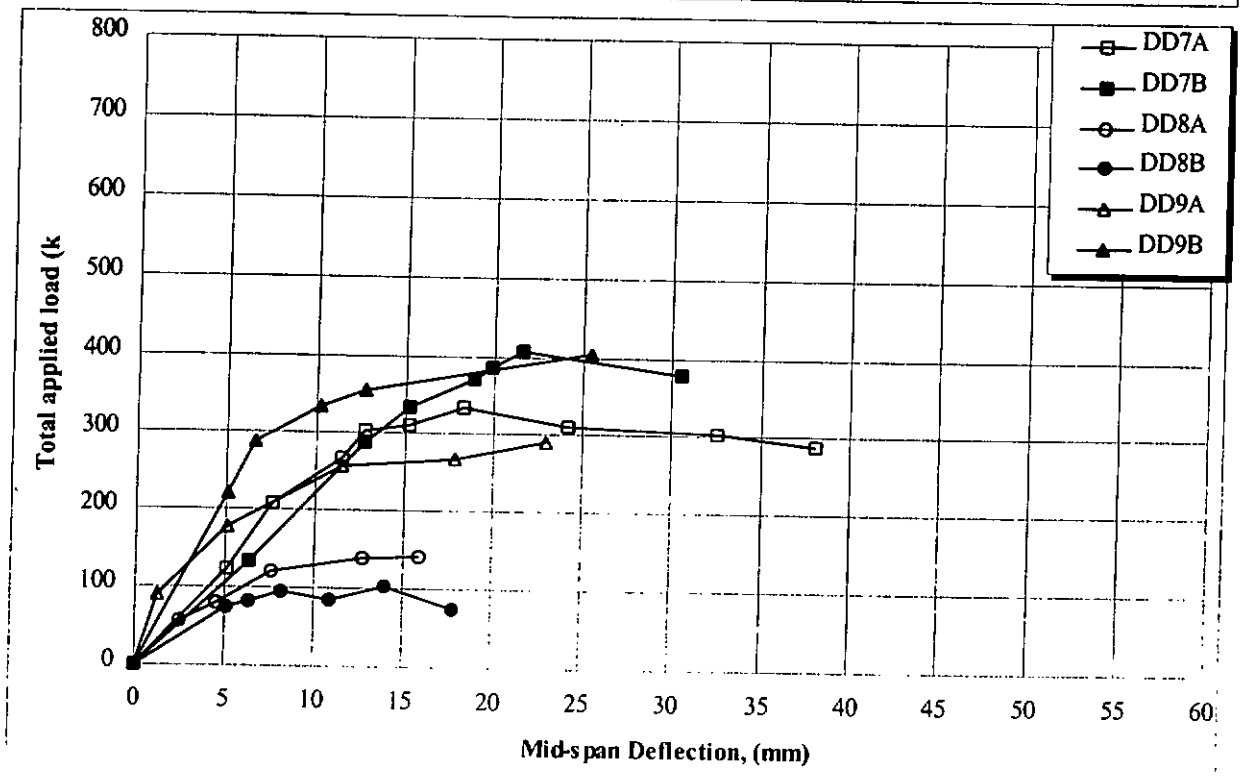

Figure A.2.3f Applied load v.s. deflections at point load near mid-span for test series Donahey & Darwin (1986)

A.2.4 Lawson, Chung, and Price (1992)

1 General

1.1	Number of beams (tests):	3(5)
1.2	Beam spans:	10 m
1.3	Steel beam sizes:	3-UB533x210x82
1.4	Steel beam grade:	309 – 349 N/mm^2
1.5	Steel beam depth:	531-532 mm
1.6	Profiled steel decking:	5-placed transversely to steel beam
1.7	Span/depth ratio:	15.3

2 Opening Configurations

2.1	Shapes of web openings:	5-rectangular
2.2	Number of eccentric openings:	1-downwards
2.3	Number of reinforced openings:	2-one sided
2.4	Length/height of openings:	1.0-3.0
2.5	Height of openings/depth of beam:	0.37-0.65
2.6	Location of opening/span:	0.03-0.29
2.7	M/V ratio at centerline of opening:	0.3-4.1 m

3 Concrete Slabs

3.1	Type of concrete:	Normal weight
3.2	Slab width:	2500 mm
3.3	Concrete height over decking:	60 mm
3.4	Height of profiled steel decking:	60 mm
3.5	Trough spacing:	300 mm
3.6	Trough width (mean):	170 mm
3.7	Thickness of decking:	0.9 mm
3.8	Height of stud shear connectors:	95 mm
3.9	Diameter of stud shear connectors:	19 mm
3.10	Welded position of shear connectors:	all favorable
3.11	Others:	

			Measured yield strength (N/mm^2)				Concrete slab
Tests	Failure loads, P (kN)	Modes of failure	Rein-forcement	Top flange	Bottom flange	Web	Cylinder strength (N/mm^2)
L1N	8x80.6	Vierendeel	315.0	316.0	316.0	338.0	31.88
L1S	8x91.9	Flexure	-	316.0	316.0	338.0	33.94
L2N	8x77.5	Flexure or Vierendeel	-	317.0	317.0	349.0	25.64
L2S	8x89.4	Vierendeel	315.0	317.0	317.0	349.0	25.64
L3N	8x92.0	Vierendeel	-	309.0	309.0	341.0	28.14
L3S	8x92.0	Vierendeel	-	309.0	309.0	341.0	28.14

Beam L1

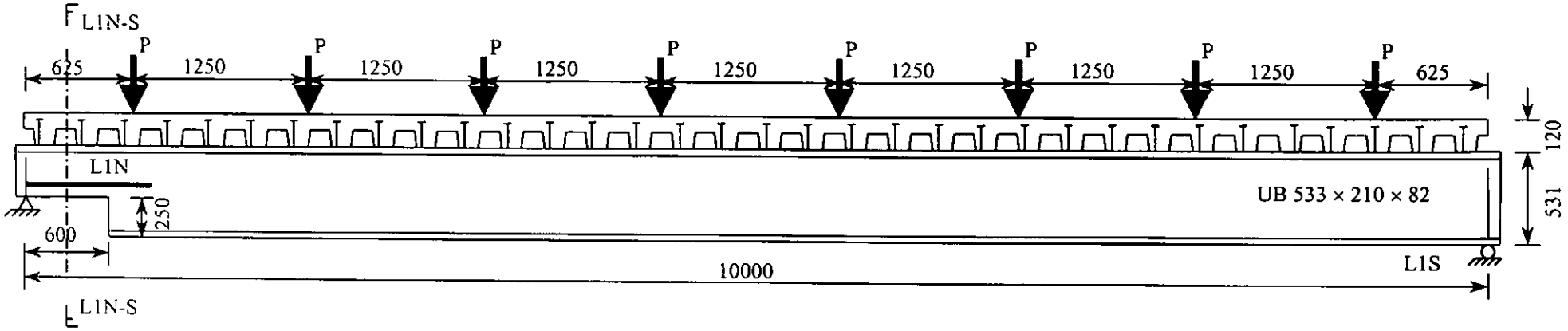

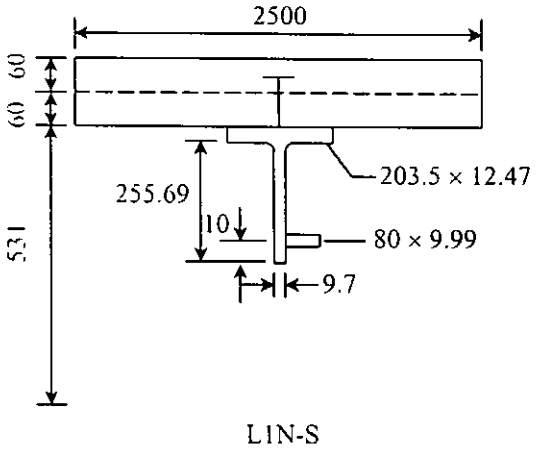

P = 80.6 kN for L1N

= 91.9 kN for L1S

Beam L2

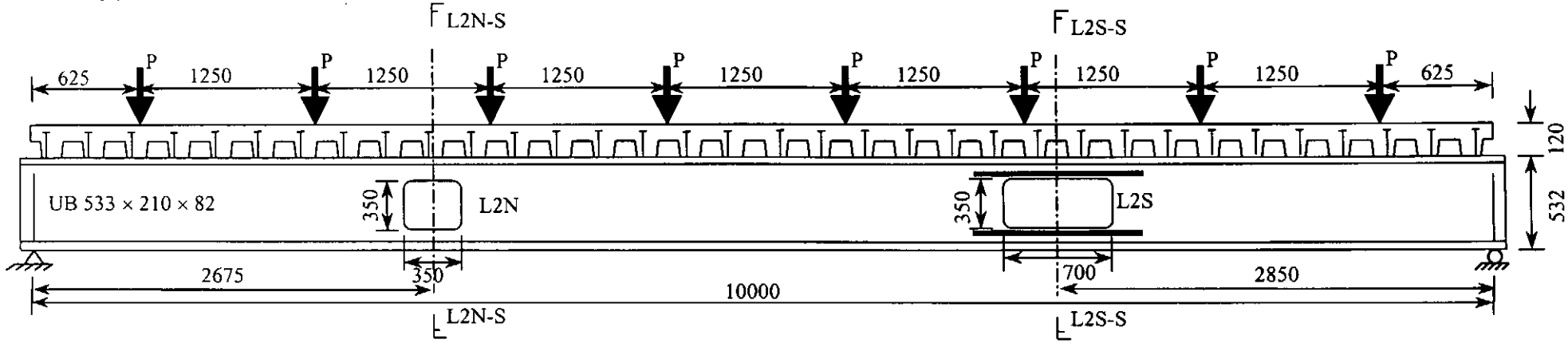

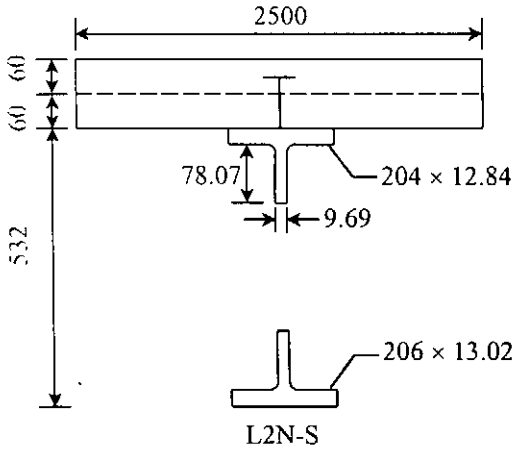

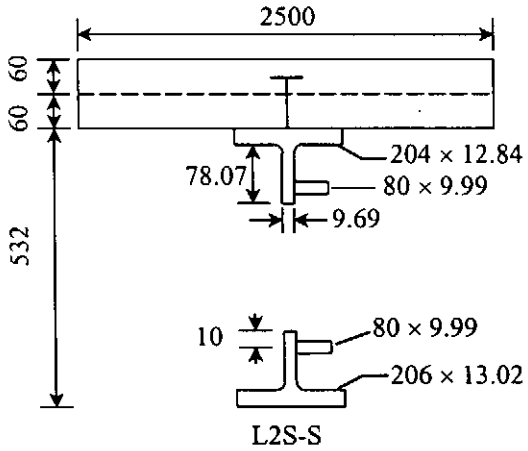

P = 77.5 kN for L2N

= 89.4 kN for L2S

Beam L3

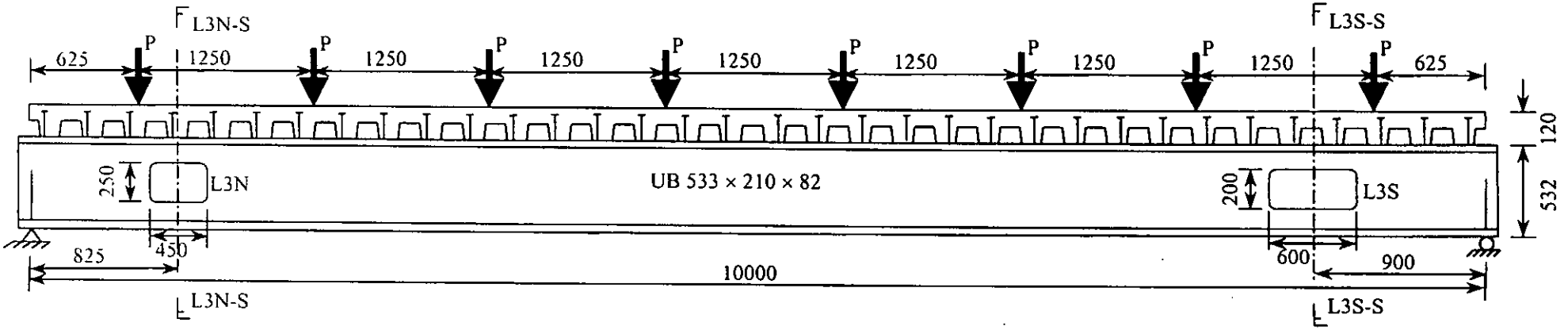

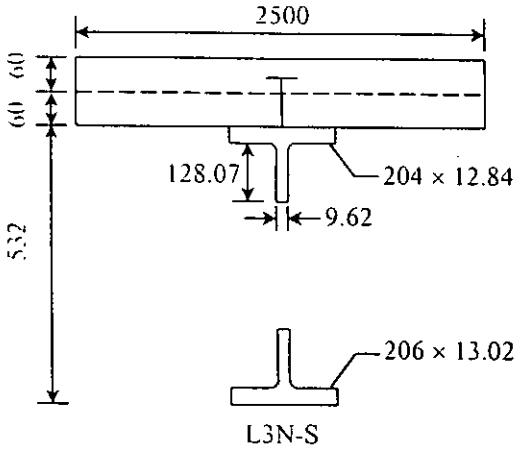

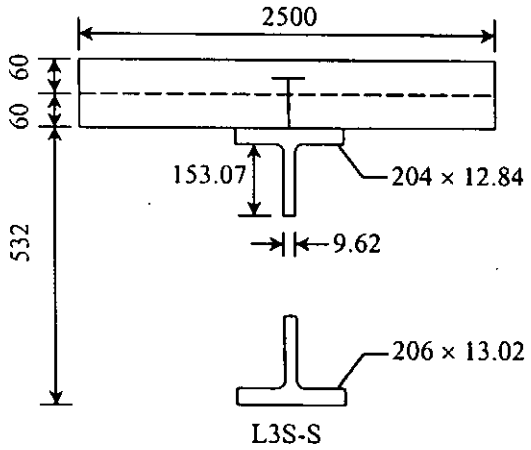

P = 92.0 kN for L3N
= 92.0 kN for L3S

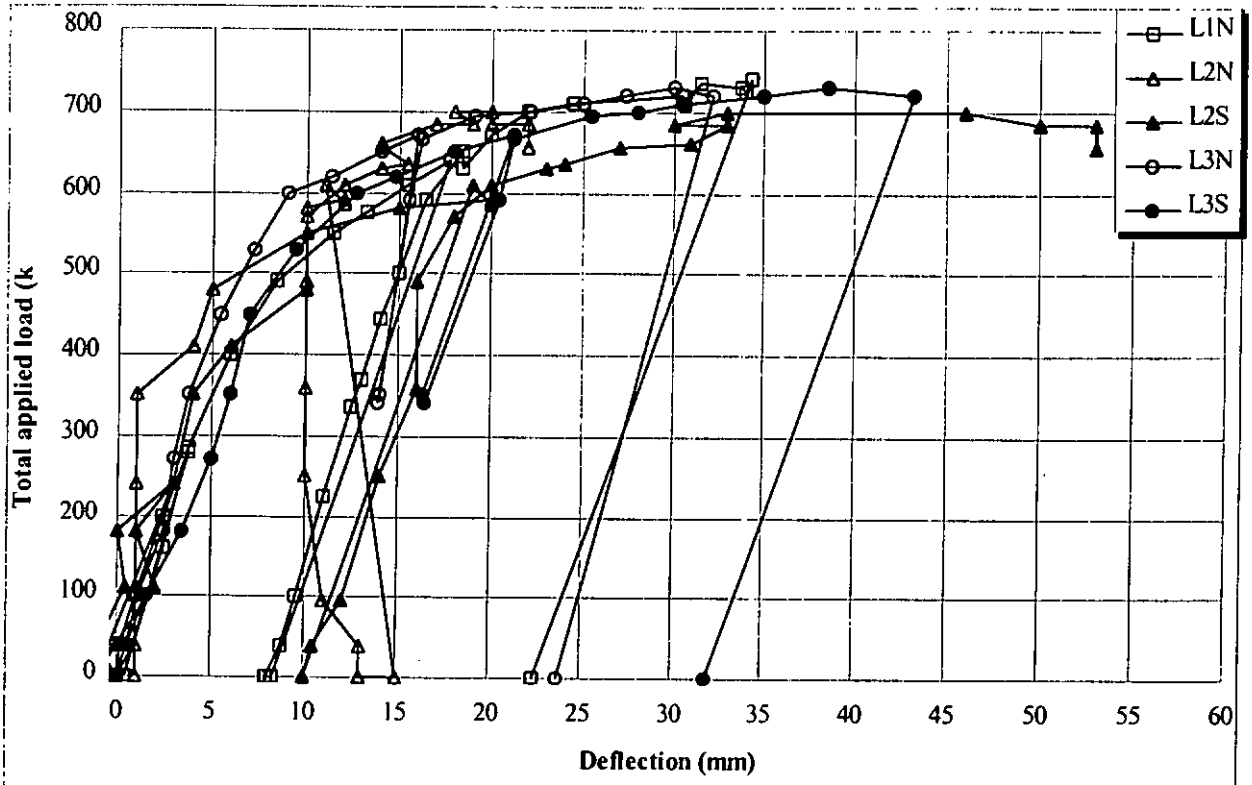

Figure A.2.4a Applied load v.s. relative deflections between opposite ends of openings for test series Lawson, Chung, and Price (1992)

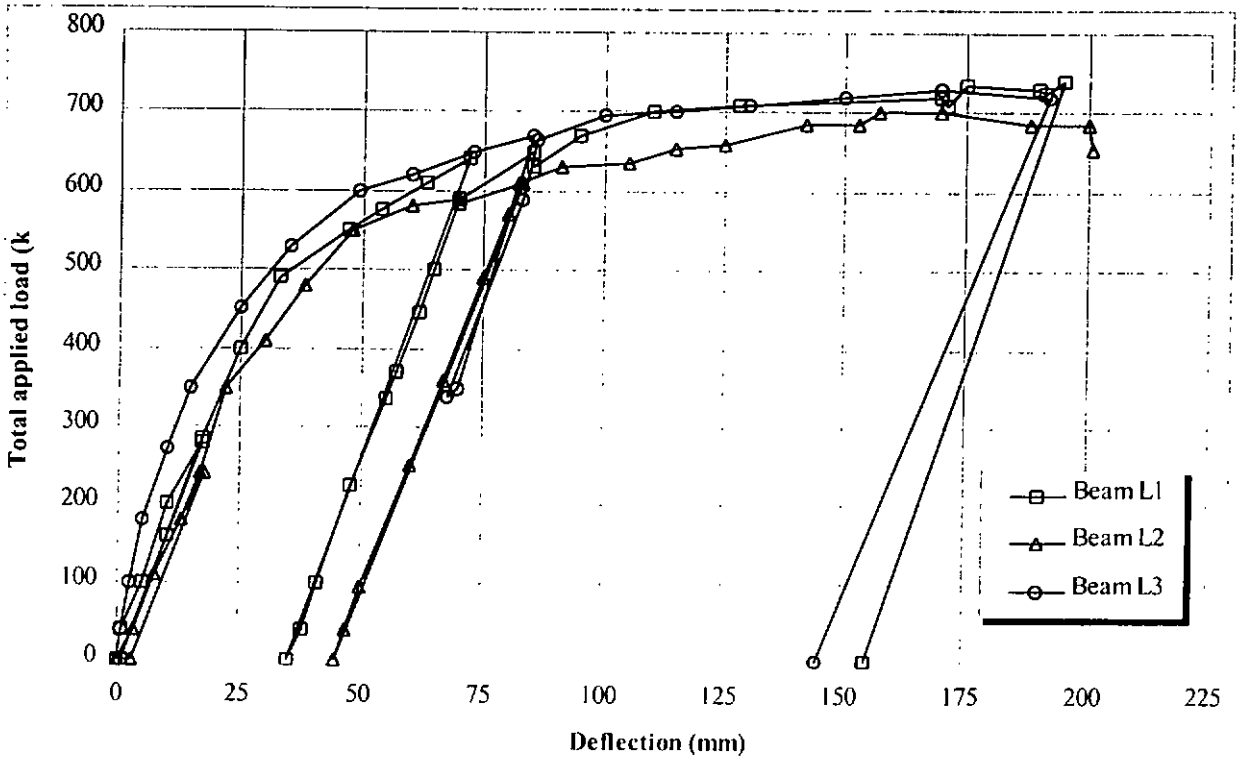

Figure A.2.4b Applied load v.s. mid-span deflections for test series Lawson, Chung, and Price (1992)

A.2.5 Redwood and Poumbouras (1983)

1 General

1.1	Number of beams (tests):	2(3)
1.2	Beam spans:	3.7 m
1.3	Steel beam sizes:	3-W360x51
1.4	Steel beam grade:	301.5 – 325.4 N/mm^2
1.5	Steel beam depth:	355 – 357 mm
1.6	Profiled steel decking:	3-placed transversely to steel beam
1.7	Span/Depth ratio:	7.6

2 Opening Configurations

2.1	Shapes of web openings:	3-rectangular
2.2	Number of eccentric openings:	0
2.3	Number of reinforced openings:	0
2.4	Length/height of openings:	2.0
2.5	Height of openings/depth of beam:	0.59 – 0.6
2.6	Location of opening/span:	0.25
2.7	M/V ratio at centerline of opening:	0.95 m

3 Concrete Slabs

3.1	Type of concrete:	Normal weight
3.2	Concrete height over decking:	65 mm
3.3	Height of profiled steel decking:	76 mm
3.4	Trough spacing:	304.8 mm
3.5	Trough width (mean):	156 mm
3.6	Thickness of decking:	0.914 mm
3.7	Height of stud shear connectors:	114 mm
3.8	Diameter of stud shear connectors:	19 mm
3.9	Weldeó position of shear connectors:	all favorable
3.10	Others:	

			Measured yield strength (N/mm^2)			Concrete slab	
Tests	Failure loads, P (kN)	Modes of failure	Top flange	Bottom flange	Web	Cylinder strength (N/mm^2)	Width (mm)
RP56	189	Vierendeel	301.5	301.5	325.4	18.80	1000.0
RP57	272	Vierendeel	301.5	301.5	325.4	18.80	1000.0
RP68	258	Vierendeel	303.7	303.7	303.2	17.10	1000.0

Beam RP5

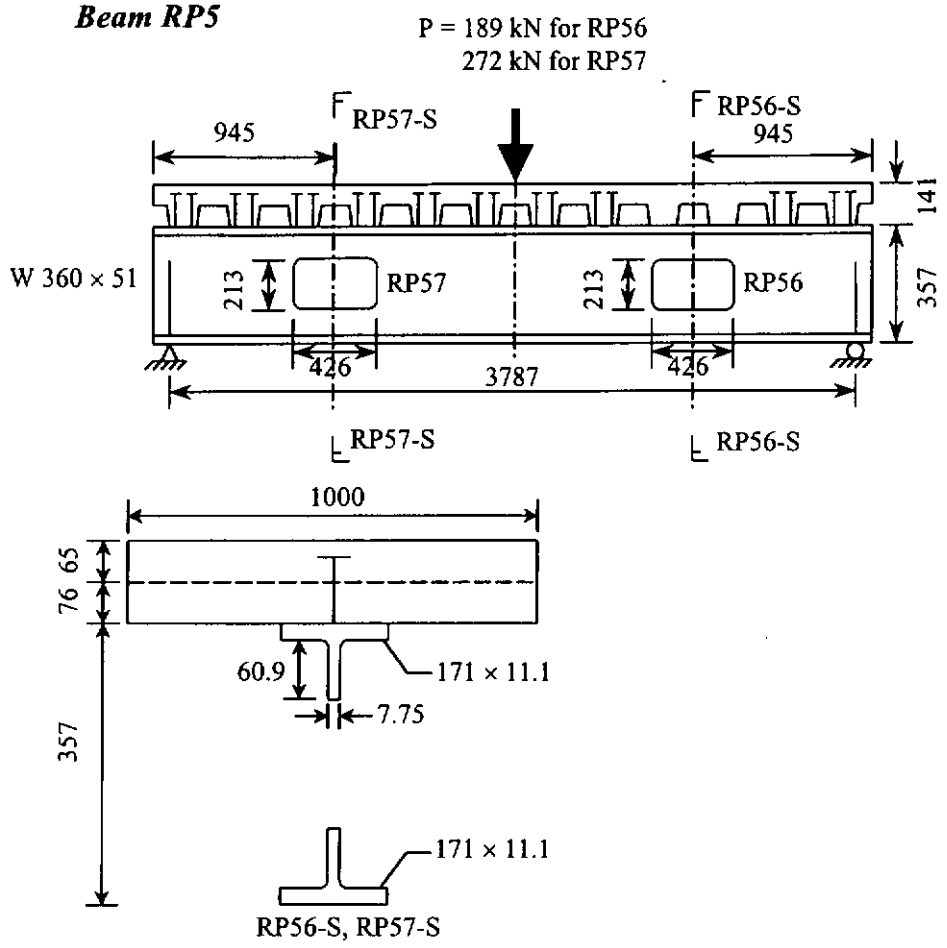

Beam RP6

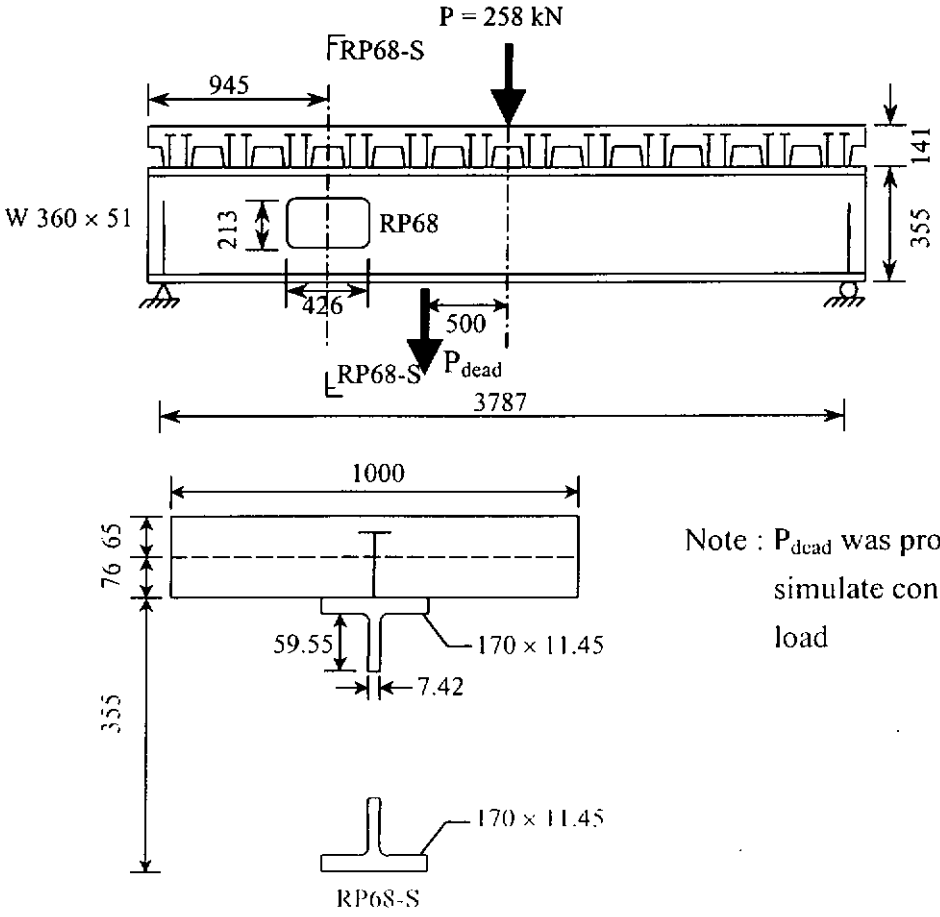

Note : P_{dead} was provided to simulate construction load

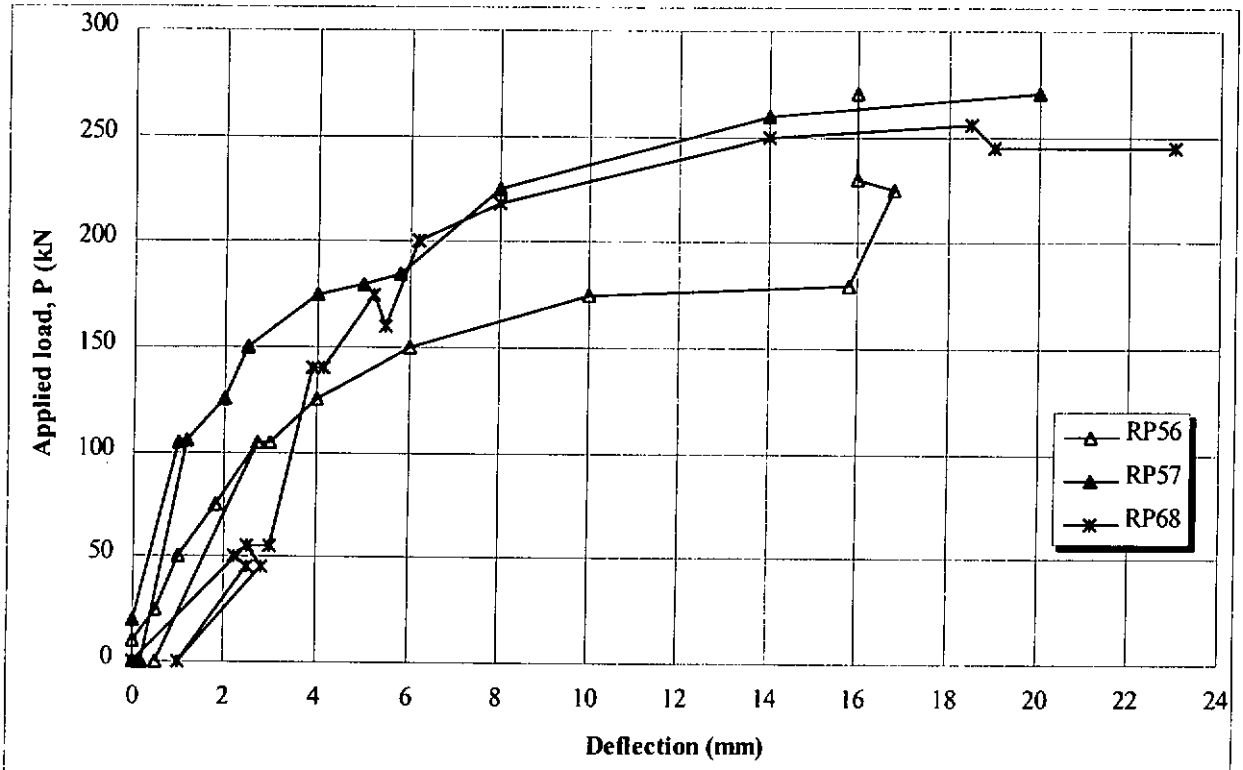

Figure A.2.5a Applied load v.s. relative deflections between opposite ends of opening for test series Redwood & Poumbouras (1983)

A.2.6 Redwood and Wong (1982)

1 General

1.1	Number of beams (tests):	5(6)
1.2	Beam spans:	3.8 - 6.0 m
1.3	Steel beam sizes:	1-W250x22, 4-W360x51
1.4	Steel beam grade:	276 – 386 N/mm^2
1.5	Steel beam depth:	253.6-356.8 mm
1.6	Profiled steel decking:	6-placed transversely to steel beam
1.7	Span/depth ratio:	7.8-12.0

2 Opening Configurations

2.1	Shapes of web openings:	6-rectangular
2.2	Number of eccentric openings:	1-upward
2.3	Number of reinforced openings:	0
2.4	Length/height of openings:	2.0
2.5	Height of openings/depth of beam:	0.59
2.6	Location of opening/span:	0.24-0.50
2.7	M/V ratio at centerline of opening:	0.94-6.0 m

3 Concrete Slabs

3.1	Type of concrete:	Normal weight
3.2	Concrete height over decking:	65 mm
3.3	Height of profiled steel decking:	76 mm
3.4	Trough spacing:	304.8 mm
3.5	Trough width (mean):	156 mm
3.6	Thickness of decking:	0.914 mm
3.7	Height of stud shear connectors:	114 mm
3.8	Diameter of stud shear connectors:	19 mm
3.9	Welded position of shear connectors:	all favorable
3.10	Others:	

			Measured yield strength (N/mm^2)			Concrete slab	
Tests	Failure loads, P (kN)	Modes of failure	Top flange	Bottom flange	Web	Cylinder strength (N/mm^2)	Width (mm)
RW00	162	Vierendeel	348.6	348.6	386.8	26.40	1000.0
RW11	225	Vierendeel	276.6	276.6	311.2	22.00	1200.0
RW22	340	Vierendeel and Flexure	301.7	301.7	326.2	19.50	1200.0
RW33	438 + 146	Flexure	291.3	291.3	325.5	29.60	1200.0
RW44	351 + 117	Flexure	302.4	302.4	331.7	27.30	1200.0
RW15	240	Vierendeel	276.6	276.6	311.2	22.00	1200.0

Beam RW0

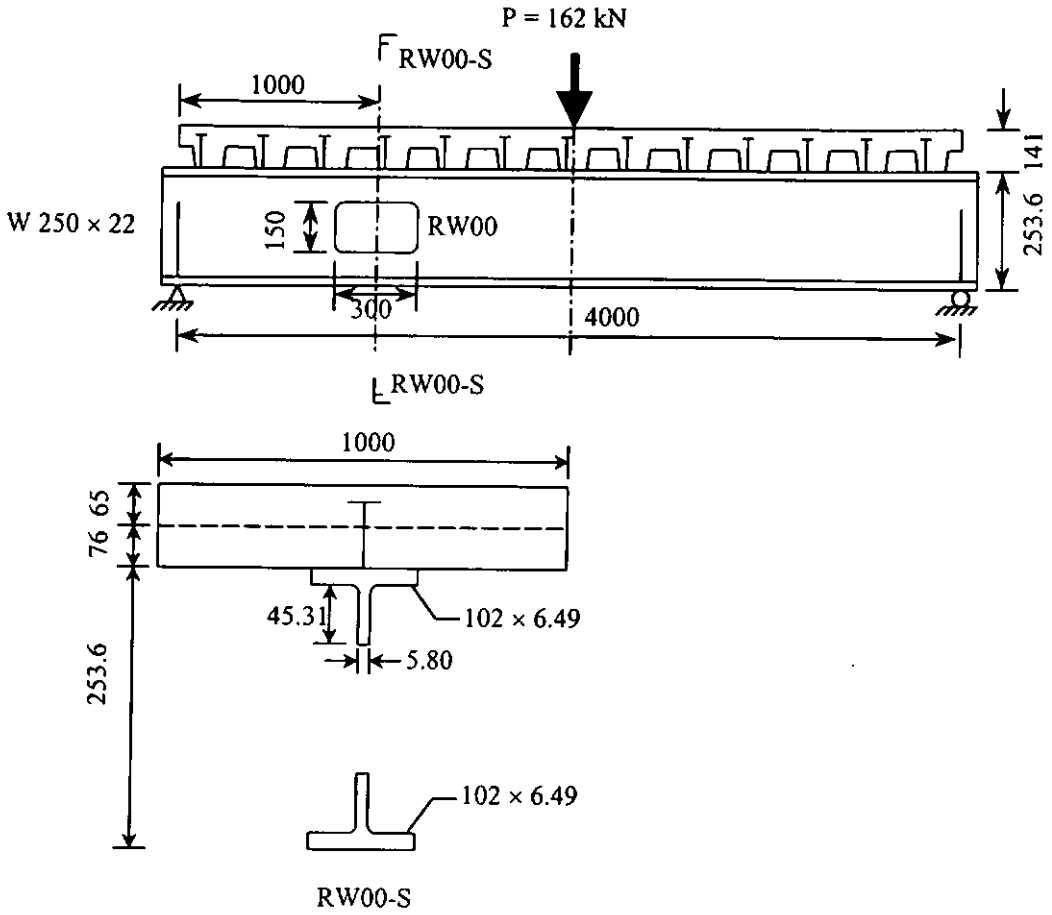

Beam RW1

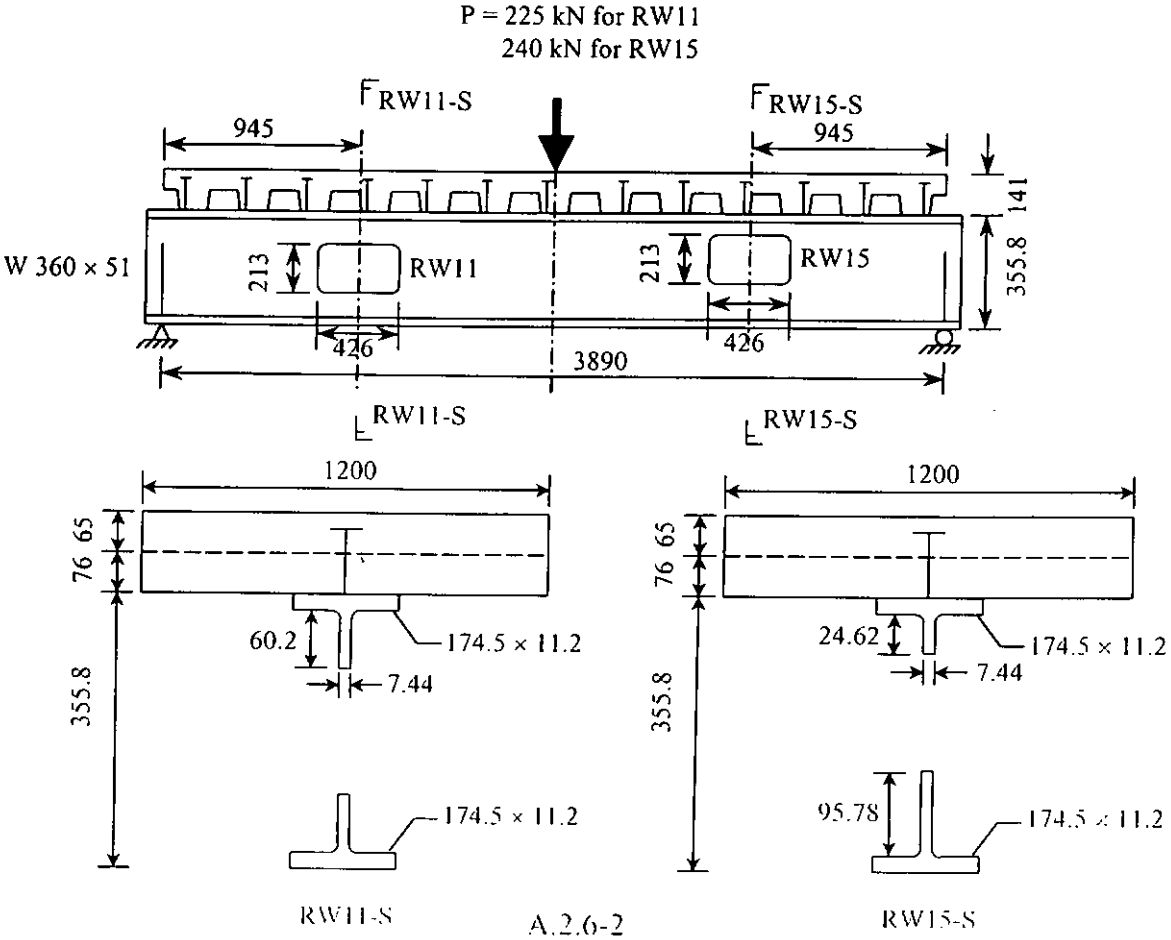

Beam RW2

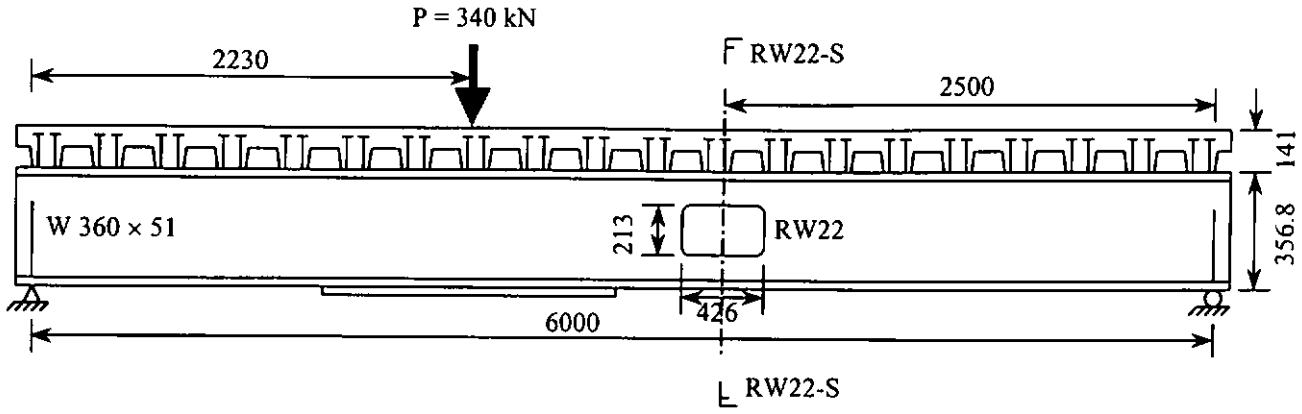

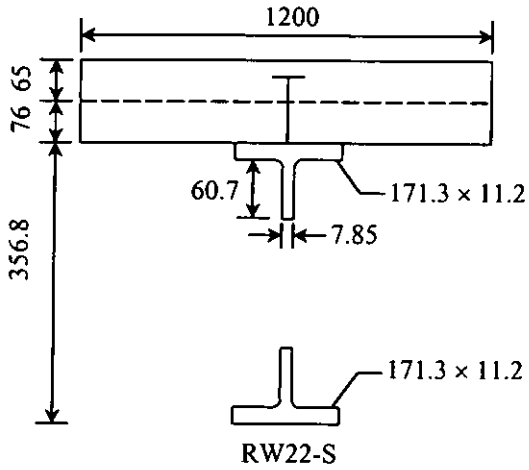

Beam RW3

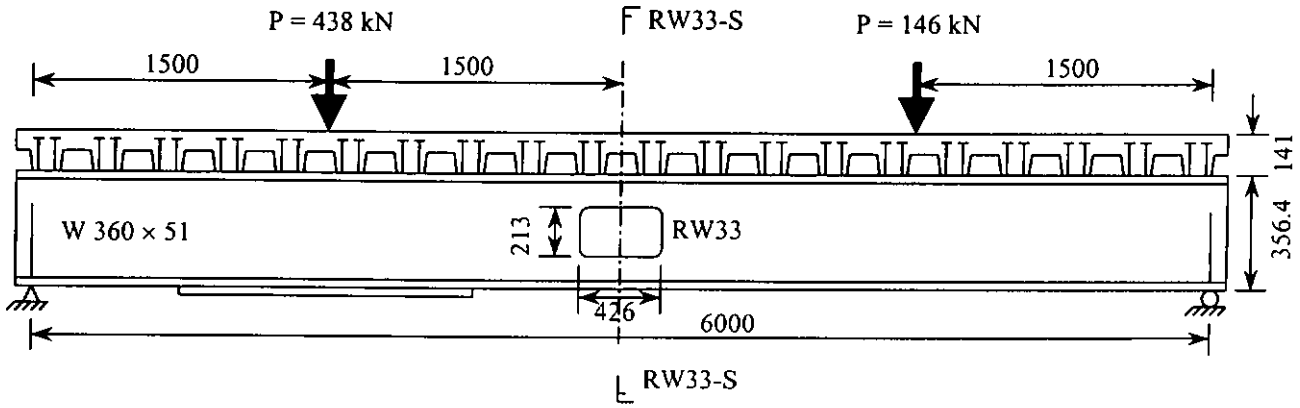

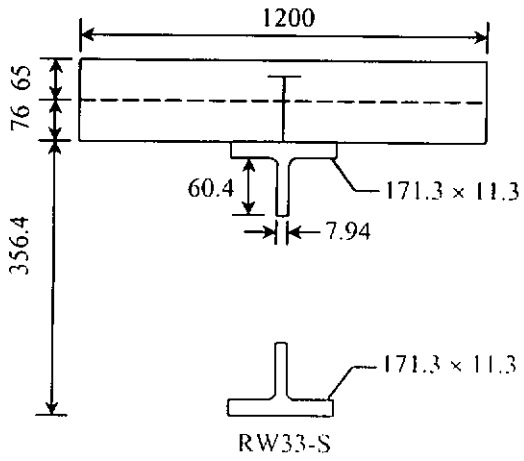

Beam RW4

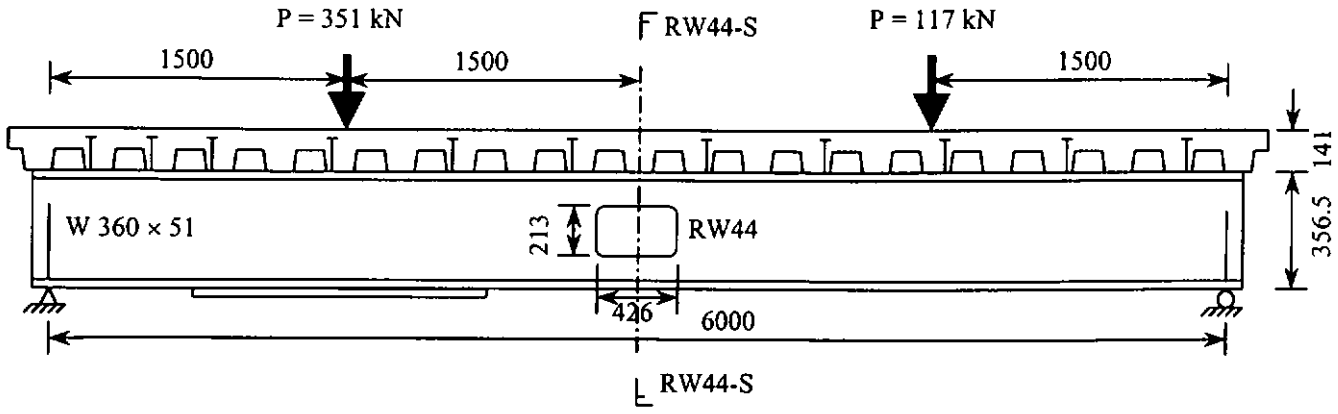
P = 351 kN
RW44-S
P = 117 kN
1500
1500
1500
141
356.5
W 360 × 51
213
RW44
426
6000
RW44-S

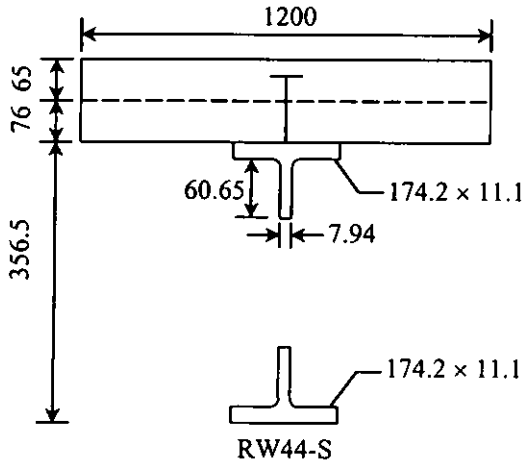
1200
76
65
356.5
60.65
174.2 × 11.1
7.94
174.2 × 11.1
RW44-S

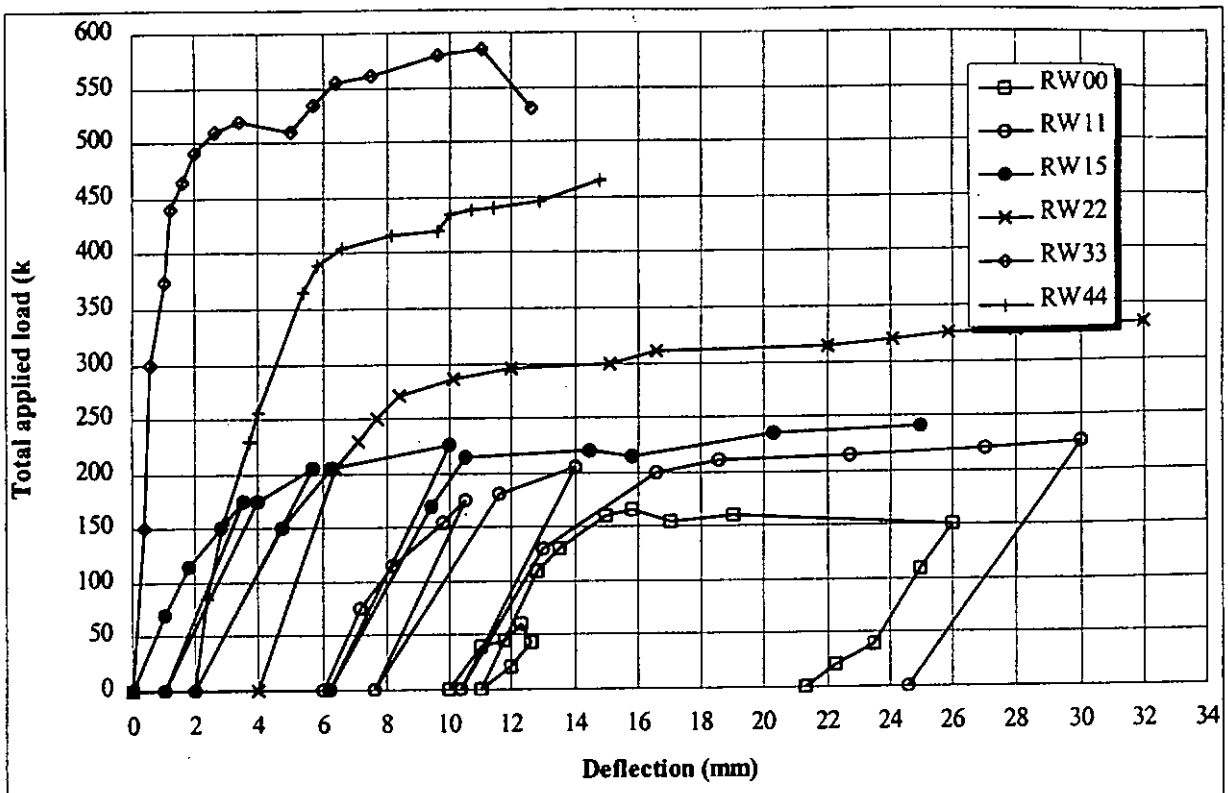

Figure A.2.6a Applied load v.s. relative deflections between opposite ends of opening for test series Redwood & Wong (1982)

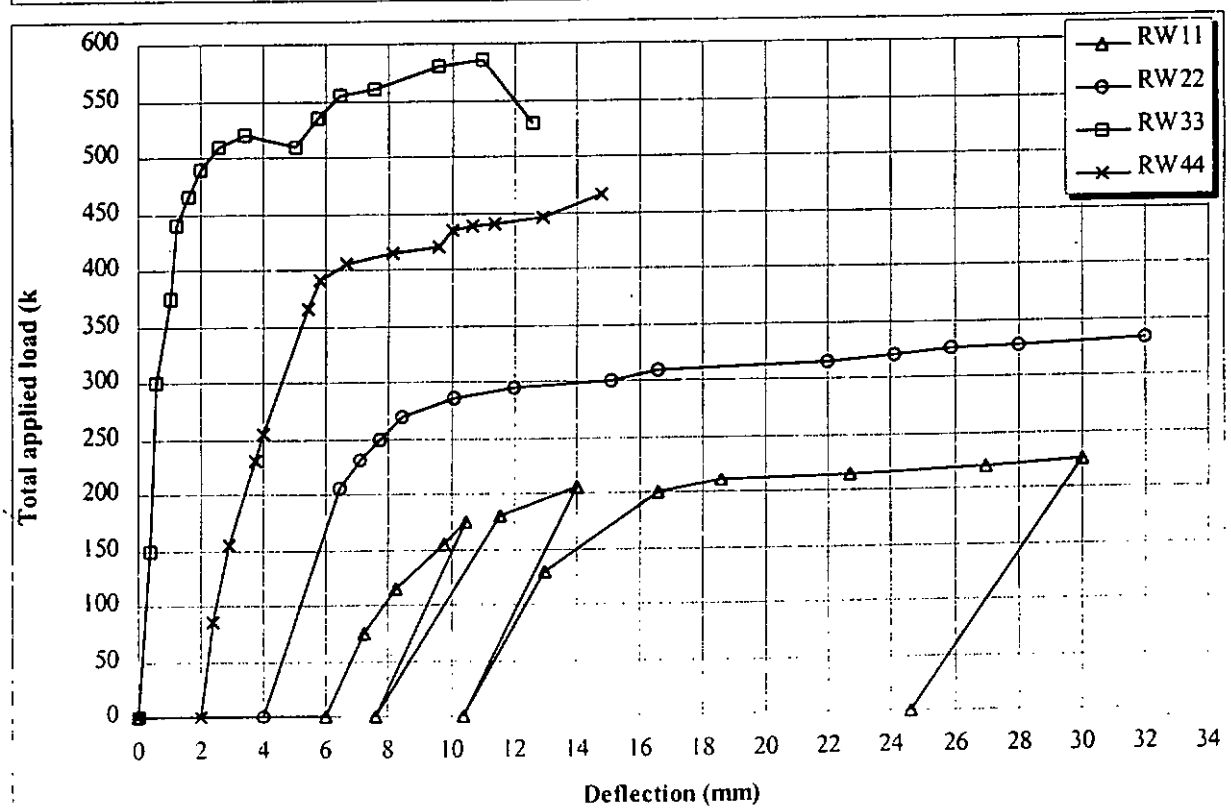

Figure A2.6b Applied load v.s. mid-span deflections for test series Redwood & Wong (1982)